Addressing Common HPLC Detector Challenges Using Silicon Photonic Microring Resonators with Applications for Polymer Separations and More

by

Emily H. Mordan

A dissertation submitted in partial fulfillment
of the requirements for the degree of
Doctor of Philosophy
(Chemistry)
in The University of Michigan
2021

Doctoral Committee:

Professor Ryan C. Bailey, Chair
Professor Robert T. Kennedy
Professor Joerg Lahann
Professor Anne J. McNeil
Dr. David Meunier, The Dow Chemical Company

Emily H. Mordan
ehmordan@umich.edu
ORCID iD: 0000-0003-0105-7458

DEDICATION

I would like to dedicate this work to my family
and all those who supported me along the way.

ACKNOWLEDGEMENTS

I think there is only way one way to start and that is with my parents, who never stopped supporting me and who always make sure to tell me how proud they are of me. My parents have always been strong role models for many aspects of my life. My Mom changed careers while I was in grammar school enrolling in a master's degree program to become a teacher. This meant that not only was she a student in night classes but she also worked full time and took care of my sister and I. Now as a 1st grade teacher for the City of Chicago, she works non-stop day and night (into the morning really) for her students, I have truly never seen anyone work as hard as my Mom. My Dad, is a firefighter for the City of Chicago who for the most part worked at least two jobs while I was growing up. More recently he studied to become a fireman engineer and also took classes to become an EMT, which was a brave move considering the last time he studied was when he was in the fireman academy back in '90s. Needless to say my parent have instilled in me the importance of always continuing to learn, that risks are worth taking, showed me what working hard looks like, and taught me to never let anyone get in the way of your success. I appreciate all you guys have done for me, I will never forget the sacrifices you have made, I could not have done it without you and I am so proud to call you Mom and Dad.

To my best friend and sister, Leanne, thank you for the telephone psych evaluations, encouraging me to always practice retail therapy and always understanding

the struggle of balancing life with graduate school. Maybe I will get lucky and your future school psychologist job will be in a city near me. Additionally, to my grandparents, who always made me feel thought of with the endless greeting cards and newspaper clippings. Their love and support means everything to me. Grandpa may still think I am becoming a teacher but that's okay, I know he would be happy to know I still have all his old chemistry books back from his teaching days.

To those at North Park University, especially Dr. Vazquez and Dr. Larazza, thank you for honestly preparing me for graduate school, trusting me with independence and shaping me into the scientist I am today. I will always value the experiences I gained as a chemistry major at North Park University whether they were independent research ventures, TAing or even attending conferences.

Other thanks are due to my boss Prof. Ryan Bailey, thank you for the opportunity to be in your lab and letting me take on my project. You definitely didn't take it easy on me, but I will always appreciate that you gave me chance and let me show you all I had.

I would also like to thank my collaborator at Dow, Dr. David Meunier. I appreciate so much your guidance, input, and passion for my project. My time at Dow as a visiting scientist in my second year was an experience I will never forget, I am grateful for the lessons I learned, the opportunities I had and the connections I made during this time. Most of all I look forward to my future at Dow and hope that our collaborations don't stop here.

To the original Bailey lab from U of I Richard, James, Ellen, Alex, Heather, Yi, Steve, and Mari, all of you truly lead by example and showed the rest of us how it is done. Thank you for welcoming the first batch of U of M students into the Bailey Lab. Special

thanks to my mentor James, thanks you for all your help over the years, for being a great teacher, and letting us bug you in Midland when we needed to stress vent. I am so happy that I had the opportunity to work with you as both a lab mate and as a collaborator, I look forward to our paths continuing to cross at Dow. Gloria, Nico, Claire, Marina, Nick, and Krista thank you for being a calm among the chaos and politely dealing with the rest of us especially as we all got more and more stressed over the years. I cannot wait to see the great things you guys accomplish in the coming years.

I was lucky enough to join the Bailey lab with a group five others, I am not sure Ryan knew but he was getting himself into but I am happy to have had them by my side through this process. Sara and Colleen, thanks for being the best desk buddies we sure did make sure to have some laughs even though we could never hear each other over the fan and all the year round space heaters. Shannon, thanks for always checking in, being considerate of everyone's best interest and keeping the candy drawer full. Cole, thank you for being comedic relief, a good distraction, and always willing to help with just about anything. Last but not least, John, we may not have planned it this way but I am so grateful to have met you and even more grateful to do life with you. Although we may not recommend anyone date their co-worker or work with their significant other, somehow we made it work and I would not have it any other way. Thank you for supporting all my endeavors, bragging about me, and being my rock. I love you so much and look forward to our future together, which will most definitely include two dogs and maybe another cat…just kidding Phoebe and Ozzy are plenty.

TABLE OF CONTENTS

LIST OF TABLES

LIST OF FIGURES

ABSTRACT

Liquid chromatography (LC) methods are powerful techniques for polymer characterization. Despite LC being a popular approach for polymer analysis, one frequently unmet challenge still persists: quantitatively determining mass concentration with conventional solvent gradient detectors. Commonly used gradient compatible high performance liquid chromatography (HPLC) detectors include UV/visible (UV/vis), charged aerosol (CAD) and evaporative light scattering (ELSD); each of which suffer critical limitations. UV/vis requires a chromophore signature for detection, limiting applicable analytes. CAD and ELSD offer universal detection, however both suffer from a non-linear response to concentration making quantification difficult. This non-linearity of CAD and ELSD is highly dependent on several factors including analyte and mobile phase composition, which means correction of the non-linear response is not a straight forward task. This then points to a demand for an improved universal detector, ideally offering gradient compatibility and linear mass detection. This dissertation addresses these demands and others by using a silicon photonic microring resonator array as an alternative HPLC detector.

Chapter one provides significant background on conventional polymer LC characterization approaches including an overview of distribution types, separation methods, and detector operation. Additionally, challenges with conventional detectors are

reviewed along with correction approaches to aerosol based non-linear detectors. Finally, much attention is brought to the ongoing challenge of quantitatively determining mass concentration with conventional solvent gradient detectors and the need for further LC detector development to meet such needs.

Initial experiments demonstrating the use of the microring resonator platform as a gel permeation chromatography (GPC) detector are presented in chapter two. Here, the microring resonator performance was directly compared to commercial detectors including differential refractive index (dRI) and UV/vis. With this comparison elevated noise in the microring resonator baseline was observed, on average the signal to noise ratio of the microrings is approximately 4 orders of magnitude smaller than UV/vis. Additionally, a molecular weight dependence was observed with analysis of large molecules which infringed on the dimensions of the evanescent field (sensitivity decay was observed at approximately 25 nm from the surface). With these limitations however, the microring resonators still offered great correlation to conventional concentration sensitive detectors in quantitating the molecular weight distributions of broadly distributed polystyrene standards. Furthermore, the linear mass detection capability of the microring resonator platform was demonstrated setting the stage for later gradient work.

Chapter three builds upon chapter two by exploring approaches for improving the microring resonator flow cell. In chapter two a molecular weight dependence of the sensor surface was observed showing a decreased sensitivity for high molecular weights. Here the flow cell was redesigned implementing a wall-jet inlet with the interest of improving the mass transfer of large molecular weight polymers to alleviate this signal fall-off. The flow cell designs themselves along with a series of chromatogram and peak area

comparison are presented throughout this chapter. It was concluded here that the main contributing factor of this trend is decreased evanescent field strength, even with enhanced mass transfer the microring resonators will likely lack sensitivity for polymers with 2Rg (radius of gyration) greater than or equal to 25 nm, which is the approximate distance from the sensor surface where there is a deviation from linearity.

Much like chapter three, chapter four also explores redesigning the microring resonator flow cell. However, here with a different interest of high temperature LC applications. A significant portion of polymer characterizations in industry is dedicated to polyolefins, which are very robust polymers with high resistance to temperature, requiring LC separations to be performed at elevated temperatures. The challenge however is that detectors compatible to such temperatures are limited, therefore the possibility of the microring resonators to be used as an alternative high temperature detector is presented here. More specifically, a successful high temperature flow cell design was tested however degraded microring resonator sensor performance at these elevated temperatures prevented further exploration of this approach.

Chapter five, continues this work to further characterize more complex polymers by chemical composition distributions, where the microrings were used as a gradient LC detector. Silicon photonic microring resonators are surface-based optical sensors that detect changes in local refractive index (RI). Unlike commercial RI detectors, microring resonators have a substantial dynamic range which allows for compatibility with gradient elution LC, which is fully demonstrated here. The microring resonator performance as a gradient elution detector was directly compared to commercial detectors including ELSD and UV/vis, utilizing an injected mass range of 0.15 to 0.75 mg. Over this range the

microring resonators and UV/vis had a linear response whereas ELSD had a mostly non-linear response. This mass range was within the working range of the ELSD calibration meaning quantification can still be achieved using the obtained non-linear curves. It is suspected that if the ELSD response was explored with injected masses below 0.15 mg and above 0.75 mg that a full sigmodal response would be observed, which is ultimately where quantification would suffer most. Additionally, with this work it was found that on average the microring resonators have a limit of detection (LOD) which is approximately 5 orders of magnitude greater than the LOD for both UV and ELSD. This however did not prevent comparable quantification of mass injected of various components of polymer blend samples by the microring resonator platform.

The microring resonator chip has a silicon surface which can be functionalized easily via silanization methods, this was pursued here in chapter six with the interest of adding another separation dimension at the chip surface. Various silanes-polymer interactions were explored in off-line experiments, as well as oxidized silicon-polymer interactions which were eventually translated to chromatography. Challenges with polymer solubility and weak interactions prevented this work from seeing completion, however the results did motivate a new direction that appears to be fruitful.

The final chapter summarizes all the work presented in this thesis, including discussion on the utility of this LC-microring resonator interface and thoroughly explain both the benefits and limitations of the silicon photonic microring resonator arrays as an HPLC detector. Research in analytical chemistry, especially with regard to LC, tend to focus on the separation side of things rather than the detector side of things, which makes this work unique. Additionally in this final chapter potential future directions are outlined

along with ongoing work which interfaces size exclusion chromatography with microring resonators chips functionalized with antibody captures.

Keywords**:** *polymer characterization, microring resonators, LC detectors, liquid chromatography, HPLC, SEC/GPC*

CHAPTER I

Future on Linear Mass Concentration Detectors for Polymer Analysis

Acknowledgements

I would like to acknowledge Dr. James Wade and Dr. David Meunier for their assistance and helpful discussions throughout the writing process for this chapter.

Abstract

One of the biggest challenges with polymer analysis is quantitatively determining mass concentration with conventional gradient elution liquid chromatography (LC) detectors. An ideal detector for polymer analysis would be a universal gradient compatible linear mass detector. UV/visible (UV/vis) detectors come close to meeting these requirements, making for a popular choice, however UV/vis requires a chemical signature for detection limiting compatible analytes. Therefore, for the solvent gradient separations of analytes without a chromophore charged aerosol (CAD) and evaporative light

scattering (ELSD) detectors are the best “universal” options. However, CAD and ELSD are non-linear in response to concentration which makes quantification difficult. These challenges with conventional LC detectors greatly impact analytical sciences both in and beyond the polymer industry. The continually ongoing advancements in formulation chemistries as well as separation technologies significantly puts strain on the utility of existing detectors. In other words, sample complexity is continually increasing overtime, therefore analysis by existing technologies are becoming more difficult. This means that equal growth in all aspects of analytical chemistry is needed especially on the detector side of things. All that being said there is great demand for an improved linear mass concentration detector for the advancement of analytical chemistry.

1. Introduction

Chemical separations are some of the most important techniques in analytical chemistry allowing for the separation, isolation and/or purification of analyte components. Liquid chromatographic (LC) separation methods remain as some of the most commonly used type of chemical separations, which is true for analytical chemistry in the polymer industry as well.[1–4] Throughout analytical chemistry history there has been continuing advancements in the separation science which persists even today. The same however cannot be said about detection technology.[5] Therefore, this review will provide an overview of polymer analysis using LC methods with much focus on the detection side of things.

As for LC detectors, much focus over the years has been placed on universal detection schemes which has led to the development and improvements of aerosol based

detectors in more recent years.[6,7] Aerosol based detectors include evaporative light scattering (ELSD)[8–15], charged aerosol (CAD),[16–25] condensation nucleation light scattering (CNLSD)[24,26,27] and chemiluminescent aerosol (CLAD)[24] detectors. These detectors all offer completive sensitivity to non-volatile analytes while also providing universal detection making for an attractive choice over other commercial detectors.[24] The drawback of these aerosol based detectors however, is their limited linear mass concentration range, as a result quantitative analysis within the non-linear portions of the response is often difficult especially with predicting unknow concentrations. More so, the non-linearity of aerosol based detectors is dependent on both mobile phase and analyte composition, therefore correcting such a response is non-trivial.[1,11,14,15,24,28,29] This brings to attention the limitations of more recently developed universal detectors and places focus on the need of a gradient compatible universal detector that offers linear mass detection capabilities.

The polymer industry is one field that is significantly craving an improved linear mass concentration detector for liquid chromatography methods. Synthetic polymers are heavily distributed by at least molecular weight and more complex samples are distributed in any of the following distributions as well; chemical composition, microstructure, end-group, and branching. Characterization of these distributions is very important to polymer chemists since one can make a connection between polymer size/structure to polymer properties, evaluating future industrial applications.[30] The numerous analytical liquid chromatography techniques have the versatility to statistically estimate each of the listed distributions.[2,3] However, very often these LC methods are challenged by the limitations of the detectors themselves.[1] Many polymer analytes lack chromophores, eliminating the

use of UV/visible (UV/vis) detectors[6,7], therefore this leaves differential refractive index detectors (dRI)[31] for isocratic separations and aerosol based detectors for gradient separations. However, as mentioned earlier the non-linearity of aerosol based detectors and the complexity of linearizing the response for gradient applications challenges quantitative analysis which is a major concern for analytical research and development in industry. There are of course other analytical techniques such as mass spectrometry[32–37] and various spectroscopy methods[38–43] (i.e. NMR and FTIR) that can also characterize these distributions as well, however characterization is represented by averages (i.e. average chemical composition or average degree of branching). LC methods are typically preferred since one obtains a better estimate of actual distributions,[44] which further motivates the development of new LC detectors.

Another concern in the LC detector space for polymer analytical chemistry is the limited number of high temperature compatible detectors. Polyolefins, including polyethylene and polypropylene, are some of the most widely used synthetic polymers. The semi-crystalline structure of polyolefins enables a highly resistant polymer to both temperature and chemical corrosion. This robust nature of polyolefins along with a range of diverse properties makes for an attractive material choice for numerous applications. However, these highly resistant properties also make for several challenges with analysis through the use of elevated temperatures and harsh solvents.[45] For this reason, high temperature liquid chromatography (HT-LC)[46–50] and thermal gradient interactive chromatography (TGIC)[51–54] methods are utilized. The problem however, is that these design constraints put significant challenges on the existing detector technologies, limiting applicable detectors.

2. Overview of Polymer Distribution Types

2.1. Molecular Weight Distributions

Linear homopolymers, probably the simplest polymer, is very easy to fully characterize. Having a uniform microstructure and single repeat unit leaving only the molecular weight (MW) dimension for characterization. However, molecular weight distributions (MWD) are useful characterizations even for the most highly distributed polymers (i.e. those with multiple distributions). Very often polymer properties are reflected with MWD, which is useful for understanding property uniformity or even specific achievable properties for future applications. Typically, with MWD statistically based averages are calculated to represent the mean MW of a sample. The two most common MW averages are number average MW (M_n) and weight average MW (M_w), M_n is a normal number average and M_w is a weight average which provides heavier weighting toward the higher molecular weight chains in the distribution. Therefore, M_w is always larger than M_n, this means M_w is more sensitive to the large MW portion of a sample and M_n is more sensitive to the small MW portion. The ratio of M_w/M_n is known as the polydispersity index (Đ) and ultimately describes the breadth of the distribution. Mathematically M_n, M_w, and Đ are defined as the following:

$$M_n = \frac{\Sigma_i N_i M_i}{\Sigma_i N_i} = \frac{\Sigma_{wi}}{\Sigma_i w_i / M_i} \qquad M_w = \frac{\Sigma_i N_i {M_i}^2}{\Sigma_i N_i M_i} = \frac{\Sigma_i w_i M_i}{\Sigma_i w_i} \qquad Đ = \frac{M_w}{M_n}$$

where N_i is the number of molecules, M_i is the MW, w_i is weight fraction.[12,13,14] Experimentally MWDs are commonly characterized with size exclusion chromatography

(SEC) separations, also often termed gel permeation chromatography (GPC) or gel filtration chromatography (GFC), and a concertation sensitive detector.

2.2. Chemical Composition Distributions

Copolymers are a class of polymers with two or more monomer repeat units, which simply means that copolymers possess a heterogenous chemical composition (CC) dimension. Therefore, that means that all copolymers are distributed in at least two dimensions, MW and CC. More specifically in this review, chemical composition distributions (CCD) refer to the heterogeneity of the polymer backbone.[62,64] Given this heterogeneity, LC separations employed for CC characterization are typically interactive in nature. This means that polymer analytes will bear an affinity for the column stationary phase and the strength of these interactions will be dictated by CC. This is very different from SEC separations where analytes do not interact with the stationary phase. There are various LC methods that can be used, many of which will be discussed in the following section.[65,66]

2.3. Functionality Distributions

Functionality type distributions are characterizations based on the polymer chain's terminal end group functionalities. Such reactive groups include hydroxyl, carboxylic acid, amine, thiol, and more. Polymers can be monofunctional, meaning only one end group of the polymer chain is functional/reactive, or bifunctional, meaning two end groups of the polymer chain are functional. In the case of branched polymers, for example star shaped polymers, polyfunctionality is also a possibility. Characterization of end group

functionalities, like many other distributions, helps one make connections to polymer properties.[67] Spectroscopic and mass spectrometry methods are more commonly used for end group analysis however LC methods are still possible. Such LC methods separate based on the number of terminal groups or the type of end groups, since the presence of functional groups will affect how the molecule interacts with the stationary phase. Typically LC methods include liquid chromatography at the critical condition (LCCC)[67–71], two-dimensional LC separations,[72] or LC hyphenated with spectroscopic techniques.[73]

2.4. Architectural Distributions

Another way polymers can be distributed is by their architecture, meaning branching, microstructure, or tacticity. Branching is mostly self-explanatory, however this simply means that there are side chains extending from the linear polymer chain and these branched can be distributed in several different parameters. Those of which include degree of branching, branch functionality, length of branches and the distance between branches. Given this complexity along with the fact that branched polymers will be distributed in other dimensions as well makes this class of polymers particularly challenging to fully characterize. However understanding branching is important since it directly translates to better understanding of crystallinity, glass transition temperature, melt rheology and solubility.[74] NMR and other spectroscopic techniques are very powerful techniques for estimating the average degree of branching,[75,76] however LC methods are useful for this as well. SEC with triple detection, typically including a light scattering detector, viscometry detector, and a concentration sensitive detectors, is also a useful method for characterizing degree of branching since this combination allows for the

correlation between molar mass and number of branches.[77–84] LCCC and interactive gradient LC methods have shown to be a viable option as well for separating based on degree of branching, as demonstrated by Al Samman et. al., however they did find that molecular weight played a role in these separations especially with low molecular weight polymers.[85] Much like characterization of end group functionality LCCC is a useful method for understanding the functionality of branches/number of functional groups including those at the terminal ends of the polymer chain.[68,70,71] High temperature approaches involving temperature gradient and solvent gradient approaches,[86,87] as well as a very recent study which performed high temperature SEC,[88] have all been used for branching characterization.

Microstructure characterization allows for a better understanding of a polymers configuration, arrangement or morphology. This is a perfect transition from discussing branching since branching is a type of microstructure. Other types of microstructures include semi-crystalline and cross-linked which can have varying degrees of crosslinking, both of which play a significant role in the properties of the polymer. Approaches for such characterizations include gradient elution at critical point of adsorption[89] and LCCC hyphenated NMR methods[41,42]. Additionally, the microstructure analysis of polyolefins tend to be performed at elevated temperatures due to their high resistance to solvent.[52]

A final microstructural parameter to be considered is tacticity. The stereochemistry of polymers containing repeat units with chiral centers are either isotactic, syndiotactic or atactic. Isotactic means all substituents are on the same side of the polymer chain/backbone and tend to be semi-crystalline in nature. Syndiotactic means the

orientation of substituents alternate down the backbone in a pattern, this stereochemistry leads to crystalline structure. Finally, atactic means the orientation of substituents is random which typically describes an amorphous polymer.[30] Characterization of tacticity with LC methods has been demonstrated with LCCC,[90,91] LCCC-NMR,[92] and HT-HPLC.[50,93–95]

3. Overview of LC Methods used for Polymer Characterization

3.1. Size Exclusion Chromatography

SEC is a hydrodynamic size based separation achieved based on the molecules steric interactions, this phenomenon is a thermodynamically driven equilibrium via the partition coefficient (K_{SEC}). K_{SEC} is simply the ratio of the average polymer concentration occupying pores to the average polymer concentration occupying interstitial space.[55,56] That being said, when performed under ideal conditions, SEC cannot distinguish based on branching/molecular architecture or chemical composition.[2] Therefore the real utility of SEC comes when coupled with a concentration sensitive detector (outlined in Table 1-1), such as UV/vis or differential refractive index (dRI), since full MWD can be determined with a single method.[57] Additionally, this technique like most analytical techniques requires calibration, in this case narrowly distributed polymers of a range of MW are utilized so that a correlation between size and elution volume can be made.

SEC columns for polymer analysis are commonly cross-linked organic polymer packing particles or porous silica particles, where pore size varies greatly for the separations on the Dalton (Da) scale all the way up to the megadalton (MDa) scale. SEC

column research has been mostly focused on improvements to the existing column technologies. This includes the development of mesoporous silica with narrower pores to improve resolution at the low MW range.[58] As well as, the development of larger pores on the 1000 angstrom scale via superficially porous particles. Which has shown substantial enhancement for mass transport, resolution, and maintaining integrity of large molecules. This is of particular interest since ultrahigh molecular weight polymers tend to be the most challenging application of SEC due to risk of shear degradation and/or deformation.[59–61] Other active areas of research include the work of Caltabiano et. al. which investigated the use of common reverse phase and hydrophilic interaction (HILIC) columns in SEC mode as alternatives to SEC dedicated columns. This is desirable due to cost, abundance and ease of equilibration for reverse phase/HILIC columns.[62]

Other recent SEC research has focused on implications of mobile phase. Conventionally SEC utilizes neat solvents, meaning pure solvents lacking additives, this is due to the fact that mixed solvents have shown to cause preferential solvation which has the potential to cause more variability in detection. However, Striegel and Sinha et. al., have recently demonstrated MW determination of polystyrene (PS) and poly (methyl methacrylate) (PMMA) with SEC using mixed solvents, here preferential solvation was avoided through use of isorefractive solvent pairing. This work is particularly useful for multi-dimensional separations since interactive separations often operate using mixed solvents, which means the SEC dimension could be performed with the same mobile phase as the other dimension.[63]

All this being said SEC is not a major focus in research today since method development is a lot more straight forward compared to interactive LC methods. And ultimately SEC as a technique has proven to be very robust and reliable for MWD characterization, which cannot always be said of methods of a similar age. In other words, traditional SEC is still used as the gold standard method for routine MWD characterization by academia and industry labs and this will continue to be the case. However, current research has placed significant focus on column improvements and ease of operation which has only further improved the utility of SEC separations.

3.2. Liquid Chromatography at the Critical Conditions

With separations where analytes interact with the stationary phase, there is an observed phenomenon named the critical point of adsorption (CPA). CPA is the transition from SEC mode to an interactive/absorption chromatography (IC) mode, where SEC mode is a state where analytes are unabsorbed and with IC mode analytes are in an absorbed state. Once proper separation conditions are met with solvent composition and temperature optimization CPA is achieved. At CPA there is an equilibrium between the number of molecules in the two states, meaning there is an equal balance between the number of molecules occupying pores of the column and interstitial space. Liquid chromatography at the critical condition (LCCC) utilizes this phenomenon as a separation method.[2] LCCC is an isocratic mode separation typically of a mixed mobile phase, which plays a significant role in determining critical conditions along with stationary phase and temperature.[96] Various approaches have been used to best determine the critical conditions, recently however many studies have taken to modeling/simulations for

establishing these conditions.[97–101] However, once a LCCC method is obtained this separation offers MW independent elution, making this a useful technique for characterizing distributions other than MW, for example tacticity[102] and end group[103] analysis. LCCC is also especially useful for block copolymers, since the CPA of one block will not be the same for the other block, which allows for the characterization one block independent of the other.[96]

3.3. Gradient Elution at Critical Point of Adsorption

Gradient elution at critical point of adsorption (GE-CPA) is another type of separation that utilizes the CPA phenomenon to achieve separations independent of MW, however unlike LCCC GE-CPA is applicable to high MW polymers. Here polymer analytes are injected into an absorption promoting solvent and are retained via enthalpy driven absorption, eventual elution is observed once CPA is met. Much like LCCC,GE-CPA is useful for the characterization of distributions other than MW such as microstructure.[89]

3.4. Liquid Adsorption Chromatography

One class of interactive chromatography (IC) is liquid adsorption chromatography (LAC), which in theory can be performed in either isocratic or gradient conditions. LAC is an enthalpy driven separation where separations are achieved based on the interaction between polymer analyte and stationary phase. LAC is more commonly run in gradient mode since, gradient elution LAC is more applicable to a broader range of applications. Therefore, in this case analyte elution is observed once the mobile phases composition promotes desorption, which is typically at CPA.[89] Where the solvent changes from weak

to strong, where weak solvents encourage adsorption and strong solvents encourage desorption.[65] Commonly this method is used for CC characterization[104–106] meaning separations are assumed to proceed based on the chemical makeup of the analyte, however it is also understood that this separation is also sensitive to MW, end groups, and chain tacticity as well. Additionally, high temperature applications of LAC are also commonly employed especially for polyolefin characterizations. Typically this consists of running a solvent gradients of "harsh" solvents at elevated temperatures (130–180 ^{o}C).[47,88,93,107,108]

This is a very versatile technique since with the right conditions many different distribution types can be characterized. There are however challenges with LAC, in isocratic mode high MW polymers tend to adsorb irreversibly limiting applications to low MW polymers.[65] Then with gradient mode LAC there is the challenge of compatible detectors, where the most commonly used options are UV, ELSD and CAD. UV detectors have limited applications for only polymers with a chromophoric signature. Then ELSD and CAD possess a non-linear response in terms of mass, and show strong solvent and polymer composition dependencies, making accurate quantification difficult.[57,109]

3.5. Liquid Precipitation Chromatography

Another IC method is liquid precipitation chromatography (LPC), this separation mechanism is also run in gradient mode where elution strength is in terms of solubility. Therefore, with LPC a polymer is injected into a poor solvent/non-soluble condition causing the analyte to precipitate out at the start of the column. As the gradient progresses additions of a good solvent is increased and the polymer analyte is eluted

once dissolution occurs.[110,111] This technique is most useful for MW and CC characterization, with previous studies showing applicability to blended samples as well.

3.6. Temperature Gradient Interaction Chromatography

Temperature gradient interaction chromatography is an isocratic solvent separation with the gradient aspect coming from temperature. Therefore, polymer is injected in a temperature that promotes adsorption and the elution strength is increased with a temperature gradient rather than a solvent gradient.[112] TGIC is sensitive to molecular weight and structural polymer chain difference, for the potential characterization of CC, chain blocks, end group and tacticity.[51–54]

4. Concentration Sensitive HPLC Detectors

4.1. Ultraviolet/Visible (UV/vis) detector

Ultraviolet/visible detection, more commonly known as UV/vis, is one of the earliest developed detectors which has evolved from early spectrophotometers dating back to the 1930s, and impressively UV/vis detection still persists as one of the most wildly used detectors. UV/vis offers optical based detection on the principle of molecular absorbance spectrometry and Beer's law, therefore absorbance is linearly proportional to sample concentration. Modern UV/vis detectors offer a range of selectable wavelengths and can operation at either fixed or variable wavelengths, this is important since sensitivity is dependent on the molar absorptivity of an analyte at a particular wavelength. The major limitation with UV/vis detections is the non-universality of this technology, where analytes lacking a chromophore cannot be analyzed. Finally, with use of UV/vis detectors special

attention should be made to the UV-cutoff of mobile phases to minimize background signal.[113–116]

4.2. Refractive Index (RI) Detector

Refractive index (RI) detectors are another class of optical detection, however unlike UV/vis, RI offers a universal response. RI detectors work by sensing the RI difference between the sample cell and reference cell which contains the mobile phase. Therefore, this means sensitivity is dependent on the RI contrast between the polymer and solvent. Additionally, this leads to the non-gradient compatibility since the mobile phase in the reference flow cell remains the same, and commercial RI detectors lack sufficient dynamic range of response to follow the mobile phase changes. This lack of dynamic range is ultimately the biggest drawback of RI detectors for gradient applications. However, RI based sensors have recently been employed as an alternative to combat this drawback therefore the future of RI detection looks promising for obtaining universal gradient compatible detection.[109,117] On the plus side however RI detectors offer linear mass detection, which is due to the refractive index increment which is a proportionality factor that relates RI to concentration. In other words, with a change of concentration a proportional change in RI will be observed. Other drawbacks to consider include low sensitivity, sensitivity to temperature changes and long equilibration times. However regardless of these drawbacks, RI continues to be the go to detector for the molecular weight distribution characterization of polymers by SEC/GPC.

4.3. Evaporative Light Scattering Detector (ELSD)

Evaporative light scattering (ELSD) is one type of aerosol based detection, the working process of ELSD consists of three parts. First, solvent flow is nebulized by a carrier gas creating a stream of droplets. Second the stream of droplets undergo desolvation, where volatile mobile phase is evaporated off leaving dried analyte particles. Then lastly, a beam of light interrogates the dried analyte particles to produce light that is scattered and measured.[8,13] ELSD rose in popularity due to the universal nature of detection. Some considerations for use of ELSD include mobile phase and analyte volatility, and for optimal performance a volatile mobile phase and non-volatile analyte is required. Additionally, ELSD drawbacks include limited sensitivity in comparison to charged aerosol detection, reproducibility issues and limited linear mass range. In terms of reproducibility issues, signal variance has been observed with different solvent compositions or even additives. Then lastly the limited linear range leads to a typically sigmodal shaped non-linear response curve (illustrated in Figure 1-1) which can challenge quantification of unknow analyte concentrations, specifically in the lower and upper portions of the calibration.[9,10,12,15]

4.4. Charged Aerosol Detector (CAD)

Charged aerosol (CAD) is another aerosol based detector and in many ways is very similar to ELSD, but offers improved sensitivity and linearity. The working principle of CAD is much like ELSD where there is first aerosol formation via nebulization which is followed by the evaporation of volatile mobile phase. Next however, the dried analyte particles are charged by an ion jet formed from a corona discharge these charged particles are then detected/measured by an electrometer. The same volatility

considerations as ELSD are at play here as well with CAD. However, in terms of drawbacks the main limitation in the non-linearity of CAD response, typically parabolic shaped, even though there is some improvement over ELSD (comparison presented in Figure 1-1).[21,25,118]

4.5. Condensation Nucleation Light Scattering Detector (CNLSD)

With the limitations of ELSD in mind, an alternative aerosol based detector was developed called condensation nucleation light scattering detector (CNLSD). CNLSD is a universal detection method similar to ELSD however lacks popularity. Early steps of the CNLSD process functions similarly to ELSD, where the effluent is aerosolized and then vaporized leaving behind dried analyte particles. The next step however involves an amplification process called condensation nucleation, here saturated vapor is condensed onto the dried analyte particles resulting in the growth of these particles. It has been reported that particles on the 2-3 nm range can increase to approximately 10 μm size droplets. This substantial increase in size greatly contributes to an increased detection efficiency, where the signal is either monitoring light scattered like ELSD or outputs a count of light pulses which is the typical signal format of commercial condensation particle counters. CNLSD may have observed low limits of detection in comparison to ELSD however challenges with a non-linear response curve persist although some improvements have been reported.[24,26,27]

4.6. Chemiluminescent Aerosol Detector (CLAD)

Chemiluminescent aerosol (CLAD) is another approach to aerosol based detection. Here the effluent is nebulized, but there is no evaporation step which means CLAD is applicable to volatile analytes unlike other aerosol based detectors. Instead, after nebulization aerosols are impacted onto a catalyst surface and then undergo chemiluminescence before detection by a photodetector.[24]

5. Other HPLC Detectors

5.1. Viscometry Detectors

Online viscometry detection is commonly utilized for isocratic detection of synthetic polymer and polysaccharides, and although rare, can also be used to study proteins and peptides. Typically with viscometry detection one can determine absolute molar mass averages/distributions by relying on universal calibration and/or determine degree of long-chain branching. Types of viscometry detectors include single-capillary viscometer, differential viscometer, and three-capillary viscometer. Single-capillary viscometers simply use a pressure transducer attached to a capillary, where pressure is measured and converted to viscosity. The challenge however with single-capillary viscometers is their sensitivity to flow fluctuations which can often cause detection to suffer. Differential viscometers are the most commonly used viscometer and works by having flow through four capillaries bridged by a differential pressure transducer, the pressure drop across is measured and translated into viscosity. Three-capillary viscometers are most commonly utilized in high temperature LC instruments, here flow is split where the one path is the first and third capillaries and the other path is the second capillary where each path has a transducer measuring the pressure.[76,119,120] Viscometry detection is commonly

employed for branching analysis, one common approach for doing such characterization is multi-detector SEC.[77,83,87,121]

5.2. Light Scattering (LS) Detectors

Light scattering (LS) detectors are commonly used for MW determinations by SEC since direct measurements of MW can be made without calibration.[84,122] Light scattering detectors include low-angle light scattering (LALS), right-angle light scattering (RALS), two-angle light scattering (TALS) and multi-angle light scattering (MALS). These are static light scattering detectors meaning the Rayleigh scattering of the incident laser beam is measured at fixed angles, as for LALS this angle is positioned at approximately 0^{o}-7^{o} from the incident beam, for RALS scattering is measured at 90^{o} from the incident beam, and finally for TALS and MALS scattering is measured at more than one fixed angle. LALS offers accurate MW determinations for polymers having radius of gyration less than 150 nm, however single angle LS cannot provide information on molecular size or radius of gyration. Radius of gyration can be determined by MALS.[123] These LS detectors are often used in triple/multi detector SEC along with viscometry and a concentration sensitive detector such as RI or UV/vis.[124]

6. Hyphenated Detection Techniques

6.1. Infrared (IR) Detectors

LC-infrared (IR) techniques are often carried out via direct interface between the LC system and the Fourier transform infrared spectrometry FTIR flow cell. The IR flow cell resembles that of a traditional UV detector. However, like other detectors mobile

phase background is of concern, therefore much work has been done to develop solvent elimination techniques. Solvent elimination is commonly carried out via nebulization and evaporation, similar to methods employed in aerosol based detection schemes.[125,126] LC-IR methods have been often applied to polymer characterization methods to achieve post-separation structural information of a complex sample.[88,127,128] Additionally, LC-IR has been often used in high temperature applications which applicable detectors are limited. One recent example, Frijns-Bruls et al., has employed a filter-based IR detector for the detection of HT-SEC which was used for the characterization of short-chain branching of polyolefins. [88,129]

6.2. Mass Spectrometry (MS) Detectors

The hyphenation of LC and MS is a powerful tool for polymer characterization with many advantages. First off LC-MS allows for MW determination of individual molecules and compositional elucidation which is especially desirable for polymer characterization. On a different note, by using LC-MS instead of MS alone, there is the added advantage of deconvoluting MS data by having a separation in-line with MS allowing for easier spectra interpretation.[33,130] Electrospray ionization (ESI) and matrix assisted laser desorption ionization (MALDI) are mass spectrometry techniques commonly hyphenated with various LC methods including GPC[34,37,131], LAC, LCCC[36] and even 2D-LC methods.[132] ESI-MS is easily interfaceable with SEC, where the eluent is passed through the ESI needle to form charged droplets which are dispersed and desolvated for ion detection. Gruendling et. al. demonstrated this with SEC-ESI, here they obtained accurate MW determinations with ESI-MS and concentration information from RI detection.[32]

MALDI-MS is not as easily interfaceable with LC given that MALDI is a solid state technique, however both online and offline techniques have been demonstrated. One particular challenge associated with MS detection of polymers is the accessible range of polymer MW which is ionizable, MALDI ionization techniques however can enable detection of larger MW fragments.[133–135]

6.3. Nuclear Magnetic Resonance (NMR) Detectors

Nuclear magnetic resonance (NMR) has often been the go to method for structure elucidation of isolated sample components via both offline and online separations. However, for the purpose of this review we are going to discuss hyphenated LC-NMR primarily. Therefore, in LC-NMR applications flow is directly coupled too the NMR flow cell commonly in either continuous or stop flow mode, in continuous flow data is acquired over time much like any other detector and with stop flow mode data is collected in static conditions. The NMR detector flow cell is comparable to a traditional 3 mm NMR tube typically of 60 µL volume. The small volume of the NMR flow cell is often a major limitation since it will often lead to under sampling of a chromatographic peak, which could be avoided with increased flow cell dimensions or by offline analysis. Other considerations for LC-NMR is the chosen flow rate, solvent system and solvent suppression technique as these factors will impact analysis. Some solvent suppression techniques include presaturation, watergate, and/or WET, one of which is necessary since the solvent signal is in greater abundance than that of the analyte but with these techniques analyte signal is often suppressed in addition. Additionally, successful operation of LC-NMR requires a very controlled system without air bubbles, sample carryover, or other sources of

contamination.[43,125] NMR is most commonly interfaced with LCCC[40–42] and SEC[42] however other LC methods are interfaceable as well. LC-NMR is a powerful technique offering structural analysis of sample components, however it is important to keep in mind the limitations and numerous consideration for proper performance/optimization.[136]

7. Efforts/Current Work Correcting ELSD and CAD Non-linearity

Of aerosol based detection methods ELSD and CAD remain as the most commonly used platforms. As mentioned earlier these techniques suffer from a limited linear response. Therefore, quantitative analysis outside the linear range or in the non-linear portions of the response can lead to less accurate analyte concentration predications. However, even with this persistent challenge ELSD and CAD remain as some of the most commonly used detectors due to the universal detection scheme and gradient compatibility. Therefore, besides finding detector alternatives another active area of research is the development of methods to linearize the responses of ELSD and CAD detectors. This is not an easy task given the non-linear response is dependent on mobile phase, detector parameters, as well as the analyte itself.[15] Such work is mostly done by correcting the response curve, one of the simplest methods for doing this is by performing a log-log transformation, illustrated in Figure 1-2 by Vervoort et. al. With a log-log transformation, the linear portion of the response can generally be increased and the previously encountered double values can mostly be eliminated for easier quantification.[19] More complex methods have been developed such as linearizing ELSD signal intensity as a function of concentration by Boborodea, A. & O'Donohue et. al., where the whole ELSD chromatogram is considered not just the peak area (Figure 1-3).

However, this correction method was only applied using isocratic separations and given that ELSD non-linearity is effected by mobile phase composition a similar approach may not be viable in a solvent gradient separation.[29] Hutchinson and colleagues investigated the factors affecting CAD non-linearity and used this insight to developed a 2 part model. This model shows the 3 dimensional relationship between CAD signal, analyte concentration and mobile phase composition (in this case % acetonitrile) (Figure 1-4). When this model is applied to determining the concentration of unknown compounds a more accurate predicted concentration was found with ~13% error where predication without the model is estimated to be ~500% error.[28] These correction methods all show improvement in the accuracy of quantitating mass concentrations within the non-linear portions of the ELSD and CAD response. However, these correction approaches are not universal meaning the process would need to be repeated with any change to the separation system. Additionally, there are still cases where a linear mass response would be preferred which ultimately highlights the need for universal gradient compatible detector that also offers linear mass detection.

8. Conclusions

Polymer characterization through various combinations of LC methods and detectors allows for the important correlation between structure and properties, which is a necessary task to support plastics manufacturing some of which have been overviewed with this review. Other techniques not mentioned in detail which can also be used for polymer characterization include, field flow fractionation, multi-dimensional LC separations and other techniques not relating to liquid phase separations, however these

techniques were beyond the scope of this review. One outstanding challenge mentioned throughout this review is the need for improved detection schemes that offer linear mass response, universal detection and gradient compatibility which is not an option with existing commercial detectors. To make this even more complicated there is also the hope that such a detector would also be HT-LC compatible, meaning able to operate at elevated temperatures. Meeting these needs in a single detector would allow for more accurate quantitative analysis with regards to polymer characterization via LC methods. As mentioned, research in this space is limited focusing mostly on hyphenation of existing technologies with LC methods and correction of the non-linear response observed with ELSD and CAD, rather than developing alternative detection technologies. Unfortunately these correction approaches still leave a desire for accurate quantitative analysis. Therefore, we hope that this review has brought more light to these issues and inspires more work towards a detector that allows for more accurate quantitative polymer analysis.

Table 1-1: Overview of Concentration Sensitive Detectors

	Detector	Universal	Detection Principle	Solvent Gradient Compatible	Response Curve
Optical Based	Ultraviolet/Visible **(UV/vis)**	No	Absorbance at given wavelength	Yes	Linear
	Refractive Index **(RI)**	Yes	Differential, Detects difference in RI between mobile phase and sample	No	Linear
Aerosol Based	Evaporative Light Scattering **(ELSD)**	Yes	Light scattering of incident beam by dried analyte particles is measured	Yes	Non-linear
	Charged Aerosol **(CAD)**	Yes	Electrometer detects dried, charged analyte particles	Yes	Non-linear
	Condensation Nucleation Light Scattering **(CNLSD)**	Yes	Count of light pulses which interrogates condensed/amplified dried analyte particles	Yes	Non-linear
	Chemiluminescent **(CLAD)**	Yes	Photodetection of the chemiluminescence of aerosols on a catalyst surface	Yes	Non-linear

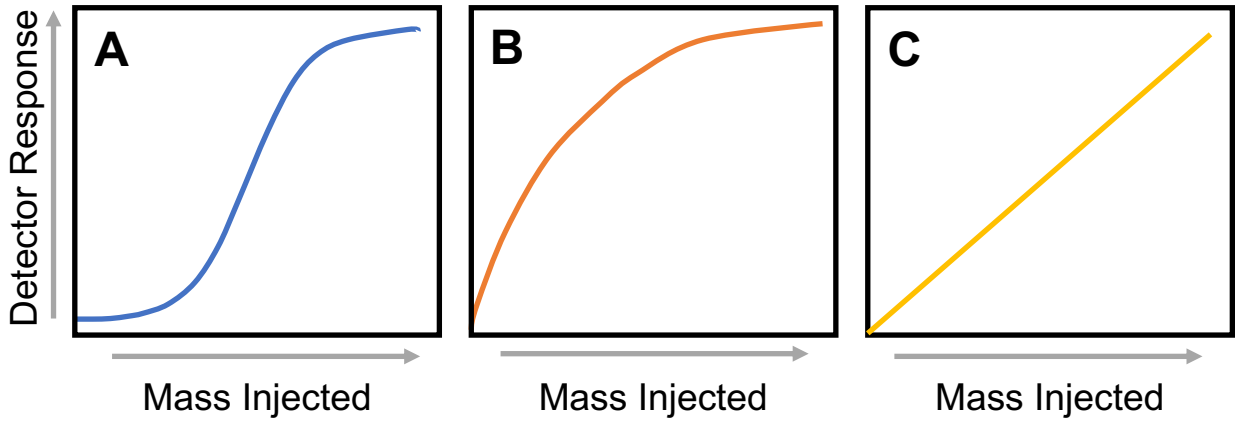

Figure 1-1: Sketch of Non-linear Response of ELSD and CAD Detectors. A. Depicts the typical sigmoidal response of evaporative light scattering detection (ELSD) signal with increasing mass injected on the column. B. Depicts the typical parabolic response of charged aerosol detection (CAD) signal with increasing mass injected on the column. C. Illustrates a linear response typically observed with detectors such as UV/vis and refractive index (RI).

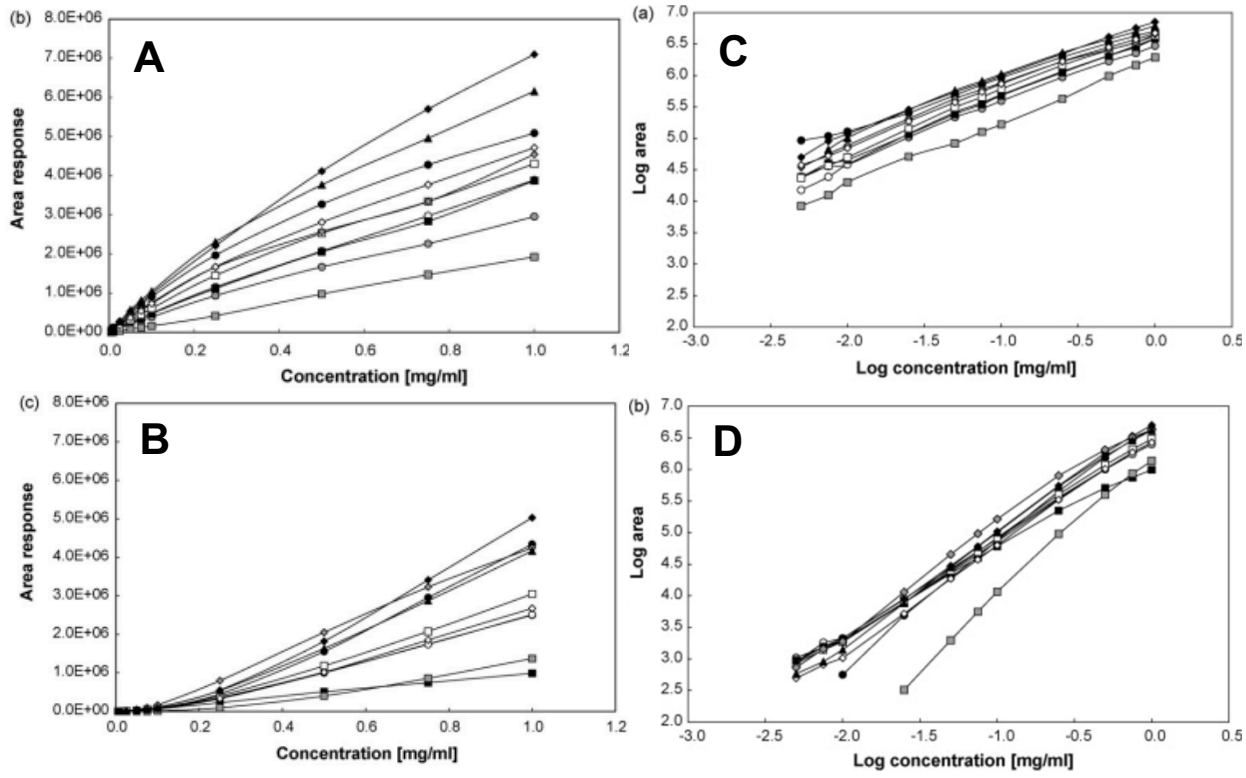

Figure 1-2: Log-log transformation of CAD and ELSD Response. (A) CAD response of increase pharmaceutical concentrations. (B) ELSD response of increase pharmaceutical concentrations. (C) Log-log transformation of CAD response (D) Log-log transformation of ELSD response. Reprinted from[19] Journal of Chromatography A, vol. 1189, N. Vervoort,D. Daemen,G. Török, "Performance evaluation of evaporative light scattering detection and charged aerosol detection in reversed phase liquid chromatography," 92-100, Copyright (2008), with permission from Elsevier.

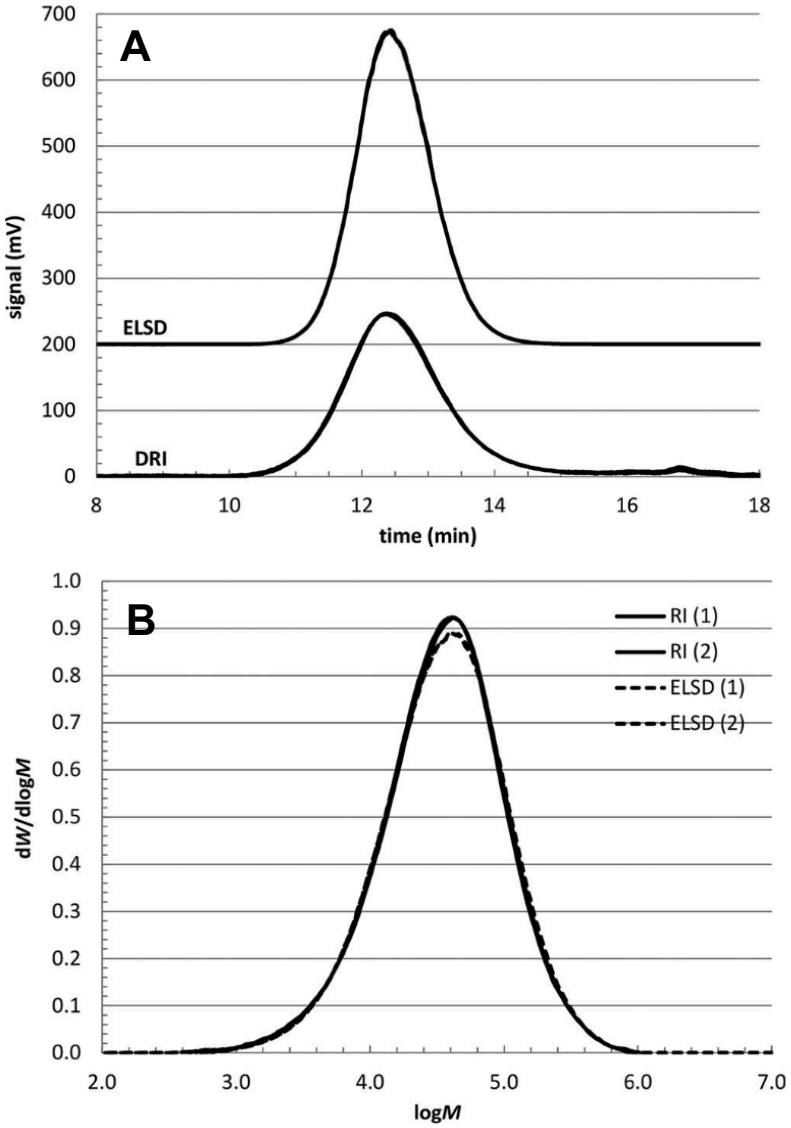

Figure 1-3: Linearized ELSD signal intensity as a function of concentration. (A) Original chromatogram comparison as obtained by RI and ELSD. (B) Comparison of RI and corrected ELSD molecular weight distributions. Reprinted from[29] International Journal of Polymer Analysis and Characterization, vol. 22, Adrian Boborodea, Stephen O'Donohue, "Linearization of evaporative light scattering detector signal," 685-691, Copyright (2017), with permission from Taylor & Francis.

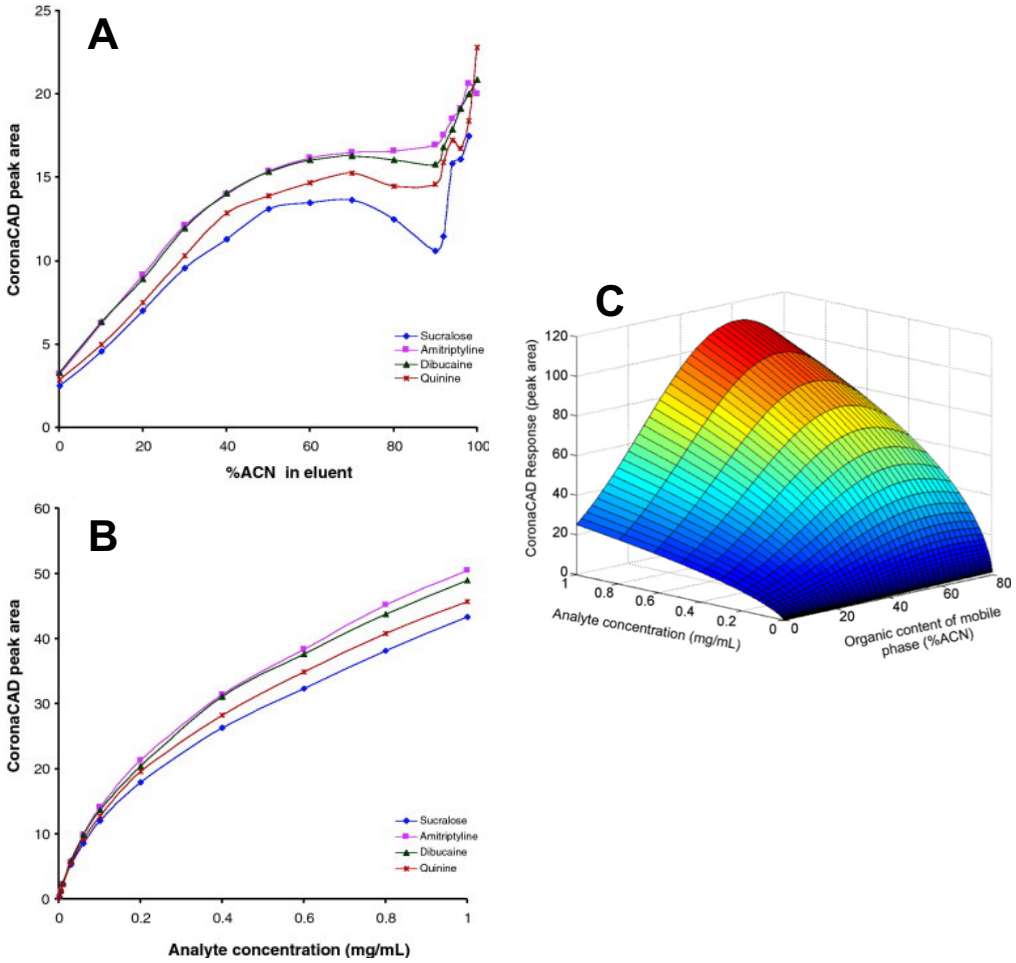

Figure 1-4: Investigation of Charged Aerosol Non-linearity. A. Flow injection analysis observing the effect of mobile phase composition on CAD response. B. Flow injection analysis observing the effect of concentration response. C. Universal response model for CAD Detector**,** which takes account the factors that contribute most to the non-linear nature of the detector. These factors include analyte concentration and mobile phase composition. Reprinted from[28] Journal of Chromatography A, vol. 1217, Joseph P. Hutchinson, Jianfeng Li, William Farrell, Elizabeth Groeber, Roman Szucs, Greg Dicinoski, Paul R. Haddad, "Universal response model for a corona charged aerosol detector," 7419-7427, Copyright (2010), with permission from Elsevier.

9. References

(1) Uliyanchenko, E.; Wal, S. van der; J. Schoenmakers, P. Challenges in Polymer Analysis by Liquid Chromatography. *Polym. Chem.* **2012**, *3* (9), 2313–2335. https://doi.org/10.1039/C2PY20274C.

(2) Chang, T. Chromatographic Separation of Polymers. In *Recent Progress in Separation of Macromolecules and Particulates*; ACS Symposium Series; American Chemical Society, 2018; Vol. 1281, pp 1–17. https://doi.org/10.1021/bk-2018-1281.ch001.

(3) Chang, T. Recent Advances in Liquid Chromatography Analysis of Synthetic Polymers. In *Liquid Chromatography / FTIR Microspectroscopy / Microwave Assisted Synthesis*; Advances in Polymer Science; Springer, Berlin, Heidelberg; pp 1–60. https://doi.org/10.1007/b11050.

(4) Grushka, E.; Grinberg, N. *Advances in Chromatography, Volume 52*; CRC Press, 2014.

(5) Drushel, H. V. Needs of the Chromatographer—Detectors. *J. Chromatogr. Sci.* **1983**, *21* (8), 375–383. https://doi.org/10.1093/chromsci/21.8.375.

(6) Zhang, B.; Li, X.; Yan, B. Advances in HPLC Detection—towards Universal Detection. *Anal. Bioanal. Chem.* **2008**, *390* (1), 299–301. https://doi.org/10.1007/s00216-007-1633-0.

(7) Zhang, K.; Kurita, K. L.; Venkatramani, C.; Russell, D. Seeking Universal Detectors for Analytical Characterizations. *J. Pharm. Biomed. Anal.* **2019**, *162*, 192–204. https://doi.org/10.1016/j.jpba.2018.09.029.

(8) Charlesworth, J. M. Evaporative Analyzer as a Mass Detector for Liquid Chromatography. *Anal. Chem.* **1978**, *50* (11), 1414–1420. https://doi.org/10.1021/ac50033a011.

(9) Arndt, J. H.; Macko, T.; Brüll, R. Application of the Evaporative Light Scattering Detector to Analytical Problems in Polymer Science. *J. Chromatogr. A* **2013**, *1310* (Supplement C), 1–14. https://doi.org/10.1016/j.chroma.2013.08.041.

(10) Megoulas, N. C.; Koupparis, M. A. Twenty Years of Evaporative Light Scattering Detection. *Crit. Rev. Anal. Chem.* **2005**, *35* (4), 301–316. https://doi.org/10.1080/10408340500431306.

(11) Mathews, B. T.; Higginson, P. D.; Lyons, R.; Mitchell, J. C.; Sach, N. W.; Snowden, M. J.; Taylor, M. R.; Wright, A. G. Improving Quantitative Measurements for the Evaporative Light Scattering Detector. *Chromatographia* **2004**, *60* (11), 625–633. https://doi.org/10.1365/s10337-004-0441-3.

(12) Dalavitsou, A.; Vasiliadis, A.; Mordos, M. D.; Markopoulou*, M. G. K. and C. K. Analytes' Structure and Signal Response in Evaporating Light Scattering Detector (ELSD) http://www.eurekaselect.com/160887/article (accessed May 18, 2020).

(13) Mourey, T. H.; Oppenheimer, L. E. Principles of Operation of an Evaporative Light-Scattering Detector for Liquid Chromatography. *Anal. Chem.* **1984**, *56* (13), 2427–2434. https://doi.org/10.1021/ac00277a039.

(14) Webster, G. K.; Jensen, J. S.; Diaz, A. R. An Investigation into Detector Limitations Using Evaporative Light-Scattering Detectors for Pharmaceutical Applications. *J. Chromatogr. Sci.* **2004**, *42* (9), 484–490.

(15) Mojsiewicz-Pieńkowska, K. On the Issue of Characteristic Evaporative Light Scattering Detector Response. *Crit. Rev. Anal. Chem.* **2009**, *39* (2), 89–94. https://doi.org/10.1080/15389580802570218.

(16) Almeling, S.; Ilko, D.; Holzgrabe, U. Charged Aerosol Detection in Pharmaceutical Analysis. *J. Pharm. Biomed. Anal.* **2012**, *69*, 50–63. https://doi.org/10.1016/j.jpba.2012.03.019.

(17) Dixon, R. W.; Peterson, D. S. Development and Testing of a Detection Method for Liquid Chromatography Based on Aerosol Charging. *Anal. Chem.* **2002**, *74* (13), 2930–2937. https://doi.org/10.1021/ac011208l.

(18) Wang, L.; He, W.-S.; Yan, H.-X.; Jiang, Y.; Bi, K.-S.; Tu, P.-F. Performance Evaluation of Charged Aerosol and Evaporative Light Scattering Detection for the Determination of Ginsenosides by LC. *Chromatographia* **2009**, *70* (3), 603–608. https://doi.org/10.1365/s10337-009-1192-y.

(19) Vervoort, N.; Daemen, D.; Török, G. Performance Evaluation of Evaporative Light Scattering Detection and Charged Aerosol Detection in Reversed Phase Liquid Chromatography. *J. Chromatogr. A* **2008**, *1189* (1), 92–100. https://doi.org/10.1016/j.chroma.2007.10.111.

(20) Takahashi, K.; Kinugasa, S.; Senda, M.; Kimizuka, K.; Fukushima, K.; Matsumoto, T.; Shibata, Y.; Christensen, J. Quantitative Comparison of a Corona-Charged Aerosol Detector and an Evaporative Light-Scattering Detector for the Analysis of a Synthetic Polymer by Supercritical Fluid Chromatography. *J. Chromatogr. A* **2008**, *1193* (1), 151–155. https://doi.org/10.1016/j.chroma.2008.04.012.

(21) Vehovec, T.; Obreza, A. Review of Operating Principle and Applications of the Charged Aerosol Detector. *J. Chromatogr. A* **2010**, *1217* (10), 1549–1556. https://doi.org/10.1016/j.chroma.2010.01.007.

(22) Wang, R.; Wang, X.; Paulino, J.; Alquier, L. Evaluation of Charged Aerosol Detector for Purity Assessment of Protein. *J. Chromatogr. A* **2013**, *1283*, 116–121. https://doi.org/10.1016/j.chroma.2013.01.109.

(23) Schilling, K.; Holzgrabe, U. Recent Applications of the Charged Aerosol Detector for Liquid Chromatography in Drug Quality Control. *J. Chromatogr. A* **2020**, 460911. https://doi.org/10.1016/j.chroma.2020.460911.

(24) Magnusson, L.-E.; Risley, D. S.; Koropchak, J. A. Aerosol-Based Detectors for Liquid Chromatography. *J. Chromatogr. A* **2015**, *1421*, 68–81. https://doi.org/10.1016/j.chroma.2015.07.045.

(25) Ligor, M.; Studzińska, S.; Horna, A.; Buszewski, B. Corona-Charged Aerosol Detection: An Analytical Approach. *Crit. Rev. Anal. Chem.* **2013**, *43* (2), 64–78. https://doi.org/10.1080/10408347.2012.746134.

(26) Allen, L. B.; Koropchak, J. A.; Szostek, Bogdan. Condensation Nucleation Light Scattering Detection for Conventional Reversed-Phase Liquid Chromatography. *Anal. Chem.* **1995**, *67* (3), 659–666. https://doi.org/10.1021/ac00099a026.

(27) Lewis, K. C.; Dohmeier, D. M.; Jorgenson, J. W.; Kaufman, S. L.; Zarrin, Fahimeh.; Dorman, F. D. Electrospray-Condensation Particle Counter: A Molecule-Counting LC Detector for Macromolecules. *Anal. Chem.* **1994**, *66* (14), 2285–2292. https://doi.org/10.1021/ac00086a014.

(28) Hutchinson, J. P.; Li, J.; Farrell, W.; Groeber, E.; Szucs, R.; Dicinoski, G.; Haddad, P. R. Universal Response Model for a Corona Charged Aerosol Detector. *J. Chromatogr. A* **2010**, *1217* (47), 7418–7427. https://doi.org/10.1016/j.chroma.2010.09.056.

(29) Boborodea, A.; O'Donohue, S. Linearization of Evaporative Light Scattering Detector Signal. *Int. J. Polym. Anal. Charact.* **2017**, *22* (8), 685–691. https://doi.org/10.1080/1023666X.2017.1367066.

(30) Hiemenz, P.; Lodge, Timothy. *Polymer Chemistry*, 2nd ed.; CRC Press.

(31) E19 Committee. *Practice for Refractive Index Detectors Used in Liquid Chromatography*; ASTM International. https://doi.org/10.1520/E1303-95.

(32) Gruendling, T.; Guilhaus, M.; Barner-Kowollik, C. Quantitative LC−MS of Polymers: Determining Accurate Molecular Weight Distributions by Combined Size Exclusion Chromatography and Electrospray Mass Spectrometry with Maximum Entropy Data Processing. *Anal. Chem.* **2008**, *80* (18), 6915–6927. https://doi.org/10.1021/ac800591j.

(33) Crotty, S.; Gerişlioğlu, S.; Endres, K. J.; Wesdemiotis, C.; Schubert, U. S. Polymer Architectures via Mass Spectrometry and Hyphenated Techniques: A Review. *Anal. Chim. Acta* **2016**, *932*, 1–21. https://doi.org/10.1016/j.aca.2016.05.024.

(34) Viodé, A.; Dagany, X.; Kerleroux, M.; Dugourd, P.; Doussineau, T.; Charles, L.; Antoine, R. Coupling of Size-Exclusion Chromatography with Electrospray Ionization Charge-Detection Mass Spectrometry for the Characterization of Synthetic Polymers of Ultra-High Molar Mass. *Rapid Commun. Mass Spectrom.* **2016**, *30* (1), 132–136. https://doi.org/10.1002/rcm.7426.

(35) Crescentini, T. M.; May, J. C.; McLean, J. A.; Hercules, D. M. Mass Spectrometry of Polyurethanes. *Polymer* **2019**, *181*, 121624. https://doi.org/10.1016/j.polymer.2019.121624.

(36) Epping, R.; Panne, U.; Falkenhagen, J. Critical Conditions for Liquid Chromatography of Statistical Copolymers: Functionality Type and Composition Distribution Characterization by UP-LCCC/ESI-MS. *Anal. Chem.* **2017**, *89* (3), 1778–1786. https://doi.org/10.1021/acs.analchem.6b04064.

(37) Nitsche, T.; Steinkoenig, J.; De Bruycker, K.; Bloesser, F. R.; Blanksby, S. J.; Blinco, J. P.; Barner-Kowollik, C. Mapping the Compaction of Discrete Polymer Chains by Size Exclusion Chromatography Coupled to High-Resolution Mass Spectrometry. *Macromolecules* **2019**, *52* (6), 2597–2606. https://doi.org/10.1021/acs.macromol.9b00203.

(38) Dwyer, J. L.; Zhou, M. Polymer Characterization by Combined Chromatography-Infrared Spectroscopy https://www.hindawi.com/journals/ijs/2011/694645/ (accessed Oct 10, 2017). https://doi.org/10.1155/2011/694645.

(39) Boyron, O.; Taam, M.; Boisson, C. Chemical Composition of Hexene-Based Linear Low-Density Polyethylene by Infrared Spectroscopy and Chemometrics. *Macromol. Chem. Phys.* **2019**, *220* (24), 1900376. https://doi.org/10.1002/macp.201900376.

(40) Hiller, W.; Sinha, P.; Pasch, H. On-Line HPLC-NMR of PS-b-PMMA and Blends of PS and PMMA: LCCC-NMR at Critical Conditions of PS. *Macromol. Chem. Phys.* **2007**, *208* (18), 1965–1978. https://doi.org/10.1002/macp.200700166.

(41) Hiller, W.; Pasch, H.; Sinha, P.; Wagner, T.; Thiel, J.; Wagner, M.; Müllen, K. Coupling of NMR and Liquid Chromatography at Critical Conditions: A New Tool for

the Block Length and Microstructure Analysis of Block Copolymers. *Macromolecules* **2010**, *43* (11), 4853–4863. https://doi.org/10.1021/ma902359e.

(42) Hiller, W.; Sinha, P.; Hehn, M.; Pasch, H.; Hofe, T. Separation Analysis of Polyisoprenes Regarding Microstructure by Online LCCC-NMR and SEC-NMR. *Macromolecules* **2011**, *44* (6), 1311–1318. https://doi.org/10.1021/ma102750s.

(43) Basic Technical Aspects and Operation of LC-NMR and LC-MS-NMR. In *LC-NMR and Other Hyphenated NMR Techniques*; John Wiley & Sons, Ltd, 2011; pp 59–94. https://doi.org/10.1002/9781118135396.ch3.

(44) Martin, K.; Spickermann, J.; Räder, H. J.; Müllen, K. Why Does Matrix-Assisted Laser Desorption/Ionization Time-of-Flight Mass Spectrometry Give Incorrect Results for Broad Polymer Distributions? *Rapid Commun. Mass Spectrom.* **1996**, *10* (12), 1471–1474. https://doi.org/10.1002/(SICI)1097-0231(199609)10:12<1471::AID-RCM693>3.0.CO;2-X.

(45) Arndt, J.-H.; Brüll, R.; Macko, T.; Garg, P.; Tacx, J. C. J. F. High Performance Liquid Chromatography of Polyolefin Plastomers/Elastomers (Ethylene/1-Octene Copolymers) – Comparison of Different Solvent Systems. *J. Chromatogr. A* **2019**, *1593*, 73–80. https://doi.org/10.1016/j.chroma.2019.01.067.

(46) Boborodea, A.; Brookes, A. Polyolefin Characterization in Dibutoxymethane by High Temperature Gel Permeation Chromatography with a New Evaporative Light Scattering Detector. *Polym. Test.* **2017**, *64*, 217–220. https://doi.org/10.1016/j.polymertesting.2017.10.002.

(47) Chatterjee, T.; Rickard, M. A.; Pearce, E.; Pangburn, T. O.; Li, Y.; Lyons, J. W.; Cong, R.; deGroot, A. W.; Meunier, D. M. Separating Effective High Density Polyethylene

Segments from Olefin Block Copolymers Using High Temperature Liquid Chromatography with a Preloaded Discrete Adsorption Promoting Solvent Barrier. *J. Chromatogr. A* **2016**, *1465*, 107–116. https://doi.org/10.1016/j.chroma.2016.08.055.

(48) Chitta, R.; Brüll, R.; Macko, T.; Monteil, V.; Boisson, C.; Grau, E.; Leblanc, A. Characterization of Ethylene Methyl Methacrylate and Ethylene Butylacrylate Copolymers with Interactive Liquid Chromatography. *Macromol. Symp.* **2010**, *298* (1), 191–199. https://doi.org/10.1002/masy.201000039.

(49) Liu, Y.; Phiri, M. J.; Ndiripo, A.; Pasch, H. Chemical Composition Separation of a Propylene–Ethylene Random Copolymer by High Temperature Solvent Gradient Interaction Chromatography. *J. Chromatogr. A* **2017**, *1522*, 23–29. https://doi.org/10.1016/j.chroma.2017.09.042.

(50) Ndiripo, A.; Pasch, H. Retention of Polypropylene Stereoisomers in Solvent Gradient Interaction Chromatography on Porous Graphitic Carbon as Influenced by Temperature and Mobile Phase Composition. *J. Chromatogr. A* **2020**, 460865. https://doi.org/10.1016/j.chroma.2020.460865.

(51) Al-Khazaal, A. Z.; Soares, J. B. P. Joint Effect of Poly(Ethyhlene-Co-1-Octene) Chain Length and 1-Octene Fraction on High-Temperature Thermal Gradient Interaction Chromatography. *Macromol. Chem. Phys.* **2017**, *218* (1), 1600332. https://doi.org/10.1002/macp.201600332.

(52) Cong, R.; deGroot, A. W.; Parrott, A.; Yau, W.; Hazlitt, L.; Brown, R.; Cheatham, M.; Miller, M. D.; Zhou, Z. High Temperature Thermal Gradient Interaction Chromatography (HT-TGIC) for Microstructure Analysis of Polyolefins. *Macromol. Symp.* **2012**, *312* (1), 108–114. https://doi.org/10.1002/masy.201100016.

(53) Inwong, N.; Anantawaraskul, S.; Soares, J. B. P.; Khazaal, A. Z. A.-. High Temperature Thermal Gradient Interaction Chromatography (HT-TGIC) of Ethylene/1-Octene Copolymers: Model Development and Validation. *Macromol. Symp.* **2015**, *356* (1), 54–60. https://doi.org/10.1002/masy.201500040.

(54) Ndiripo, A.; Albrecht, A.; Monrabal, B.; Wang, J.; Pasch, H. Chemical Composition Fractionation of Olefin Plastomers/Elastomers by Solvent and Thermal Gradient Interaction Chromatography. *Macromol. Rapid Commun.* **2018**, *39* (6), 1700703. https://doi.org/10.1002/marc.201700703.

(55) Striegel, A. M. Chapter 10 - Size-Exclusion Chromatography. In *Liquid Chromatography (Second Edition)*; Fanali, S., Haddad, P. R., Poole, C. F., Riekkola, M.-L., Eds.; Elsevier, 2017; pp 245–273. https://doi.org/10.1016/B978-0-12-805393-5.00010-5.

(56) Chen, Q. P.; Schure, M. R.; Siepmann, J. I. Using Molecular Simulations to Probe Pore Structures and Polymer Partitioning in Size Exclusion Chromatography. *J. Chromatogr. A* **2018**, *1573*, 78–86. https://doi.org/10.1016/j.chroma.2018.08.049.

(57) Mordan, E.; Wade, J. H.; Wiersma, Z. S. B.; Pearce, E.; Pangburn, T. O.; deGroot, A. W.; Meunier, D. M.; Bailey, R. C. Silicon Photonic Microring Resonator Arrays for Mass Concentration Detection of Polymers in Isocratic Separations. *Anal. Chem.* **2018**. https://doi.org/10.1021/acs.analchem.8b04263.

(58) Nassivera, T.; Eklund, A. G.; Landry, C. C. Size-Exclusion Chromatography of Low-Molecular-Mass Polymers Using Mesoporous Silica. *J. Chromatogr. A* **2002**, *973* (1), 97–101. https://doi.org/10.1016/S0021-9673(02)01200-1.

(59) Wagner, B. M.; Schuster, S. A.; Boyes, B. E.; Shields, T. J.; Miles, W. L.; Haynes, M. J.; Moran, R. E.; Kirkland, J. J.; Schure, M. R. Superficially Porous Particles with 1000Å Pores for Large Biomolecule High Performance Liquid Chromatography and Polymer Size Exclusion Chromatography. *J. Chromatogr. A* **2017**, *1489*, 75–85. https://doi.org/10.1016/j.chroma.2017.01.082.

(60) Ahmed, A.; Skinley, K.; Herodotou, S.; Zhang, H. Core–Shell Microspheres with Porous Nanostructured Shells for Liquid Chromatography. *J. Sep. Sci.* **2018**, *41* (1), 99–124. https://doi.org/10.1002/jssc.201700850.

(61) Meunier, D. M.; Li, Y.; Gao, W. Characterization of Ultralarge Polymers by Gel Permeation Chromatography: Challenges and Opportunities. In *Recent Progress in Separation of Macromolecules and Particulates*; ACS Symposium Series; American Chemical Society, 2018; Vol. 1281, pp 89–109. https://doi.org/10.1021/bk-2018-1281.ch006.

(62) Caltabiano, A. M.; Foley, J. P.; Barth, H. G. Size Exclusion Chromatography of Synthetic Polymers and Biopolymers on Common Reversed Phase and Hydrophilic Interaction Chromatography Columns. *J. Chromatogr. A* **2016**, *1437*, 74–87. https://doi.org/10.1016/j.chroma.2016.01.055.

(63) Striegel, A. M.; Sinha, P. Absolute Molar Mass Determination in Mixed Solvents. 1. Solving for the SEC/MALS/DRI “Trivial” Case. *Anal. Chim. Acta* **2019**, *1053*, 186–195. https://doi.org/10.1016/j.aca.2018.11.051.

(64) Philipsen, H. J. A. Determination of Chemical Composition Distributions in Synthetic Polymers. *J. Chromatogr. A* **2004**, *1037* (1), 329–350. https://doi.org/10.1016/j.chroma.2003.12.047.

(65) Brun, Y.; Rasmussen, C. J. Chapter 11 - Interaction Polymer Chromatography. In *Liquid Chromatography (Second Edition)*; Fanali, S., Haddad, P. R., Poole, C. F., Riekkola, M.-L., Eds.; Elsevier, 2017; pp 275–318. https://doi.org/10.1016/B978-0-12-805393-5.00011-7.

(66) Wang, Y. Theory and Principles of Interaction Chromatography. In *ACS Symposium Series*; Wang, Y., Gao, W., Orski, S., Liu, X. M., Eds.; American Chemical Society: Washington, DC, 2018; Vol. 1281, pp 19–30. https://doi.org/10.1021/bk-2018-1281.ch002.

(67) Gorshkov, A. V.; Much, H.; Becker, H.; Pasch, H.; Evreinov, V. V.; Entelis, S. G. Chromatographic Investigations of Macromolecules in the “Critical Range” of Liquid Chromatography: I. Functionality Type and Composition Distribution in Polyethylene Oxide and Polypropylene Oxide Copolymers. *J. Chromatogr. A* **1990**, *523*, 91–102. https://doi.org/10.1016/0021-9673(90)85014-M.

(68) Jiang, X.; Schoenmakers, P. J.; Lou, X.; Lima, V.; van Dongen, J. L. J.; Brokken-Zijp, J. Separation and Characterization of Functional Poly(n-Butyl Acrylate) by Critical Liquid Chromatography. *J. Chromatogr. A* **2004**, *1055* (1), 123–133. https://doi.org/10.1016/j.chroma.2004.08.136.

(69) Jiang, X.; Lima, V.; Schoenmakers, P. J. Robust Isocratic Liquid Chromatographic Separation of Functional Poly(Methyl Methacrylate). *J. Chromatogr. A* **2003**, *1018* (1), 19–27. https://doi.org/10.1016/j.chroma.2003.08.035.

(70) Rollet, M.; Glé, D.; Phan, T. N. T.; Guillaneuf, Y.; Bertin, D.; Gigmes, D. Characterization of Functional Poly(Ethylene Oxide)s and Their Corresponding Polystyrene Block Copolymers by Liquid Chromatography under Critical Conditions

in Organic Solvents. *Macromolecules* **2012**, *45* (17), 7171–7178. https://doi.org/10.1021/ma301199m.

(71) Ahn, J.; Chang, T.; Wang, X.; Limpouchová, Z.; Procházka, K. Influence of the Chain Architecture and the Presence of End-Groups or Branching Units Chemically Different from Repeating Structural Units on the Critical Adsorption Point in Liquid Chromatography. *Macromolecules* **2017**, *50* (21), 8720–8730. https://doi.org/10.1021/acs.macromol.7b01786.

(72) Jiang, X.; van der Horst, A.; Lima, V.; Schoenmakers, P. J. Comprehensive Two-Dimensional Liquid Chromatography for the Characterization of Functional Acrylate Polymers. *J. Chromatogr. A* **2005**, *1076* (1), 51–61. https://doi.org/10.1016/j.chroma.2005.03.135.

(73) Jiang, X.; Schoenmakers, P. J.; van Dongen, J. L. J.; Lou, X.; Lima, V.; Brokken-Zijp, J. Mass Spectrometric Characterization of Functional Poly(Methyl Methacrylate) in Combination with Critical Liquid Chromatography. *Anal. Chem.* **2003**, *75* (20), 5517–5524. https://doi.org/10.1021/ac034556r.

(74) Apel, N.; Uliyanchenko, E.; Moyses, S.; Rommens, S.; Wold, C.; Macko, T.; Brüll, R. Separation of Branched Poly(Bisphenol A Carbonate) Structures by Solvent Gradient at Near-Critical Conditions and Two-Dimensional Liquid Chromatography. *Anal. Chem.* **2018**, *90* (8), 5422–5429. https://doi.org/10.1021/acs.analchem.8b00618.

(75) Zhou, Z.; Baugh, D.; Fontaine, P. P.; He, Y.; Shi, Z.; Mukhopadhyay, S.; Cong, R.; Winniford, B.; Miller, M. Long-Chain Branch Measurement in Substantially Linear Ethylene Polymers by 13C NMR with Halogenated Naphthalenes as Solvents.

Macromolecules **2017**, *50* (20), 7959–7966. https://doi.org/10.1021/acs.macromol.7b01692.

(76) Simon, P. F. W.; Müller, A. H. E.; Pakula, T. Characterization of Highly Branched Poly(Methyl Methacrylate) by Solution Viscosity and Viscoelastic Spectroscopy. *Macromolecules* **2001**, *34* (6), 1677–1684. https://doi.org/10.1021/ma0014766.

(77) Farmer, B. S.; Terao, K.; Mays, J. W. Characterization of Model Branched Polymers by Multi-Detector SEC in Good and Theta Solvents. *Int. J. Polym. Anal. Charact.* **2006**, *11* (1), 3–19. https://doi.org/10.1080/10236660500484213.

(78) Gaborieau, M.; Castignolles, P. Size-Exclusion Chromatography (SEC) of Branched Polymers and Polysaccharides. *Anal. Bioanal. Chem.* **2011**, *399* (4), 1413–1423. https://doi.org/10.1007/s00216-010-4221-7.

(79) Netopilík, M.; Janata, M. Decomposition of Size-Exclusion Chromatography Elution Curves of Complex Branched Polymers. *J. Chromatogr. A* **2014**, *1330*, 14–19. https://doi.org/10.1016/j.chroma.2014.01.005.

(80) Yang, H.; Wang, Z.; Zheng, Y.; Huang, W.; Xue, X.; Jiang, B. Synthesis of Highly Branched Polymers by Reversible Complexation-Mediated Copolymerization of Vinyl and Divinyl Monomers. *Polym. Chem.* **2017**, *8* (14), 2137–2144. https://doi.org/10.1039/C7PY00174F.

(81) Suárez, I.; Coto, B. Determination of Long Chain Branching in PE Samples by GPC-MALS and GPC-VIS: Comparison and Uncertainties. *Eur. Polym. J.* **2013**, *49* (2), 492–498. https://doi.org/10.1016/j.eurpolymj.2012.11.015.

(82) Striegel, A. Long-Chain Branching Macromolecules: SEC Analysis; 2009; pp 1417–1420.

(83) Pathaweeisariyakul, T.; Narkchamnan, K.; Thitisuk, B.; Yau, W. Methods of Long Chain Branching Detection in PE by Triple-Detector Gel Permeation Chromatography. *J. Appl. Polym. Sci.* **2015**, *132* (28), n/a-n/a. https://doi.org/10.1002/app.42222.

(84) Podzimek, S.; Vlcek, T.; Johann, C. Characterization of Branched Polymers by Size Exclusion Chromatography Coupled with Multiangle Light Scattering Detector. I. Size Exclusion Chromatography Elution Behavior of Branched Polymers. *J. Appl. Polym. Sci.* **2001**, *81* (7), 1588–1594. https://doi.org/10.1002/app.1589.

(85) Al Samman, M.; Radke, W.; Khalyavina, A.; Lederer, A. Retention Behavior of Linear, Branched, and Hyperbranched Polyesters in Interaction Liquid Chromatography. *Macromolecules* **2010**, *43* (7), 3215–3220. https://doi.org/10.1021/ma902537e.

(86) Lee, S.; Chang, T. Branching Analysis of Comb-Shaped Polystyrene with Long Chain Branches. *Macromol. Chem. Phys.* **2017**, *218* (12), 1700087. https://doi.org/10.1002/macp.201700087.

(87) Lee, H.; Yang, J.; Chang, T. Branching Analysis of Star-Shaped Polybutadienes by Temperature Gradient Interaction Chromatography-Triple Detection. *Polymer* **2017**, *112*, 71–75. https://doi.org/10.1016/j.polymer.2017.01.070.

(88) Frijns-Bruls, T.; Ortin, A.; Weusten, J.; Geladé, E. Studies on the Use of Filter-Based IR Detector for Short-Chain Branching Characterization of Polyolefin Copolymers with High Temperature Size Exclusion Chromatography. *Polymer* **2019**, *180*, 121600. https://doi.org/10.1016/j.polymer.2019.121600.

(89) Brun, Y.; Foster, P. Characterization of Synthetic Copolymers by Interaction Polymer Chromatography: Separation by Microstructure. *J. Sep. Sci.* **2010**, *33* (22), 3501–3510. https://doi.org/10.1002/jssc.201000572.

(90) Berek, D.; Janco, M.; Hatada, K.; Kitayama, T.; Fujimoto, N. Separation of Poly(Methyl Methacrylate)s According to Their Tacticity II. Chromatographic Investigations of Poly(Methyl Methacrylate)s with Different Tacticity at the Critical Adsorption Point. *Polym. J.* **1997**, *29* (12), 1029–1033. https://doi.org/10.1295/polymj.29.1029.

(91) Janco, M.; Hirano, T.; Kitayama, T.; Hatada, K.; Berek, D. Discrimination of Poly(Ethyl Methacrylate)s According to Their Molar Mass and Tacticity by Coupling Size Exclusion Chromatography and Liquid Chromatography at the Critical Adsorption Point. *Macromolecules* **2000**, *33* (5), 1710–1715. https://doi.org/10.1021/ma990518r.

(92) Kitayama, T.; Janco, M.; Ute, K.; Niimi, R.; Hatada, K.; Berek, D. Analysis of Poly(Ethyl Methacrylate)s by On-Line Hyphenation of Liquid Chromatography at the Critical Adsorption Point and Nuclear Magnetic Resonance Spectroscopy. *Anal. Chem.* **2000**, *72* (7), 1518–1522. https://doi.org/10.1021/ac991065r.

(93) Macko, T.; Pasch, H. Separation of Linear Polyethylene from Isotactic, Atactic, and Syndiotactic Polypropylene by High-Temperature Adsorption Liquid Chromatography. *Macromolecules* **2009**, *42* (16), 6063–6067. https://doi.org/10.1021/ma900979n.

(94) Macko, T.; Arndt, J.-H.; Brüll, R. Elution Behavior of Polypropylene with Different Tacticity – An Overview. *Macromol. Symp.* **2015**, *356* (1), 77–86. https://doi.org/10.1002/masy.201500045.

(95) Kot, D.; Macko, T.; Arndt, J.-H.; Brüll, R. Porous Graphite as Platform for the Separation and Characterization of Synthetic Polymers – an Overview. *J. Chromatogr. A* **2019**, *1606*, 360038. https://doi.org/10.1016/j.chroma.2019.02.029.

(96) Striegel, A. M. Method Development in Interaction Polymer Chromatography. *TrAC Trends Anal. Chem.* **2020**, *130*, 115990. https://doi.org/10.1016/j.trac.2020.115990.

(97) Ahn, J.; Chang, T.; Wang, X.; Limpouchová, Z.; Procházka, K. Influence of the Chain Architecture and the Presence of End-Groups or Branching Units Chemically Different from Repeating Structural Units on the Critical Adsorption Point in Liquid Chromatography. *Macromolecules* **2017**, *50* (21), 8720–8730. https://doi.org/10.1021/acs.macromol.7b01786.

(98) Yang, S.; Neimark, A. V. Critical Conditions of Polymer Chromatography: An Insight from SCFT Modeling. *J. Chem. Phys.* **2013**, *138* (24), 244903. https://doi.org/10.1063/1.4810747.

(99) Cimino, R. T.; Rasmussen, C. J.; Brun, Y.; Neimark, A. V. Critical Conditions of Polymer Adsorption and Chromatography on Non-Porous Substrates. *J. Colloid Interface Sci.* **2016**, *474*, 25–33. https://doi.org/10.1016/j.jcis.2016.04.002.

(100) Cimino, R. T.; Rasmussen, C. J.; Brun, Y.; Neimark, A. V. Mechanisms of Chain Adsorption on Porous Substrates and Critical Conditions of Polymer Chromatography. *J. Colloid Interface Sci.* **2016**, *481*, 181–193. https://doi.org/10.1016/j.jcis.2016.07.019.

(101) Ziebarth, J. D.; Gardiner, A. A.; Wang, Y.; Jeong, Y.; Ahn, J.; Jin, Y.; Chang, T. Comparison of Critical Adsorption Points of Ring Polymers with Linear Polymers. *Macromolecules* **2016**, *49* (22), 8780–8788. https://doi.org/10.1021/acs.macromol.6b01925.

(102) Bhati, S. S.; Macko, T.; Brüll, R.; Mekap, D. Liquid Chromatography at Critical Conditions of Poly(Propylene). *Macromol. Chem. Phys.* **2015**, *216* (22), 2179–2189. https://doi.org/10.1002/macp.201500303.

(103) Apel, N.; Uliyanchenko, E.; Moyses, S.; Rommens, S.; Wold, C.; Macko, T.; Rode, K.; Brüll, R. Selective Chromatographic Separation of Polycarbonate According to Hydroxyl End-Groups Using a Porous Graphitic Carbon Column. *J. Chromatogr. A* **2017**, *1488*, 77–84. https://doi.org/10.1016/j.chroma.2017.01.075.

(104) Schunk, T. C. Chemical Composition Separation of Synthetic Polymers by Reversed-Phase Liquid Chromatography. *J. Chromatogr. A* **1993**, *656* (1), 591–615. https://doi.org/10.1016/0021-9673(93)80821-O.

(105) Striegel, A. M. Determining the Vinyl Alcohol Distribution in Poly(Vinyl Butyral) Using Normal-Phase Gradient Polymer Elution Chromatography. *J. Chromatogr. A* **2002**, *971* (1), 151–158. https://doi.org/10.1016/S0021-9673(02)00960-3.

(106) Macko, T.; Arndt, J.-H.; Brüll, R. HPLC Separation of Ethylene–Vinyl Acetate Copolymers According to Chemical Composition. *Chromatographia* **2019**, *82* (4), 725–732. https://doi.org/10.1007/s10337-019-03697-x.

(107) Miller, M. D.; deGroot, A. W.; Lyons, J. W.; Van Damme, F. A.; Winniford, B. L. Separation of Polyolefins Based on Comonomer Content Using High-Temperature

Gradient Adsorption Liquid Chromatography with a Graphitic Carbon Column. *J. Appl. Polym. Sci.* **2012**, *123* (2), 1238–1244. https://doi.org/10.1002/app.33809.

(108) Macko, T.; Brüll, R.; Alamo, R. G.; Thomann, Y.; Grumel, V. Separation of Propene/1-Alkene and Ethylene/1-Alkene Copolymers by High-Temperature Adsorption Liquid Chromatography. *Polymer* **2009**, *50* (23), 5443–5448. https://doi.org/10.1016/j.polymer.2009.09.057.

(109) Mordan, E. H.; Wade, J. H.; Pearce, E.; Meunier, D. M.; Bailey, R. C. A Linear Mass Concentration Detector for Solvent Gradient Polymer Separations. *Analyst* **2020**. https://doi.org/10.1039/C9AN02533B.

(110) Schultz, R.; Engelhardt, H. HPLC of Synthetic Polymers Characterization of Polystyrenes by High Performance Precipitation Liquid Chromatography (HPPLC). *Chromatographia* **1990**, *29* (5), 205–213. https://doi.org/10.1007/BF02317905.

(111) Jančo, M.; Sýkora, D.; Svec, F.; Fréchet, J. M. J.; Schweer, J.; Holm, R. Rapid Determination of Molecular Parameters of Synthetic Polymers by Precipitation/Redissolution High-Performance Liquid Chromatography Using "Molded" Monolithic Column. *J. Polym. Sci. Part Polym. Chem.* **2000**, *38* (15), 2767–2778. https://doi.org/10.1002/1099-0518(20000801)38:15<2767::AID-POLA170>3.0.CO;2-B.

(112) Cong, R.; deGroot, W.; Parrott, A.; Yau, W.; Hazlitt, L.; Brown, R.; Miller, M.; Zhou, Z. A New Technique for Characterizing Comonomer Distribution in Polyolefins: High-Temperature Thermal Gradient Interaction Chromatography (HT-TGIC). *Macromolecules* **2011**, *44* (8), 3062–3072. https://doi.org/10.1021/ma200304e.

(113) Knol, W. C.; Pirok, B. W. J.; Peters, R. A. H. Detection Challenges in Quantitative Polymer Analysis by Liquid Chromatography. *J. Sep. Sci. n/a* (n/a). https://doi.org/10.1002/jssc.202000768.

(114) Uliyanchenko, E.; Wal, S. van der; Schoenmakers, P. J. Challenges in Polymer Analysis by Liquid Chromatography. *Polym. Chem.* **2012**, *3* (9), 2313–2335. https://doi.org/10.1039/C2PY20274C.

(115) Glöckner, G. Detection in Gradient High-Performance Liquid Chromatography. In *Gradient HPLC of Copolymers and Chromatographic Cross-Fractionation*; Glöckner, G., Ed.; Springer Berlin Heidelberg: Berlin, Heidelberg, 1991; pp 87–98. https://doi.org/10.1007/978-3-642-75799-0_7.

(116) Swartz, M. Hplc Detectors: A Brief Review. *J. Liq. Chromatogr. Relat. Technol.* **2010**, *33* (9–12), 1130–1150. https://doi.org/10.1080/10826076.2010.484356.

(117) Ye, D.; Wang, W.; Moline, D.; Islam, M. S.; Chen, F.; Wang, P. A Microwave Flow Detector for Gradient Elution Liquid Chromatography. *Anal. Chem.* **2017**, *89* (20), 10761–10768. https://doi.org/10.1021/acs.analchem.7b01924.

(118) Kou, D.; Manius, G.; Zhan, S.; Chokshi, H. P. Size Exclusion Chromatography with Corona Charged Aerosol Detector for the Analysis of Polyethylene Glycol Polymer. *J. Chromatogr. A* **2009**, *1216* (28), 5424–5428. https://doi.org/10.1016/j.chroma.2009.05.043.

(119) Garamszegi, L.; Nguyen, T. Q.; Plummer, C. J. G.; Månson, J.-A. E. Characterization of Hyperbranched Aliphatic Polyesters and Their Trimethylsilylated Derivatives by GPC-Viscometry. *J. Liq. Chromatogr. Relat. Technol.* **2003**, *26* (2), 207–230. https://doi.org/10.1081/JLC-120017164.

(120) Striegel, A. M. Viscometric Detection in Size-Exclusion Chromatography: Principles and Select Applications. *Chromatographia* **2016**, *79* (15–16), 945–960. https://doi.org/10.1007/s10337-016-3078-0.

(121) Saunders, G.; Cormack, P. A. G.; Graham, S.; Sherrington, D. C. Use of Rapid Triple Detection Size Exclusion Chromatography To Evaluate the Evolution of Molar Mass and Branching Architecture during Free Radical Branching Copolymerization of Methyl Methacrylate and Ethylene Glycol Dimethacrylate. *Macromolecules* **2005**, *38* (15), 6418–6422. https://doi.org/10.1021/ma0501693.

(122) Se, K.; Sakakibara, T.; Ogawa, E. Molecular Weight Determination of Star Polymers and Star Block Copolymers Using GPC Equipped with Low-Angle Laser Light-Scattering. *Polymer* **2002**, *43* (20), 5447–5453. https://doi.org/10.1016/S0032-3861(02)00410-X.

(123) Liu, Y.; Bo, S.; Zhu, Y.; Zhang, W. Determination of Molecular Weight and Molecular Sizes of Polymers by High Temperature Gel Permeation Chromatography with a Static and Dynamic Laser Light Scattering Detector. *Polymer* **2003**, *44* (23), 7209–7220. https://doi.org/10.1016/j.polymer.2003.08.037.

(124) Wang, W.-J.; Kharchenko, S.; Migler, K.; Zhu, S. Triple-Detector GPC Characterization and Processing Behavior of Long-Chain-Branched Polyethylene Prepared by Solution Polymerization with Constrained Geometry Catalyst. *Polymer* **2004**, *45* (19), 6495–6505. https://doi.org/10.1016/j.polymer.2004.07.035.

(125) Pasch, H. Hyphenated Separation Techniques for Complex Polymers. *Polym. Chem.* **2013**, *4* (9), 2628–2650. https://doi.org/10.1039/C3PY21095B.

(126) Coulier, L.; Kaal, E.; Hankemeier, T. Hyphenation of Infrared Spectroscopy to Liquid Chromatography for Qualitative and Quantitative Polymer Analysis: Degradation of Poly(Bisphenol A)Carbonate. *J. Chromatogr. A* **2006**, *1130* (1), 34–42. https://doi.org/10.1016/j.chroma.2006.04.070.

(127) Beskers, T. F.; Hofe, T.; Wilhelm, M. Development of a Chemically Sensitive Online SEC Detector Based on FTIR Spectroscopy. *Polym. Chem.* **2014**, *6* (1), 128–142. https://doi.org/10.1039/C4PY01043D.

(128) Carson, W. W.; Dwyer, J. L.; Boumajny, B. Copolymer Compositional Drift across Molecular Weight Measured by LC-FTIR. *Int. J. Polym. Anal. Charact.* **2008**, *13* (6), 463–470. https://doi.org/10.1080/10236660802503017.

(129) Frijns-Bruls, T.; Ortin, A.; Weusten, J.; Geladé, E. Studies on the Application of Filter-Based IR Detector for Polyolefin Characterization with HT-SEC. *Macromol. Symp.* **2015**, *356* (1), 87–94. https://doi.org/10.1002/masy.201500077.

(130) Gruendling, T.; Weidner, S.; Falkenhagen, J.; Barner-Kowollik, C. Mass Spectrometry in Polymer Chemistry: A State-of-the-Art up-Date. *Polym. Chem.* **2010**, *1* (5), 599–617. https://doi.org/10.1039/B9PY00347A.

(131) Muneeruddin, K.; Thomas, J. J.; Salinas, P. A.; Kaltashov, I. A. Characterization of Small Protein Aggregates and Oligomers Using Size Exclusion Chromatography with Online Detection by Native Electrospray Ionization Mass Spectrometry. *Anal. Chem.* **2014**, *86* (21), 10692–10699. https://doi.org/10.1021/ac502590h.

(132) Murgasova, R.; Hercules, D. M. Polymer Characterization by Combining Liquid Chromatography with MALDI and ESI Mass Spectrometry. *Anal. Bioanal. Chem.* **2002**, *373* (6), 481–489. https://doi.org/10.1007/s00216-002-1332-9.

(133) Cho, D.; Park, S.; Kwon, K.; Chang, T.; Roovers, J. Structural Characterization of Ring Polystyrene by Liquid Chromatography at the Critical Condition and MALDI−TOF Mass Spectrometry. *Macromolecules* **2001**, *34* (21), 7570–7572. https://doi.org/10.1021/ma0108012.

(134) Montaudo, G.; Samperi, F.; Montaudo, M. S. Characterization of Synthetic Polymers by MALDI-MS. *Prog. Polym. Sci.* **2006**, *31* (3), 277–357. https://doi.org/10.1016/j.progpolymsci.2005.12.001.

(135) Trimpin, S.; Weidner, S. M.; Falkenhagen, J.; McEwen, C. N. Fractionation and Solvent-Free MALDI-MS Analysis of Polymers Using Liquid Adsorption Chromatography at Critical Conditions in Combination with a Multisample On-Target Homogenization/Transfer Sample Preparation Method. *Anal. Chem.* **2007**, *79* (19), 7565–7570. https://doi.org/10.1021/ac070986w.

(136) Hiller, W.; Sinha, P.; Hehn, M.; Pasch, H. Online LC-NMR – From an Expensive Toy to a Powerful Tool in Polymer Analysis. *Prog. Polym. Sci.* **2014**, *39* (5), 979–1016. https://doi.org/10.1016/j.progpolymsci.2013.10.001.

CHAPTER II

Silicon Photonic Microring Resonator Arrays for Mass Concentration Detection of Polymers in Isocratic Separations

Acknowledgements

This chapter has been reproduced with permission from: Mordan, E.; Wade, J. H.; Wiersma, Z. S. B.; Pearce, E.; Pangburn, T. O.; deGroot, A. W.; Meunier, D. M.; Bailey, R. C. Silicon Photonic Microring Resonator Arrays for Mass Concentration Detection of Polymers in Isocratic Separations. *Anal. Chem*. **2018**. https://doi.org/10.1021/acs.analchem.8b04263. Copyright 2020 American Chemical Society.[⊥]

My contribution to this work is the following: LC system optimization, execution of all experiments, development of R code for data processing, all data analysis and workup,

[⊥] https://pubs.acs.org/pb-assets/acspubs/Migrated/dissertation.pdf

full investigation of molecular weight dependence, and finally I wrote the presented article. James H. Wade assisted with experimental interface, development of R code, data interpretation, and article revisions. Zachary S. B. Wiersma executed early trial experiments which verified the project design. Todd O. Pangburn and A. Willem deGroot provided valuable insight throughout experimental process. Eric Pearce, and David M. Meunier contributed in choice of system, experimental design, data interpretation, as well as article revisions.

Finally, we acknowledge financial support from The Dow Chemical Company through the University Partnership Initiative Program.

Abstract

Molecular weight distribution (MWD) is often the most informative analytical parameter in polymer analysis, with gel permeation chromatography (GPC) being the most common approach for determining the MWD for polymer samples. Many industrially relevant polymers lack chromogenic or fluorogenic signatures, precluding use of spectroscopy-based detection. Universal detectors, such as evaporative light scattering and charged aerosol detectors, are nonlinear, limiting quantitative polymer analysis. Differential refractive index (dRI) detectors show linear mass concentration sensitivity but are limited for some analyses given that they are incompatible with gradient-based separations, have a limited dynamic range, and require extended thermal equilibration times. In this study, we investigated the utility of silicon photonic microring resonator arrays as a quantitative mass concentration detector for industrial polymer analysis. Microring resonators have optical properties that are sensitive to changes in refractive

index, offer an extended dynamic range, have a broad solvent compatibility, and have a linear mass concentration detection for a range of molecular weights. Linear mass concentration detection for microrings was demonstrated through a series of isocratic GPC separations using narrow MWD polystyrene (PS) standards. This detection technology was then utilized in conjunction with conventional GPC detectors to analyze a series of broad MWD PS standards, with results in good agreement with dRI and UV/visible. These results demonstrate the potential of the microring resonator platform as a detector for industrial polymer analysis.

1. Introduction

Polymers are an enormously diverse class of analytes broadly defined as organic chain macromolecules of repeating monomer units. These macromolecules have innumerable commercial applications, ranging from packaging and adhesives to tires and clothing.[1] The properties of a synthetic polymer are controlled through monomer chemistry and composition, monomer arrangement, chain length, and chain branching.[1] Molecular weight (MW) and molecular weight distribution (MWD) are requisite parameters for polymer characterization, as they profoundly influence physical properties. Gel permeation chromatography (GPC) remains the gold standard for MWD analysis of polymers. Other techniques include Fourier transform infrared spectroscopy (FTIR) and nuclear magnetic resonance spectroscopy (NMR) for functional or end-group analysis and determining monomer ratios in polymer blends.[2] These and other spectroscopic methods rely on GPC for distributional analysis and are collectively used for comprehensive industrial polymer characterization.[3,4]

Polydispersity is a metric of the breadth of the MWD, and the degree of polymerization for a given polymer describes the number of monomer repeat units per chain at a particular average MW in the distribution (e.g., number-average or weight-average). The polydispersity index (Đ) is defined as the ratio of the weight-average molecular weight (M_W) to the number-average molecular weight (M_n).

$$Đ = \frac{M_w}{M_n} \qquad (1)$$

The number-average molecular weight is defined as

$$M_n = \frac{\Sigma_i N_i M_i}{\Sigma_i N_i} = \frac{\Sigma_i w_i}{\Sigma_i w_i / M_i} \qquad (2)$$

where N_i is the number of molecules, and M_i is the molecular weight. M_n can also be written in terms of the polymer weight fraction (w_i), which is more simply referred to as the mean molecular weight. The weight-average molecular weight M_W is defined as

$$M_w = \frac{\Sigma_i N_i M_i^2}{\Sigma_i N_i M_i} = \frac{\Sigma_i w_i M_i}{\Sigma_i w_i} \qquad (3)$$

The more disperse a polymer distribution, the greater divergence of M_n and M_W. Đ values are an important characteristic of industrial polymers because many important physical properties, such as resin processability, depend on Đ. [1]

Methods for determining polymer MW include light scattering, sedimentation, chromatography, and mass spectrometry. [1,2] Light scattering and sedimentation velocity are often used for M_W determinations. [5] Methods using osmotic pressure, colligative

properties, or end group analysis are typically used for M_n determination. GPC and mass spectrometric methods, such as matrix-assisted laser desorption ionization mass spectrometry (MALDI-MS), can determine both M_w and M_n,[6-10] enabling Đ determination using a single technique. MALDI-MS has the notable advantage of high- resolution mass determination in comparison to separation- based methods. Unlike GPC, though, MALDI-MS methods have challenges with determining broad polymer distributions, and high MW polymers can often not reach a sufficient charge state for analysis.[11] As a result, separation-based methods are most commonly used for Đ determination.

Polymer analysis using GPC requires the use of a concentration detector, such as UV/visible (UV), differential refractive index (dRI), evaporative light scattering (ELSD), or charged aerosol (CAD) detectors.[7,12,13,2] UV absorbance is nondestructive and concentration-dependent, but it is limited to analytes with chromogenic signatures. Because of the above limitations, dRI is one of the most commonly used detectors with GPC separations of industrially relevant polymer samples. dRI is also nondestructive, but it has the added advantage of being a universal detector. [14] However, dRI has some limitations, including incompatibility with gradient separations, for which the refractive index (RI) change of the solvent gradient exceeds the dynamic range of the commercial dRI detectors. Although incompatibility with gradients is not relevant for GPC detection, identifying a universal detector for gradient separations of polymers would be an important breakthrough for polymer analysis. Polymer separations routinely require two-dimensional methods, where solvent gradients are often applied in the first dimension, preventing the use of dRI detectors for the first dimension.[15,16]

In ELSD, the solvent is nebulized and evaporated, leaving only the analyte particles, and the light scattering of these particles is measured. ELSD is a universal gradient-compatible detector commonly implemented for polymer analysis, but it has some notable limitations. ELSD detectors are destructive and require a volatile mobile phase. Importantly, ELSD is not a linear mass detector, prohibiting quantitation of low concentrations of high molecular weight polymers and/or polymers at high concentrations.[15,17-19] CAD detectors similarly rely on a nebulized spray, like ELSD detectors, but for CAD, particles are charged by a corona wire.[20] These particles create a current which is proportional to analyte concentration. Much like ELSD, CAD is gradient compatible, destructive, requires a volatile mobile phase, and is only linear over a narrow mass range.[15,22,21]

The silicon photonic microring resonator platform has the potential to be an improved universal detector for polymer analysis. Similar to dRI detectors, microring resonators can measure changes in RI. However, unlike conventional dRI, microring resonator arrays offer solvent gradient compatibility due to their enormous linear dynamic range for bulk RI measurements. Most implementations of microring resonators leverage the exquisite surface sensitivity to detect molecular binding events to specific recognition elements tethered to the sensor surface (e.g., antibodies or DNA).[23,24] It was this surface sensitivity and dynamic range previously that enabled implementation of the platform as a high-performance liquid chromatography (HPLC) detector for gradient elution separation of small molecules.[14] Using a similar approach, a microwave interferometer was recently interfaced with HPLC, demonstrating isocratic and gradient compatibility.[25]

Additionally, similar optical resonator detectors have been interfaced with separations, including gas chromatography and capillary electrophoresis.[26-29]

Herein, we demonstrate microring resonators as a quantitative mass concentration detector for polymer applications. Microring resonators combine the appealing capabilities of wide solvent compatibility and mass concentration detection of dRI detectors and the gradient compatibility provided by CAD and ELSD into a single detection platform. To demonstrate the linear mass detector capability of the microring resonator platform, isocratic separations of polystyrene standards (PS) by GPC with the microring resonator platform as a detector were performed. Parallel isocratic separations of the same narrow range polystyrene samples were performed using UV and dRI, allowing a direct comparison of the two RI-sensitive-based detectors. MWD of polystyrene standards with broad MWD were determined by calibrating the microring resonators for polystyrene MW. Much like the narrow range PS experiments, MWD were also determined using dRI and UV as the GPC detectors, to compare Đ values calculated for each standard by each method. A direct comparison of MWD assessment for UV, dRI, and microring resonator analysis are provided. These results demonstrate the suitability and limitations of microring resonator arrays for polymer analysis.

2. Experimental Section

2.1. Materials

All solvents were purchased from Sigma-Aldrich (St. Louis, MO) at the highest purity available. Narrow and broad range polystyrene standards were purchased from

Polymer Standards Service-USA, Inc. (Amherst, MA) and were used as received. Ten narrow MWD polystyrene standards ranging in MW (1.3, 3.2, 9, 18, 33, 62, 120, 280, 560, and 1400 kDa) were prepared in tetrahydrofuran (THF) at various concentrations from 0.3 to 0.7 mg/mL. Three broad MWD polystyrene standards (20, 47, and 60 kDa) were prepared in THF at a concentration of 1.0 mg/mL.

2.2. Microring Resonators

The microring resonator system (Maverick M1 optical scanning instrumentation) and sensor array chips were purchased from Genalyte, Inc. (San Diego, CA). Detailed descriptions of sensor fabrication and instrument operation have been described elsewhere.[14] Briefly, microring resonators are ring shaped optical cavities with adjacent linear waveguides. The individual microrings are probed by an external tunable cavity diode laser centered at 1550 nm, and optical transmission is monitored as a function of wavelength. Dips in transmittance signal occur at resonant wavelengths defined by

$$\lambda_r = \frac{2\pi r n_{eff}}{m} \qquad (4)$$

where r is the ring radius, n_{eff} is the effective refractive index, and m is a constant. Changes in n_{eff} at the sensor surface, such as a changing mobile phase composition, resulted in a change of the resonant wavelength, which was measured and referred to as the relative shift in picometers (Δpm).[30,31] These changes in resonance wavelengths corresponded to changes in n_{eff} and were monitored as a function of time.[31]

Sensor array chips have a 4 mm × 6 mm footprint with 128 individually addressable microring sensors.[30] Sensor chips were fabricated from silicon-on-insulator (SOI) wafers with an SiO_2 surface that was highly chemically resistant. The chips also have a protective photoresist coating that was removed before use. Photoresist was removed by successively immersing chips in acetone and isopropanol baths, followed by an acetone rinse.

2.3. HPLC

Chromatographic separations were performed on a Waters Alliance e2695 separation module (Milford, MA) furnished with a Waters 2489 UV/Visible Detector and a Waters 2414 refractive index detector. The column used was an Agilent MiniMIX-C column (Santa Clara, CA), with dimensions of 250 mm × 4.6 mm, and a packing particle size of 5 μm. The flow rate was maintained at 0.3 mL/min, sample temperature was kept at 5 °C, and the column oven at 35 °C. The Waters 2489 UV/Visible detector wavelength was set to 260 nm with a sampling frequency of 10 HZ. The Waters 2414 RI detector was kept at a constant temperature of 40 °C. For all separations, the mobile phase solvent was THF.

2.4. GPC-Microring Resonator Interface

Sensor chips were placed into an anodized aluminum cartridge holder. A polyethylene terephthalate (Mylar) gasket was sandwiched onto the top of the sensor chip followed by a polytetrafluoroethylene (Teflon) cartridge top. The HPLC outlet was connected to a 0.25 mm flangeless 1/4−28 and then to a ZDV 10−32 PEEK low pressure

union. The PEEK union adapted the HPLC fittings to the microring resonator cartridge. Once assembled, the function of the GPC-microring resonator interface was analogous to a detector flow cell. A diagram of the GPC-microring resonator interface can be found in Figure 2-1.[14]

2.5. Data Analysis

Data analysis was carried out using custom software written in R (version 3.4.1). Chromatograms were obtained for all the detection methods by plotting signal intensity as a function of time. There was an additional step for microring resonator chromatograms, where responses from 20 microrings were averaged and plotted as a function of time, with 20 rings being averaged each time. Prior to each run, signal response for all 128 microring sensors was collected, 20 rings with the lowest variance in baseline noise were selected for data collection, and the average of these 20 rings was used as the signal response (Figure 2-2). A Whittaker smoothing function, i.e., a penalized least-squares smoothing function, was applied to the averaged raw data response.[32] An asymmetrically reweighted least-squares (arPLS) approach was used to baseline correct the averaged chromatogram.[33] Processed chromatograms were then normalized by concentration. Evaporative losses of THF caused slight differences in standard concentrations, and these variations were accounted for using exact concentrations (determined by UV absorption). This data treatment process and a comparison to uncorrected data is provided in Figure 2-3.

2.6. Đ Determinations

Đ values were calculated directly using eqs 5 and 6. These equations represent modified M_n and M_w equations, which use refractive index intensity (RI_i) directly instead of w_i.

$$M_n = \frac{\Sigma_i RI_i}{\Sigma_i RI_i / M_i} \qquad (5)$$

$$M_w = \frac{\Sigma_i RI_i M_i}{\Sigma_i RI_i} \qquad (6)$$

This is due to the relationship between refractive index (n) and concentration (c), changes in n are proportional to changes in c. The proportionality factor, referred to as the refractive index increment $^{\partial n}/_{\partial c}$, depends on the differences in polymer and solvent refractive indices at a given wavelength and temperature. This relationship allows for the calculation of M_n and M_w from refractive index-based detector chromatograms.[1] Microring resonators are sensitive to refractive index differences due to changes in mass concentrations of analytes as they flow past the detector.

3. Results and Discussion

3.1. Narrow Range PS Standards

Isocratic separations of 0.5 mg/mL narrow range PS standards utilizing the GPC-microring resonator interface were performed, with the resulting chromatograms shown in Figure 2-4A. This demonstrates the applicability of the microring resonator platform for GPC detection. Using the described separation method, 100 µL injections of the 0.5 mg/mL narrow range PS standards were made for 10 standards ranging from 1.3 to 1400

kDa. The observed elution order for the GPC-microring resonator experiment was as expected, with the largest MW standard (1400 kDa) eluting first, and lower MWs followed consecutively. By comparing the detection of narrow range PS standards by the microring resonator platform to dRI (Figure 2-4B) and UV (Figure 2-4C), the trends are the same across the various detection methods. A drawback from the microring resonator detection method is that it has the greatest amount of noise in the baseline when compared to commercial detectors. The greater noise is attributed to un-thermostated temperature and flow fluctuations; however, further investigations need to be performed to isolate various contributions to detector noise. Figure 2-3 visually depicts the raw data processing methods for noise reduction, and a comparison of processed and raw data is provided.

3.2. Investigating MW Dependence

Comparing the chromatograms of the various detection methods, it is observed that there is an MW trend with the microring resonators with detector response decreasing with increasing MW. The trend is further visualized by integrating the microring resonator chromatogram peaks. Peak areas decrease with increasing MW (Figure 2-4D), and this is not the case for the dRI (Figure 2-4E) or UV (Figure 2-4F), which show comparable peak areas for the full MW range. This dependence on MW is due to the size of the dissolved polymer chain and surface sensitivity of the sensor. Light travels through the waveguide via total internal reflection, and therefore, the sensitivity falls off exponentially according to the decay profile of the evanescent field in the following equation:

$$I(z) = I_0 e^{-2\gamma z} \qquad (7)$$

where I(z) is the intensity of the evanescent field as a function of distance, z, from the surface. I_0 is the initial evanescent field intensity, and γ is the exponential decay constant. The evanescent field was previously directly probed via layer-by- layer polymer deposition on the sensors, and the 1/e decay constant (where the light intensity, I_0, has decreased to 36.7%),was found to be 63 nm.[34] In the previous work, the ring resonators exhibited a quasi-linear response up to a total layer-by-layer polymer thickness of about 20−25 nm from the surface. Because of the exponential decrease in the evanescent wave intensity, deviations from linearity became obvious at thicknesses greater than 25 nm, and a plateauing effect was observed at thicknesses greater than about 150 nm. A similar trend may be expected for polymer chains dissolved in solution, and indeed, such is the case. At lower MWs (smaller sizes), there is a MW independent region of microring resonator response, as indicated by the roughly constant peak area for MWs less than ~120 kDa (radius of gyration, R_g ~ 13 nm).[35] For MWs exceeding ~120 kDa, there is an obvious size dependence to the detector response, as indicated by the monotonic decrease in peak area with increasing MW (see Figure 2-5 and Table 2-1).

For any given size, or MW, the detector response may be linear with polymer concentration, but the sensitivity (slope of the calibration curve) is expected to decrease with increasing MW. The key factor influencing this behavior is the actual mass concentration of polymer contained within an approximately 25 nm distance from the ring surface (surface concentration), compared to the bulk mass concentration. At $2R_g$ sizes less than ~ 25 nm, the bulk concentration and surface concentration appear to be the same, as indicated by the observed MW independent detector response for chains in this size regime. As the sizes of polymer chains exceed a $2R_g$ distance of ~25 nm, the surface

concentration begins to differ from the bulk. In this region, an MW dependent response is observed.

3.3. MW Calibration

By using the narrow range PS standards, the linear mass concentration detector capability of the microring resonator platform was demonstrated, as shown in Figure 2-6. Again, utilizing the GPC-microring resonator interface, isocratic separations were performed with 100 µL injections and various concentrations (0.3, 0.5, and 0.7 mg/ mL). Overlaid chromatograms of various concentrations, obtained by microring resonator detection, show that signal intensity as well as peak area are dependent on the mass injected (Figure 2-6A−C). This mass concentration dependence on peak area was further analyzed by integrating the area under the curve for each standard and each concentration. Plotting the integrated area against the mass injected on the column for each detection method shows a strong positive linear correlation for all MW standards used (Figure 2-6D−F). For the microring resonator plots, the slopes are comparable for all standards except the 560 kDa standard. This result is consistent with the decreasing sensitivity for higher MW polymers, as previously described. The 560 kDa is clearly in the MW dependent regime of sensor response and has a much shallower calibration slope. Additionally, MW and R_g trends were again investigated at the various concentrations in Figure 2-7 and Table 2-2, these trends are reproducible regardless of mass, verifying that the MW dependence behaves in a predictable manner. UV and dRI, in comparison, have comparable slopes for all standards (Figure 2-6E,F), as expected for MW independent

mass concentration detection since they are bulk, rather than surface-sensitive. The fitting parameters for linear mass concentration detection plots are found in Table 2-3.

The microring resonator platform was used for detection of narrow range PS MW standards (n = 3), and calibration curves were constructed by plotting the log of standard MW versus elution volume for each detection method (Figure 2-8A−C). The resulting MW calibration curves for each method were fit with a first-order polynomial, and all exhibited R^2values of greater than 0.99 and near identical slopes (Table 2-4), which when plotted on the same axes show direct overlap (Figure 2-8D). This demonstrates the good alignment and reproducibility among methods, which is further demonstrated by Figures 2-9 and 2-10.

3.4. Broad Range PS Standards Separations

GPC separations of 1.0 mg/mL broad MWD PS standards utilizing the GPC-microring resonator interface were performed (100 µL injection of 1.0 mg/mL standards). Separation conditions were the same as those used for the narrow range PS standard experiments. Much like the narrow range PS standard separations, detection by the microring resonators had the greatest level of noise. However, the S/N ratio was greatly improved following the data processing methods described previously (Figure 2-3). Obtained chromatograms using microring resonators, dRI, and UV are shown in Figure 2-11.

3.5. Determination of MWD

Using the broad range PS standard's elution volume and the PS MW calibration curve, M_W can be determined at each retention time increment across the peak. Equations 5 and 6 were used to calculate M_n, M_W, and Đ (eq 1) for the three broad standards. By comparing the obtained M_n and M_W values via each detection method, good agreement was observed among values for all three detection methods (Figure 2-12A,B). By comparing obtained Đ values, we see very good agreement for all standards for all detection methods. Although good agreement was observed for the microring resonators results when compared to both UV and dRI results, the three broad PS materials analyzed had very little (if any) fractions of their distributions exceeding 100 kDa. As such, these standards were in a range where the M_W- dependent sensitivity was not pronounced for the microring resonators. The larger wider standard deviations for values determined by the microring resonators is unsurprising, given the higher noise floor of the sensor.

Given the observed MW dependence of the microring resonators, there could be some challenges with determining the Đ of high MW polymers. An improved understanding of MW trends of the sensor along with the fact that these trends are independent of mass concentration for a given MW could provide a tool for correcting and predicting this effect and fully characterize the MWD to include the high MW regime.

4. Conclusions

Isocratic separations using PS standards with GPC demonstrated the linear mass concentration detection of the silicon photonic microring resonator. A MW dependence was observed where the sensors were less responsive to larger polymers due to the

evanescent surface sensitivity of the resonators. However, this dependence is consistent and was fit via a polynomial function. In addition, Đ was determined with the microring resonator platform and found to be in good agreement compared to UV and dRI detectors. This demonstrates the applicability of the microring resonator for industrial polymer analysis.

Future work will focus on accounting for the observed MW dependence of the sensor surface, implementing the microring resonator platform as a gradient elution detector for polymer separations, and using the facile chemical modification of the sensor surface.

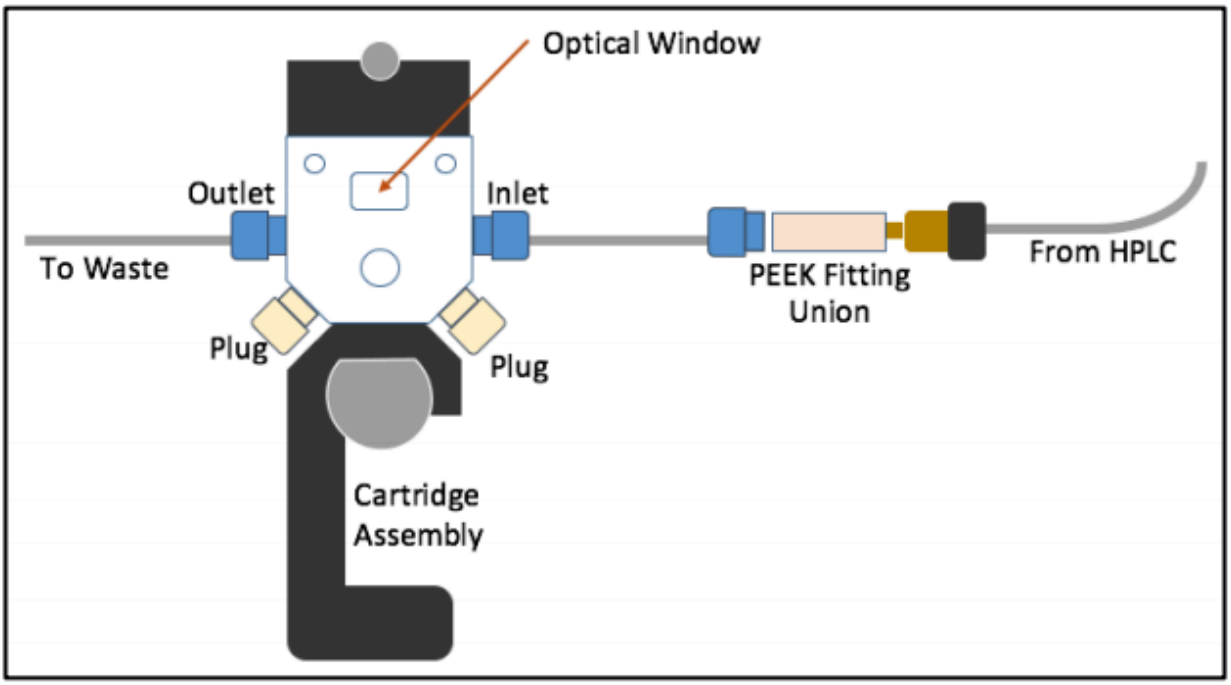

Figure 2-1: GPC-Microring Resonator Interface. Samples separated by the HPLC on a GPC column, detected by UV/Vis detector which is the connected to MRR (in series), via a 0.25mm flangeless ¼-28 and a ZDV 10-32 PEEK low pressure union. The elutant enters the right side of cartridge top, flows across a blank chip, and exits left side of cartridge top to waste.

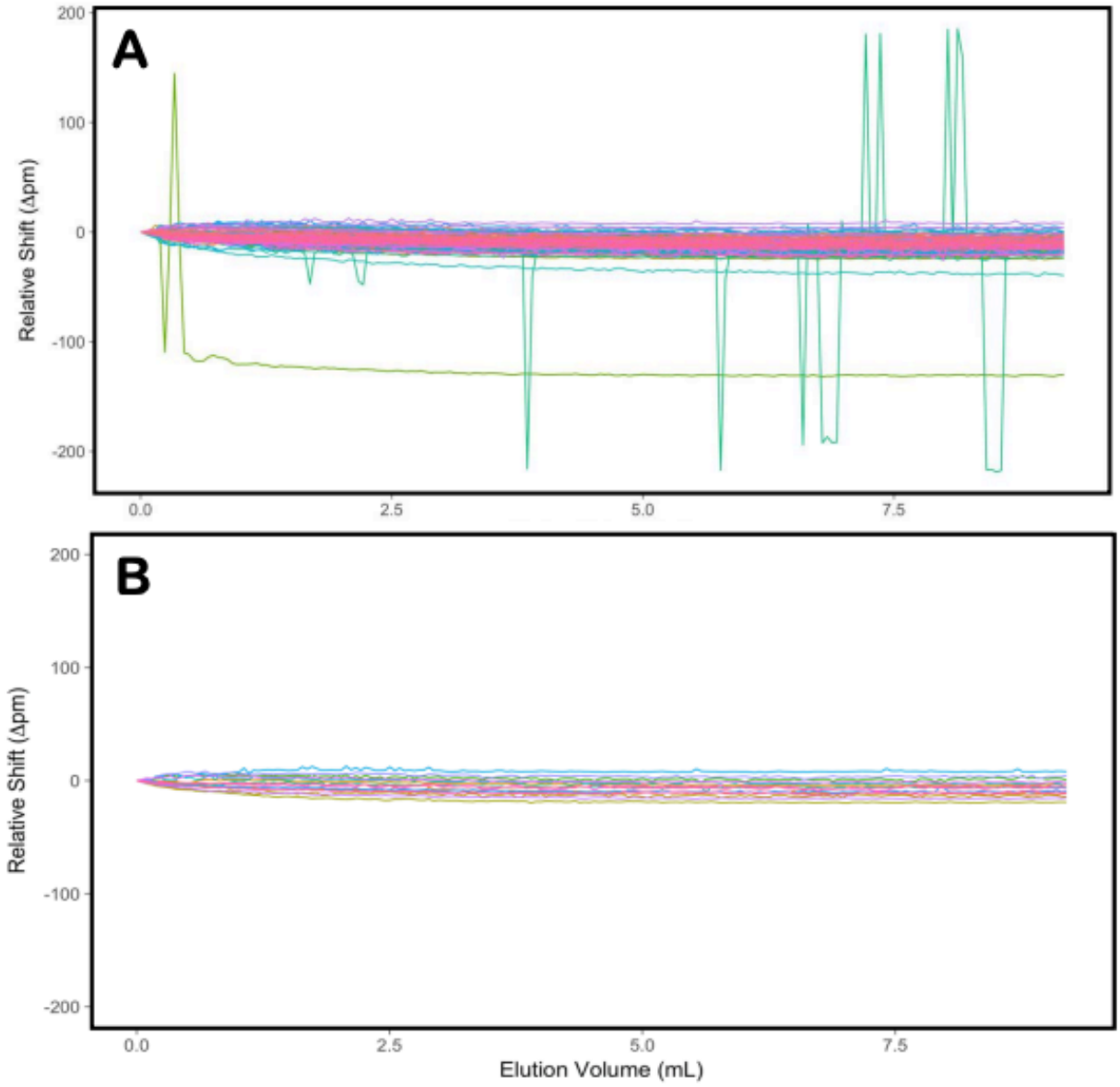

Figure 2-2: Automated Ring Selection. (A.) Initial experiment performed by running THF across 128 rings. (B.) Obtained data is processed and top 20 rings are identified based on minimum variance. Experiment is performed, in this case 100 µL injections of 1.0 mg/mL broad standards, scanning only the identified 20 rings with the least amount of variance in the baseline.

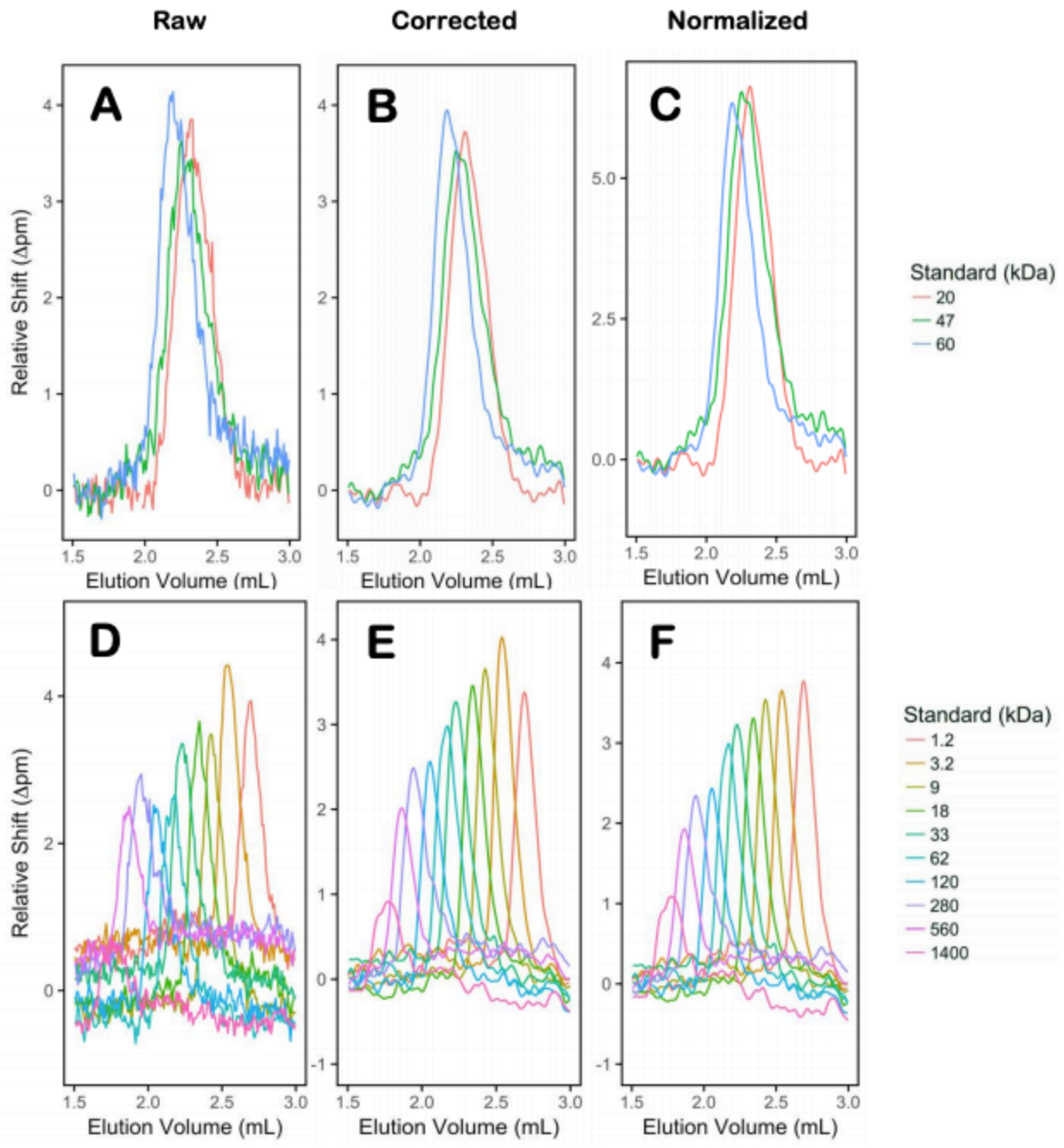

Figure 2-3. Data Treatment Process for Microring Resonators. Raw microring resonator chromatograms of broad standards (A) and narrow standards (D). These traces show increased noise and baseline drift compared to other detection methods. Noise was reduced by applying an arPLS smoothing function. Smoothing allows for reducing drift and noise without impacting the integrity of the peaks. This is illustrated for both broad (B) and narrow polystyrene separations (E) Data are then normalized by concentration for both broad (C) and narrow (F) PS, as slight differences in standard concentration impacts peak height. Therefore normalizing for concentration removes this factor.

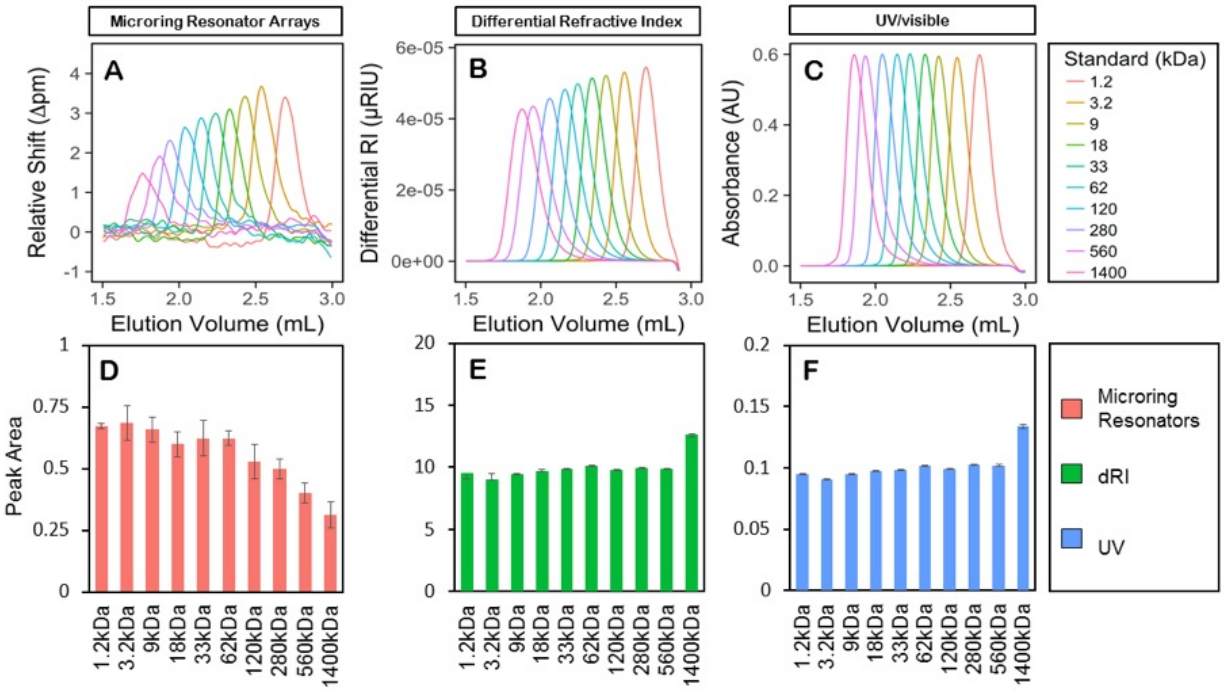

Figure 2-4: Various GPC Detection Methods for Narrow Standard Analysis. The following chromatograms are representative of minimum n = 3 and were obtained using narrow range polystyrene standards with an MW range of 1.2−1400 kDa. (0.5 mg/mL concentration and 100 µL injections). (A) The microring resonator chromatogram (average of 20 rings), (B) dRI chromatogram, and (C) UV chromatogram. Plotting the average peak areas for all MW standards shows that dRI (E) and UV (F) have comparable peak areas for all standards. Whereas with the microring resonators (D), there is a trend of decreasing peak areas with increasing MW.

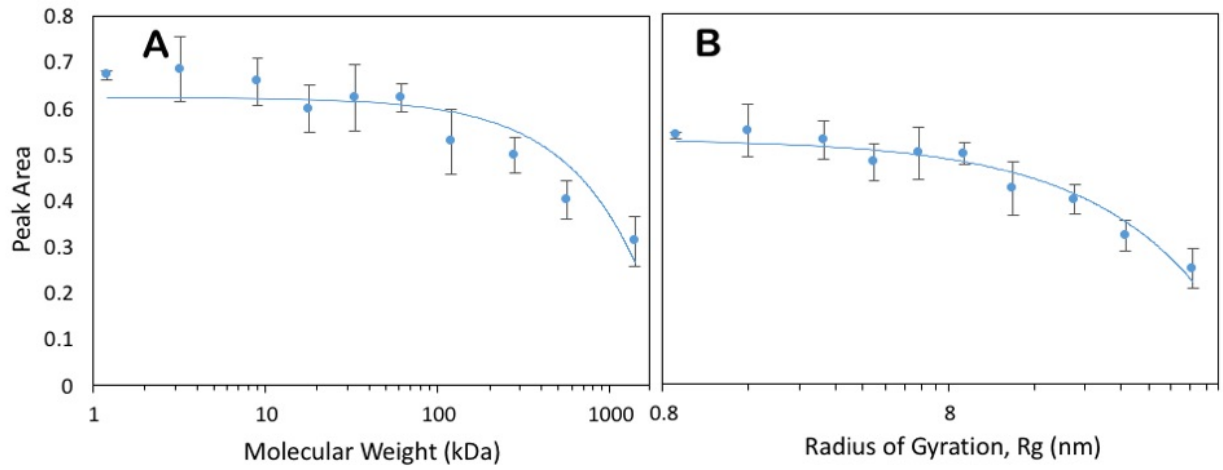

Figure 2-5: MW Dependence of Microring Resonators. Further investigating the MW dependence shows MW and radius of gyration trends. (A) Plotting the full MW range on a log scale against peak area shows an exponential decay. (B) In addition, plotting peak area against radius of gyration on a log scale shows a similar exponential decay. Both (A) and (B) show that there is a flat linear region with no MW dependence. In addition, these plots demonstrate that the microring resonator platform has increased sensitivity at lower MW.

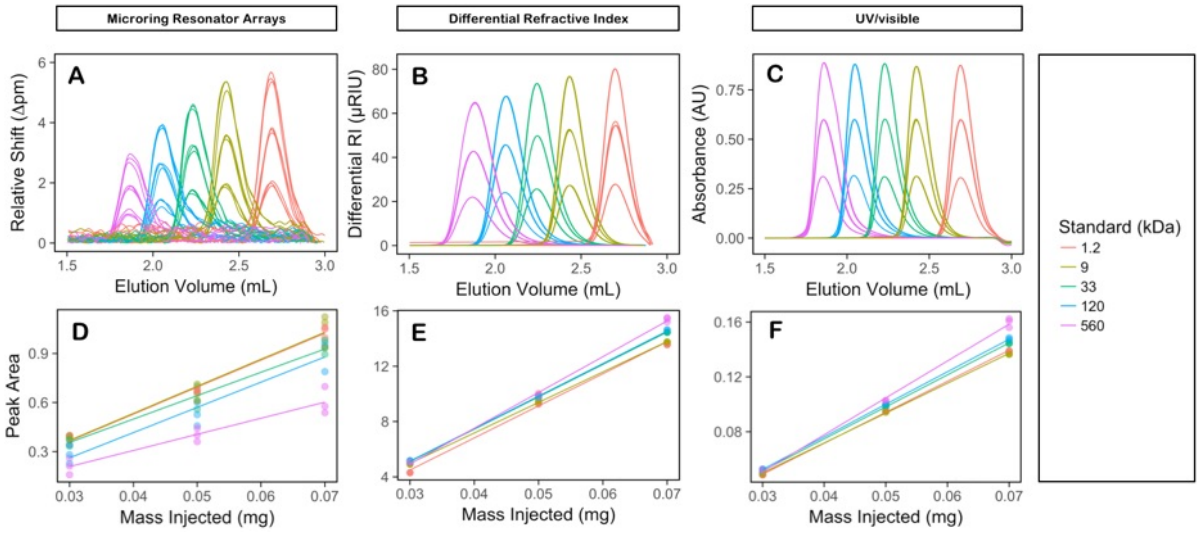

Figure 2-6: Microring Resonators as a Linear Mass Detector. Utilizing the same narrow range polystyrene standards (MW range of 1.2−560 kDa) at various concentrations (0.3, 0.5, and 0.7 mg/mL) the linear mass detection capability of the microring resonators can be demonstrated. The detector signal is expected to increase linearly with increasing concentration. (A) Overlapping GPC-microring resonator chromatogram at various concentrations (n = 3) show that the microring resonator signal intensity/chromatogram peak area increases with concentration peak area verifying concentration dependence. The same is true for dRI detection (B) and UV detection (C). Integrating the chromatogram peaks and plotting against mass injected further illustrates this linear relationship (D−F).

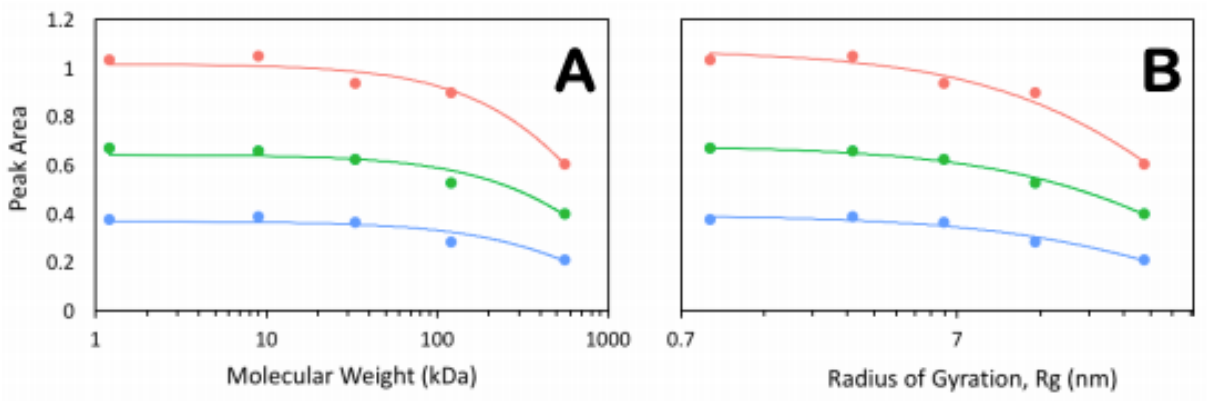

Figure 2-7. MW Dependence of Microring Resonators at Varying Concentrations. Repeating the initial investigation of the molecular weight dependence at the 3 varying linear mass detection experiment concentrations (0.3, 0.5, 0.7 mg/mL) shows that MW and radius of gyration trends are independent of concentration. (A.) Plotting the full MW range on a log scale against peak area shows a linear trend. (B.) Plotting peak area against radius of gyration on a log scale shows the same trend. These plots show that these trends behave in a reproducible and predictable manner.

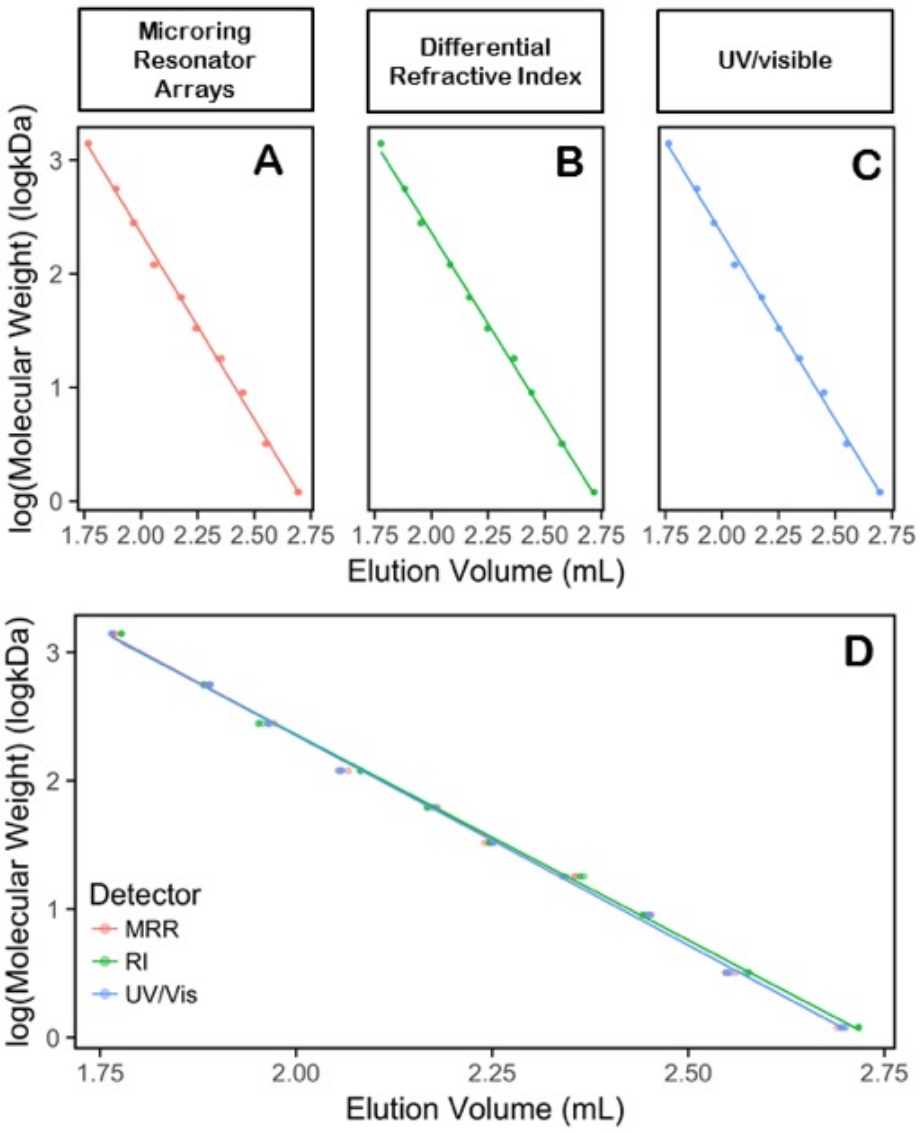

Figure 2-8: Calibration Curves for Narrow Range Polystyrene Standards (0.5 mg/mL concentration and 100 µL injections). (A) Microring resonator calibration curve. (B) UV calibration curve. (C) dRI calibration curve. (D) Overlapping calibration curves, which shows reproducible slopes by each method.

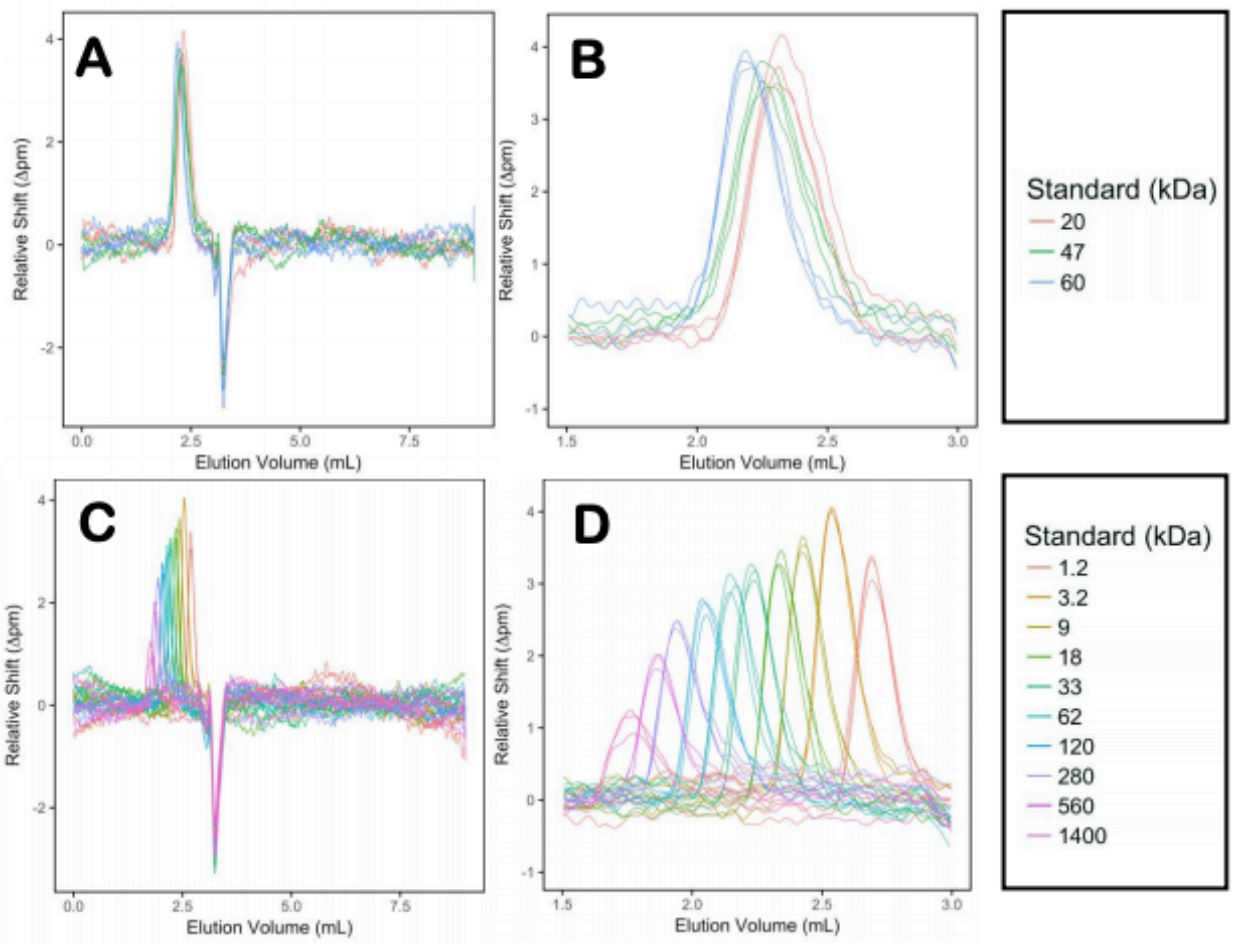

Figure 2-9: Full Microring Resonator Chromatogram and Reproducibility. These chromatograms represent the smoothed full run traces of the microring resonators for both (A) broad and (C) narrow standards. Zooming in on these traces are represented by (B) for the broad and (.) for the narrow polystyrene standards. (A-D) Also represent the reproducibility of detection by the microring resonators, as all separations were repeated three times, with the triplicate traces shown here. Comparing the individual traces show comparable peak shapes and intensities as well as identical elution volumes.

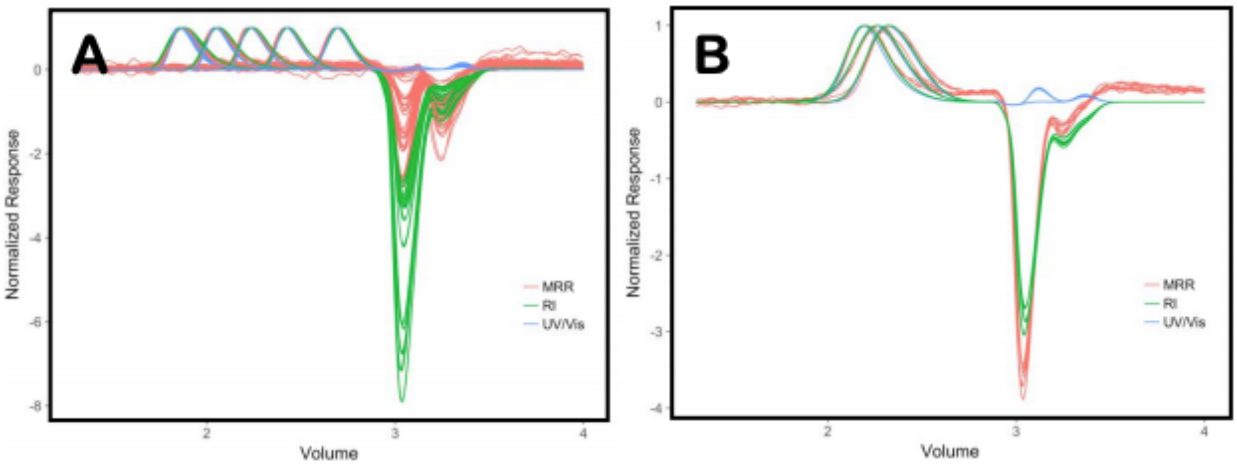

Figure 2-10: Correction for Volume Delay Between Detectors. Normalizing all three detector's signal to 1 and plotting on the same axis verifies the alignment and agreement. All standards have the same elution volume regardless of the detection method, verifying that there is no delay or compromise of the separation caused by the interface. This is evident in the normalized signal response chromatograms for both the linear mass detection experiments using narrow range polystyrene standards (A) and the broad range polystyrene chromatograms (B).

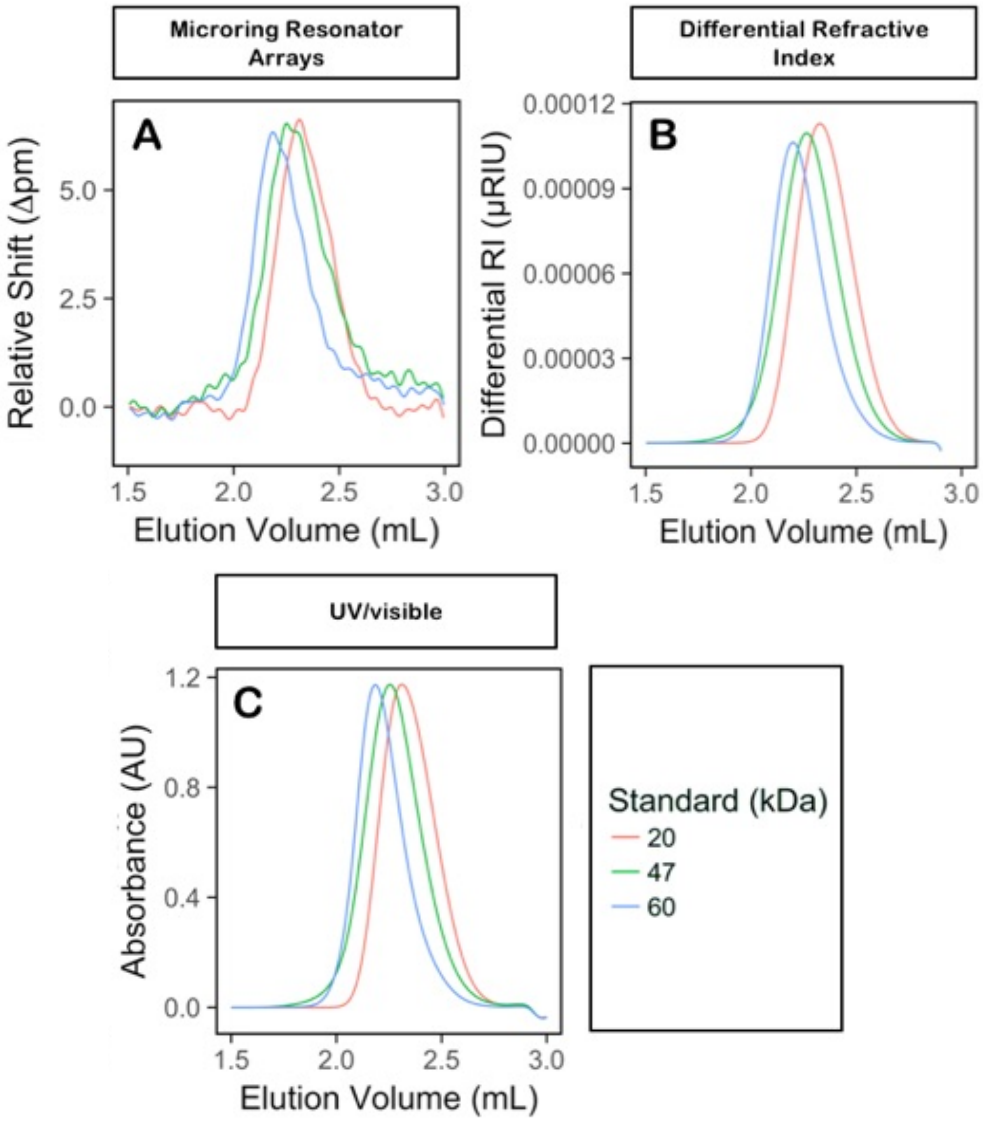

Figure 2-11: Comparison of Various GPC Detection Methods for Broad Range Polystyrene Standards, MW range of 20−60 kDa (1.0 mg/mL concentration and 100 μL injections). (A) Microring resonator (average of 20 rings), (B) dRI, and (C) UV. The representative traces of n = 3 by all three detection methods demonstrate comparable detection and very good reproducibility. These broad standards were then used to demonstrate the quantitative ability of the microring resonators by determining their full MWDs.

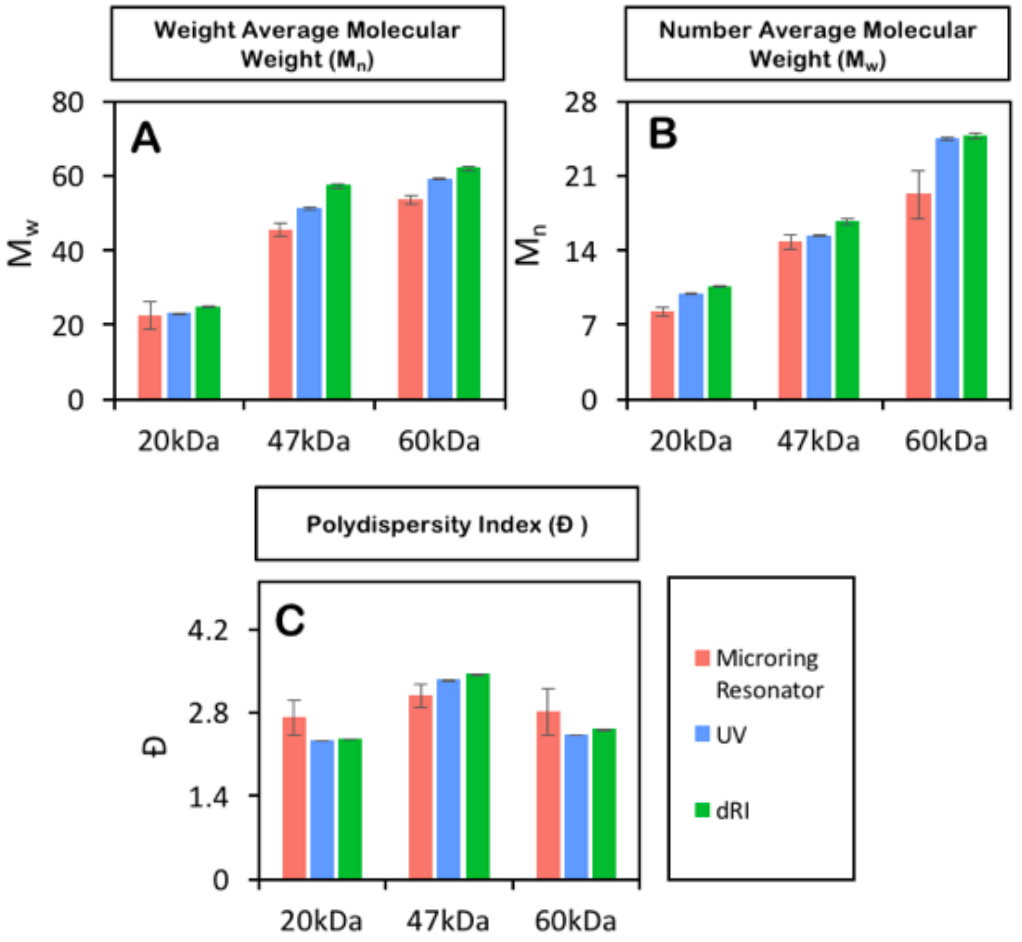

Figure 2-12: MWD Determination for Broad Standards. All three detection methods were calibrated for MW using narrow range polystyrene, these calibrations allowed for the MWD determination of broad range polystyrene. (A) M_W, (B) M_n, and (C) Đ were determined for each broad standard with all three detection methods. Microring resonator values are represented in red, UV values are represented in blue, and dRI values are in green. By comparing the determined MWs and PDIs by the various methods, the same trends are observed. The microring resonators have the largest error in comparison, which is mostly attributed to noise in the baseline; however, these values are still comparable to those determined by UV and dRI.

Table 2-1: Fitting Parameter for MW Dependence

	Plot	Ae^{Bx}		R^2
		A	B	
A	Peak area vs MW	0.6250	-0.0006	0.8995
B	Peak area vs Rg	0.6743	-0.0140	0.9759

Table 2-2: Fitting Parameter for MW Dependence at Varying Concentrations

Plot		Mass Injected (mg)	*Ax + B*		R^2
			B	*C*	
A	Peak area vs MW	0.03	-0.0007	1.0122	0.95514
		0.05	-0.0005	0.642	0.90059
		0.07	-0.0003	0.3677	0.86218
B	Peak area vs Rg	0.03	-0.0056	0.3881	0.93598
		0.05	-0.0085	0.6729	0.97579
		0.07	-0.0135	1.0584	0.97692

Table 2-3: Fitting Parameters for Linear Mass Concentration Detection

	Detector	Standard (kDa)	$Bx + C$		R^2
			B	C	
A	Microring Resonators	1.2	16.5	-0.13	0.99
		9	16.5	-0.127	0.95
		33	14.3	-0.0724	0.97
		120	15.4	-0.2	0.93
		560	9.84	-0.0866	0.91
B	Differential Refractive Index	1.2	2.26	-0.0187	1.0
		9	2.18	-0.0153	1.0
		33	2.34	-0.0187	1.0
		120	2.37	-0.0187	1.0
		560	2.69	-0.0298	1.0
C	UV/Visible	1.2	232	-2.46	0.99
		9	220	-1.64	1.0
		33	234	-1.92	1.0
		120	235	-1.91	1.0
		560	259	-2.83	1.0

Table 2-4: Fitting Parameters for Calibration Curves

	Detector	$Bx + C$		R^2
		B	C	
A	Microring Resonators	-3.276	8.9095	0.99781
B	Differential Refractive Index	-3.205	8.7701	0.99804
C	UV/visible	-3.2657	8.8834	0.99791

5. References

(1) Hiemenz, P.; Lodge, T. *Polymer Chemistry*, 2nd ed.; CRC Press, **2007**; Vol. 1−141,360−372.

(2) Uliyanchenko, E.; van der Wal, S.; Schoenmakers, P. *J. Polym. Chem*. **2012**, 3 (9), 2313−2335.

(3) Dwyer, J. L.; Zhou, M. *Int. J. Spectrosc.* **2011**, 2011, 694645.

(4) Otte, D. A. L.; Borchmann, D. E.; Lin, C.; Weck, M.; Woerpel, K. A. *Org. Lett*. **2014**, 16 (6), 1566−1569.

(5) Farmer, B. S.; Terao, K.; Mays, J. W. *Int. J. Polym. Anal. Charact*. **2006**, 11 (1), 3−19.

(6) Kostanski, L. K.; Keller, D. M.; Hamielec, A. E. *J. Biochem. Biophys. Methods* **2004**, 58 (2), 159−186.

(7) Striegel, A. M. *Anal. Bioanal. Chem*. **2008**, 390 (1), 303−305.

(8) Schriemer, D. C.; Li, L. *Anal. Chem*. **1996**, 68 (17), 2721−2725.

(9) Liu, J.; Loewe, R. S.; McCullough, R. D. *Macromolecules* **1999**, 32 (18), 5777−5785.

(10) Murgasova, R.; Hercules, D. M. *Anal. Bioanal. Chem*. **2002**, 373 (6), 481−489.

(11) Martin,K.;Spickermann,J.;Raӧder,H.J.;Müllen,K.Rapid Commun. *Mass Spectrom*. **1996**, 10 (12), 1471−1474.

(12) Schoenmakers, P.; Aarnoutse, P. *Anal. Chem*. **2014**, 86 (13), 6172−6179.

(13) Gentekos, D. T.; Dupuis, L. N.; Fors, B. P. *J. Am. Chem. Soc.* **2016**, 138 (6), 1848−1851.

(14) Wade, J. H.; Bailey, R. C. *Anal. Chem*. **2014**, 86 (1), 913−919.

(15) Kou, D.; Manius, G.; Zhan, S.; Chokshi, H. P. *J. Chromatogr. A* **2009**, 1216 (28), 5424−5428.

(16) ASTM E1303-95(2017). *Practice for Refractive Index Detectors Used in Liquid Chromatography*; ASTM International: West Conshohocken, PA, **2017**.

(17) Mojsiewicz-Pieńkowska,K. J.*Chromatogr.B Anal.Technol. Biomed. Life Sci*. **2008**, 865 (1−2), 1−6.

(18) Arndt, J. H.; Macko, T.; Brüll, R. *J. Chromatogr. A* **2013**, 1310, 1−14.

(19) Boborodea, A.; O'Donohue, S. Int. *J. Polym. Anal. Charact*. **2017**, 22 (8), 685−691.

(20) Dixon, R. W.; Peterson, D. S. *Anal. Chem.* **2002**, 74 (13), 2930−2937.

(21) Vehovec, T.; Obreza, A. J*. Chromatogr. A* **2010**, 1217 (10), 1549−1556.

(22) Takahashi, K.; Kinugasa, S.; Senda, M.; Kimizuka, K.; Fukushima, K.; Matsumoto, T.; Shibata, Y.; Christensen, J. *J. Chromatogr. A* **2008**, 1193 (1), 151−155.

(23) Washburn, A. L.; Shia, W. W.; Lenkeit, K. A.; Lee, S.-H.; Bailey, R. C. *Analyst* **2016**, 141 (18), 5358−5365.

(24) Graybill, R. M.; Para, C. S.; Bailey, R. C. *Anal. Chem*. **2016**, 88 (21), 10347−10351.

(25) Ye, D.; Wang, W.; Moline, D.; Islam, M. S.; Chen, F.; Wang, P. *Anal. Chem*. **2017**, 89 (20), 10761−10768.

(26) Shopova, S. I.; White, I. M.; Sun, Y.; Zhu, H.; Fan, X.; Frye- Mason, G.; Thompson, A.; Ja, S. *Anal. Chem*. **2008**, 80 (6), 2232− 2238.

(27) Scholten, K.; Collin, W. R.; Fan, X.; Zellers, E. T. *Nanoscale* **2015**, 7 (20), 9282−9289.

(28) Zhu, H.; White, I. M.; Suter, J. D.; Zourob, M.; Fan, X. *Anal. Chem*. **2007**, 79 (3), 930−937.

(29) Kim, D. C.; Dunn, R. C. *Anal. Chem*. **2016**, 88 (2), 1426−1433.

(30) Iqbal, M.; Gleeson, M. A.; Spaugh, B.; Tybor, F.; Gunn, W. G.; Hochberg, M.; Baehr-Jones, T.; Bailey, R. C.; Gunn, L. C. *IEEE J. Sel. Top. Quantum Electron*. **2010**, 16 (3), 654−661.

(31) Wade, J. H.; Bailey, R. C. *Annu. Rev. Anal. Chem*. **2016**, 9, 1− 25.

(32) Eilers, P. H. C. *Anal. Chem*. **2003**, 75 (14), 3631−3636.

(33) Baek, S.-J.; Park, A.; Ahn, Y.-J.; Choo, J. *Analyst* **2015**, 140 (1), 250−257.

(34) Luchansky, M. S.; Washburn, A. L.; Martin, T. A.; Iqbal, M.; Gunn, L. C.; Bailey, R. C. *Biosens. Bioelectron*. **2010**, 26 (4), 1283− 1291.

(35) Van Kreveld, M. E.; Van Den Hoed, N. *J. Chromatogr. A* **1973**, 83, 111−124.

Chapter III

Investigation into Alternative Fluidic Geometries for Improvement of Observed Molecular Weight Dependence of Microring Resonator Platform

Acknowledgements

I would like to acknowledge the many contributions of John D. Orlet, including assistance with designing flow cells (both cartridge lid and gasket), drawing SolidWorks files, assisting with experimental design, assisting with executing experiments, and assisting with editing this chapter. My contributions include sample preparation, LC method development, development of R code for data work up, data processing, and writing up this chapter.

The authors would like to thank Dr. James Wade and Dr. David Meunier for providing valuable insight throughout experimental process. Additionally, we acknowledge financial support from The Dow Chemical Company through the University

Partnership Initiative Program. We would also like to thank the lab of Professor Adam Matzger especially his student Ryan Dodson for training us and allowing us to use the CO_2 laser cutter. Then finally we would like to thank the Machine Shop and The Fabrication Studio of the University of Michigan for fabricating necessary parts for this project.

Abstract

Silicon photonic microring resonators, much like other optical sensors, are attractive for many analytical applications because of their high level of surface sensitivity. However, this sensitivity falls off exponentially with increasing distance from the sensor surface which correlates with the decay profile of the evanescent field. This sensitivity fall-off has been well characterized for the microring resonators with previous studies. One study directly probed the evanescent field by layer-by-layer polymer deposition on the sensor surface, where deviation from a linear response was observed at approximately 25 nm from the surface. In a more recent study, which utilized the microring resonators as a liquid chromatography (LC) detector, it was observed that with increasing polystyrene (PS) molecular weight (MW) there was a decrease in peak areas tracking with the same decay profile of the evanescent field. Therefore, the goal of this study was to explore alternative fluidic geometries for the microring resonator flow cell to improve the mass transfer/sensitivity of the high MW regime. In other words, if we alter the way eluent is delivered to the chip, is there any observed improvement in the previously visualized MW dependence? Here experimental conditions of LC interfaced polymer separations were emulated and analytical narrow range PS standards were used as a

model system to fully probe potential improvements for the detection of large MW analytes.

1. Introduction

Silicon photonic microring resonators are a type of optical resonant sensors. These resonant sensors rely on the coupling of light into microcavities for various sensing applications. Light propagates on the principle of total internal reflection through waveguides and under proper conditions the light couples into the adjacent microcavity. At the interface of the core and cladding of the waveguide there is an evanescent optical field that extends from the surface. This evanescent field is inherent for sensing since light-matter interactions with the evanescent field are measured over time. The strength of the evanescent field is dependent on proximity to the sensor surface, this has been well characterized and has been found to decay exponentially with increasing distance from the sensor surface. The following equation describes the discussed exponential decay of the evanescent field strength (*I*):

$$I(z) = I_0 e^{2\gamma z} \qquad \textit{Eq. 1}$$

where I_0 is the evanescent field strength at the sensor surface, z is the distance from the surface and γ is the exponential decay constant or rate of fall-off in field strength.[1,2] As for the microring resonator platform, the exponential decay of the evanescent field was probed directly by layer-by-layer polymer deposition on the sensor surface. Here deviation from a linear response was observed 25 nm from the surface.[2] This can be a challenge for the sensing of dissolved large molecules whose hydrodynamic diameter

infringes on such dimensions. For example a 120 kDa polystyrene standard has a radius of gyration (R_g) of approximately 13 nm when dissolved in tetrahydrofuran (THF) this equals a diameter of 26 nm which falls beyond the linear sensing region. More so as polystyrene molecular weight increases so does Rg, which means sensitivity of the microring resonator platform tracks with molecule size.[3] This challenge however is something more likely to occur in liquid chromatography (LC) applications rather than biological binding applications which are estimated to extend tens of nanometers.[3]

Previous work has utilized silicon photonic microring resonators as an alternative detection scheme to combat some commonly encountered challenges in commercially available LC detectors, for example detection of signature (i.e. chromophore or florescence) lacking analytes or linear mass detection for gradient separations. Here the major advantages of LC detection by the microrings was demonstrated with polymer characterization. Our gel permeation chromatography (GPC) application demonstrated applicability to LC detection with linear mass detection capability, high correlation to conventional detectors, as well as our ability to quantify molecular weight distributions of broadly distributed polystyrene (PS).[3] As for our adsorption LC application we fully demonstrated the gradient detection capability of our platform which is unique for a refractive index based detection mechanism.[4] All that being said there were some challenges with these experiments, most of which could simply be improved if we were to develop our platform further to function as an LC detector. However, one challenge observed was the molecular weight dependence of the sensor surface. This means as the molecular weight of our analytes increased there was a decrease in peak area for a fixed injection mass. Specifically, a MW dependent region is observed for polymer chains

which exceed a $2R_g$ distance of ~25 nm.[3] This dependence is most likely a result of both lower sensitivity to larger molecules due to evanescent field limitations and less efficient mass transfer of larger molecules regardless of injected concentration.

The mass transfer contribution to this trend was investigated with this work, which was heavily motivated by other pervious work which utilized the microring resonator platform as a capillary electrophoresis (CE) detector. With these studies mass concertation linearity and detection of sugars lacking chromophores was observed, but what was especially clear was the improved sensitivity of microring resonator platform when used in this format as opposed to LC interfaced work.[5] This sensitivity difference is mostly attributed to the inherent flow profile differences between the two different separation methods. More specifically, LC flow is pressure driven which by nature possesses a laminar flow profile, which is typically described as rounded and orderly. Laminar flow is conventionally considered mass transfer limited and subjective to diffusion which can greatly contribute to the sensitivity issues. On the other hand, due to the applied potential, CE is driven by electroosmotic flow (EOF). EOF delivers a flow that has a square profile, this characteristic reduces band broadening effects and enhances the number of theoretical plates.

In other words, by comparing our labs' work it is observed that the laminar flow profile of our separation greatly effects the sensitivity of the microring resonators. Therefore, with this project we sought out an alternative flow cell configuration for our LC interface with the microring resonators to alter the laminar flow profile and induce

improved mass transfer. The method we sought to explore our hypothesis was to employ a “wall-jet” configuration often utilized in electrochemical applications.

A wall-jet geometry utilizes a “T” like flow path where the inlet comes in from the vertical portion and flow is split in opposite directions horizontally. With this configuration the inlet stream strikes the detection portion (hence the name “wall-jet”), which for electroanalytical applications is typically an electrode, that is positioned perpendicular with regards to the inlet flow. This wall-jet flow path has shown to enhance mass transport and sensitivity when compared to conventional/parallel flow geometries. [6–10] Recently, Munshi and Martin et. al. 3-D printed a wall-jet microfluidic device where the electrode was placed perpendicular to the inlet stream and compared the performance to a thin-layer electrode configuration where the electrode was placed laterally to flow. With use of the wall-jet device they observed 16 times higher sensitivity along with improved mass transport over the thin-layer device. They also compared the wall-jet electrode device to UV and mass spectrometry detectors in an HPLC applications, with this they observed a comparable number theoretical plate across all the detectors.[10]

Therefore, with this study an alternative geometry to our conventional flow cell was explored as a method to experimentally improve the mass transfer of higher molecular weights, which as a result should also enhance microring sensitivity. This was done by taking inspiration from wall-jet electrode work. In other words we redesigned the microring resonator flow cell to place the inlet stream perpendicular to the microring resonator chip. We did this through a series of flow cell lid and gasket designs. A series of chromatogram comparisons and quantified peak areas are presented here to illustrate the design

progression. These results show the successful implication of a wall-jet design to our microring resonator flow cell. However, much of this work shows that the molecular weight dependence of our sensor remains reproducible regardless of the flow cell geometry, eliminating limited mass transfer as the cause of this trend. On a more positive note some improvement of our data representation, for example noise reduction, is observed with our final wall-jet design. This observation is promising for future work that will further optimize the microring resonator flow cell to better serve LC applications.

2. Experimental

2.1. Materials

Solvents were purchased from Sigma-Aldrich (St. Louis, MO) at the highest purity available and polystyrene standards (narrowly distributed) were purchased from Polymer Standards Service-USA, Inc. (Amherst, MA), all reagents were used as received. Polystyrene standards (1.3, 3.2, 9, 18, 33, 62, 120, 280, 560, and 1400 kDa) were prepared at various concentrations in tetrahydrofuran (THF) or ethyl acetate depending on compatibility with cartridge top material.

2.2. Microring Resonators

The microring resonator system (Maverick M1 optical scanning instrumentation) and sensor array chips were purchased from Genalyte, Inc. (San Diego, CA). Detailed descriptions of sensor fabrication and instrument operation have been described elsewhere.[11] However, the microring resonators are ring shaped optical cavities with adjacent linear waveguides. An external tunable cavity diode laser centered at 1550 nm

individually probes each microring, monitoring optical transmission as a function of wavelength. Dips in transmittance signal are observed at resonant wavelengths (λ_r) defined by the following equation:

$$\lambda_r = \frac{2\pi n_{eff}}{m} \qquad \textit{Eq. 2}$$

Here r is the ring radius, n_{eff} is the effective refractive index, and m is a constant. n_{eff} changes with observed changes at the sensor surface, such as analyte elution or changing mobile phase composition, resulting in a change of the resonant wavelength, which is measured and referred to as relative shift in picometers (Δpm). These changes in resonance wavelengths corresponded to changes in n_{eff} and are monitored as a function of time.[1,3,12]

Sensor chips consist of an array of 128 individual microring resonators on a 4 × 6 mm silicon-on-insulator (SOI) wafer which has a SiO_2 surface that is highly chemically resistant. Prior to use a protective photoresist coating was removed by successively immersing chips in acetone and isopropanol baths, followed by an acetone rinse.[3]

2.3. Wall-Jet Cartridge Top and Gasket Fabrication

Early generations of the flow cell lid designs versions 1-2 of Figure 3-1 B-C were manually machined by the University of Michigan machine shop out of Teflon, designs were provided via SolidWorks. For later generations of the flow cell lid designs, versions 3-4 of Figure 3-1 D-E, were 3D printed using the Strasys J750 in Vero resin printed by the University of Michigan Fabrication Studio. Then for reference the original flow cell lid

design is provided in Figure 3-1A, which was purchased from Genalyte and was constructed out of Teflon.

New fluidic gaskets were laser cut out of polyethylene terephthalate (Mylar) using a CO_2 laser cutter provided by the lab of Prof. Adam Matzger in the department of chemistry at the University of Michigan. Gasket designs are presented in Figure 3-2A. Design 0 represents the original Mylar 2 channel gasket purchased from Genalyte, which was used here with the original flow cell lid design (Figure 3-1A) and for preliminary wall-jet design 1 (Figure 3-1B) data shown in Figure 3 B-C. Gasket design 1 of Figure 3-2A was used with wall-jet designs 1 and 2 (Figure 3-1 B and C respectively), data shows this pairing in Figures 3-6 and 3-7. Gasket design 2 of Figure 3-2A was used with wall-jet designs 3 and 4 of (Figure 3-1 D and E respectively), data obtained using this combination is presented in Figure 3-9 B-C.

2.4. HPLC

Gel permeation chromatographic (GPC) separations were performed on a Waters Alliance e2695 separation module (Milford, MA) furnished with a Waters 2489 UV/Visible Detector. The column used was an Agilent MiniMIX-C column (Santa Clara, CA), with dimensions of 250 mm × 4.6 mm, and a packing particle size of 5 μm. The utilized flow rates ranged from 0.6-0.9 mL/min, sample temperature was kept at 5 °C, and the column oven at 35 °C. Mobile phase solvent was either THF or ethyl acetate depending on compatibility with cartridge top material.

2.5. GPC-Microring Resonator Interface

An anodized aluminum cartridge holder housed sensor chips and were topped with the appropriate Mylar gasket and flow cell lid. This whole assembly, which is analogous to a detector flow cell, was interfaced to the HPLC via the following connections. The HPLC outlet was connected to a 0.25 mm flangeless 1/4−28 and then to a ZDV 10−32 PEEK low pressure union. The PEEK union adapted the HPLC fittings to the microring resonator cartridge. The same interface HPLC-microring resonator interface has been discussed previously.[3,4,12]

2.6. Data Analysis

Data analysis was carried out using custom software written in R (version 3.4.1), previously described in more detail.[3] Briefly, microring resonator chromatograms typically show an averaged responses from 4-128 microrings depending on the experiment. The averaged signal intensity is plotted as a function of time which is further smoothed and baseline corrected using a Whittaker smoothing function[13] and an asymmetrically reweighted least-squares (arPLS) approach.[14]

3. Results and Discussion

3.1. Designing a Wall-Jet Flow Cell for the Microring Resonator Platform

The microring resonator flow cell sits under the instrument's optical head in very close proximity. Positioning of the flow cell with regards to the optical head needs to be exact for consistent performance, and built in alignment features allow for positioning to be very robust. With this in mind it was very important to keep certain aspects of the existing flow cell and maintain the same footprint with new designs in order to not interfere

with instrument performance. As a result the base of the flow cell, which has several alignment features, was used as it exists and the actual geometry changes to incorporate a wall-jet came from newly designed flow cell lids (Figure 3-1) and gaskets (Figure 3-2). The design progression of the flow cell lids in presented in Figure 3-1, with the original design illustrated in Figure 3-1A and the flow path shown in Figure 3-1F. As for the gasket designs, Figure 3-2A shows the design progression with design 0 illustrating the original gasket design.

3.2. Testing Operation and Optimization of the First Wall-Jet Flow Cell Design

The first wall-jet design is shown in Figure 3-1 B and G. With this design the inlet of the bottom fluidic channel of the flow cell lid was extended into the top channel and then dropped down so that the inlet would be in-line with the outlet. The angle of the flow cell lid ports was maintained from the original design, and because of this the new inlet did not fall in the middle of the chip, rather it was offset to the right. This feature brought on many early challenges. The shorter flow path was often favored which meant we were not seeing an equal split in flow. To combat this the outlet tubing length was manually adjusted until equal flow rates were measured out of both outlets.

Once flow rates out the outlets were balanced with the first wall-jet design, the operation of the new flow cell was investigated with the original gasket. Here two different flow rates 0.6 mL/min and 0.9 mL/min were used for the analysis of 0.2 mg injections of various polystyrene standards. The chromatograms obtained are presented in Figure 3-3, where Figure 3-3A is the original flow cell (0.6 mL/min), Figure 3-3B is the first wall-jet design operated at 0.6 mL/min, and Figure 3-3C in the first wall-jet design operated at 0.9

mL/min. All three chromatograms present comparable detection, initial inspection shows the expected molecular weight trend in Figure 3-3A and possible deviation from this trend in Figure 3-3B and C. However, comparing the actual peak areas, Figure 3-4, shows that this is most likely not the case since the trends look mostly the same. Figure 3-4C does show that the peak areas of the chromatogram obtained with the wall-jet operated at 0.9 mL/min to have minimally increased peak sizes over the other chromatogram however, this is mostly attributed to the flow rate rather than the alternative flow cell geometry. This logic is further verified by investigating the cluster dependence of the wall-jet signal at this 0.9 mL/min flow rate (Figure 3-5). In other words, if we were seeing increased mass transfer with the 1st wall-jet design when operated at 0.9 mL/min we would expect this effect to be greatest at the actual junction of where our inlet meets our microring resonator chip. Given the offset design of our flow cell lid we would expect our inlet to drop down around cluster 28 and in Figure 3-5 we show the average peak area per cluster. It is observed here that there is fairly consistent peak areas across the whole channel with no obvious dependence of proximity to the inlet. Concluding on this it appears that we are seeing little to no change with the utilization of our 1st wall-jet design under these experimental conditions, consequently some design considerations were reconsidered.

An often-mentioned feature of wall-jet geometry devices is the dimension of the outlet channel with regards to the inlet channel. Previous research recommends having an outlet channel that is at least equivalent in size to the inlet.[10] This was not something we were achieving. For Figures 3-5 our inlet dimension was 0.4 mm and our outlet dimension was 0.16 mm. With this is mind we redesigned the gaskets within our flow cell. The original design “0” is presented in Figure 3-2 and the new designs “1” and “2” are

presented as well. The goal of the new designs was to eliminate the confining channels and increase the gasket thickness to achieve an outlet which is larger than the inlet to better promote a wall-jet effect.

3.3. Exploring the First Wall-Jet Flow Cell Design With an Alternative Fluidic Gasket

The first wall-jet design was revisited using a new gasket design (design 1 of Figure 3-2), and the obtained chromatogram is shown in Figure 3-6B. Here the inlet dimension remained the same, 0.4 mm, however the outlet dimension of the wall-jet flow cell was increased significantly to 0.75 mm. The chromatogram presented in Figure 3-6A utilized the original flow cell lid (design 0) and gasket (design 0). A comparison of the two designs is provided in Figure 3-6C, where it can be observed that the peak areas obtained vary slightly even though the experimental conditions/sample concentrations are identical. The original flow cell shows the expected molecular weight dependence whereas the wall-jet flow cell exhibits less of an obvious molecular weight trend. Other observations that can be made is that the wall-jet peak areas tend to have larger error bars, which may mean that with our new flow cell we experience more variation in its performance. However, the more comparable peak areas across the significant molecular weight range seen with the wall-jet flow cell is still a potential promising improvement.

3.4. Testing Operation of the Second Wall-Jet Flow Cell Design

Although some promising improvements were observed, our confidence in the reproducibility was still a concern. The performance of this flow cell design seemed variable most likely due to the manual balancing of flow rates out of the two outlets, which

is simply due to the off-center inlet. Therefore, because of these concerns the flow cell was redesigned to center the inlet. The 2nd new wall-jet flow cell is presented in Figure 3-1C and the flow diagram is presented in Figure 3-1H. With this design the inlet comes in through the top fluidic channel and drops down in the center of the top channel with the outlets out the two ports of the bottom channel. Initial fluidic testing of this 2nd wall-jet flow cell and new gasket design 1 (Figure 3-2A) showed more balanced outlet flow rates which was promising for pursuing this design further. The obtained chromatogram with this combination, wall-jet flow cell lid design 2 and new gasket design 1, is presented in Figure 3-7C. Figure 3-7A shows the chromatogram obtained with the original flow cell and Figure 3-7B shows the chromatogram obtained with the 1st wall-jet flow cell. The integrated peak areas and peak heights from these experiments are seen in Figure 3-8. Looking at both peak areas (Figure 3-8A) and peak heights (Figure 3-8B) it is observed that design 2 shows minimal increase in both metrics. However, the molecular weight fall-off remains very reproducible regardless of the design.

3.5. Testing Operation of the Third and Fourth Wall-Jet Flow Cell Design

The designs of our first two wall-jet flow lids were heavily limited by the constrains of the machining method. These wall-jet lids were made in the University of Michigan Machine Shop which means that the fluidic ports were manually drilled through Teflon, and so the length of the channels was limited by the length of the drill bit and the 90° angle integrity was dependent on the skill of the operator. Given these limitations and the numerous challenges along the way we sought an alternative method for constructing our flow cell lids, and chose 3-D printing. A redesigned wall-jet flow cell lid used a centered

outlet. We also sought to improve upon the prior designs, including having the two outlets in-line with the inlet (within the same channel) and eliminate the right angle of the inlet. We expected that these abrupt change in right angle flow path could potentially be disrupting any possible mass transfer improvements. That being said the inlet of wall-jet designs 3 and 4 replace the right angle channel with a curved fluidic path. Figure 3-9 presents the collected chromatograms using the last two wall-jet flow cell designs and the 2 new gasket designs. Results from wall-jet design 3 can be seen in Figure 3-9B, while results from wall-jet design 4 can be seen in Figure 3-9C and results obtained with the original flow cell design can be seen in Figure 3-9A. It is important to point out that 3-D printing gave us more freedom in our design, but with a compromise in solvent compatibility. The experiments presented prior to this point used a THF mobile phase whereas the results shown in Figure 3-9 employed ethyl acetate as the mobile phase since it was compatible with the 3-D printed material. This solvent change did not compromise the collected data, which is verified by comparing Figure 3-9A to Figures 3-9B-C. With this comparison we see very comparable chromatograms, arguably we are seeing minimally increased peak heights and reduced noise in the baseline with the final/4th wall-jet flow cell design. However, these improvements are again minimal and the molecular weight trend seems unchanged as indicated by the peak height fall-off with increasing molecular weight.

4. Conclusion

We have thoroughly explored a series of flow cell designs to employ a wall-jet inlet in the hopes of improving the mass transfer of large molecular weight polymers. Through

all the data that has been collected we have observed uncompromised chromatograms, however the molecular weight trend has shown to be heavily reproducible, as illustrated further in Figure 3-10. Here we can see that regardless of the fluidic delivery to the microring resonators there remains the challenge of decreased sensitivity to larger molecular weight polymers. There are variations in peak areas calculated from flow cell to flow cell. Any observed differences lack statistical significance to conclude that changes in flow cell geometry provide improved sensitivity toward larger polymer solutes.

Therefore, with these conclusions, at this present time we have stopped ongoing experiments that utilize an alternative flow cell for the improvement of the mass transfer of large molecular weight molecules. Future work includes modeling the flow of the various presented flow cell designs to determine if we were ever experiencing increased mass transfer or a “wall-jet effect.” It is possible that our channel dimensions and/or device footprint is not conducive to allowing such an effect, if this is the case we hope that with the help of modeling we can better determine the necessary factors needed in order to promote an enhanced mass transfer. Additionally, investigating the microring resonators response to polymer chains which have experienced shear deformation could also provide valuable insight into the molecular weight dependence. The potential of once again pursuing this challenge experimentally persists however the decreased evanescent field strength is likely a significant contributor to this trend.

With original observation of the microring resonator’s molecular weight dependence, it was hypothesized that both the size of the evanescent field relative to the polymer in solution as well as limited mass transfer for larger molecular weights were

contributing factors.[3] Given that the presented approach for enhancing the mass transfer of large molecular weight polymers was heavily reproducible, it can be concluded that the main contributing factor of this trend is decreased evanescent field strength. In other words, even with enhanced mass transfer the microring resonators will likely lack sensitivity for polymers with 2Rg greater than or equal to 25 nm, which is the approximate distance from the sensor surface where there is a deviation from linearity.[3] However, given that this trend has proven to be highly reproducible, tracking heavily with the dimensions of the evanescent field, active consideration is going into mathematically correcting the molecular weight fall-off in the mean-time.

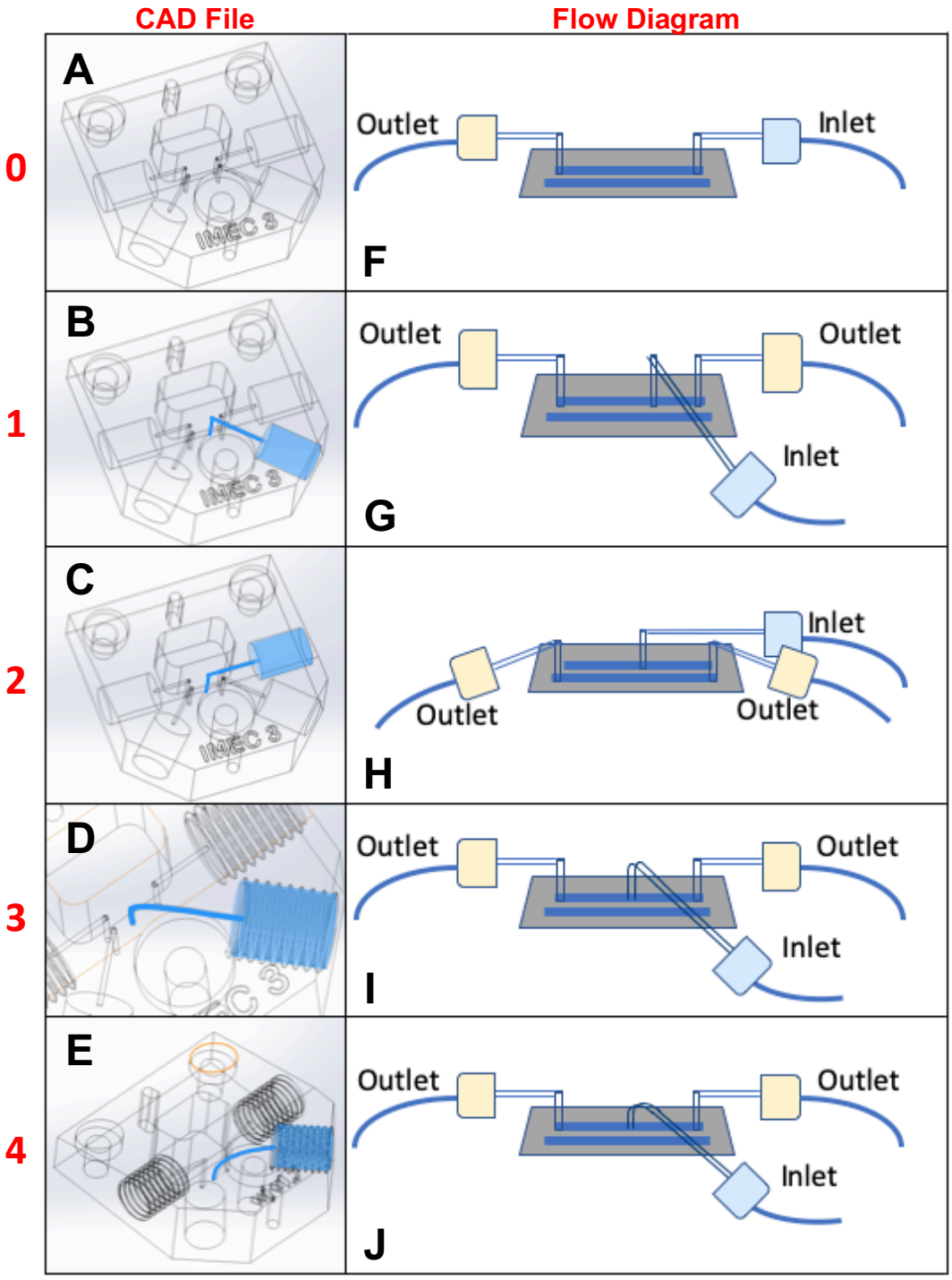

Figure 3-1: Series of Wall-Jet Flow Cell Designs. (A) Skeleton sketch generated with AutoCAD of the original flow cell lid. (B-E) Skeleton sketch generated with AutoCAD of a series of wall-jet flow cell designs. (F) Schematic of the flow path of the original flow cell design. (G-J) Schematic of the flow path of a series of wall-jet flow cell designs.

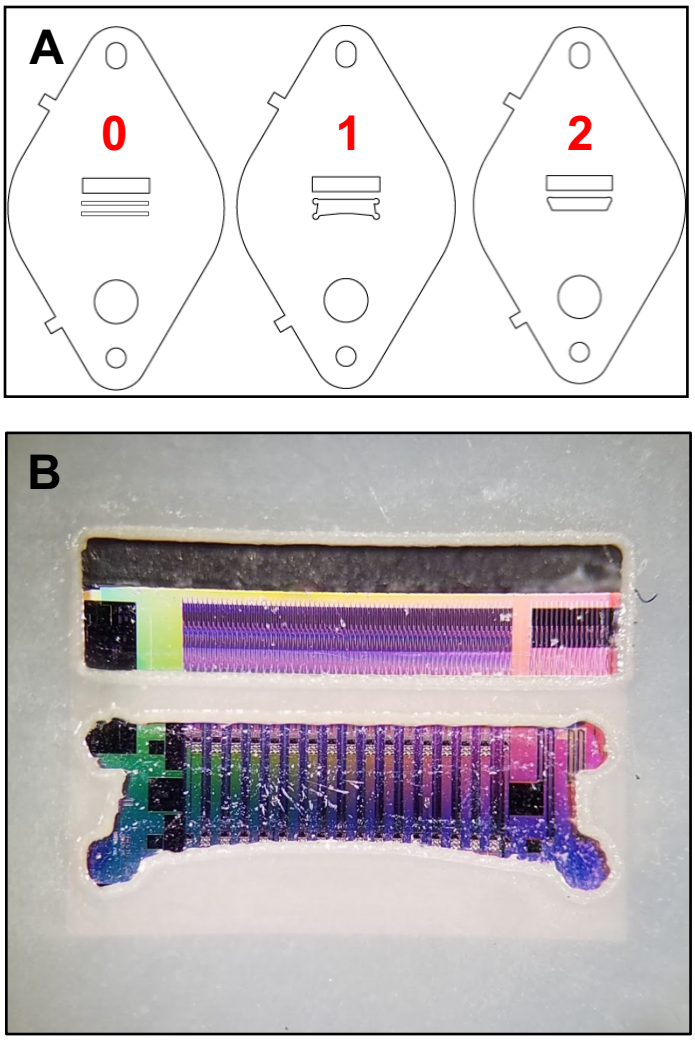

Figure 3-2: Series of Wall-Jet Gasket Designs. (A) Illustrations of gasket designs: *0* Original 2-channel gasket, *1* and *2* new gasket designs eliminating channel confinement of flow. (B) Shows a photo of gasket 1 over a microring resonator chip.

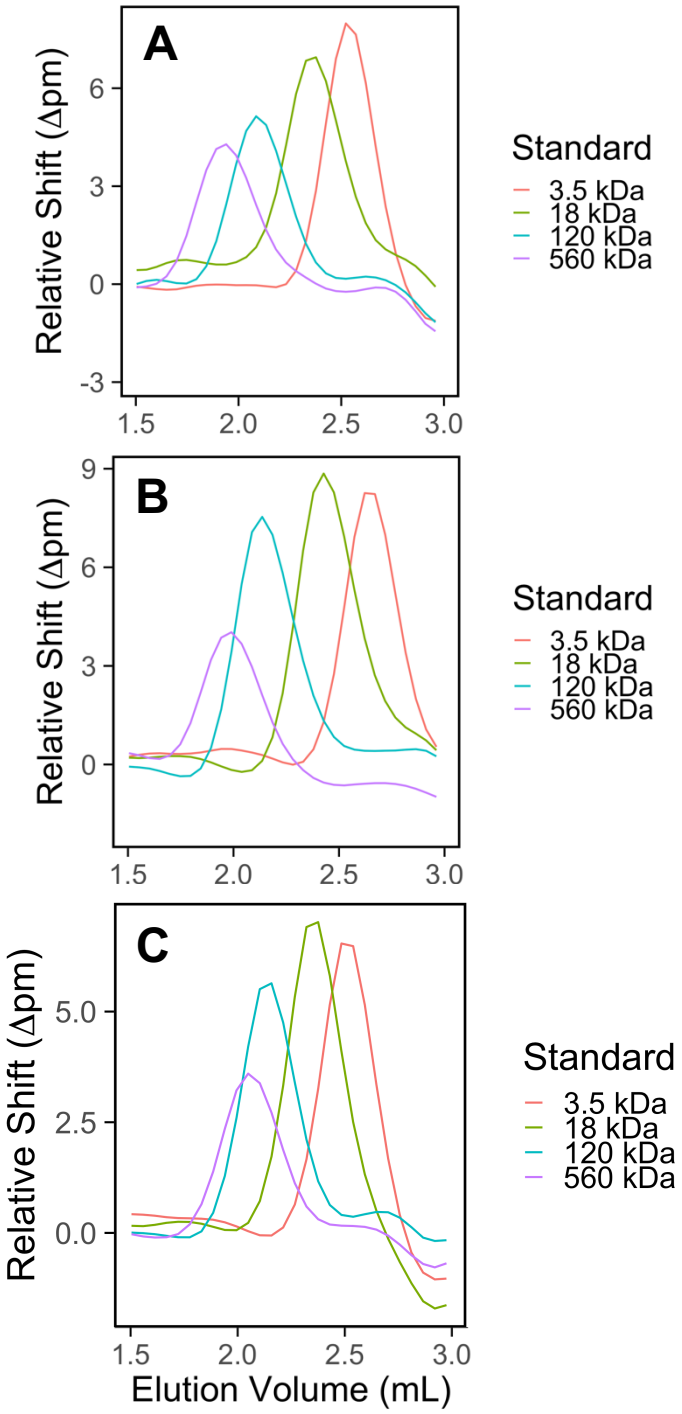

Figure 3-3: Chromatogram Comparison Between Original and First Wall-Jet Flow Cell Designs. (A) Representative chromatogram of a single microring resonator cluster obtained with the original flow cell design. (B-C) Representative chromatogram of a single microring resonator cluster obtained with the 1st wall-jet flow cell design. (A) and (B) use identical experimental conditions at a 0.6 mL/min flow rate (C) uses a faster flow rate of 0.9 mL/min, all consecutive experiments.

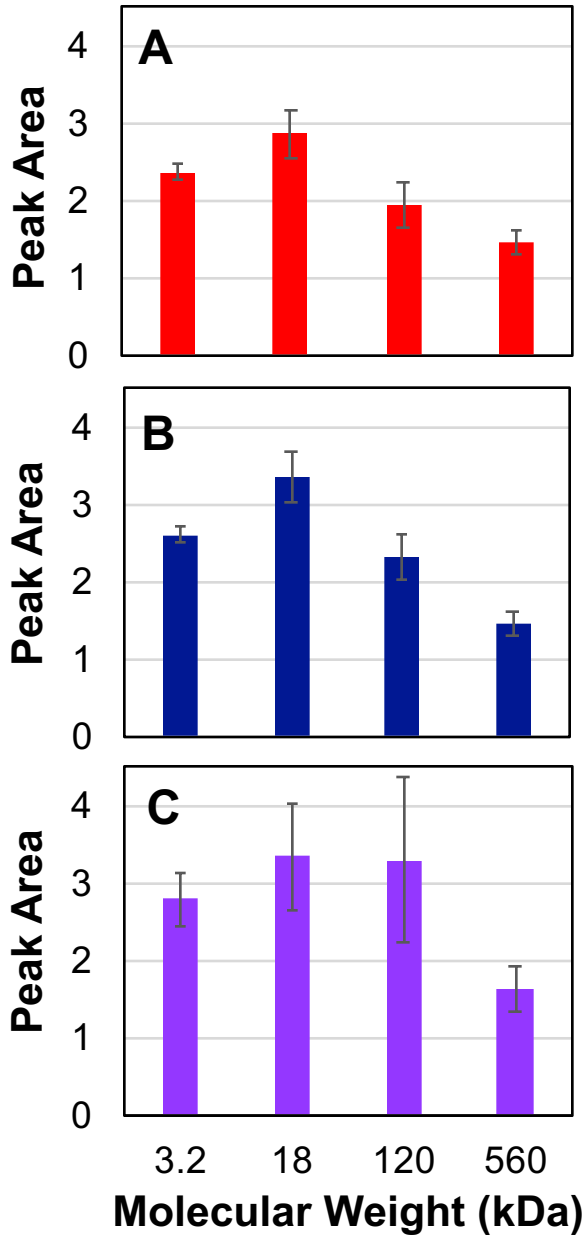

Figure 3-4: Peak Area Comparison Between Original and First Wall-Jet Flow Cell Designs. (A) Peak areas obtained with original flow cell design. (B-C) Peak areas obtained with fist wall-jet flow cell design. (A) and (B) use identical experimental conditions at a 0.6 mL/min flow rate (C) uses a faster flow rate of 0.9 mL/min, all consecutive experiments. Flow rate shows to have limited impact on mass transfer.

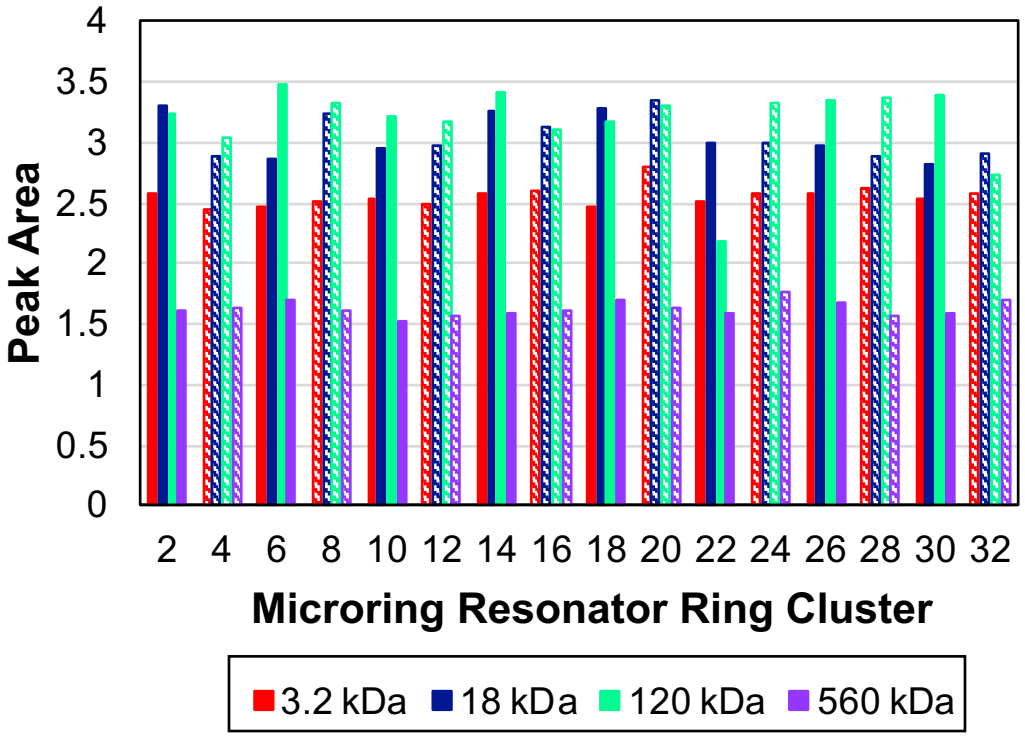

Figure 3-5: Investigating Cluster Dependence of First Wall-Jet Flow Cell Design. Histogram showing peak areas per cluster obtained using the 1st wall-jet flow cell design at 0.9 mL/min flow rate.

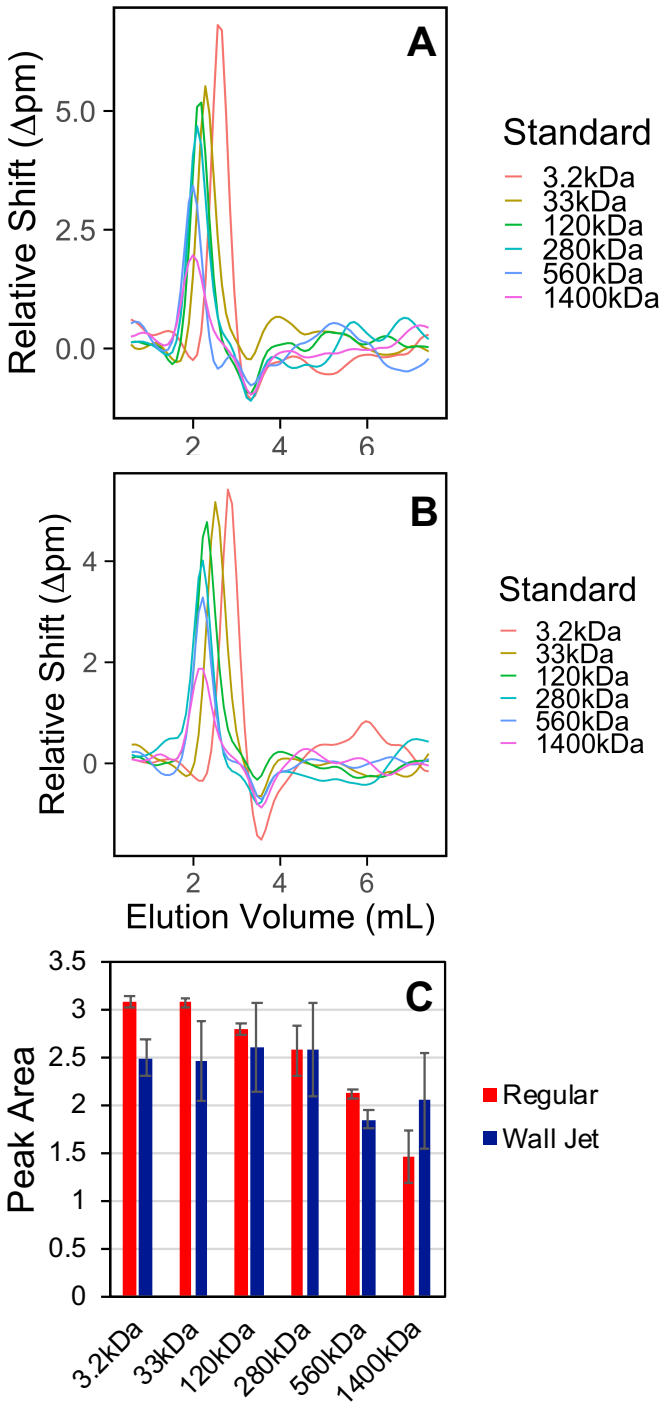

Figure 3-6: Obtained Chromatogram with First Wall-Jet Flow Cell Designs and New Gasket. (A) Chromatogram obtained using original flow cell design and conventional 2 channel gasket. (B) Chromatogram obtained using 1st wall-jet flow cell design and new gasket design 1 from Figure 3-2. (A) and (B) use identical experimental conditions at a 0.6 mL/min flow rate. (C) Offers a peak area comparison for the two different flow cell and gasket designs.

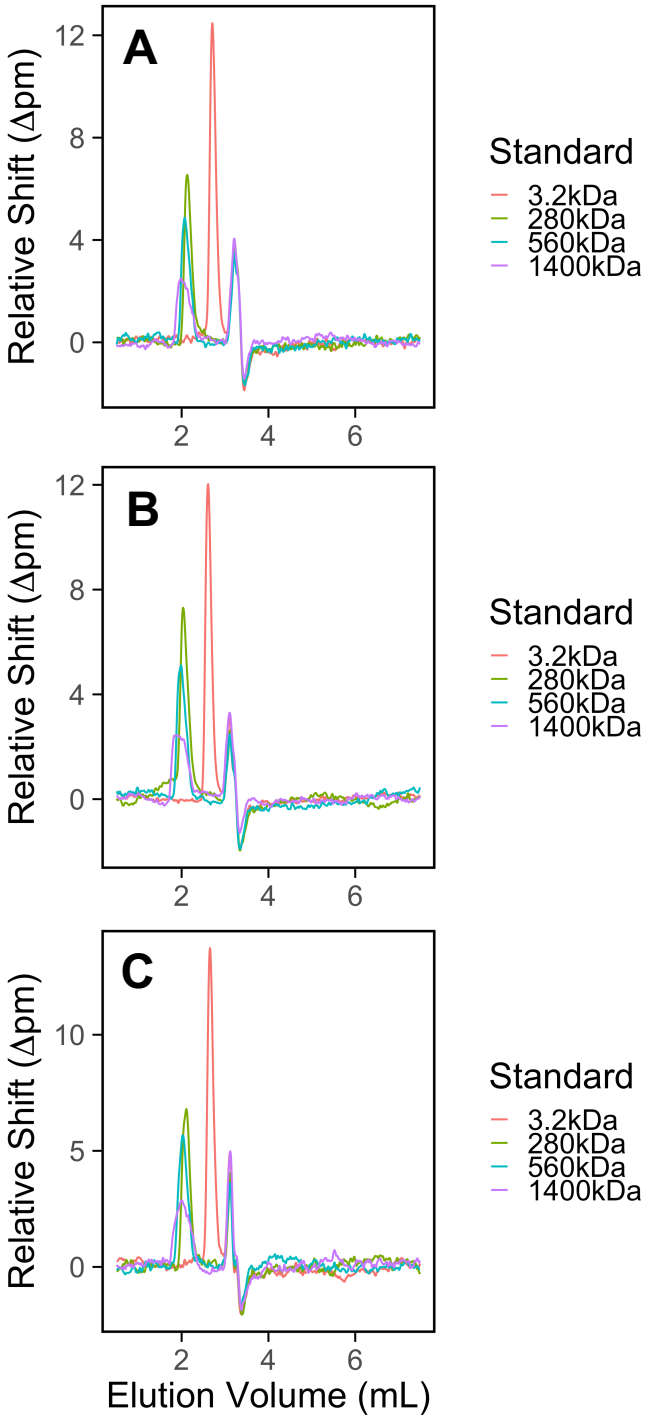

Figure 3-7: Chromatogram Comparison Between Original, First and Second Wall-Jet Flow Cell Designs. (A) Representative chromatogram obtained with the original flow cell design and original 2-channel gasket. (B) Representative chromatogram obtained with the 1st wall-jet flow cell design and 1st new gasket design. (C) Representative chromatogram obtained with the 2nd wall-jet flow cell design and 1st new gasket design.

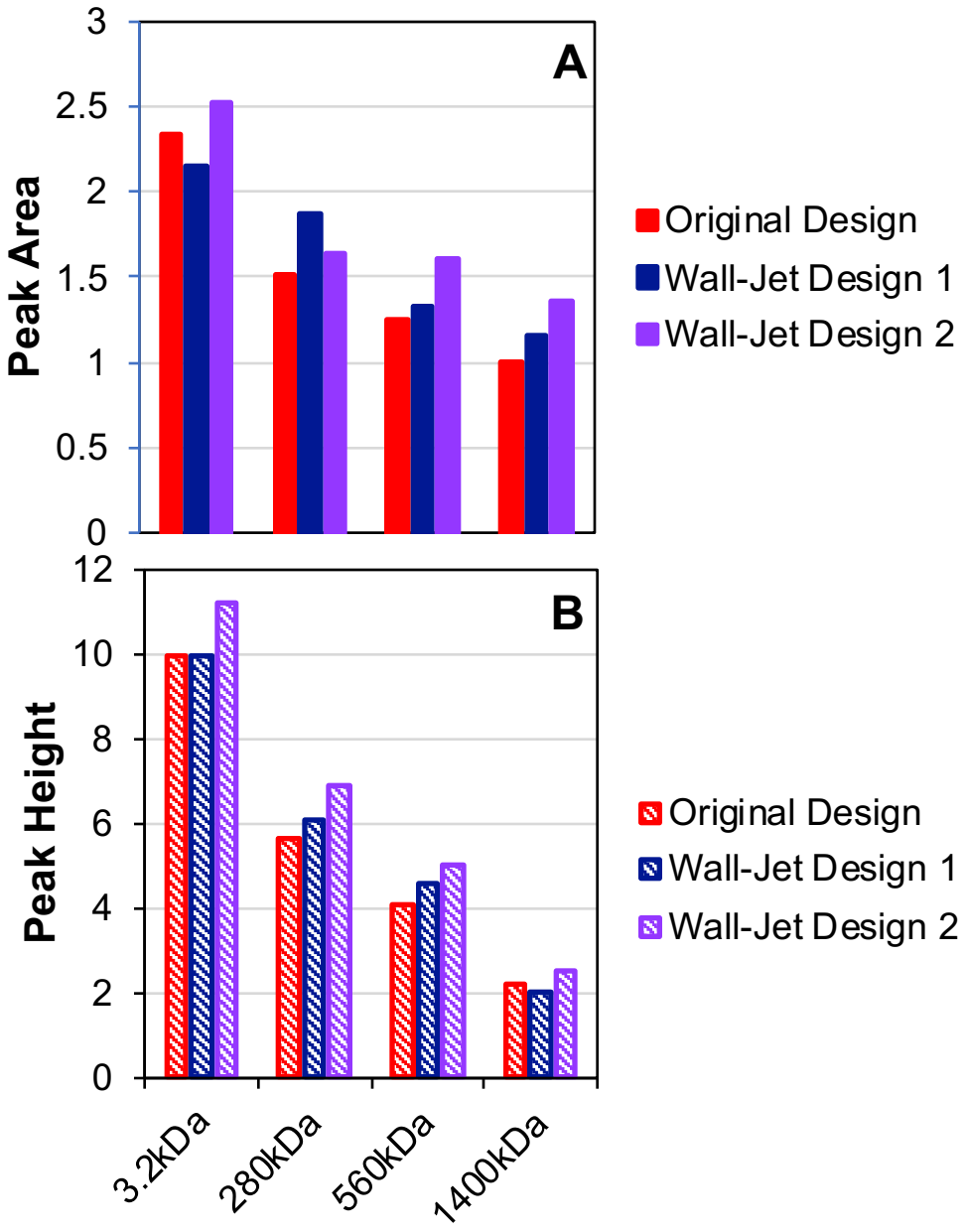

Figure 3-8: Peak Comparison Between Original, First and Second Wall-Jet Flow Cell Designs. (A) Illustrates a peak area comparison for the first two wall-jet designs to the original flow cell. (B) Illustrates a peak height comparison for the first two wall-jet designs to the original flow cell.

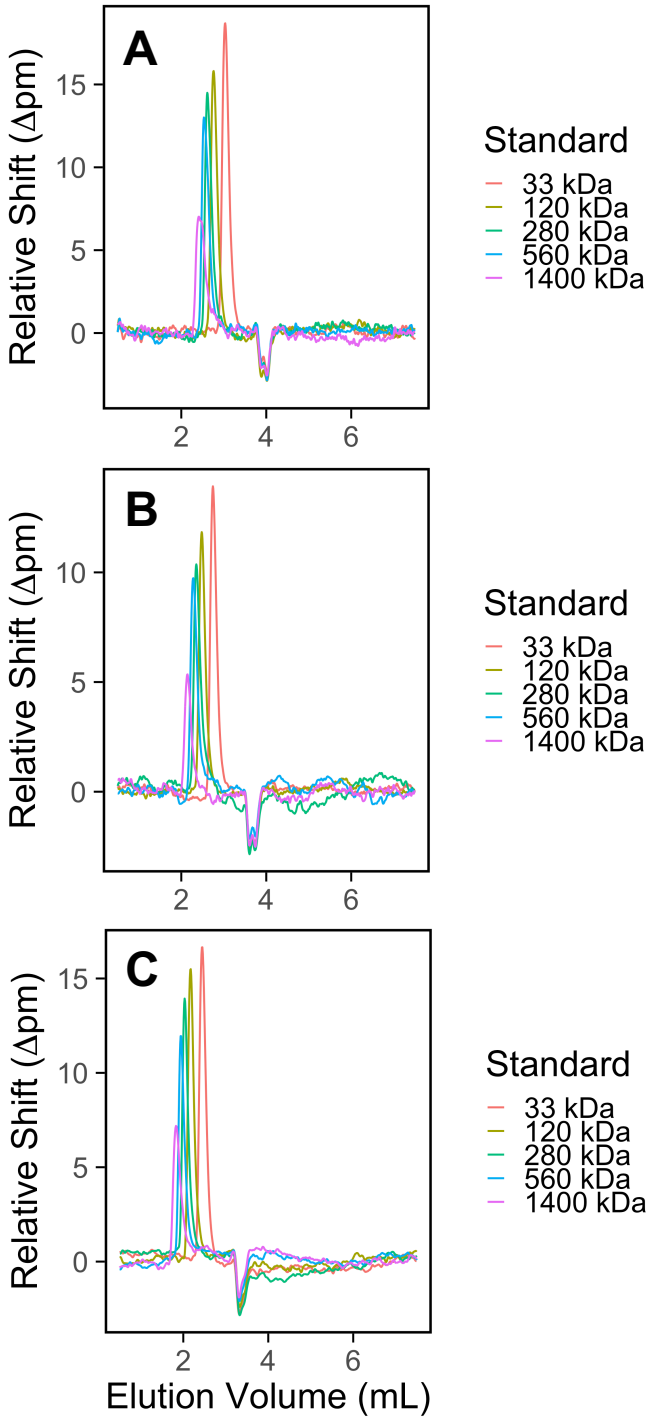

Figure 3-9: Chromatogram Comparison of Final Wall-Jet Designs. (A) Chromatogram obtained with original flow cell design. (B) Chromatogram obtained with 3rd wall-jet flow cell design and 2nd new gasket design. (C) Chromatogram obtained with 4th wall-jet flow cell design and 2nd new gasket design.

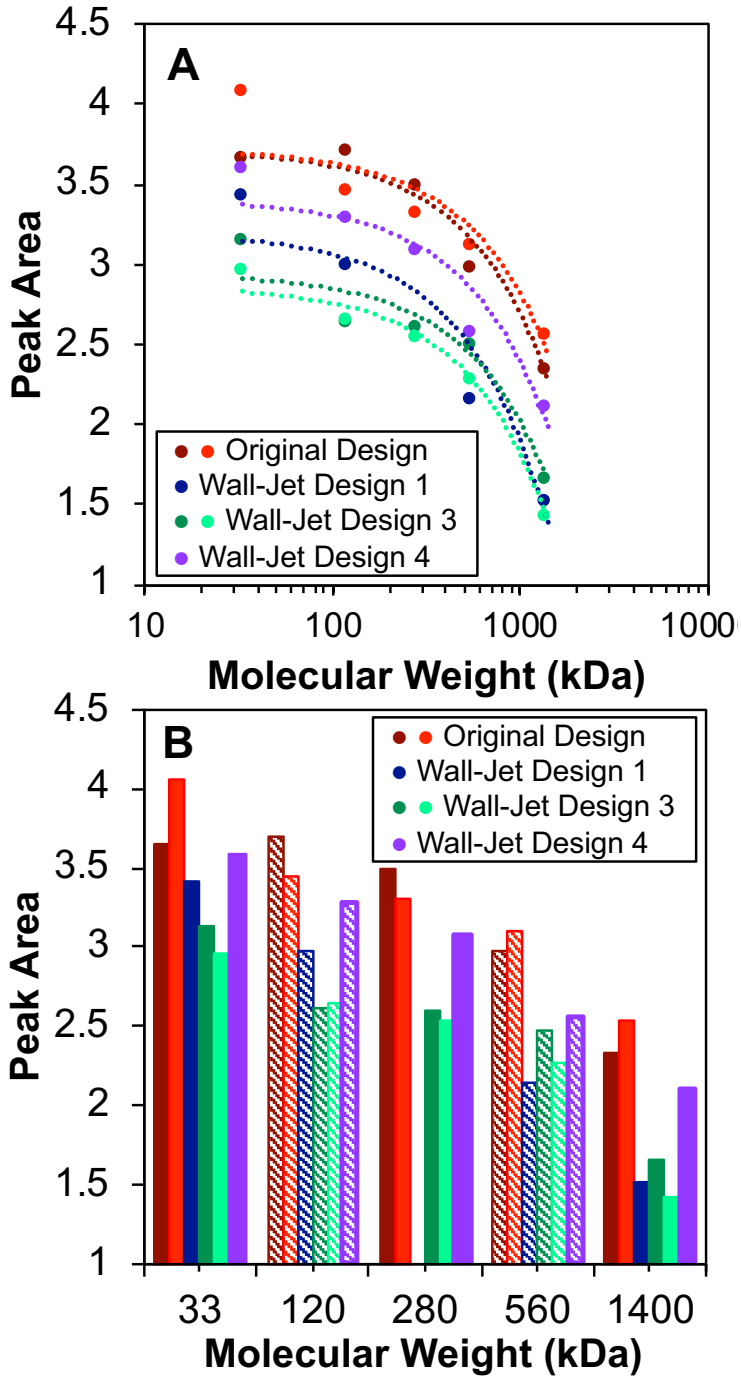

Figure 3-10: Peak Area Comparison of Series of Wall-Jet Designs. (A) Plotting peak area against log of molecular weight for a series of flow cell designs shows the reproducibility of the microring resonators molecular weight trend. (B) The same data presented as a histogram, verifies this further.

5. References

(1) Wade, J. H.; Bailey, R. C. Applications of Optical Microcavity Resonators in Analytical Chemistry. *Annu. Rev. Anal. Chem.* **2016**, *9*, 1–25. https://doi.org/10.1146/annurev-anchem-071015-041742.

(2) Luchansky, M. S.; Washburn, A. L.; Martin, T. A.; Iqbal, M.; Gunn, L. C.; Bailey, R. C. Characterization of the Evanescent Field Profile and Bound Mass Sensitivity of a Label-Free Silicon Photonic Microring Resonator Biosensing Platform. *Biosens. Bioelectron.* **2010**, *26* (4), 1283–1291. https://doi.org/10.1016/j.bios.2010.07.010.

(3) Mordan, E. H.; Wade, J. H.; Wiersma, Z. S. B.; Pearce, E.; Pangburn, T. O.; deGroot, A. W.; Meunier, D. M.; Bailey, R. C. Silicon Photonic Microring Resonator Arrays for Mass Concentration Detection of Polymers in Isocratic Separations. *Anal. Chem.* **2019**, *91* (1), 1011–1018. https://doi.org/10.1021/acs.analchem.8b04263.

(4) Mordan, E. H.; Wade, J. H.; Pearce, E.; Meunier, D. M.; Bailey, R. C. A Linear Mass Concentration Detector for Solvent Gradient Polymer Separations. *Analyst* **2020**. https://doi.org/10.1039/C9AN02533B.

(5) Orlet, J. D.; Bailey, R. C. Silicon Photonic Microring Resonator Arrays as a Universal Detector for Capillary Electrophoresis. *Anal. Chem.* **2020**, *92* (2), 2331–2338. https://doi.org/10.1021/acs.analchem.9b05271.

(6) Chin, D.-T.; Tsang, C.-H. Mass Transfer to an Impinging Jet Electrode. *J. Electrochem. Soc.* **1978**, *125* (9), 1461–1470. https://doi.org/10.1149/1.2131697.

(7) Ball, J. C.; Compton, R. G.; Brett, C. M. A. Theory of Anodic Stripping Voltammetry at Wall-Jet Electrodes. Simulation of Spatially Differential Stripping and Redeposition

Phenomena. *J. Phys. Chem. B* **1998**, *102* (1), 162–166. https://doi.org/10.1021/jp9720810.

(8) Compton, R. G.; Fisher, A. C.; Latham, M. H.; Brett, C. M. A.; Brett, A. M. C. F. O. Wall-Jet Electrode Linear Sweep Voltammetry. *J. Phys. Chem.* **1992**, *96* (21), 8363–8367. https://doi.org/10.1021/j100200a028.

(9) Laevers, P.; Hubin, A.; Terryn, H.; Vereecken, J. A Wall-Jet Electrode Reactor and Its Application to the Study of Electrode Reaction Mechanisms Part I: Design and Construction. *J. Appl. Electrochem.* **1995**, *25* (11), 1017–1022. https://doi.org/10.1007/BF00241950.

(10) Munshi, A. S.; Martin, R. S. Microchip-Based Electrochemical Detection Using a 3-D Printed Wall-Jet Electrode Device. *The Analyst* **2016**, *141* (3), 862–869. https://doi.org/10.1039/C5AN01956G.

(11) Iqbal, M.; Gleeson, M. A.; Spaugh, B.; Tybor, F.; Gunn, W. G.; Hochberg, M.; Baehr-Jones, T.; Bailey, R. C.; Gunn, L. C. Label-Free Biosensor Arrays Based on Silicon Ring Resonators and High-Speed Optical Scanning Instrumentation. *IEEE J. Sel. Top. Quantum Electron.* **2010**, *16* (3), 654–661. https://doi.org/10.1109/JSTQE.2009.2032510.

(12) Wade, J. H.; Bailey, R. C. Refractive Index-Based Detection of Gradient Elution Liquid Chromatography Using Chip-Integrated Microring Resonator Arrays. *Anal. Chem.* **2014**, *86* (1), 913–919. https://doi.org/10.1021/ac4035828.

(13) Eilers, P. H. C. A Perfect Smoother. *Anal. Chem.* **2003**, *75* (14), 3631–3636. https://doi.org/10.1021/ac034173t.

(14) Baek, S.-J.; Park, A.; Ahn, Y.-J.; Choo, J. Baseline Correction Using Asymmetrically Reweighted Penalized Least Squares Smoothing. *Analyst* **2014**, *140* (1), 250–257. https://doi.org/10.1039/C4AN01061B.

CHAPTER IV

A High Temperature Flow Cell for Microring Resonator Array Detector

Acknowledgements

This chapter is an adapted from an internal report from The Dow Chemical Company which has been used here with permission.[∴] The citation to the original publication is the following: Wade, J. H.; Mordan, E. H.; Meunier, D. M.; Bailey, R. C. Pearce, E.; deGroot, A. W. A High Temperature Flow Cell for Microring Resonator Array Detector, *Central Report Index (CRI) Report The Dow Chemical Company*, Report number *ACCN 2018007894,* Issued October 8th, 2018.

James Wade designed the high temperature flow cells, organized their production, put experimental plans in place, and wrote the majority of report. My contribution to this

[∴] Approval for reprint has been received from Dow through an information release request (ref. number 20202584).

work is assistance with flow cell designs, execution of bench top temperature testing of flow cells, developed flow cell insulation method, investigation of microring performance at elevated temperature, data analysis/workup, and assisted with writing report. Eric Pearce, Willem DeGroot, and David Meunier provided valuable insight and contributed to experimental design.

The authors would like to acknowledge Jacob Crosthwaite for his assistance with the flow cell temperature controllers as well as Warren Dillon and Gary Prather for their fantastic work machining the flow cell components. Additionally, much thanks is due to James Wade, David Meunier, and other Dow employees for coordinating and assisting with getting Emily Mordan access to Dow's facilities in order to contribute to this work.

Abstract

This chapter describes the design, prototyping, and testing of a high temperature flow cell as part of a University Partnership Initiative (UPI) in collaboration with Prof. Ryan Bailey's research group at the University of Michigan. The purpose of the UPI was to develop a gradient compatible linear mass concentration detector for applications in polymer separations. The detector consists of silicon photonic microring resonators, a class of whispering gallery mode sensors with exquisite surface sensitivity. Polyolefins are of greatest interest to Dow as related to this detector, but polyolefin separations place significant design constraints on the detection, due to detector operation at elevated temperature and chemical resistance to strong organic solvents (e.g., trichlorobenzene). To adapt the microring resonator platform for polyolefin separations, a new flow cell was needed that could withstand the harsh experimental conditions. The flow cell was

successfully built and tested internally. During testing, it was observed that the detector has significantly reduced performance at higher temperatures. Possible avenues to improve detector performance are described here.

1. Introduction

A university partnership initiative (UPI) in partnership with Prof. Ryan Bailey's research group at the University of Michigan aimed at expanding the detectors that could be used for polyolefin analysis. The goal of the UPI was to develop a gradient compatible concentration detector. The detector could have broad applications for polymer separation, but the focus was on polyolefins. Characterizing the molecular architecture of polyolefins requires a suite of analytical methods. Critical components of polyolefin characterization include molecular weight distribution (MWD) and chemical composition distribution (CCD), commonly referred to as short chain branding distribution. Separations methods are widely used for characterizing these distributional measurements.

High performance liquid chromatography (HPLC) detection methods for polyolefin separations are constrained by the elevated temperatures required to analyze samples. Polyolefin separations require elevated temperatures to dissolve samples for analysis. For most samples, temperatures requirements exceed 130 ^{o}C and can be as high as 180 ^{o}C. Elevated temperatures limit the detectors available for these separations, as most manufacturers do not build detectors capable of withstanding such harsh conditions. Additionally, most detectors used for high temperature separations are placed into a detector oven, which adds geometrical and size constraints to the detector footprint.

There are five detectors that are in current use within industry for high temperature applications: light scattering (LS), infrared (IR), capillary viscometer (CV), ultraviolet (UV), and evaporative light scattering (ELSD) detectors. LS, IR, and viscometer detectors are placed into a detector oven, such as the separations system from PolymerChar (Valencia, Spain) or the PL-220 from Agilent (Santa Clara, CA). ELSD and UV detectors operate as standalone models with independent heating control and heated transfer lines. For all detectors, most sensitive electronic components (e.g., control boards) of the detectors are kept in a separate compartment at near ambient temperature.

For the UPI work, silicon photonic microring resonators were proposed as the detector to achieve linear mass concentration detection under gradient conditions. Microring resonator arrays are a class of refractive index (RI) sensitive detectors that are part of analytical sensors known as whispering gallery mode optical resonators.[1] The advantage of the microring resonator platform is the exquisite surface sensitivity (1×10^{-7} RIU) combined with an enormous dynamic range (>0.1 RIU). A number of recent reports detail progress toward the development of this detection platform.[2,3]

The experiment conditions for polyolefin separations required the development of a flow cell that could withstand the elevated temperatures (up to 180°C) and solvents that dissolve materials currently used in flow cell construction (e.g., polyetheretherketone (PEEK), polytetrafluoroethylene (PTFE), polypropylene). In collaboration with Dow's Tool and Dye Shop, a series of prototype materials were designed, built, and evaluated in-house. The following results detail the various designs and highlight key learnings as part of the prototyping process. Importantly, these learnings of high temperature flow cells are

not limited to the development of polymer separation detectors. This is because many analytical methods for polyolefins require elevated temperatures and strong organic solvents, lessons from this work are likely broadly applicable to analytical measurements, automation, and robotics for polyolefins.

2. Experimental Procedures

2.2. Chemicals and Materials

All chemicals for this study were purchased from ThermoFisher Scientific (Waltham, MA). Trichlorobenzene (TDB) was used a solvent. Prior to use, TCB was supplemented with 200 ppm of ionol (butylated hydroxytoluene [BHT]) as an antioxidant. Previous lots of TCB contained particulate matter that interfered with light scattering detection. After the addition of ionol, TCB underwent recirculation through a 0.07 μm nylon filter from Pall Corporation (Port Washington, NY) for a minimum of 3 hours prior to use.

2.3. Microring Resonator Detection Platform

Microring resonator sensor array chips and Maverick M1 detection system were purchased from Genalyte Inc. (San Diego, CA). Sensor fabrication and instrument operation have been described previously.[4] Briefly, the sensor array chips are batch fabricated on silicon-on-insulator wafers using deep UV photolithography. Each chip contains 128 individually addressable microring sensors. A schematic of a sensor chip is provided in Figure 4-1A. Sensors are serially interrogated using a tunable infrared laser centered at 1550 nm. Light is coupled onto the chip via free space coupling with grating

couplers from an optical head directly above the chip surface. Light transmittance through the sensor chip is continuously monitored. Under specific resonance conditions define by the following equation results in dips in the transmittance signal at narrow wavelengths:

$$m\lambda_{res} = 2\pi r n_{\text{eff}} \qquad \textit{Equation 1}$$

where λ_{res} is the resonant wavelength, m is an integer, $2\pi r$ is the circumference of the microring sensor, and n_{eff} is the effective RI at the sensor surface. Changes in n_{eff} at the sensor surface result in changes in λ_{res}, which is monitored over time. In this way, each microring resonator sensor operates as a RI sensor sensitive to RI changes at the sensor surface. A schematic of sensor operation is provided in Figure 4-1B-C. Additional details on instrument components including the flow cell are provided below. The components for the ambient temperature flow cell were purchased from Genalyte. All high temperature flow cell components were fabricated in-house.

3. Results and Discussion

3.1. Ambient Temperature Flow Cell Design

Solvent is guided across the sensor surface with a fluidic assembly. This assembly sandwiches the sensor chip between a cartridge base and a fluidic gasket. A cartridge top secures the gasket atop the sensor chip and allowed for chip-to-world connections for easy interfacing to other instrumentation or pumps. The cartridge holder was machined from aluminum and the sensor chip was placed in a cut out. The base snaps into the instrument below the optical head for fast and reproducible optical alignment. The fluidic gasket was laser cut from 0.007” biaxially oriented polyethylene terephthalate (Mylar®),

and the cartridge top was fabricated from polytetrafluoroethylene (PTFE/Teflon). Schematics of flow cell components are provided in Figure 4-2.

3.2. Material Selection for High Temperature Flow Cell Design

The material choice for the high temperature flow cell was guided by two characteristics: (1) chemical resistance to solvents for high temperature polymer separations and (2) stable operation at temperatures up to 180°C. The gasket and cartridge top components of the ambient temperature flow cell met neither criterion. Stainless steel was chosen for the cartridge top and was machined in-house by the Tool & Dye shop at Dow. The cartridge base was also machined at Dow out of stainless steel, replacing the original anodized aluminum base. Kalrez ® and Viton™ were chosen as gasket materials. These are fluoropolymer rubbers that can be manufactured as thin sheets. The gasket consists of an optical window and two fluidic channels, which were added using a punch. The punch was also machined in-house at Dow.

3.3. 1st Generation High Temperature Flow Cell

The first-generation flow cell was designed to position the cartridge heater away from the cartridge top to prevent contact between the heater and solvents. This consisted of a winged flow cell design where the one wing held the temperature probe, and the other wing held the cartridge heater. See Figure 4-3 for a schematic of this design.

Initial testing indicated that the heat transfer across the flow cell was slow. Consequently, the zone near the cartridge heater reached extreme heats (>300 °C) with only slight changes observed for the temperature probe zone. Additionally, the anodized

aluminum flow cell handle heated much faster than the rest of the flow cell. Table 4-1 provides a table of heat transfer coefficients for materials used in the flow cell construction. The low thermal conductivity of stainless steel was judged to be too slow to allow for effective temperature control for the cell.

3.4. 2nd Generation High Temperature Flow Cell

The second-generation design sought to address the poor heat transfer of stainless steel by placing the cartridge heater and temperature probe in the cartridge top (Figure 4-4). The cartridge top has both inlet and outlet for the solvent and is of greatest concern to maintain temperature. The ambient temperature flow cell contains 4 fluidic ports: two inlets and two outlets (see Figure 4-2). For this design, the bottom two fluidic ports were replaced with ports for the cartridge heater and temperature probe, and the schematic presented in Figure 4-4. However, given the size constraints of the cartridge top, only a portion of the heater fit into the top. As such, the heater produced a significant amount of heat that caused significant oxidation to the heater probe itself and posed a significant fire hazard even when set to modest temperature settings (e.g., 60 °C). Note that in the 1st and 2nd generation prototyping phase, no flammable solvents were introduced into the flow cell because of solvent proximity to the heater.

To address the safety concern of the exposed heater, a stainless steel piece was added to the flow cell for both the heater and temperature probe (Figure 4-5). This assisted with securing the components in place, but heat transfer to the cartridge top was still poor. The temperature differential between the cartridge top and heater sheathing was >60°C. As such, this design was untenable.

The key learnings from the second-generation design was that: (1) the cartridge heater must be fully enclosed in the flow cell for safety concerns and (2) the temperature probe and heater must be in direct proximity for adequate temperature control.

3.5. 3rd Generation High Temperature Flow Cell

The final iteration of the high temperature flow cell design enabled successful operation of the microring resonator system at temperature. The design was a hybrid of the 1st and 2nd generation experiments. This design included two cartridge heaters and two temperature probes in the winged format from the 1st generation (Figure 4-3). Each probe was placed next to each heater. This was done to prevent overheating of parts of the flow cell near the heater and avoids prolong waiting periods for the thermal equilibration. As in the 1st generation design, the heated portions of the flow cell were separated from the fluidic connections to minimize potential fire hazards with flammable solvents. A schematic of the third-generation design is provided in Figure 4-6.

The initial testing of the 3rd generation prototype on the benchtop (i.e., not placed into the microring resonator instrument) found an approximately 50 °C temperature difference between ends where the heater and temperature probes are located and the cartridge top. The cartridge top reached 60 °C with the temperature controller set to 120 °C. When placed into the instrument the temperature difference between heater and cartridge top was reduced to 20 °C after a 15 minute thermal equilibration period. However, significant heat was lost to the surrounding area.

To minimize heat loss, woven fiberglass insulation was placed around the flow cell (insulation can be observed in Figure 4-9). This resulted in the cartridge reaching 95 °C with the temperature controllers set to 180 °C after a 20 minute thermal equilibration. However, insulation of the flow cell caused issues with instrument operation. This was attributed to insulation particles on the optical head interfering the positional registration of the laser. This was solved with periodic cleaning of the optical head, but insulation was eventually abandoned because of the registration issues that it caused.

3.6. Microring Resonator Instrument Operation at Elevated Temperature

3.6.1. Sensor Operation at 100 °C

To first probe the quality of sensor operation at temperature, the flow cell temperature was held to 100 °C in air (i.e., no solvent flowing). This resulted in continuous oscillation of the sensor response (Figure 4-7). The variable response was attributed to temperature oscillations caused by the temperature controllers attempting to maintain the fixed temperature. This could pose a significant challenge for subsequent polymer chromatography. For reference, typical microring resonator response from polystyrene standards is on the order of 10 pm. If the oscillations are reproducible across both channels (see Figure 4-1A), one channel could be used as a reference to remove temperature-driven signal response. Additionally, the temperature controller manufacturer (Fluke Corporation, Everett, WA) recommends that the heating area is well insulated with a continuous airflow. These requirements are not feasible for these initial prototyping experiments.

3.6.2. Sensor Operation Under Dynamic Temperature Conditions

Unpublished results from Prof. Bailey's lab had previously indicated stable operation of the platform at temperatures near 100 °C, but thermal cycling or temperature ramping at temperatures above 100 °C were unknown. To determine sensor robustness to changing temperatures, data collection was started under ambient conditions followed by setting the temperature controller to a modest 30 °C and increasing at 10 °C increments once thermal equilibrium was reached at a given setting. Figure 4-8 shows the effect of increasing temperature during data acquisition. For the lower temperatures (<40 °C), the signal response is uniform across the rings with minimal deviation in the signal over time. However, as the temperature continues to increase, the variance of the ring response continues to increase. Additionally, of the 64 ring sensor being actively monitored, only 5 rings produced useable responses during the course of the full run. Comparatively, in a standard run with aqueous solutions under ambient conditions, all 128 rings remain usable for more than 4 hours of continuous data acquisition. Consequently, the temperature variation appears to play a significant role in sensor operation.

3.6.3. Flowing Hot Trichlorobenzene through the Flow Cell

The dynamic temperature conditions resulted in poor sensor performance, but detector temperature is typically fixed for high temperature polymer separations. To assess sensor performance under relevant conditions, trichlorobenzene (TCB) was used a solvent. The TCB was pumped using a PolymerChar (Valencia, Spain) unit maintained at 160 °C, and a heated transfer line was used to connect the eluent from

the PolymerChar system to the flow cell inlet (Figure 4-9). The top picture here shows the side view of the flow cell in the flow cell holder, and the bottown shows a head-on perspective of the same setup.

Leaking occurred at flow rates exceeding 0.2 mL/min. With the Mylar gasket from the ambient flow cell, leaking can be addressed by increased tightening of the fluidic assembly using the 3 screws in the cartridge top. However, additional tightening with the Kalrez® gaskets appears to compress the fluidic channels and cause leaking. To prevent leaking, the screws were tightened enough to hold the cartridge top in place but not so much that it compressed the fluidic channels. Proper tightening was determined through trial and error, but no leaking was observed after more than an hour of flow at 1 mL/min after the optimal tightness was found.

After the leaking issue was addressed, proper registration of the laser beam with the grating couplers on the chip emerged as another limiting factor. It was observed that flowing TCB through the flow cell caused the Kalrez® gasket to swell. The gasket expansion extended onto the grating couplers. The grating couplers are used for the free space coupling of the laser light onto the sensor chip, and any obstruction of this region of the chip prevents sensor operation. An alternative fluoropolymer elastomer material was then tested to circumvent the swelling issue. Viton^{TM} appeared to swell more slowly than the Kalrez® material but swelling occurred nonetheless. The solution to the registration issues was to remove a portion of the gasket material between the optical window and the first fluidic channel (Figure 4-10).

3.6.4. Sensor Operation at High Temperature with Flowing Trichlorobenzene

With the solvent leaking and registration issues addressed, sensor operation could be tested under relevant temperature and solvent conditions for high temperature separations. Compared to a conventional detector, the amount of instrumentation required to operate the detector was remarkable. Figure 4-11 is an image taken of the entire assembly with TCB flowing through the flow cell. Importantly, a commercial version of the detector would not be feasible with such extensive equipment.

Unfortunately, the diminished performance observed at 100 °C in air were worse at 160 °C with flowing heated TCB. An example of detector performance under th conditions is provided in Figure 4-12. The data included Figure 4-7 and Figure 4-8 removed poorly performing microring sensors from the provided plots. In Figure 4-12, all microrings are included in the plot, with each sensor having a unique color. The beginning of the run shows a general increase in sensor response oscillating in a similar manor as observed in Figure 4-7. However, over the course of the run, the response from the majority of rings becomes unusable. After less than 1 hour of flowing TCB, all but 64 of the microrings is lost. The microring sensor loss is reproducible and all microring sensors are lost within 2 hours after beginning data acquisition.

The cause of reduced performance at elevated temperatures is unclear. One hypothesis is that the increased temperature of the air gap between the optical head and grating couplers causes poor coupling of the light onto the chip. The coupling efficiency onto the chip varies exponentially with insertion angle. Therefore, a significant increase in temperature could alter the coupling angle by changing the RI of the air. Alternatively, light propagation in the linear waveguides is dependent upon the RI contrast between the

sensor chip and the environment directly at the sensor surface. The higher refractive index of TCB (1.57) versus aqueous solutions (1.3-1.4) could provide poorer confinement of light in the waveguides.

4. Conclusions and Future Directions

The design, prototyping, and testing of the high temperature flow cell for the microring resonator detection platform was able to successfully operate under the experimental conditions demanded for polyolefin separations. However, an undetermined aspect of the experimental setup described in more detail below prevented polyolefin separations with the current flow cell prototype because of the degraded sensor performance.

There are several possible avenues that could improve the sensor performance. The most important next step is to identify the key drivers of reduced performance. The variables to consider are temperature, temperature variation, and solvent. Adding an insulation housing for the flow cell would substantially reduce the temperature oscillations during a run. Reduced temperature fluctuation would allow for assessment of whether the poor sensor performance is caused by elevated temperatures, temperature oscillations, or a combination of the two. If the insertion angle of light into the gradient couplers is the issue, this could be solved by altering the optical head positioning, though this would likely confine sensor operation to either high temperature or ambient sensor operation but not both. If TCB is the cause of poor ring performance independent of gasket swelling, various alternative solvents (e.g., dibutoxymethane) are available.

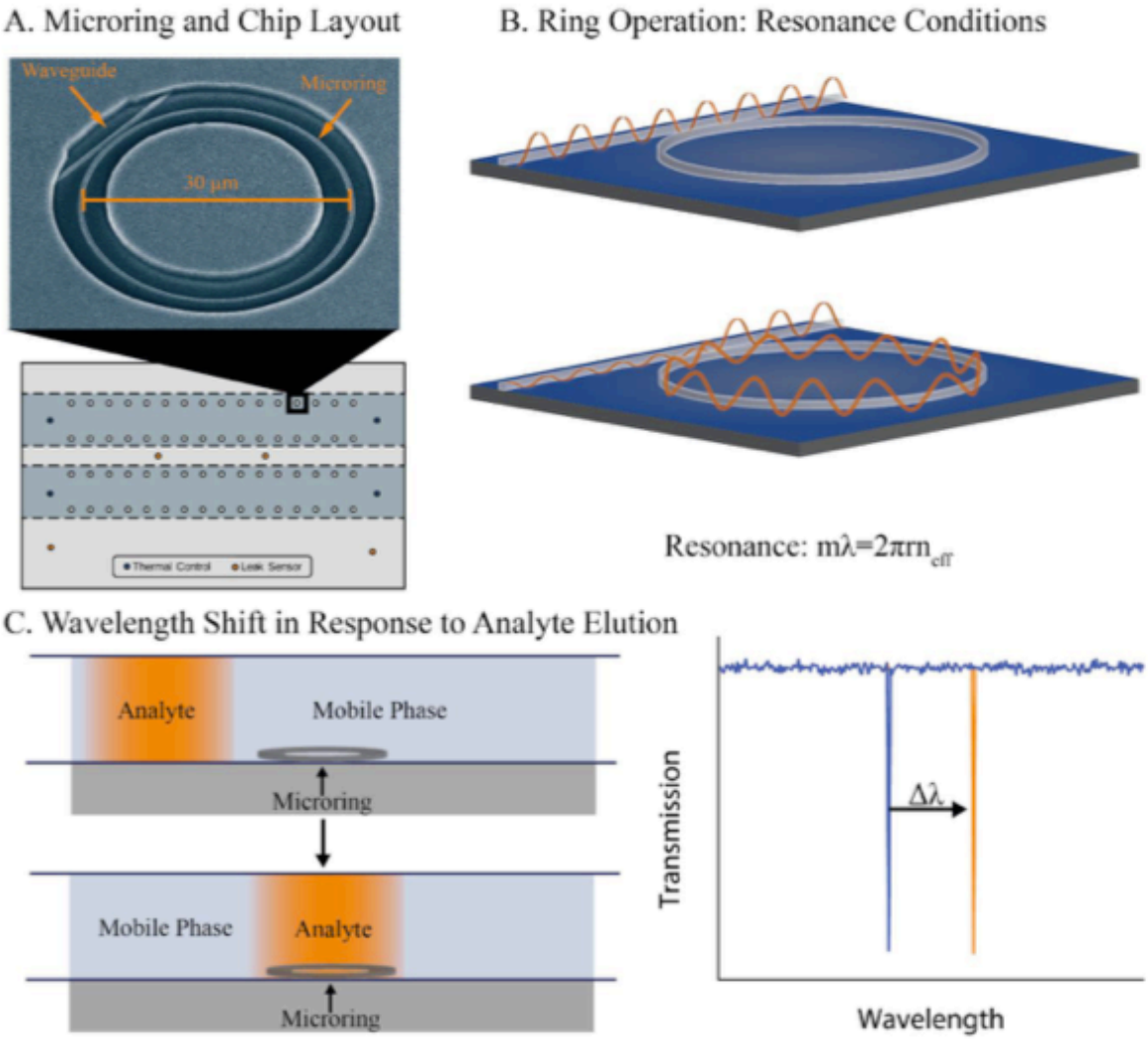

Figure 4-1. Microring Resonator Sensor Array Chip Layout and Schematic of Sensor Operation. (A) The schematic of the sensor layout consists of 2 fluidic channels and each channel consists of 32 clusters of 4 microring sensor. (B) Under non-resonance conditions, light propagates down the waveguide and does not couple into the microring. The resonance condition shows light coupling into the microring and attenuation of light that continues to propagate down the waveguide. (C) Upon a shift in RI at the sensor surface (for example analyte elution) the resonant wavelength (λ_{res}) will shift (see Equation 1), and shifts in resonant wavelength are monitored over time. Reprinted with permission from J. H. Wade, R. C. Bailey, Refractive Index-Based Detection of Gradient Elution Liquid Chromatography using Chip-Integrated Microring Resonator Arrays. *Analytical Chemistry* **86**, 913-919 (2014); published online 2014/01/07 (10.1021/ac4035828). Copyright (2014), American Chemical Society.

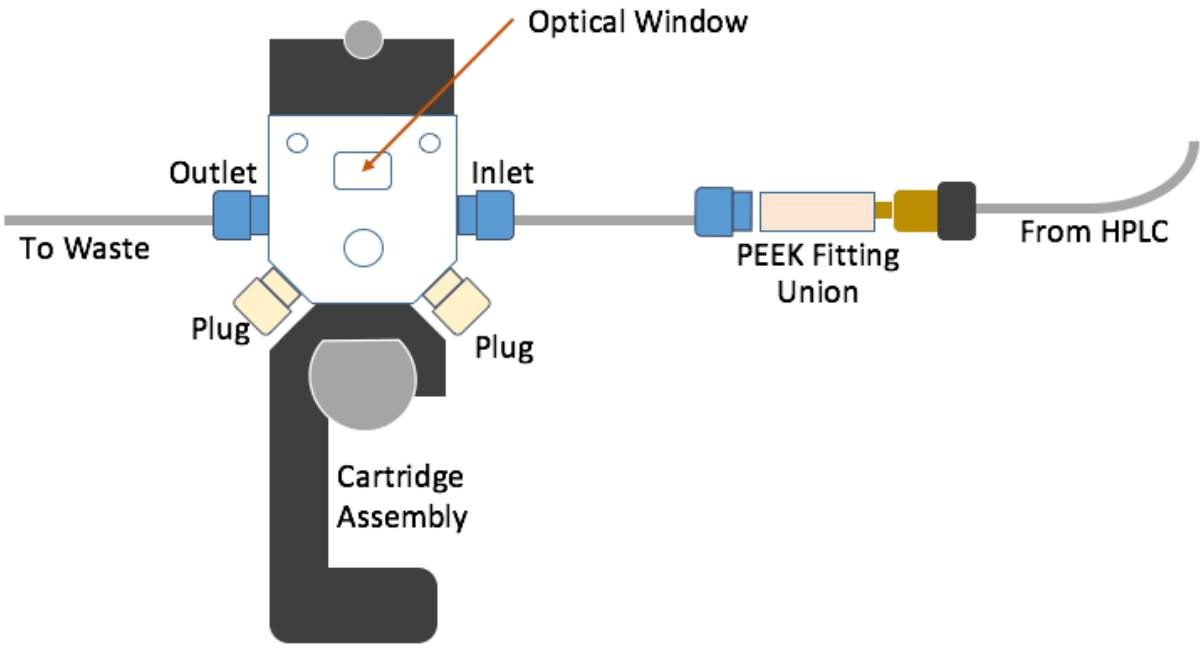

Figure 4-2. Schematic of Flow Cell for Ambient Temperature Operation.

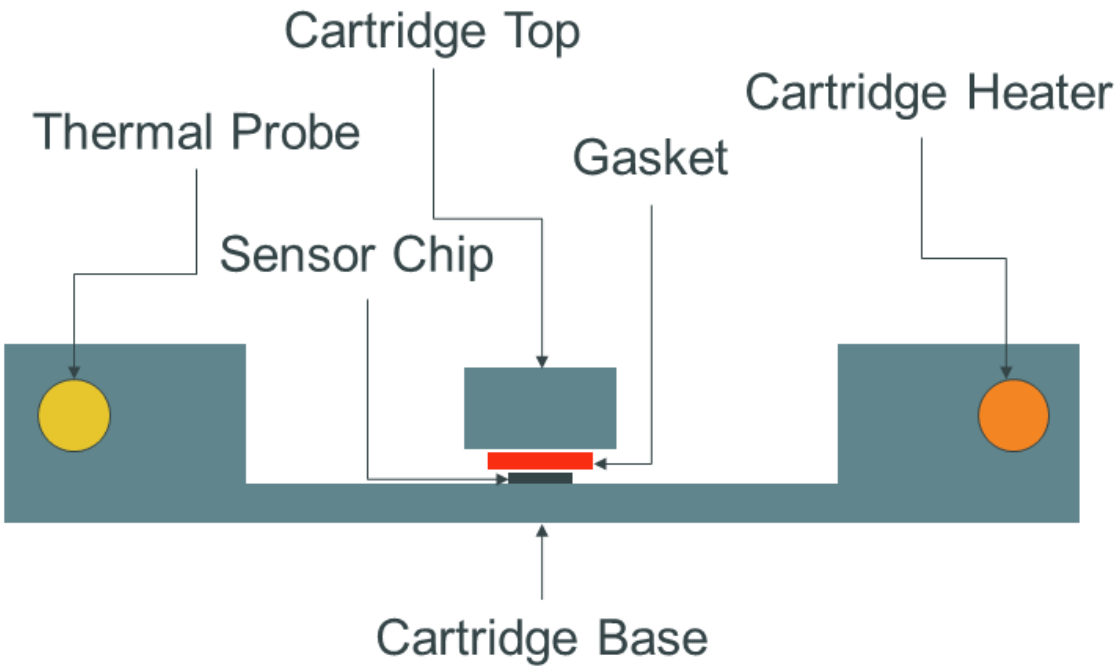

Figure 4-3. First-Generation Schematic of High Temperature Flow Cell Design.

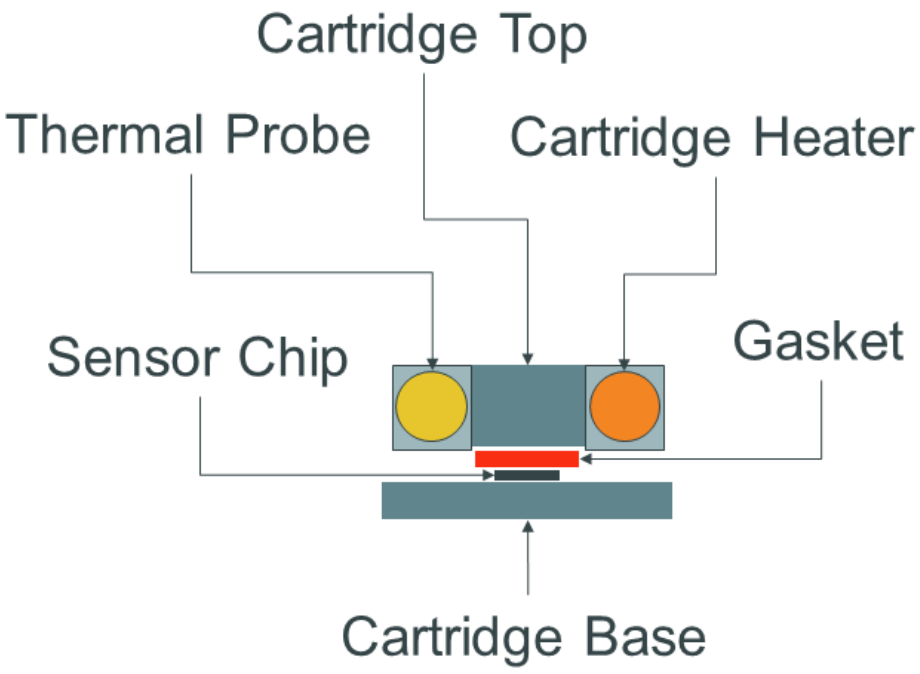

Figure 4-4. Second-Generation Schematic of High Temperature Flow Cell Design.

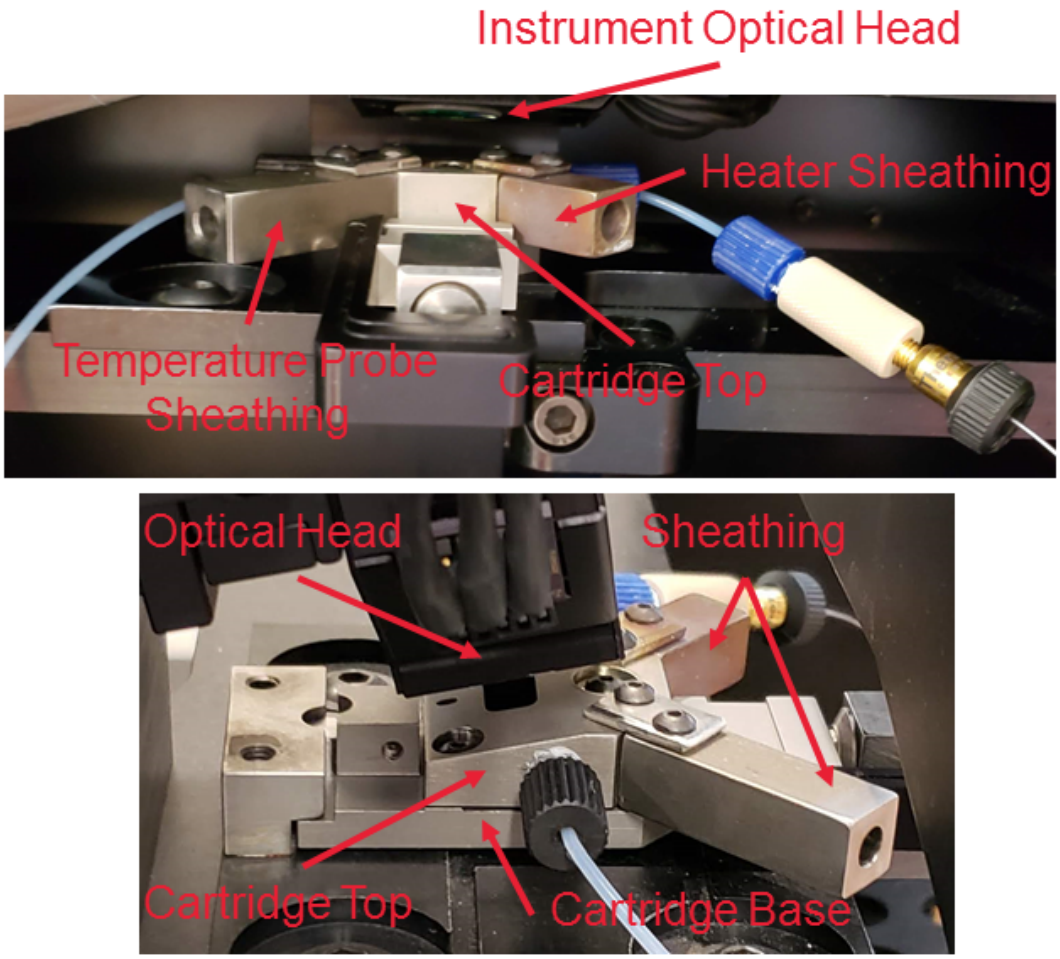

Figure 4-5. Second-Generation Flow Cell Prototype Testing. The images show the flow cell placed into the microring resonator instrument. The optical head must be directly above the sensor chip for instrument operation, which placed significant constraints on the flow cell design.

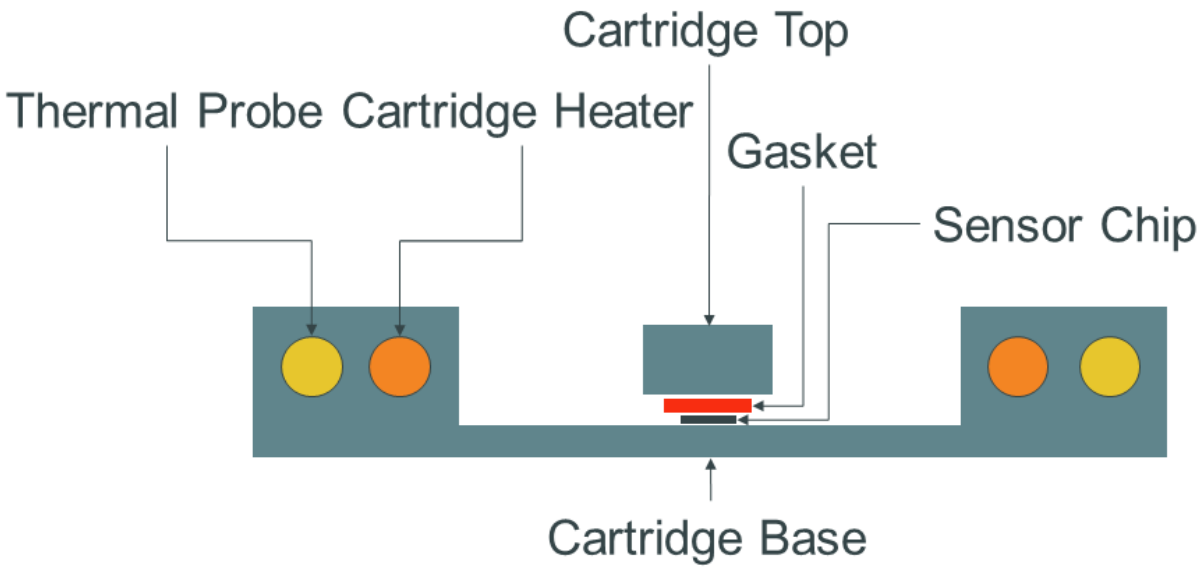

Figure 4-6. Third-Generation Schematic of High Temperature Flow Cell Design.

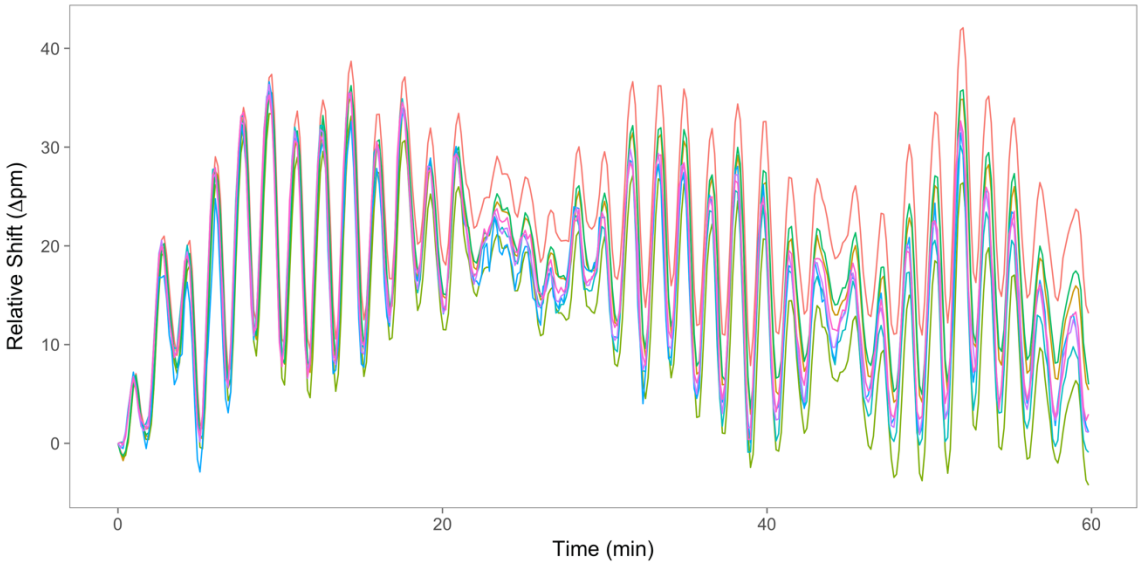

Figure 4-7. Microring Resonator Array Response at Elevated Temperature (100°C). Each trace corresponds to a single ring of the 128 on the sensor chip. This is a subset of the 10 best performing rings at 100°C. The periodic oscillations are caused by the temperature controllers attempting to maintain a constant temperature.

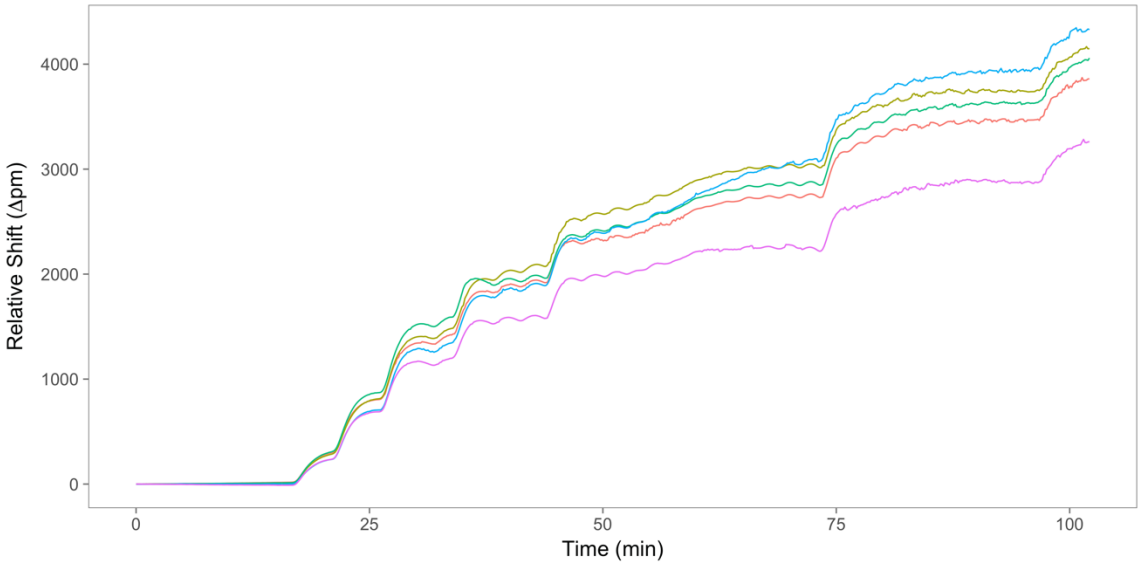

Figure 4-8. Microring Resonator Sensor Operation while Increasing Temperature.

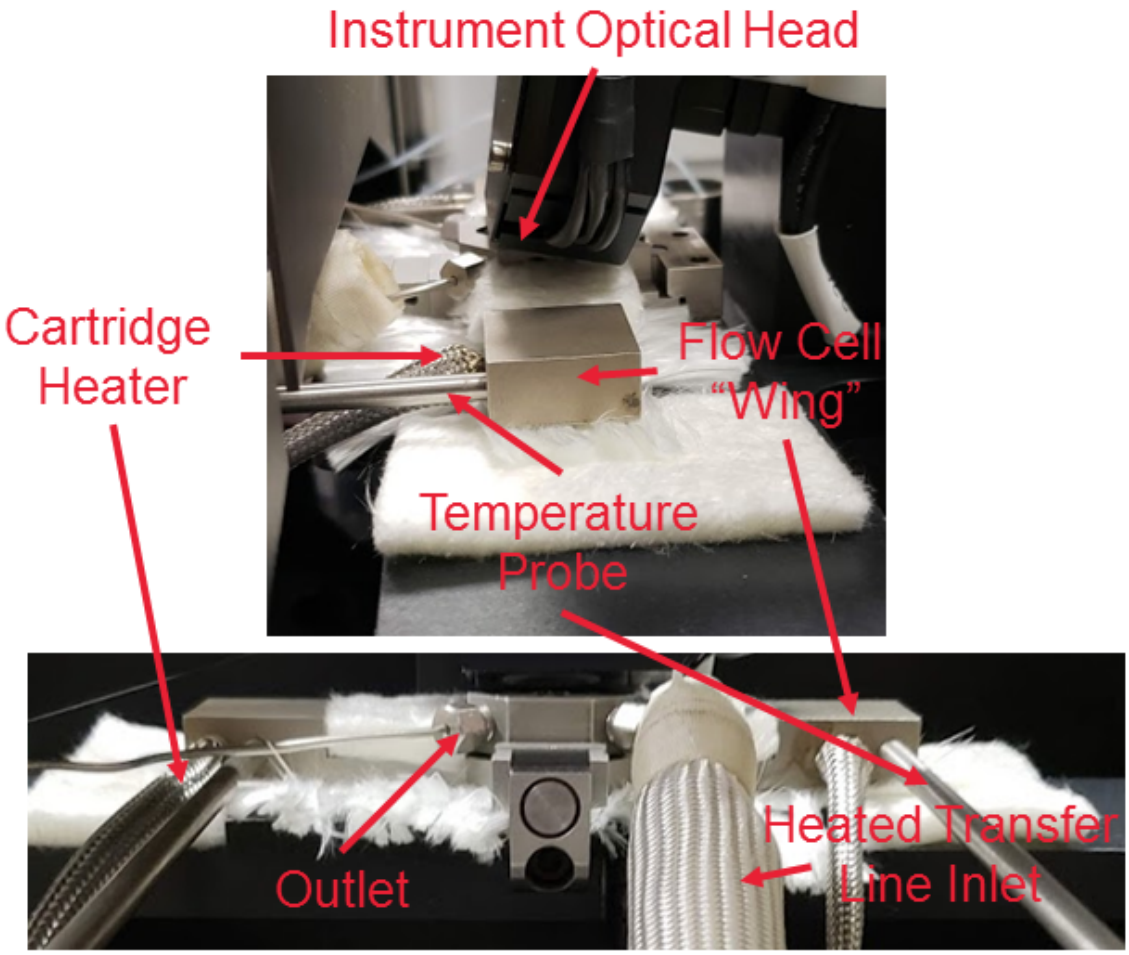

Figure 4-9. Flow Cell Placed into Microring Resonator Instrument. The flow cell with heated transfer line connected and insulated. The top image shows the side view of the flow cell in the flow cell holder, and the bottown shows a head-on perspective of the same setup. Both pictures highight the geometrical contraints on the flow cell design.

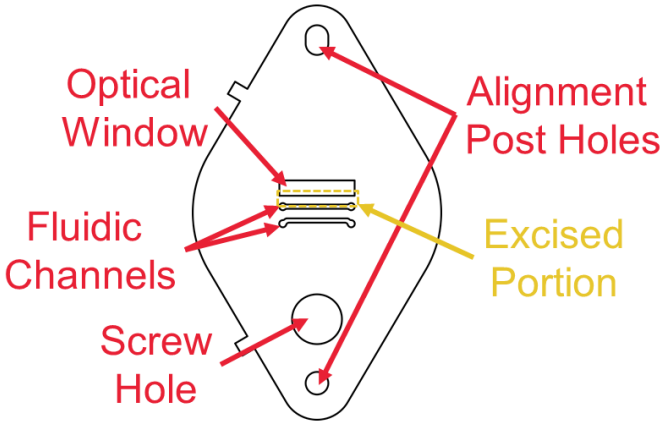

Figure 4-10. Fluidic Gasket Schematic. Due to gasket swelling issues material which interfered with grating couplers was removed to enabled laser registration of the chip.

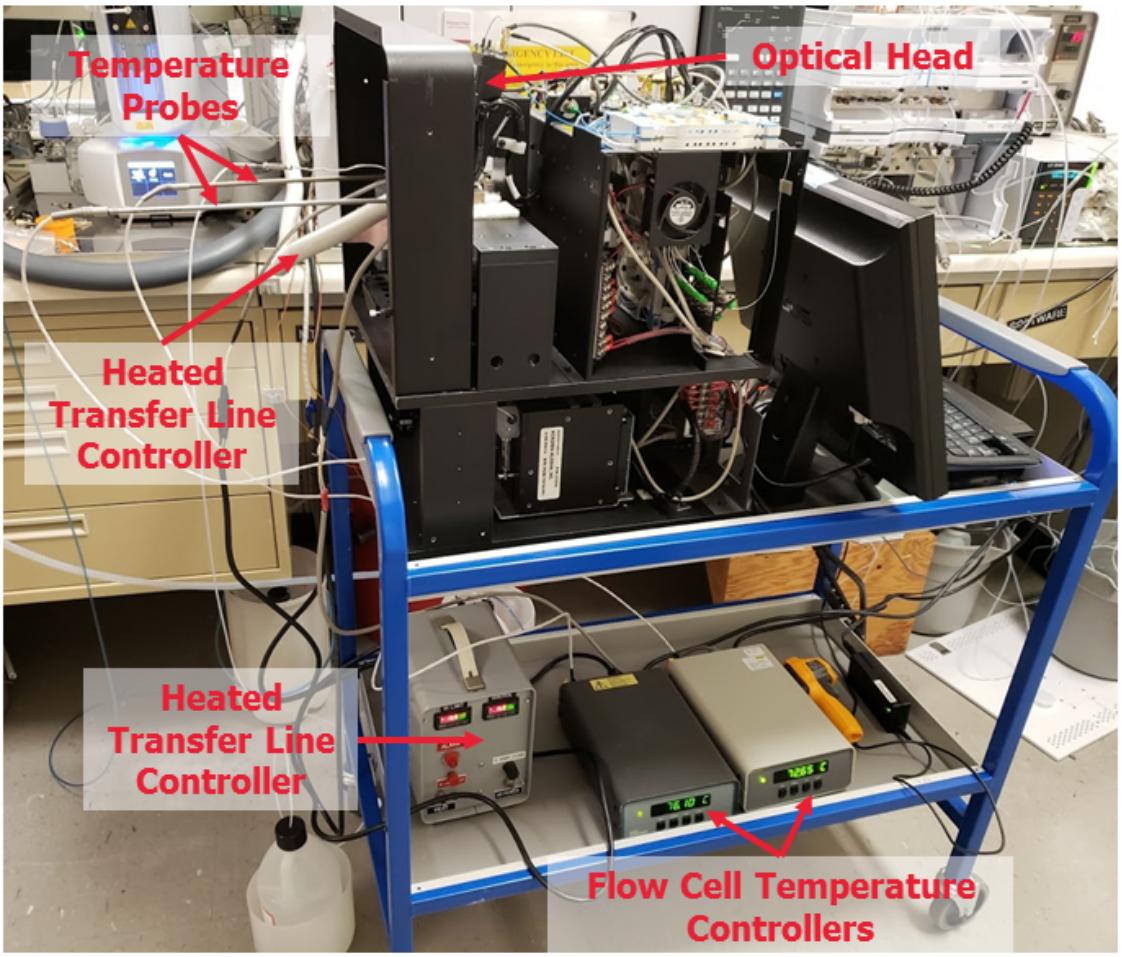

Figure 4-11. Complete Detector Assembly with Temperture Controllers.

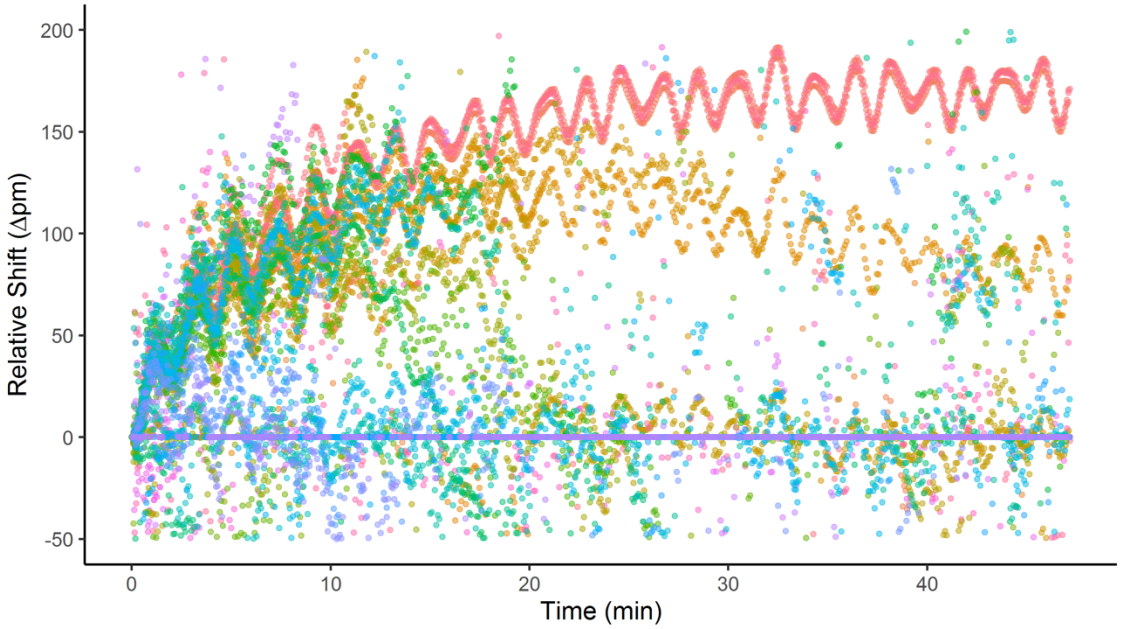

Figure 4-12. Microring Resonator Sensor Operation at 160°C and Flowing TCB. Signal is no longer useable under these conditions. Each microring has a unique color.

Table 4-1. Thermal Conductivity of Flow Cell Construction Materials

Material	Thermal Conductivity ($W\ m^{-1}\ K^{-1}$)	Flow Cell Component
Stainless Steel	16-24	Cartridge base and top
Aluminum	160-220	Cartridge handle and instrument body
SOI wafer	0.5-1.4	Sensor Chip
Mylar	0.15-0.4	Fluidic Gasket
Kalrez	0.17-0.19	Fluidic Gasket
Viton	0.15-0.30	Fluidic Gasket

5. References

(1) J. H. Wade, R. C. Bailey, Applications of Optical Microcavity Resonators in Analytical Chemistry. *Annual Review of Analytical Chemistry* **9**, 1-25 (2016)10.1146/annurev-anchem-071015-041742).

(2) J. H. Wade, R. C. Bailey, Refractive Index-Based Detection of Gradient Elution Liquid Chromatography using Chip-Integrated Microring Resonator Arrays. *Analytical Chemistry* **86**, 913-919 (2014); published online Epub2014/01/07 (10.1021/ac4035828).

(3) D. Meunier, T. Pangburn, W. Degroot, P. O'Connor, Z. Wiersma, J. Wade, R. Bailey, Towards the Development of a Refractive Index-Based Optical Microcavity Mass Concentration Detector Compatible with Gradient Elution Liquid Chromatography: First Year Progress Report on UPI Project 226772AE with University of Illinois. Dow CRI Report ACCN 2016074852, Issued October 7th, 2016. (2016); published online Epub10/7

(4) M. Iqbal, M. A. Gleeson, B. Spaugh, F. Tybor, W. G. Gunn, M. Hochberg, T. Baehr-Jones, R. C. Bailey, L. C. Gunn, Label-Free Biosensor Arrays Based on Silicon Ring Resonators and High-Speed Optical Scanning Instrumentation. *IEEE Journal of Selected Topics in Quantum Electronics* **16**, 654-661 (2010)10.1109/JSTQE.2009.2032510).

CHAPTER V

A Linear Mass Concentration Detector for Solvent Gradient Polymer Separations

Acknowledgements

This chapter has been reproduced here with permission from the Royal Society of Chemistry © 2020.[+] The citation to the original publication is the following:

Mordan, E.H.; Wade, J. H.; Pearce, E.; Meunier, D. M.; Bailey, R. C. A Linear Mass Concentration Detector for Solvent Gradient Polymer Separations. *Analyst.* **2020**, 145,4484-4493. https://doi.org/10.1039/C9AN02533B.

My contribution to this work is the following: solvent gradient method development and optimization, execution of all experiments, development of R code for data processing and baseline subtraction, all data analysis and workup, and finally I wrote the

[+]https://www.rsc.org/journals-books-databases/journal-authors-reviewers/licences-copyright-permissions/#deposition-sharing

presented article. James Wade, Eric Pearce, and David Meunier contributed in choice of system, experimental design, data interpretation, as well as article revisions.

Lastly, the authors acknowledge financial support from The Dow Chemical Company through the University Partnership Initiative Program. Ryan C. Bailey acknowledges support from the National Science Foundation through Award 1744105.

Abstract

Characterization of copolymers requires the measurement of two distributions—molecular weight (MW) and chemical composition (CC). Molecular weight distributions (MWD) are traditionally determined using size exclusion chromatography (SEC) run under isocratic solvent conditions. Chemical composition distributions (CCD) are often determined using liquid adsorption chromatography (LC) with solvent gradients. The use of solvent gradients, however, often limits options of compatible detectors. A gradient compatible, universal linear mass concentration detector is a longstanding unmet need. Many industrially-relevant polymers lack chromophores or other discriminating moieties requiring detectors with a universal response. Differential refractive index (dRI) is incompatible with gradient elution due to its small dynamic range. Charged aerosol detectors (CAD) and evaporative light scattering detectors (ELSD) are probably the most promising options for gradient elution detection, but both suffer from a non-linear mass concentration response and a solvent dependence. Silicon photonic microring resonators are optical sensors that are responsive to changes in the local refractive index (RI). The substantial dynamic range of this technology makes it attractive for refractive index-based detection during solvent gradient elution. Previously, the microring resonator platform was

used as a SEC detector to characterize the MWD of broadly dispersed polystyrene (PS) standards. In this study, we demonstrate the gradient compatibility of the microring resonator platform for polymer detection by quantifying the CCD of polymer blend components. Control experiments were run with UV and ELSD detection, highlighting the uniqueness of the platform as a linear mass concentration detector with a universal detector response.

1. Introduction

Characterizing polymeric samples by size, composition, structure, and purity can help solve many challenges in industrial polymer manufacturing. Comprehensive characterization of polymers requires a suite of analytical methods with the ultimate goal of establishing structure property relationships.[1] Continuing advances in polymer chemistry and advanced manufacturing have enabled commercial viability of increasingly complex polymer systems. This complexity demands continued advances in polymer characterization methods.[2] For instance, homopolymers such as polystyrene or high density polyethylene can be well characterized by molecular weight distributions (MWD).[1] The standard bearer for MWD determination is size exclusion chromatography (SEC) coupled to a UV/Visible (UV) or differential refractometer (dRI) for linear mass concentration detection.[3-5]

Nearly all modern product development in the polymer industry involves copolymer commercialization because of the need for a balance of properties in most new materials. Polymers with two or more incorporated monomers leads to an inherent chemical composition distribution (CCD). Much like MWD, CCD dictates many physical properties

of polymers including melt temperature, thermal stability, solubility, and mechanical properties such as tensile strength.[1,6] As such, CCD measurements are a vital component of copolymer characterization.

Traditional techniques for characterizing chemical composition (CC) of copolymers include mass spectrometry (MS), various spectroscopic methods, and liquid chromatography (LC). MS and spectroscopic methods (e.g., NMR, FT-IR) provide an averaged measure of CC rather than a distribution. Given that copolymers are heterogeneous in both CC and MW, a compositional average does not provide the most comprehensive characterization.[7] More informative distribution measurements require a separation of polymer components. Therefore, CC characterizations by MS or NMR often use preparative fractions obtained by SEC or LC, or these techniques are often hyphenated directly in-line with these separations methods.[8-12] However, the complexity of these hyphenated techniques is such that gradient elution high performance liquid chromatography (HPLC) has emerged as the most commonly used approach for CCD measurements in practice.[13]

Gradient elution LC achieves separations based on CC and functions by increasing the elution strength of the mobile phase throughout the experiment. Analytes with a high affinity for the stationary phase adsorb onto the column and are eluted once there is a higher affinity for the mobile phase.[14] The challenge, however, with gradient LC is a lack of available/ compatible detectors.

The most common options for GPC characterization of polymers include dRI, UV, charged aerosol detectors (CAD),[4,15,16] and evaporative light scattering detectors

(ELSD);[17-20] however, each of these has limitations for certain applications. dRI lacks the dynamic range to track the gradient baseline and obviously any analytes eluting during the gradient. UV detectors, widely used in gradient LC, give linear mass concentration response, but many industrial polymers, including polyolefins, polyacrylates, and polyalkoxides lack chromo- phores.[21] Because of their universal response, CAD and ELSD are preferred as gradient compatible detectors for polymer analysis. Both CAD and ELSD nebulize and evaporate off the mobile phase prior to detection, but they give a non-linear response as a function of polymer concentration and solvent composition. This non-linearity is a major limitation of both CAD and ELSD for industrial polymer CCD as it substantially complicates quantitative measurements.[20,22,23] It is important to mention that one approach to overcoming ELSD non-linearity is actually linearizing the response. This is often done by applying a correction to the ELSD signal and has been shown to give good correlation with isocratic GPC data compared to traditional detectors.[24]

Silicon photonic microring resonators are a type of whispering gallery mode optical sensor that detects small changes in refractive index (RI) at the sensor surface.[25] The microring resonator platform offers a very large RI dynamic range making the sensor gradient compatible, as has been previously demonstrated.[26] This is in contrast to conventional dRI detectors, which are not gradient compatible because of their small dynamic range. As a result, dRI detectors can only be used for CCD type measurements as a concentration detector for an isocratic dimension in concert with multidimensional separations.[27]

Typically, the microring resonator platform is implemented as a biosensor for monitoring molecular binding events on the sensor surface.[25, 28-30] Much work has also been done interfacing similar optical resonator detectors with various separation methods such as gas chromatography[31] and capillary electrophoresis,[32-34] and recently a microwave interferometer was interfaced with HPLC for gradient separations.[35] In addition, our previous work demonstrated the applicability of microring resonator platform for industrial polymer analysis. Here we interfaced SEC separations with the microring resonators to determine the MWD of broad range polystyrene (PS) standards. These experiments were performed in conjunction with separate dRI and UV experiments to demonstrate the agreement of MWD determined by the microrings to these conventional detectors.[36]

Herein, we demonstrate the quantification of CC by utilizing the microring resonator platform as a RI based gradient elution detector. Using poly(styrene-co-methyl methacrylate) (PS-PMMA) copolymer standards, the microring resonator platform was calibrated for polystyrene (PS)/polymethacrylate (PMMA) composition. The mass linearity of the microring resonators was demonstrated and directly compared to identical experiments performed with UV and ELSD detection. Additionally, copolymer blends were created using the same PS-PMMA standards and these blends were analyzed using all three detection methods. The composition calibration allowed for identification of blend components, while mass calibrations allowed for quantification of the abundance of each component. These results demonstrate the versatility and applicability of the microring resonator platform for characterizing industrial polymers with a single detector.

2. Experimental

2.1. Materials

High purity solvents were all purchased from Sigma-Aldrich (St Louis, MO). Poly(styrene-co-methyl methacrylate) (PS-PMMA) standards were purchased from Polymer Source, Inc. (Dorval, QC). Polystyrene (PS) and polymethacrylate (PMMA) homopolymer standards were purchased from Agilent (Santa Clara, CA). All polymer standards were used as received. Four 10 mg mL^{-1} PS-PMMA standards varying in PS content (82%, 54%, 31%, and 14% mol PS, provided by vendor) were prepared in chloroform and two 10 mg mL^{-1} homopolymer samples (70 kDa PS and 70 kDa PMMA) were prepared in chloroform.

2.2. Microring Resonators

The microring resonator system (Maverick M1 optical scanning instrumentation) and sensor array chips were purchased from Genalyte, Inc. (San Diego, CA). Detailed descriptions of sensor fabrication and instrument operation has been described elsewhere.[26] Microring resonators are ring-shaped optical cavities of 30 μm diameter with adjacent linear waveguides. 128 individually addressable microring sensors are arranged in an array on a 4 mm × 6 mm chip. Sensor chips have a protective photoresist coating that is removed before use by successively immersing chips in acetone and isopropanol baths, followed by an acetone rinse.

Each individual microring is probed by an external tunable cavity diode laser centered at 1550 nm. Optical transmission is monitored as a function of wavelength, and

dips in transmittance signal occur at resonant wavelengths defined by the following equation.

$$\lambda_r = \frac{2\pi r n_{eff}}{m}$$

where r is the ring radius, n_{eff} is the effective refractive index, and m is a constant. As the refractive index environment surrounding the sensor surface changes, such as analyte elution or a switching mobile phase composition, the resonant wavelength will shift. These changes in resonance wavelengths correspond to changes in n_{eff} which are monitored as a function of time and referred to as relative shift in units of delta picometers (Δpm).[25,37]

2.3. HPLC

Chromatographic separations were performed on a Waters Alliance e2695 separation module (Milford, MA) equipped with a Waters 2489 UV/Visible detector and a Waters 2424 ELSD detector. A Kromasil (Bohus, Sweden) column was used for all separations. Column dimensions were 250 mm × 4.6 mm and the packing material was 5 µm silica particles with 60 Å pores.[20,38-40] A 0.4 mL min^{-1} flow rate was maintained for a gradient of 95% cyclohexane (spiked with 5% tetrahydrofuran (THF)) to 90% THF (Table 5-1) and the column oven was held at 35 °C. To increase mass on the column, multiple 5 µL injections of polymer were injected in isocratic mode using initial gradient conditions.[41,42] This method was utilized to maintain small injections and prevent polymer breakthrough.[43] The Waters 2489 UV/Visible detector wavelength was set to 260 nm with a sampling frequency of 10 Hz. The Waters 2424 ELSD detector operated at a gain of

20, gas pressure of 20 psi, drift tube temperature of 50 °C, and a nebulizer temperature of 12 °C.

2.4. HPLC-Microring Resonator Interface

The microring resonator cartridge was assembled by placing the sensor chip on an anodized aluminum cartridge base followed by a polyethylene terephthalate (Mylar) gasket and a polytetrafluoroethylene (Teflon) cartridge top. The Mylar gasket and Teflon cartridge top direct fluid flow across the chip and the whole assembly is secured together by screws. 1/16″ PEEK tubing with a 0.25 mm flangeless 1/4-28 interface were used to couple the HPLC directly to the microring resonator cartridge, as described previously.[36] For a diagram of the cartridge assembly see Figure 5-1.

Once assembled the cartridge can be handled much like a flow cell, with a volume of approximately 2 µL, requiring no further handling of the sensor chip. Additionally the chip which is composed of silicon dioxide is robust enough to be used repeatedly without degraded sensor performance. Fouling is often an issue with surface based sensors especially with biological applications, however that is not an area of concern here since with LC methods analytes only come in contact with the sensor chip once they are in favorable solvents which mitigate any affinity they might have for the surface.

2.5. Data Analysis

Data analysis was carried out using custom software written in R (version 3.4.1) and RStudio (version 1.0153). Chromatograms were obtained for all the detection methods by plotting signal intensity as a function of time. Microring resonator data was

obtained for each individual ring and individual ring responses were averaged to obtain the averaged response. This averaged raw data was then baseline corrected to account for the sloping baseline resulting from the continually changing mobile phase composition (Figure 5-2). The sloping baseline spans over a relative shift exceeding 800 Δpm, therefore peaks on a scale of 2–15 Δpm are initially obscured by the background baseline and overlapping traces (see Figure 5-2A and B). Peaks begin to become slightly visible by zooming in on the raw chromatogram, dashed lines are used to guide the eye toward peak location, (Figure 5-2B) but this is still not sufficient for any useful identification or quantification. An alternative plot of Figure 5-2B is presented with Figure 5-3, which allows for better visibility of peaks before correction. Baseline correction was necessary to remove the background baseline caused by the solvent gradient. Baseline correction was performed by fitting the sloping gradient observed in Figure 5-2B to a third order polynomial and subtracting the fit from the raw data (seen in Figure 5-2C). The resultant chromatogram was smoothed with a locally estimated scatterplot smoothing function (LOESS), a common smoothing function for time series data.[44] The final corrected microring resonator chromatogram resembles chromatograms obtained by more traditional detectors, as shown in Figure 5-2D. All chromatographic calculations were performed on baseline corrected and smoothed data. Lastly, this baseline correction process is very robust since identical gradient methods will always observe the same RI change since this is a function of mobile phase, therefore baseline response is very reproducible making correction for this routine.

3. Results and Discussion

3.1. Gradient Separation of PS-PMMA Copolymers

The described gradient method outlined in Table 5-1 was applied to 0.15 mg injections of PS-PMMA copolymer samples prepared in chloroform, and varying in PS content covering the full range of 100%–0% moles PS (0%–100% moles PMMA). Peaks begin to elute from the column with increasing THF content, with 100% PS eluting the earliest in the gradient given that it is the least polar. Therefore, elution order is highest to lowest PS content (lowest to highest PMMA content), with the 100% PMMA standard taking the longest to elute from the column. Detection of the described separation was implemented using three detection methods; microring resonators (Figure 5-4A), ELSD (Figure 5-4B) and UV (Figure 5-4C). UV and microring resonators were connected in series, ELSD data was obtained in a separate experiment due to the destructive nature of the detection technique. A chart of the used flow path can be found in Figure 5-5.

A comparison of the UV, ELSD, and microring resonator detectors is shown in Figure 5-4. The most notable difference between the ELSD and microring resonator detectors is increased noise of the microring resonator chromatograms, where the average signal to noise ratio of the microrings is approximately 4 orders of magnitude smaller than UV and ELSD. This increased level of noise was somewhat expected since the microring resonator platform is held under ambient conditions susceptible to temperature fluctuations, whereas the UV and ELSD detectors are far less sensitive to temperature variations. The impact of temperature on the microring resonator signal has been discussed elsewhere, however, it is estimated that a 0.1 °C change in temperature

results in ~4.5 Δpm change in microring resonator response (this estimate was determined in a related study).[26,36]

Other comparisons that can be made are the differences of peak heights observed as the PS content changes. For the microring resonators (Figure 5-4A) this decrease in peak height is due to the changing RI contrast as PMMA content is increased. The respective RI (n) of PS, PMMA, cyclohexane and THF are as follows; 1.59,[45] 1.49,[46] 1.43, and 1.41, at 20 °C and 632.8 nm. The 31% PS-PMMA peak provided the smallest response from the microring resonators. This is caused by a combination of the RI contrast and the decreased sensitivity of the microring resonator platform for high molecular weights. With increasing molecular weight, the radius of gyration of a random polymer coil in solution also increases, and polymers with larger radiuses of gyration have portions that extend beyond the evanescent field of the sensor causing this sensitivity fall-off. This molecular weight dependence has been investigated and described previously.[36,47] All PS-PMMA standards have a molecular weight within a range of 60–80 kDa, with the exception of 31% PS which has a molecular weight of 117 kDa. These were available choices at the time of purchase. As for the changing peak heights with the ELSD chromatogram (Figure 5-4B) this is most likely due to scattering differences resulting from shape and size of analyte particles varying with different PS : PMMA ratios and elution solvent composition. Finally, for the UV chromatogram (Figure 5-4C) there is a consistent decrease in peak height as PMMA content is increased, corresponding to the decrease in the UV-active PS component. These visual observations of peak height/area are further supported by a more quantitative comparison of peak integrations for the three detectors' chromatograms (Figure 5-6).

3.2. Verification of Interface Integrity

Retention times were obtained from chromatograms of all three detection methods (microring resonators, ELSD, and UV) and representative chromatograms are presented in Figure 5-4. This was used to calibrate for copolymer composition, the % moles of PS were plotted against the PS/PMMA peak elution time for each polymer composition standard, as shown in Figure 5-7. Data points represent the average retention times for three replicated experiments (n = 3). There is very little variance among individual retention times so error bars are small, this verifies interface robustness. Overlaying all three calibrations on the same axis highlights indistinguishable slopes attributed by the agreement across detectors and lack of significant dead volume in the flow path. The fitting parameters of these curves can be found in Table 5-2. Additionally, these compositional calibrations can be useful for the identification of unknown PS-PMMA samples or blend samples that have multiple components or for computing the chemical composition distribution of a broad PS-PMMA copolymer of unknown composition.

3.3. Mass Concentration Response Curves

Using the same PS-PMMA copolymer samples prepared in chloroform and the same experimental method discussed earlier, gradient separations were performed for various injected masses ranging from 0.15 to 0.75 mg for each detector. The 31% PS standard was measured over a narrower mass range because of the pressure limits of the HPLC system. Injecting too much mass of the later eluting standards caused the HPLC system to go over pressure. These standards are least soluble in the initial gradient conditions, resulting in precipitation onto the column and increased pressure. The mass

concentration response was investigated by plotting mass injected against the integrated peak area for each detection method allowing for mass calibrations of 4 PS-PMMA standards, as seen in Figure 5-8. Here all y-intercepts were set to 0 as a means to normalize across detectors. Comparing these mass calibration curves demonstrates the linearity of the microring resonator response (Figure 5-8A). The UV detector also has a linear response for the 4 PS-PMMA standards and slope offset correlates with PS content (Figure 5-8B). The fitting parameters for the microring resonator and UV response curves are found in Table 5-3. As for the ELSD, the response is non-linear (Figure 5-8C) and the fitting parameters are provided in Table 5-4. As mentioned this non-linearity makes quantification difficult especially in the portions of the response curve where double values are observed. Therefore, the presented curve in Figure 5-8C are within the working range of the response for this particular system, this allows for a fair comparison across detector types. Calibration curve points represent the average of three replicate experiments, and error bars represent the standard deviation from visible over the plot range presented. As mentioned above, we attribute the increased error of the microring resonator platform to inherent noise of the detector and the reduced precision of baseline fitting for peak integration. Finally, limits of detection (LOD) and limits of quantification (LOQ) were calculated for each detector (Table 5-5), on average the LOD of the microring resonators is approximately 5 orders of magnitude greater than the LOD for both UV and ELSD. LOD and LOQ are dependent on the standard composition since detection differs slightly due to differing RI contrast for the microrings, though this changes depending on the analyte/ mobile phase pairing. Therefore in cases where RI contrast is low increasing sample size can be advantageous especially in polymer separations where sample size

is rarely a limitation. The LODs and LOQs for UV also depend on standard composition or more specifically chromophore content, this however is a more difficult challenge when the analyte of interest lacks such chemical signature.

3.4. Polymer Blend Separations

Polymer blends were prepared as mixtures of the various PS-PMMA copolymers at different ratios. These included varying amounts of 100%, 82%, and 54% PS with the 31% PS standard used as an internal control having constant concentration across all 4 synthetic blends. For blend separations a total mass of 0.75 mg was injected on the column and detection was carried out using all three detectors. Representative chromatograms for n = 3 blend separations are shown in Figure 5-9 (peak areas presented in Figure 5-10), with the same elution order as in Figure 5-4 (highest to lowest PS). Using the compositional calibration presented in Figure 5-7 we can identify each individual component of the blends, the first eluted peak is 100%, second 82%, third 54% and last eluted is the 31%. The 31% component was used as an internal standard and the consistency of the sample preparation across blends is verified by looking at the overlapping 31% blend component.

3.5. Quantification and Analysis of Polymer Blend Samples

The quantification of mass injected was done using the corresponding calibration curve for each peak component. Peak components were identified by retention time. A comparison of quantification across detectors for each blend can be found in Figure 5-11 and Table 5-6, additionally actual mass are provided in Table 5-7. In this comparison,

similar values are observed for each method, verifying the quantitative ability of the microring resonators. The microring resonator platform appears to offer some significant advantages over traditional HPLC detectors. Its large dynamic range of response enables detection of analytes on top of a strongly sloping gradient baseline. Observation of the gradient baseline (i.e., the gradient composition) itself is another advantage, which is not possible with traditional LC detectors (Figure 5-12). Real-time monitoring of the solvent gradient can account for fluctuations in pump performance and detection of non-ideal gradients serving as a diagnostic tool to monitor run integrity. Additionally, observation of the gradient baseline enables detection of gradient distortion which can compromise resolution. This in practice is demonstrated in Figure 5-12, where a 100% cyclohexane to 100% THF gradient was utilized without injections. Using the programmed methods of Figure 5-12A the raw gradient traces in Figure 5-12B were transformed into relative shift (Δpm) as a function of % THF Figure 5-12C. Here (Figure 5-12C) it is observed that with a steep gradient (i.e. 8 minutes), which is equivalent to approximately 1 column volume, there is a non-linear distortion in the raw gradient traces that is not observed in methods of multiple column volumes. The 100 min trace covers >10 column volumes and illustrates a linear gradient which is ideal for separations of better resolution. Gritti and Guiochon observed these same distortion trends using reverse phase gradients.[48] On a side note, comparing raw gradient traces of different lengths (Figure 5-12B) there is the observation of different gradient slopes due to varied rates of solvent mixing however the overall change in RI is consistent. Therefore, if run integrity was compromised it would be obvious early on before translating to traces into a function of solvent composition. In fact closer examination of Figure 5-2A, which utilizes a truncated gradient (95% (95 : 5 cyclohexane

: THF) to 10% cyclohexane) and has a gradient length of 20 minutes, reveals a slight bit of curvature in a nominally linear gradient. This curvature may indicate that our gradient was slightly steeper than optimal, however further investigation implied that time is not a factor since the curvature was nearly the same across methods of various lengths (Figure 5-13).[48] Similar curvature among the various gradients does not appear to be an artifact of the method itself but is likely due to the use of 5% strong solvent in reservoir A or inadequate solvent mixing. The use of strong solvent in reservoir A was necessary to maintain complete solubility of all analytes on injection. Although its presence appears to offer an advantage in terms of gradient ideality, it limits retention of copolymers with larger % styrene. The reason for minimal gradient distortion is that THF is always present in the column so there is minimal loss of THF as the gradient begins due to interaction of THF with the column. Further, UV absorbing solvents (e.g., toluene) are compatible with microring resonator platform, meaning direct monitoring of the gradient is possible. Finally, although all detectors used in this study required calibration for mass concentration determination, the microring resonator platform is believed to have an advantage over ELSD. Although not obvious for the system studied here, the ELSD typically exhibits both a solvent and polymer composition dependence to its response,[24,49] and both of these dependencies are typically non-linear. On the other hand, the microring resonator response is only dependent on the polymer composition eluting at a particular time in the gradient, and the response to that component is linear with concentration.

4. Conclusions

Commercial detectors compatible with gradient elution HPLC, such as ELSD and UV, have limitations for quantitative CCD measurements of industrially relevant polymers. Using microring resonators as gradient detectors for the separation of various PS-PMMA copolymers demonstrates advantages of the platform for complex polymer analysis. Foremost, the gradient compatibility of the microring resonator platform was exhibited, showing that refractive index based detection of gradient elution LC can be achieved unlike commercial dRI detectors. Here it was also observed that polymers like PMMA, which do not have a chromophore, can be detected by the microrings, providing an advantage over the commonly used UV detector. Additionally, various calibrations were performed for composition and mass injected, where mass calibrations illustrated the linearity of the microring resonator response. Linearity is where commonly used detectors like ELSD struggle since linearity is important for the ability to quantify mass concentrations. The quantitative results further support the applicability of the microring resonator platform for quantitative polymer analysis in solvent gradients.

However, it is important to also point out the challenges of the microring resonator platform as a solvent gradient chromatography detector. In comparison to commercial detectors, the baseline noise is larger. Because of the increased noise, there are additional processing steps for data analysis. Also, the decreased surface sensitivity with high molecular weights is another limitation. Commercial development of this platform for chromatographic separations would likely require improvements in each of these areas, which is an active area of continued research.

In summary, microring resonators offer much applicability to polymer analysis with broad versatility in a single detector. A universal linear mass concentration detector for use in solvent gradient HPLC is a longstanding challenge for separations. Despite the described limitations of the platform, this work represents an advancement toward a new detector technology for industrial copolymer analysis.

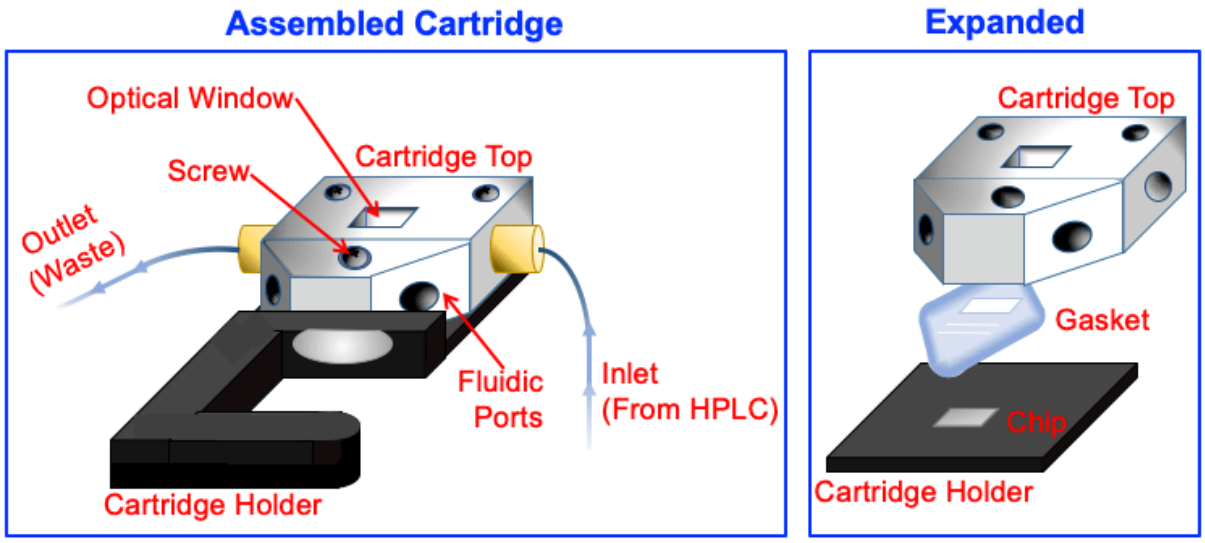

Figure 5-1: Microring Resonator Cartridge Assembly/HPLC Interface. Sensor chip and gasket are sandwiched between cartridge top and holder, which is aligned and held in place by screws. The UV/visible detector is connected directly to one of the fluidic ports on the cartridge top, the gasket directs eluents across the rings, and waste exits the opposite port. Only one of two fluidic channels is used in this work.

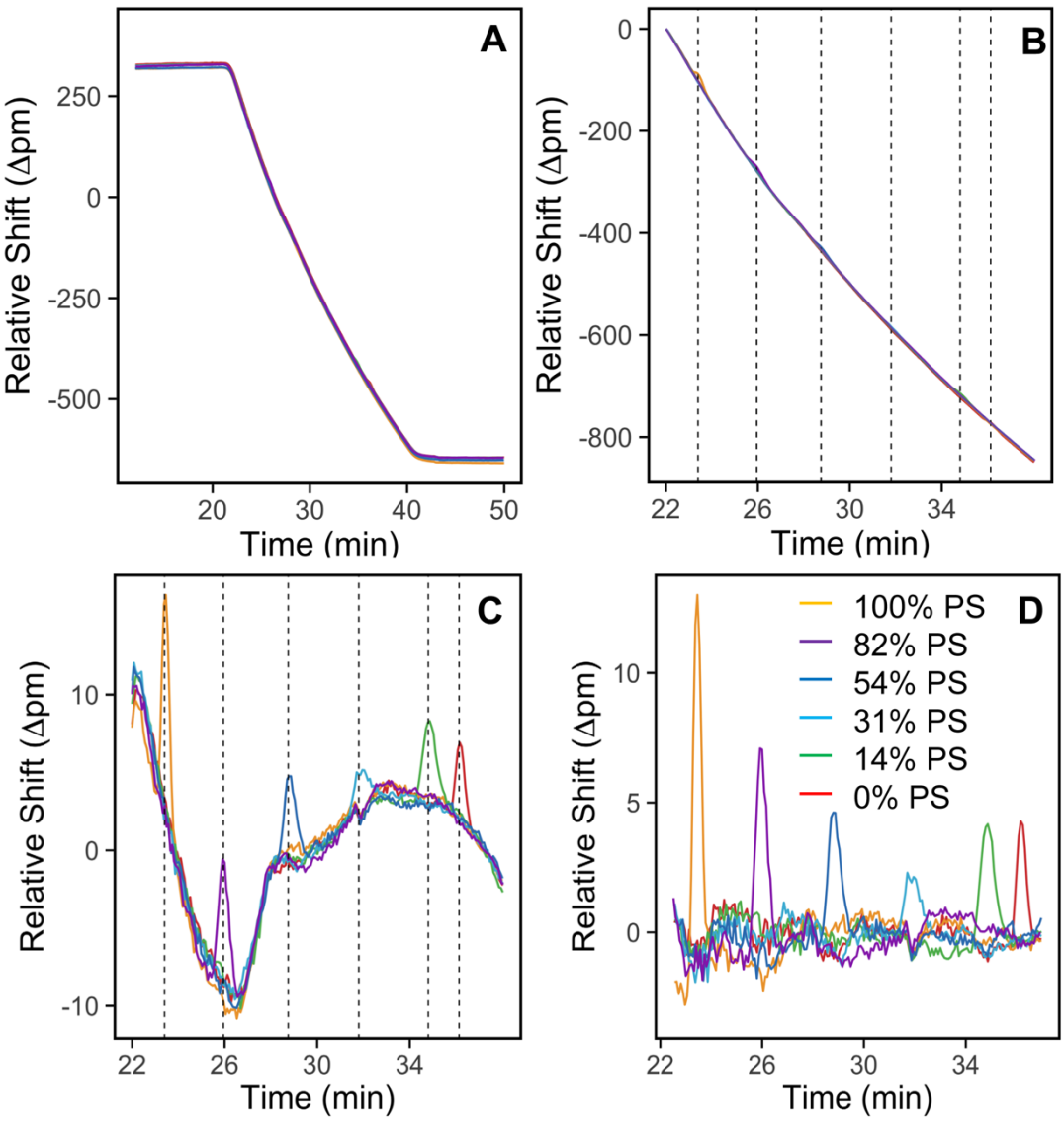

Figure 5-2: Data Treatment Process for Microring Resonators. A. Raw overlapping microring traces shows direct monitoring of gradient mixing though experiment since RI changes with changing mobile phase, this means gradient shape/slope is very reproducible for identical methods. B. A subset of (A) shows small peaks can be observed on the sloping baseline (peak location is indicated by dashed lines). This sloping baseline is fit to a third order polynomial which is then used to baseline correct the data. C. The fit obtained from the baseline observed in (B) is extrapolated and subtracted from the raw data. D. Then finally the subtracted chromatogram can be further corrected by applying a LOESS function.

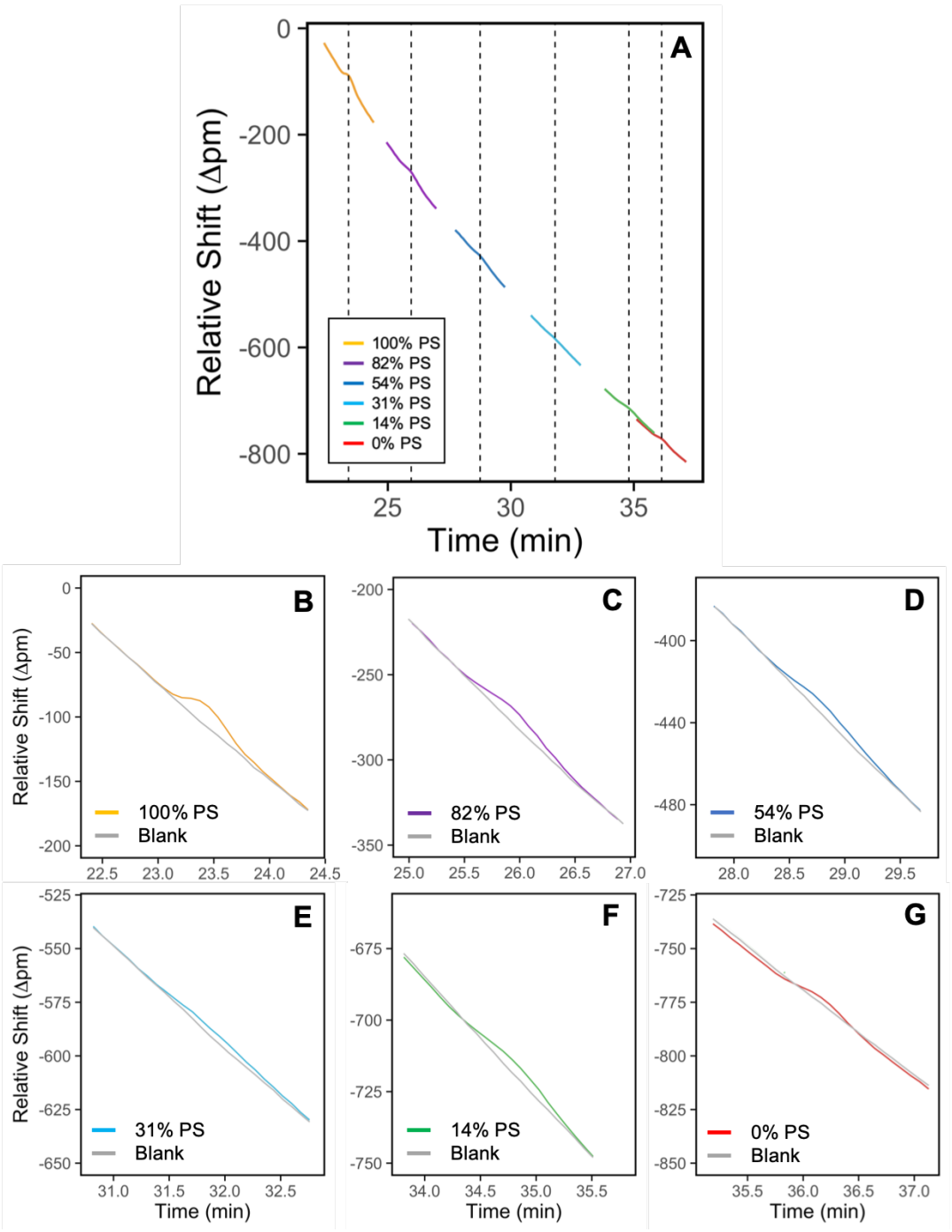

Figure 5-3: Closer Look at Peaks Before Baseline Correction. A. The data from Figure 1B is plotted here highlighting only the portions of the traces that are relevant to peak location. The observed bumps or slight non-linearity on the slopping baseline coordinates to peak elution, which is not as visible in Figure 1B due to obstruction from overlapping baselines. Additionally, the dashed lines from Figure 1 are continued here to indicate peak location throughout the correction process. The relevant trace portions from A are plotted individually with a blank trace in panels B-G, allowing for the observation of peaks before baseline correction.

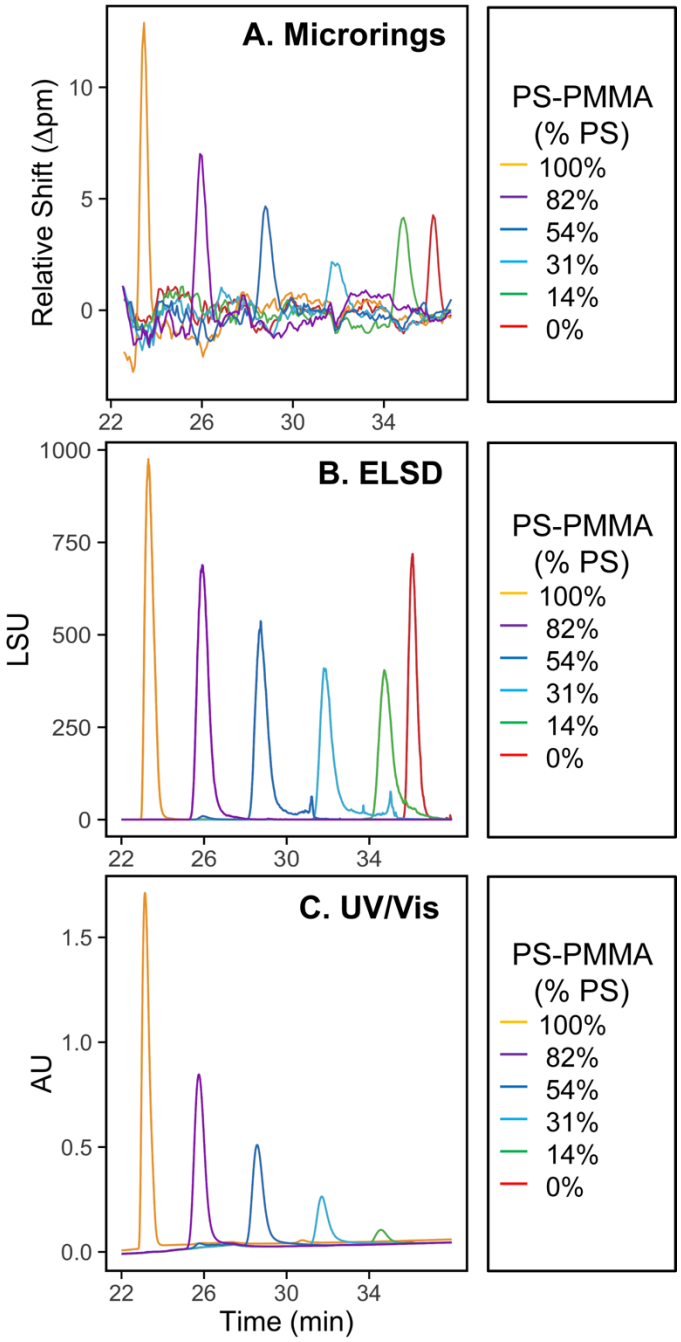

Figure 5-4 Gradient LC Chromatogram Comparison. Separations of PS-PMMA copolymers with a cyclohexane to THF gradient. Samples were prepared in chloroform at a concentration of 10 mg mL^{-1} and a mass of 0.15 mg was injected. Chromatograms were obtained by all three detectors A. microring resonator platform, B. evaporative light scattering (ELSD), and C. UV/visible (UV).

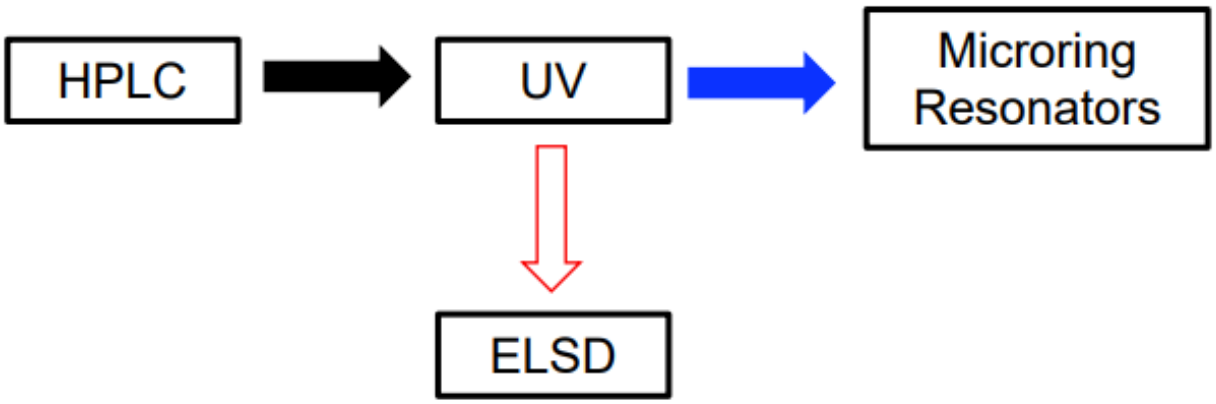

Figure 5-5: Fluidic Flow Path. Eluents flow off the column to the UV detector and then the microring resonators which are connected in-line. The interface from figure 5-1 is represented here by the blue arrow. ELSD data needs to be collected last in series due to the destructive nature of the detector. ELSD data were collected in a separate experiment.

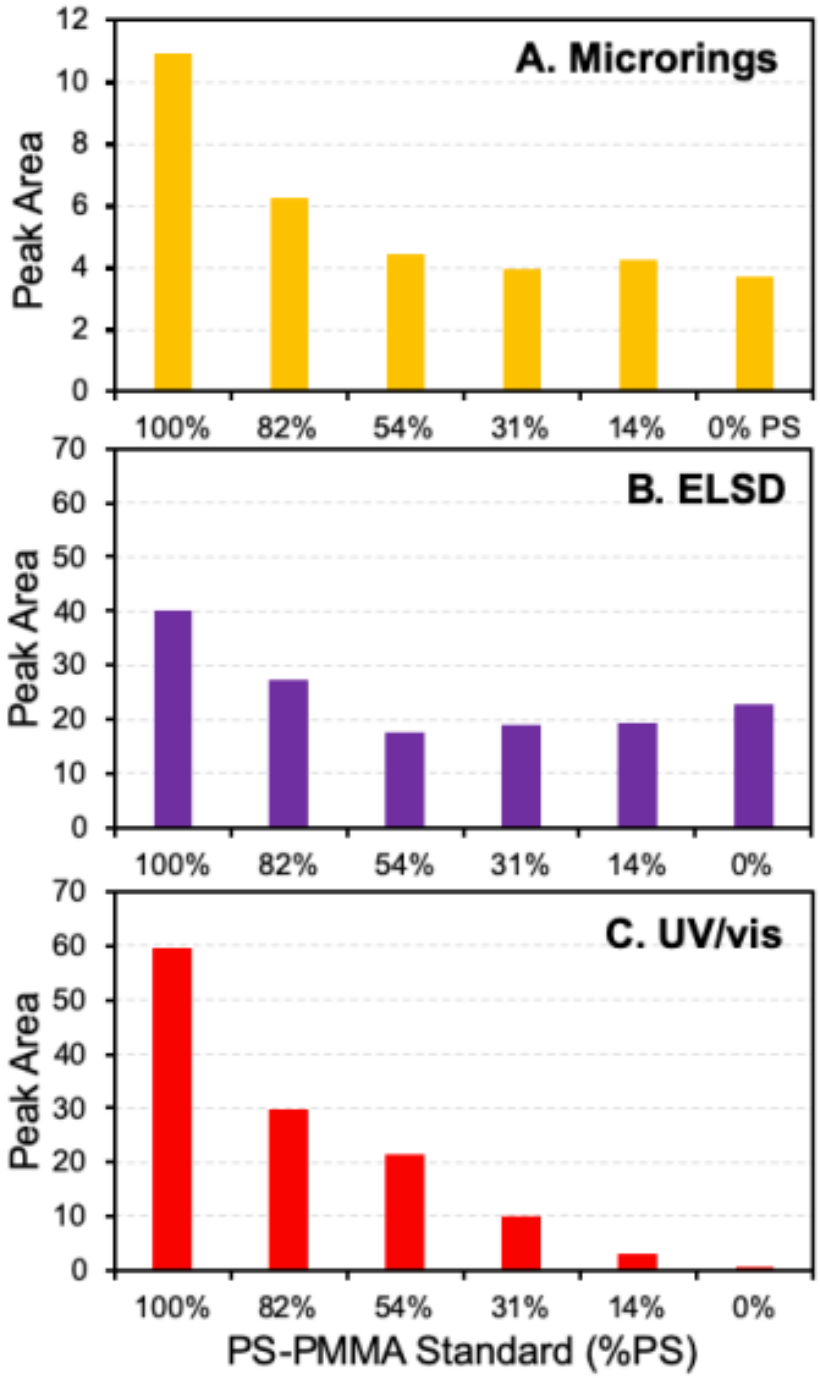

Figure 5-6: Peak Integrations for Gradient LC Chromatogram. Corresponding peak areas from Figure 5-4. A. Microring peak area decreases with decreasing RI contrast with increasing PMMA content. B. ELSD peak areas show a non-monotonic trend with polymer composition due to the solvent dependence and polymer composition dependence of the ELSD response. C. UV/vis peak areas decrease as a result of decreasing chromophore content/PS content.

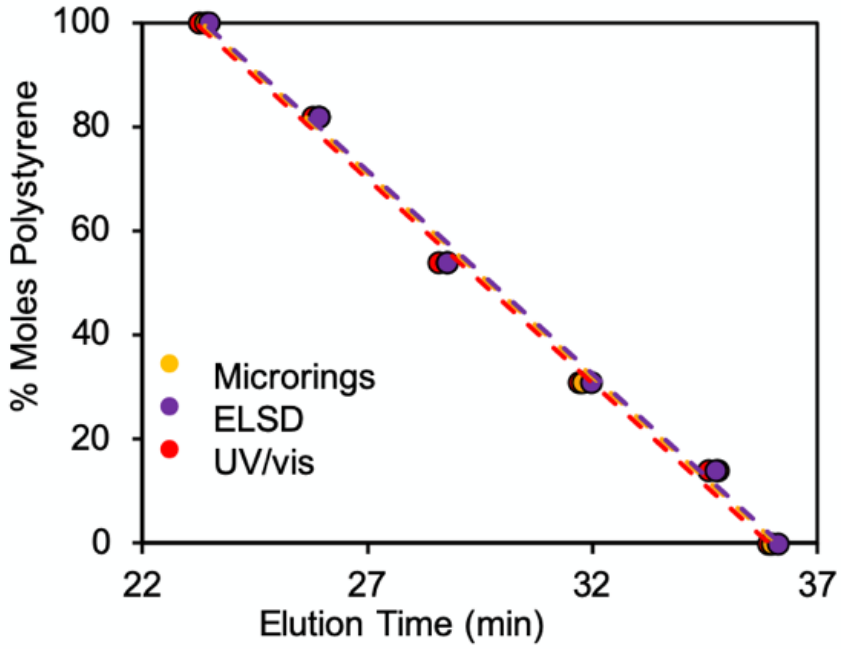

Figure 5-7: Copolymer Composition Versus Elution Times. Elution times from the chromatograms obtained in Fig. 5-2 were plotted against % moles of polystyrene for each copolymer. Resulting in calibrations for copolymer composition. Plotting all three calibrations on the same axis show over- lapping curves, verifying interface integrity such as no dead volume or delay between detectors.

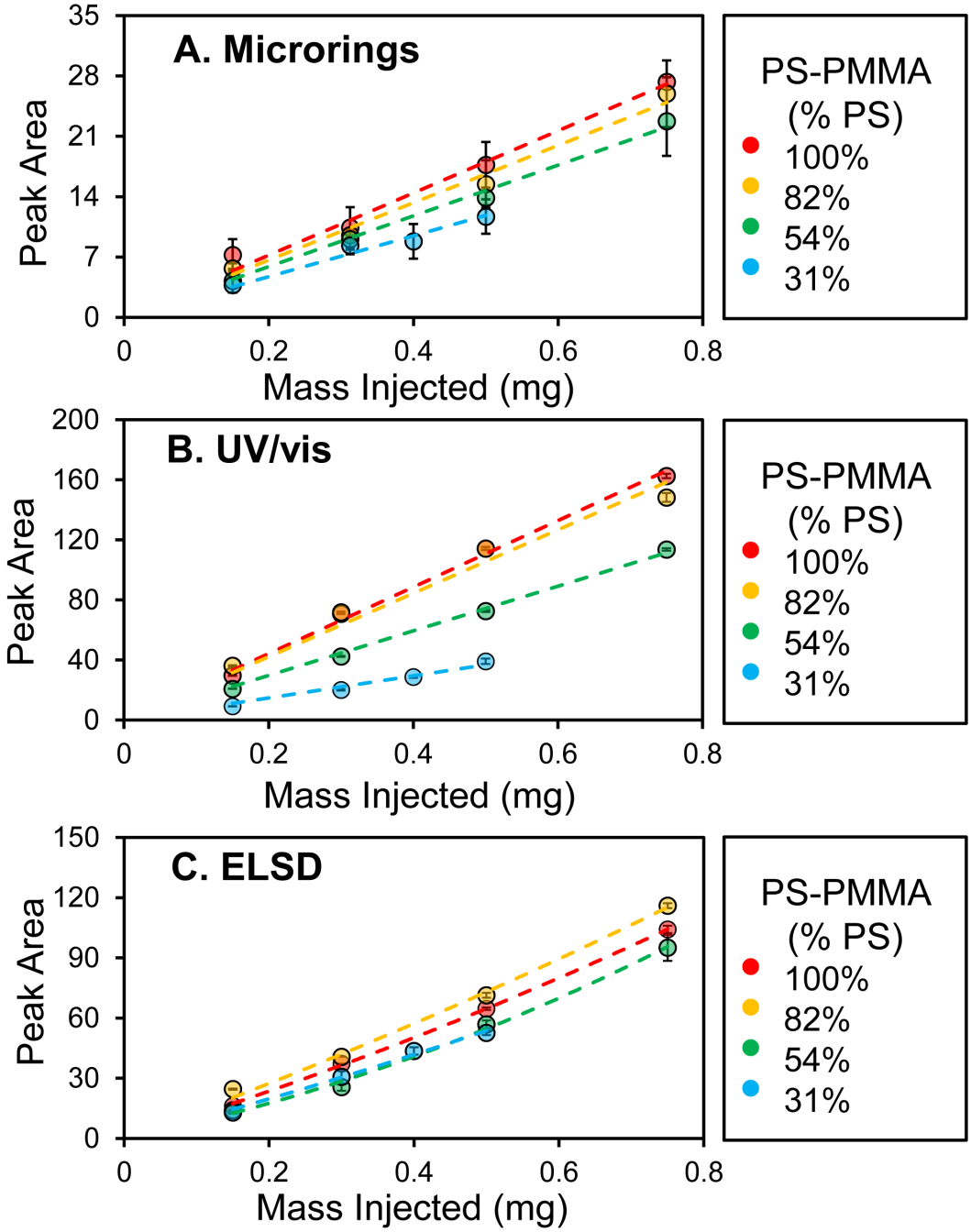

Figure 5-8: Mass Detection Calibrations. A. Repeating cyclohexane : THF gradient separations of PS-PMMA copolymers at 4 different injected masses for 4 standards demonstrated the linearity of the microring resonators. Plotting mass injected against peak area illustrates this linear correlation. B. Comparable linear correlation is also observed by UV/ visible (UV) detection. C. However plotting mass injected against peak area for evaporative light scattering (ELSD) demonstrates the non-linearity of the detector (mass range: 0.15–0.75 mg).

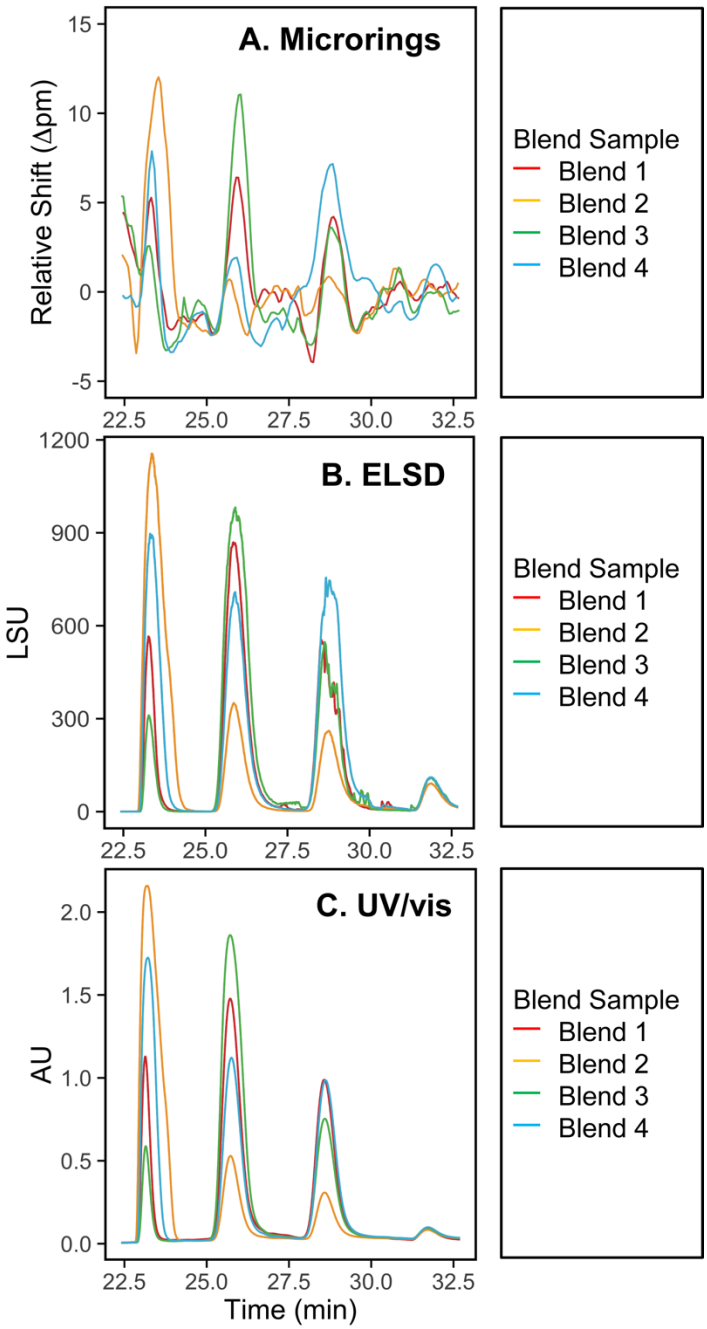

Figure 5-9: Copolymer Blend Analysis by Various Detectors. Polymer blends were made by mixing three PS-PMMA copolymers at various ratios all with a concentration of 11 mg mL^{-1} in chloroform. Separations were achieved based on composition using a cyclohexane : THF gradient. Chromatograms were obtained by detection with the A. microring resonators, B. evaporative light scattering (ELSD) and C. UV/visible (UV).

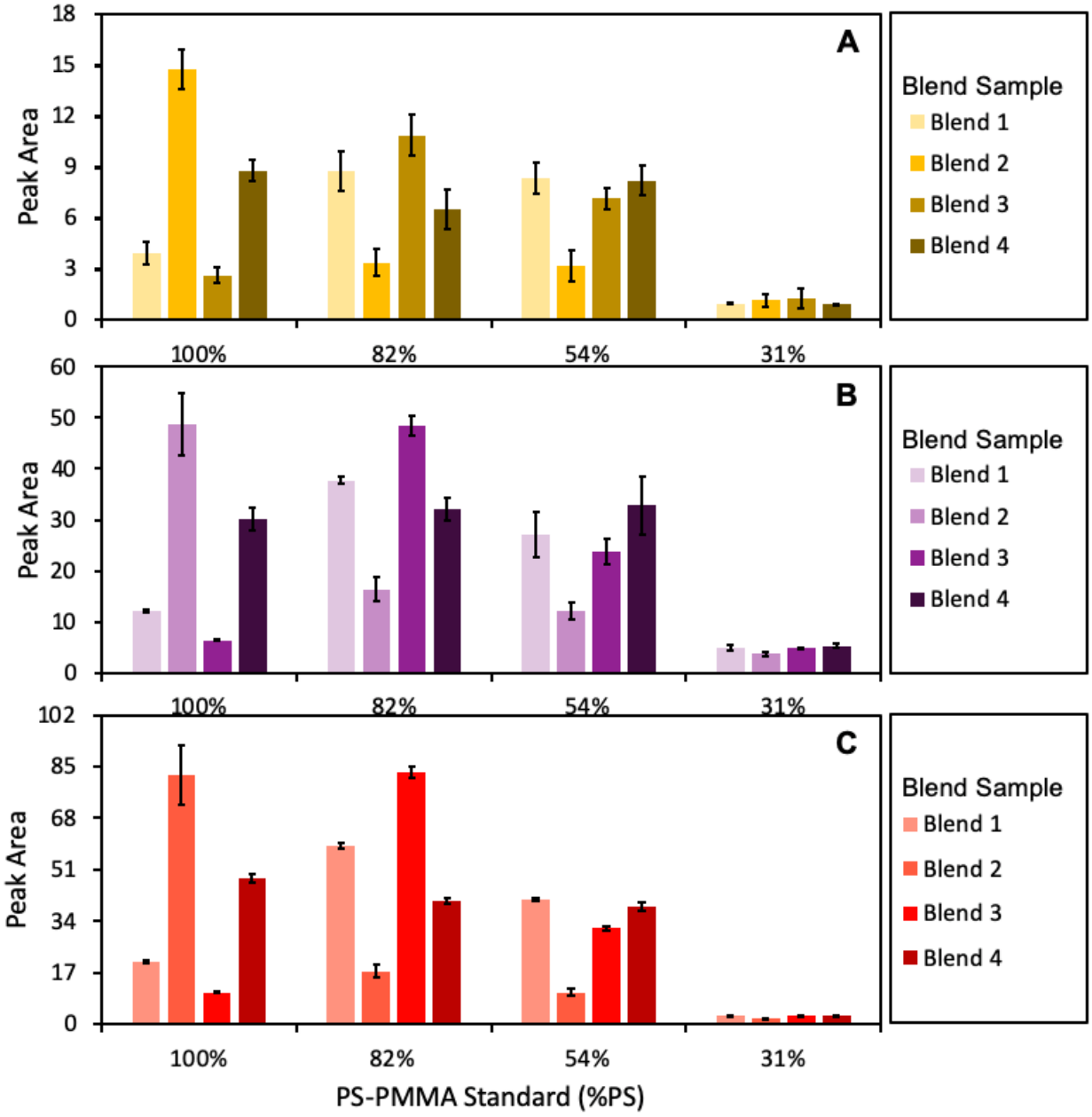

Figure 5-10: Peak Integrations for Polymer Blend Analysis. Peak areas were integrated and then plugged into mass calibration curves to determine the mass of each blend component. Here is a comparison of these compiled peak areas, from the A. microring resonator, B. ELSD, and C. UV/vis.

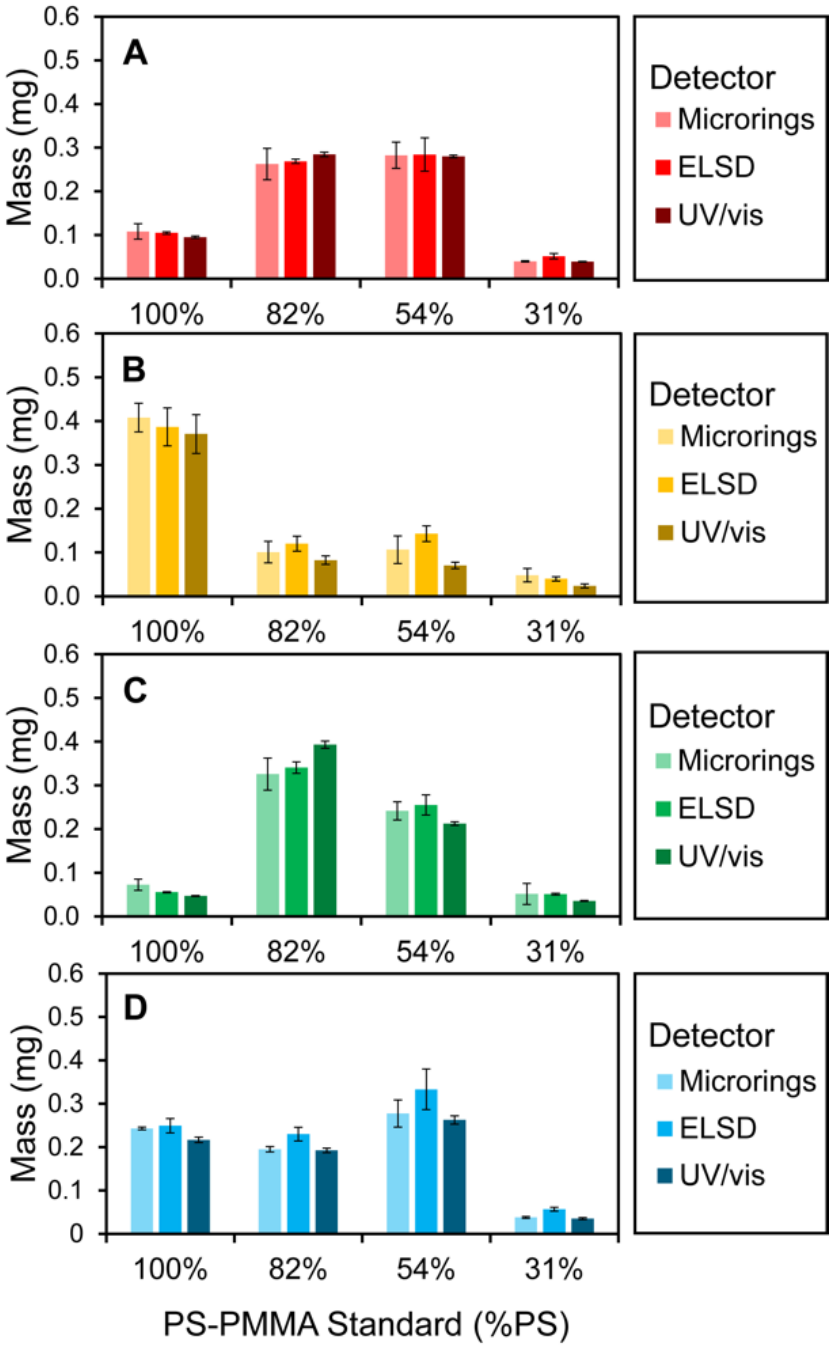

Figure 5-11: Quantitative Analysis of Polymer Blends. Integrating each peak area allowed for the quantification of mass detected for each component of the sample. This was done across all detectors allowing for a direct comparison, good correlation is observed since comparable mass values were obtained for each component by each method. Each histogram represents a different blend sample of the same three components A. Blend 1, B. Blend 2, C. Blend 3, and D. Blend 4.

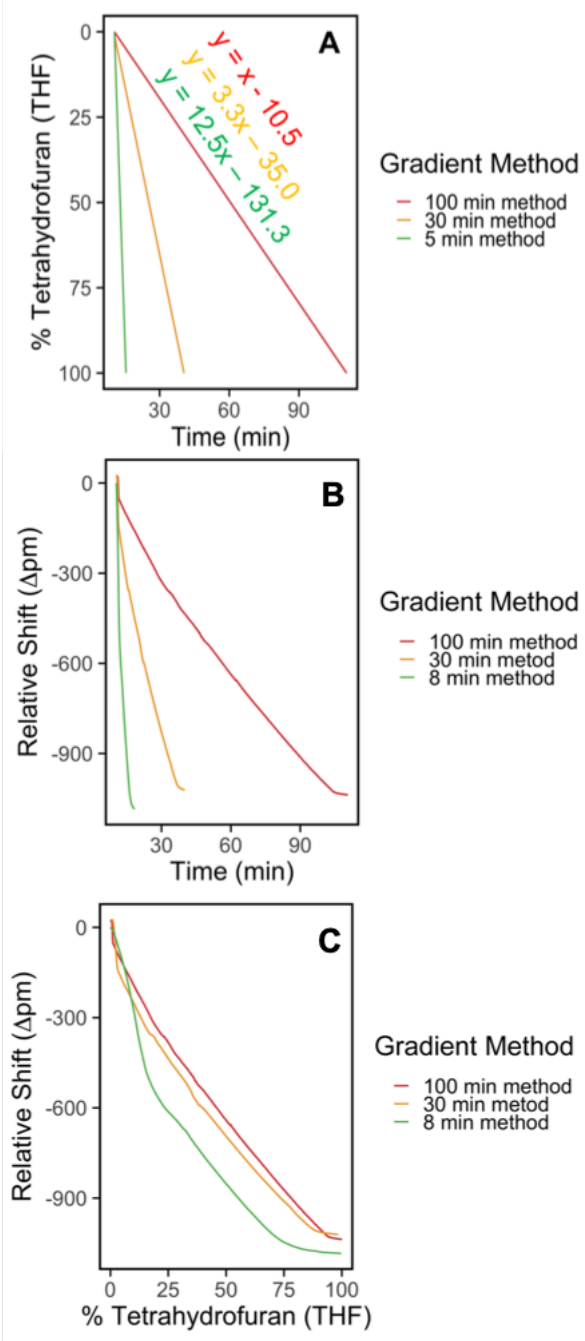

Figure 5-12: Real Time Monitoring of Solvent Gradient Baseline. (A) Here we wrote three gradient methods (100% cyclohexane to 100% THF) of varying length. By plotting zoomed in traces (B) as relative shift versus time and (C) as a function of solvent composition demonstrates how gradient ideality can be directly evaluated and optimized. For example, the 8 min method (equivalent to 1 column volume) shows a non-ideal distorted trace which will limit resolution. An optimized trace is rep- resented by the 100 min method which covers over 10 column volumes.

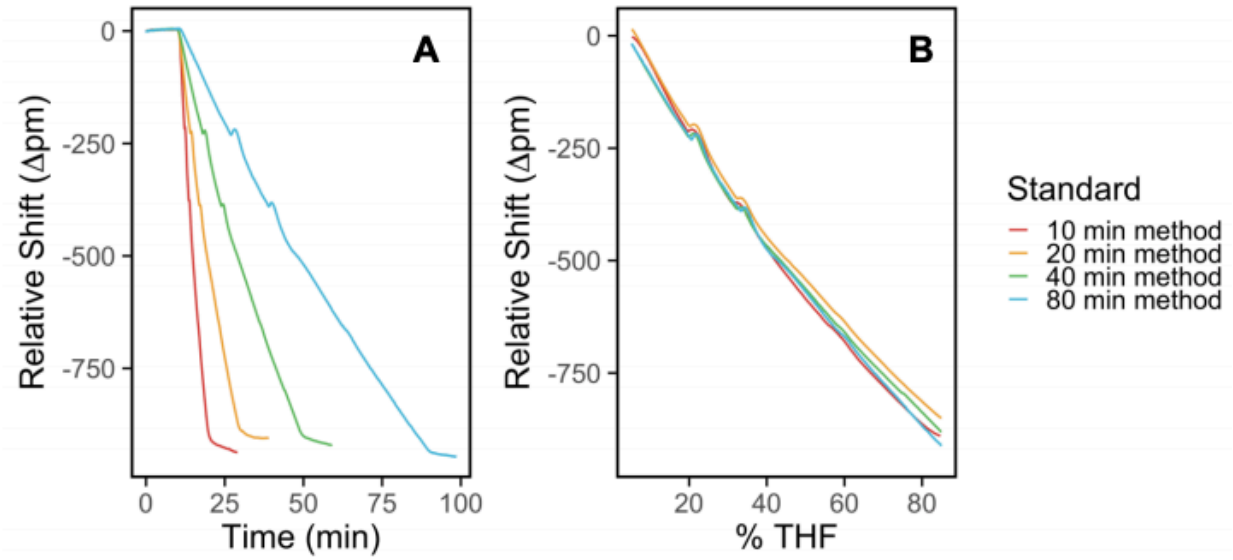

Figure 5-13: Investigation of Curvature in Raw Microring Traces. The slight curvature of the observed gradient traces suggests that the gradient may be too steep. A. However, upon investigation of gradient length the observed curvature was independent of time. B. The time independence was verified by plotting the traces as a function of nominal% THF. The time independence is likely due to the presence of 5% strong solvent (THF) in solvent A.

Table 5-1: Gradient HPLC Method

	Time	Mobile Phase	
		95:5 cyclohexane:THF	THF
Starting Condition	0	95%	5%
Isocratic Hold	10.5	95%	5%
Gradient Time	30.5	5%	95%
Purging	40.5	5%	95%
Re-conditioning	60.5	95%	5%

Table 5-2: Fitting Parameters for Polystyrene Content Calibration

	Detector	$bx + c$		R^2
		b	c	
A	Microrings	-7.830	281.4	0.9954
B	ELSD	-7.834	283.1	0.9962
C	UV/vis	-7.829	282.5	0.9947

Table 5-3: Linear Fitting Parameters for Mass Detection

	Detector	Standard (%PS)	$bx + 0$ / b	R^2
A	Microrings	100	36.10	0.9819
		82	33.25	0.9848
		54	29.53	0.9924
		31	23.66	0.9585
B	UV/vis	100	221.4	0.9942
		82	211.2	0.9621
		54	148.6	0.9971
		31	73.68	0.9727

Table 5-4: ELSD Fitting Parameters for Mass Detection

	Detector	Standard (%PS)	$bx^2 + cx + 0$		R^2
			b	c	
C	ELSD	100	38.35	110.3	0.9996
		82	30.07	131.1	0.9953
		54	72.11	73.34	0.9961
		31	29.35	92.81	0.9921

Table 5-5: LOD and LOQ Comparison

	Detector	Standard (%PS)	LOD (µg)	LOQ (µg)
A	Microrings	100	220	550
		82	240	590
		54	270	670
		31	340	840
B	UV/vis	100	0.0055	0.011
		82	0.0057	0.011
		54	0.0082	0.016
		31	0.016	0.032
C	ELSD	100	0.0017	0.0043
		82	0.0015	0.0036
		54	0.0026	0.0065
		31	0.0021	0.0051

Table 5-6: Polymer Blend Analysis, Mass Quantification

		Quantified Mass for Each Blend Component (mg)							
		100% PS		82% PS-PMMA		54% PS-PMMA		31% PS-PMMA	
Detector	Blend	Average	Standard Deviation	Average	Standard Deviation	Average	Standard Deviation	Average	Standard Deviation
Microrings	1	0.11	0.018	0.26	0.036	0.28	0.030	0.040	0.0016
	2	0.41	0.033	0.10	0.024	0.11	0.031	0.048	0.015
	3	0.072	0.013	0.33	0.037	0.24	0.021	0.052	0.024
	4	0.24	0.0033	0.19	0.0061	0.28	0.031	0.038	0.0021
UV	1	0.093	0.0025	0.28	0.0053	0.28	0.0030	0.038	0.00090
	2	0.37	0.044	0.083	0.0098	0.070	0.0074	0.024	0.0048
	3	0.047	0.0011	0.39	0.0082	0.21	0.0041	0.036	0.00084
	4	0.22	0.0061	0.19	0.0052	0.26	0.0095	0.035	0.0023
ELSD	1	0.11	0.0028	0.27	0.0049	0.29	0.038	0.052	0.0062
	2	0.39	0.043	0.12	0.017	0.15	0.018	0.040	0.0048
	3	0.057	0.0013	0.34	0.013	0.26	0.023	0.051	0.0020
	4	0.25	0.017	0.23	0.016	0.34	0.047	0.057	0.0043

Table 5-7: Actual mass injected for each individual blend component

	Mass Injected for Each Blend Component (mg)				
	100% PS	82% PS-PMMA	54% PS-PMMA	31% PS-PMMA	Total Mass
Blend 1	0.09	0.28	0.33	0.05	0.75
Blend 2	0.52	0.09	0.09	0.05	0.75
Blend 3	0.05	0.42	0.24	0.05	0.75
Blend 4	0.23	0.19	0.28	0.05	0.75

5. References

(1) P. Hiemenz and T. Lodge, *Polymer Chemistry*, CRC Press, 2nd edn, 2007.

(2) E. Uliyanchenko, S. v. d. Wal and P. J. Schoenmakers, Challenges in Polymer Analysis by Liquid Chromatography, *Polym. Chem*., 2012, **3**(9), 2313–2335.

(3) S. Podzimek, Molar Mass Distribution by Size Exclusion Chromatography: Comparison of Multi-Angle Light Scattering and Universal Calibration, *J. Appl. Polym. Sci*., 2019, **136**, 47561.

(4) D. Kou, G. Manius, S. Zhan and H. P. Chokshi, Size Exclusion Chromatography with Corona Charged Aerosol Detector for the Analysis of Polyethylene Glycol Polymer, *J. Chromatogr. A*, 2009, **1216**(28), 5424–5428.

(5) A. M. Striegel, Multiple Detection in Size-Exclusion Chromatography of Macromolecules, *Anal. Chem*., 2005, **77**(5), 104A–113A.

(6) A. Södergård and M. Stolt, Properties of Lactic Acid Based Polymers and Their Correlation with Composition, *Prog. Polym. Sci*., 2002, **27**(6), 1123–1163.

(7) G. Glöckner, *Chemical Heterogeneity of Copolymers, in Gradient HPLC of Copolymers and Chromatographic Cross-Fractionation*, ed. G. Glöckner, Springer Berlin Heidelberg,

(8) R. Murgasova and D. M. Hercules, Polymer Characterization by Combining Liquid Chromatography with MALDI and ESI Mass Spectrometry, *Anal. Bioanal. Chem*., 2002, **373**(6), 481–489.

(9) J. D. Campbell, J. A. Allaway, F. Teymour and M. Morbidelli, High-Temperature Polymerization of Styrene: Mechanism Determination with Preparative Gel Permeation Chromatography, Matrix-Assisted Laser Desorption/ Ionization Time-

of-Flight Mass Spectrometry, and 13C Nuclear Magnetic Resonance, *J. Appl. Polym. Sci.,* 2004, **94**(3), 890–908.

(10) R. X. E. Willemse, B. B. P. Staal, E. H. D. Donkers and A. M. van Herk, Copolymer Fingerprints of Polystyrene- Block-Polyisoprene by MALDI-ToF-MS, *Macromolecules*, 2004, **37**(15), 5717–5723.

(11) E. Uliyanchenko, Applications of Hyphenated Liquid Chromatography Techniques for Polymer Analysis, *Chromatographia*, 2017, **80**(5), 731–750.

(12) J. L. Dwyer and M. Zhou, Polymer Characterization by Combined Chromatography-Infrared Spectroscopy, *Int. J. Spectrosc.*, 2011, **2011**, 694645, https://www.hindawi.com/ journals/ijs/2011/694645/.

(13) G. Glöckner, Separation of Copolymers by Composition through Gradient High-Performance Liquid Chromatography, in *Gradient HPLC of Copolymers and Chromatographic Cross- Fractionation*, ed. G. Glöckner, Springer Berlin Heidelberg, Berlin, Heidelberg, 1991, pp. 113–147.

(14) L. R. Snyder, J. J. Kirkland and J. W. Dolan, Gradient Elution, in *Introduction to Modern Liquid Chromatography*, John Wiley & Sons, Ltd, 2010, pp. 403–473.

(15) R. W. Dixon and D. S. Peterson, Development and Testing of a Detection Method for Liquid Chromatography Based on Aerosol Charging, *Anal. Chem*., 2002, **74**(13), 2930–2937.

(16) T. Vehovec and A. Obreza, Review of Operating Principle and Applications of the Charged Aerosol Detector, *J. Chromatogr. A*, 2010, **1217**(10), 1549–1556.

(17) J. M. Charlesworth, Evaporative Analyzer as a Mass Detector for Liquid Chromatography, *Anal. Chem*., 1978, **50**(11), 1414–1420.

(18) J. H. Arndt, T. Macko and R. Brüll, Application of the Evaporative Light Scattering Detector to Analytical Problems in Polymer Science, *J. Chromatogr. A*, 2013, **1310**(Supplement C), 1–14.

(19) K. Mojsiewicz-Pieńkowska, Size-Exclusion Chromatography with Evaporative Light Scattering Detection: Method for Determination of Polydimethylsiloxanes. I. Testing Dependence of Molecular Weight of Polydimethylsiloxanes and Injected Mass upon the Detector Signal, J. Chromatogr. B: *Anal. Technol. Biomed. Life Sci.*, 2008, **865**(1–2), 1–6.

(20) K. Takahashi, S. Kinugasa, M. Senda, K. Kimizuka, K. Fukushima, T. Matsumoto, Y. Shibata and J. Christensen, Quantitative Comparison of a Corona- Charged Aerosol Detector and an Evaporative Light- Scattering Detector for the Analysis of a Synthetic Polymer by Supercritical Fluid Chromatography, *J. Chromatogr. A*, 2008, **1193**(1), 151–155.

(21) L. R. Snyder, J. J. Kirkland and J. W. Dolan, *Biochemical and Synthetic Polymer Separations, in Introduction to Modern Liquid Chromatography*, John Wiley & Sons Ltd, 2010, pp. 569–663.

(22) N. Vervoort, D. Daemen and G. Török, Performance Evaluation of Evaporative Light Scattering Detection and Charged Aerosol Detection in Reversed Phase Liquid Chromatography, *J. Chromatogr. A*, 2008, **1189**(1), 92–100.

(23) G. K. Webster, J. S. Jensen and A. R. Diaz, An Investigation into Detector Limitations Using Evaporative Light- Scattering Detectors for Pharmaceutical Applications, *J. Chromatogr. Sci.*, 2004, **42**(9), 484–490.

(24) A. Boborodea and S. O'Donohue, Linearization of Evaporative Light Scattering Detector Signal, *Int. J. Polym. Anal. Charact.,* 2017, **22**(8), 685–691.

(25) J. H. Wade and R. C. Bailey, Applications of Optical Microcavity Resonators in Analytical Chemistry, *Annu. Rev. Anal. Chem*., 2016, **9**, 1–25.

(26) J. H. Wade and R. C. Bailey, Refractive Index-Based Detection of Gradient Elution Liquid Chromatography Using Chip-Integrated Microring Resonator Arrays, *Anal. Chem*., 2014, **86**(1), 913–919.

(27) P. Schoenmakers and P. Aarnoutse, Multi-Dimensional Separations of Polymers, *Anal. Chem*., 2014, **86**(13), 6172–6179.

(28) R. M. Graybill, C. S. Para and R. C. Bailey, PCR-Free, Multiplexed Expression Profiling of MicroRNAs Using Silicon Photonic Microring Resonators, *Anal. Chem*., 2016, **88**(21), 10347–10351.

(29) A. L. Washburn, W. W. Shia, K. A. Lenkeit, S.-H. Lee and R. C. Bailey, Multiplexed Cancer Biomarker Detection Using Chip-Integrated Silicon Photonic Sensor Arrays, *Analyst*, 2016, **141**(18), 5358–5365.

(30) J. H. Wade, A. T. Alsop, N. R. Vertin, H. Yang, M. D. Johnson and R. C. Bailey, Rapid, Multiplexed Phosphoprotein Profiling Using Silicon Photonic Sensor Arrays, *ACS Cent. Sci.,* 2015, **1**(7), 374–382.

(31) S. I. Shopova, I. M. White, Y. Sun, H. Zhu, X. Fan, G. Frye- Mason, A. Thompson and S. Ja, On-Column Micro Gas Chromatography Detection with Capillary-Based Optical Ring Resonators, Anal. Chem., 2008, 80(6), 2232–2238.

(32) H. Zhu, I. M. White, J. D. Suter, M. Zourob and X. Fan, Integrated Refractive Index Optical Ring Resonator Detector for Capillary Electrophoresis, *Anal. Chem*., 2007, **79**(3), 930–937.

(33) D. C. Kim and R. C. Dunn, Integrating Whispering Gallery Mode Refractive Index Sensing with Capillary Electrophoresis Separations Using Phase Sensitive Detection, Anal. Chem., 2016, 88(2), 1426–1433.

(34) J. D. Orlet and R. C. Bailey, Silicon Photonic Microring Resonator Arrays as a Universal Detector for Capillary Electrophoresis, *Anal. Chem*., 2020, **92**(2), 2331–2338.

(35) D. Ye, W. Wang, D. Moline, M. S. Islam, F. Chen and P. Wang, A Microwave Flow Detector for Gradient Elution Liquid Chromatography, *Anal. Chem*., 2017, **89**(20), 10761–10768.

(36) E. Mordan, J. H. Wade, Z. S. B. Wiersma, E. Pearce, T. O. Pangburn, A. W. deGroot, D. M. Meunier and R. C. Bailey, Silicon Photonic Microring Resonator Arrays for Mass Concentration Detection of Polymers in Isocratic Separations, *Anal. Chem*., 2018, **91**, 1011–1018.

(37) M. Iqbal, M. A. Gleeson, B. Spaugh, F. Tybor, W. G. Gunn, M. Hochberg, T. Baehr-Jones, R. C. Bailey and L. C. Gunn, Label-Free Biosensor Arrays Based on Silicon Ring Resonators and High-Speed Optical Scanning Instrumentation, *IEEE J. Sel. Top. Quantum Electron*., 2010, **16**(3), 654–661.

(38) Y. Brun and P. Alden, Gradient Separation of Polymers at Critical Point of Adsorption, *J. Chromatogr. A*, 2002, **966**(1), 25–40.

(39) G. Glöckner, Special Features of Polymer HPLC, in *Gradient HPLC of Copolymers and Chromatographic Cross- Fractionation*, ed. G. Glöckner, Springer Berlin Heidelberg, Berlin, Heidelberg, 1991, pp. 45–55.

(40) T. H. Mourey, Polymer Adsorption Chromatography with Evaporative Light-Scattering Detection, *J. Chromatogr. A*, 1986, **357**, 101–106.

(41) D. Mekap, T. Macko, R. Brüll, R. Cong, W. deGroot, A. Parrott and W. Yau, Multiple-Injection Method in High- Temperature Two-Dimensional Liquid Chromatography (2D HT-LC), *Macromol. Chem. Phys*., 2014, **215**(4), 314–319.

(42) Y. Mengerink, R. Peters, M. Kerkhoff, J. Hellenbrand, H. Omloo, J. Andrien, M. Vestjens and S. van der Wal, Analysis of Linear and Cyclic Oligomers in Polyamide-6 without Sample Preparation by Liquid Chromatography Using the Sandwich Injection Method: II. Methods of Detection and Quantification and Overall Long-Term Performance, *J. Chromatogr. A*, 2000, **878**(1), 45–55.

(43) X. Jiang, A. van der Horst and P. J. Schoenmakers, Breakthrough of Polymers in Interactive Liquid Chromatography, *J. Chromatogr. A*, 2002, **982**(1), 55–68.

(44) W. S. Cleveland and S. J. Devlin, Locally Weighted Regression: An Approach to Regression Analysis by Local Fitting, *J. Am. Stat. Assoc*., 1988, **83**(403), 596–610.

(45) C. Smart and E. Willis, Determination of Refractive Indices of Polystyrene Latices by Light Scattering, *J. Colloid Interface Sci.*, 1967, **25**(4), 577–583.

(46) G. Beadie, M. Brindza, R. A. Flynn, A. Rosenberg and J. S. Shirk, Refractive Index Measurements of Poly(Methyl Methacrylate) (PMMA), *Appl. Opt*., 2015, **54**(31), F139–F143.

(47) M. S. Luchansky, A. L. Washburn, T. A. Martin, M. Iqbal, L. C. Gunn and R. C. Bailey, Characterization of the Evanescent Field Profile and Bound Mass Sensitivity of a Label-Free Silicon Photonic Microring Resonator Biosensing Platform, *Biosens. Bioelectron*., 2010, **26**(4), 1283–1291.

(48) F. Gritti and G. Guiochon, Separations by Gradient Elution: Why Are Steep Gradient Profiles Distorted and What Is Their Impact on Resolution in Reversed-Phase Liquid Chromatography, *J. Chromatogr. A*, 2014, **1344**, 66–75.

(49) T. H. Mourey and L. E. Oppenheimer, Principles of Operation of an Evaporative Light-Scattering Detector for Liquid Chromatography, *Anal. Chem*., 1984, **56**(13), 2427– 2434.

Chapter VI

Quasi 2-D Liquid Chromatography, Exploration of Column Mimics at the Chip Surface

Acknowledgements

I would like to acknowledge John D. Orlet for teaching me the chip functionalization protocol. I would also like to acknowledge Sara M. Medfisch for teaching me the piranha treatment protocol as well as piranha treating chips for me. Additionally, I would like to acknowledge Cole A. Chapman's assistance with on-line functionalization as well as well as piranha treating chips for me. Finally, I would like to acknowledge Nicolas Mesyngier for oxygen plasma treating chips for me. My contributions include all experimental design, all chip silanization, much of the piranha treatments, all sample preparation, all experimental execution, development of R code for data work up, and all data work up.

The authors would like to thank Dr. James Wade and Dr. David Meunier for providing valuable insight throughout experimental process. Additionally, we

acknowledge financial support from The Dow Chemical Company through the University Partnership Initiative Program.

Abstract

Complex copolymers with multiple dimensions of structural heterogeneity are often characterized with multi-dimensional separations, where more than one column is run in-line each often separating based on different modalities (e.g., molecular weight and chemical composition). Multi-dimensional separations allow for the characterization of multiple distributions in a single experiment making them useful for complex polymers. This is especially true once the numerous combinations of separations are considered. Although it should be noted that multidimensional dimensional separations often take hours and require much more optimization in comparison to single dimension separations. However, a possible alternative to conventional multidimensional separations is integrating a second dimension with an affinity based detector. The silicon photonic microring resonator platform, which has been previous explored for the detection of liquid chromatography methods, offers functionalizable sensor chips that have the potential to provide affinity-like data once modified. Here this capability was leveraged and various silanes were investigated as potential chip modification chemistries in hopes of creating affinity based separation column mimics at the chip surface. This ultimately adds a quasi-second dimension for characterizing analytes that are not easily analyzed by a single dimension. Therefore with this method there is the potential of obtaining as much data as a two-dimensional separation with a single dimensional separation.

1. Introduction

Polymers by nature are complex, structurally heterogenous mixtures of analytes, where each aspect of structure is broadly distributed. Even the simplest of polymers, linear homopolymers, require at least characterization of molecular weight distribution. However in the real world polymeric samples are complex meaning they are distributed in more than one dimension, which can include molecular weight, chemical composition, functionality, branching, and tacticity. All such distributions greatly impact physical and mechanical properties, and therefore characterization of these distributions is necessary for better understanding the material at hand. Liquid chromatography techniques are often the go-to method for characterization of these various distributions. However, for those polymers that have multidimensional distributions one separation is not enough to fully characterize the material. In these cases multidimensional separations are often utilized to fully characterize the polymer analyte.[1,2]

Multidimensional separations, typically two-dimensional (2D) separations, work by combining two independent separation mechanisms to characterize two distributions in a single experiment, this is typically referred to as an on-line or comprehensive approach. More specifically with this approach, an analyte is separated by the first column, in the first dimension (^{1}D), these fractions which elute from the ^{1}D are further separated by the second dimension (^{2}D). The collected data is typically combined into three-dimensional contour plots, consisting of retention times for ^{1}D plotted on the x-axis, retention times for ^{2}D plotted on the y-axis, and peak intensity dictated by color constructing the three-dimensional peaks, which is very information dense.

The numerous combinations of separations make the capabilities of 2D-LC truly expansive. However, this does come at the price of time, with regards to both separation optimization and length/speed of experiment[1,3] which is where this current study could make improvements. Here we investigate the possibility of a quasi-2D LC separation where the second separation occurs at the detection source. This is through the hyphenation of LC with the microring resonator platform, which uses a silicon photonic chip that can be functionalized with column mimicking chemistries.

The microring resonator platform is conventionally run in stand-alone operation for the observation of molecular binding events/immunoassays, often employed as a diagnostic tool. This works by placing a multiplexed chip which has an array of tethered capture agents such as antibodies, DNA, and much more. Samples in complex matrices are flown across the multiplexed microring resonator chip and specific analytes bind to their corresponding capture agent resulting a Langmuir binding response. These experiments provide insight on binding kinetics and components of complex matrices.[4–9] Combining this utility of the microring resonators with recent work interfacing the microring resonator platform with up-stream separations[10–13] has the potential for adding another dimension of data post separation.

Previous work utilizing the microring resonators in separation applications has shown the versatility and robustness of this universal detection scheme as an alternative detector for both LC and capillary electrophoresis[12]. Work with the microring resonators as an LC detector for polymer analysis first demonstrated the linear mass detection capability which is an improvement over commercialized universal detectors such as

evaporative light scattering (ELSD) and charged aerosol detectors (CAD).[10,11] Both ELSD and CAD suffer from a non-linear response, meaning with increasing mass injected peak area does not increase linearly. This non-linearity leads to complications with quantification, especially in the lower and upper portions of the curves. However, even with this complication ELSD and CAD are still widely used because they are universal detection schemes that are also gradient compatible. UV/visible (UV/vis) detectors are not universal and differential refractive index detectors (dRI) are not gradient compatible. The microring resonators offer an RI-based detection scheme and provide gradient compatibility due to their substantial dynamic range, which has been previously demonstrated with both normal phase and reverse phase gradients.[11,13] All of this work has shown the great potential of the microring resonators as a detector for in-line separations and this current work hopes to expand this further by utilizing the functionalizable chip surface.

With this study the microring resonator platform will be hyphenated with LC. However, the difference from previous work is that the sensor chip will be treated with various chemical modifications prior to detection. Such treatments include silanization of the silicon surface with various silanes and oxidation methods for treating the surface. Two experimental approaches were used, the first approach utilized the stand-alone operation of the microring resonator platform to investigate polymer interactions with the sensor surface treatment. Once decent interactions were observed with a given surface modification, a second experimental approach which interfaced with LC to deliver injections and solvent gradients without a column in place was pursued. Promising interactions were observed with oxidized chip surfaces, however these experiments were

less promising when translated to chromatography. The challenges encountered however were mostly due to the experimental system rather than the set-up itself, therefore future work with a similar design is still worth further pursuit.

2. Experimental

2.1. Materials

High purity solvents were all purchased from Sigma-Aldrich (St Louis, MO). Poly(styrene-co-methyl methacrylate) (PS-PMMA) standards were purchased from Polymer Source, Inc. (Dorval, QC), varying in PS content (82%, 54%, 31%, and 14% mol PS). Polymethacrylate (PMMA) homopolymer standard was purchased from Agilent (Santa Clara, CA). All polymer standards were used as received and were typically prepared at a 1 mg/mL concentration in either chloroform or toluene. Silanes including 3-aminopropyltriethoxy silane (APTES), N,N-bis(2-Hydroxylethyl)-3-aminopropyltriethoxy silane (BH-APTES), cyanopropyltriethoxy silane (CPTES), 2-hydroxy-4-(3-triethoxysilylpropoxy)diphenylketone) silane (HTDS), N-(3-triethoxysilylpropyl)gluconamide silane (TGS), and octadecyltriethoxy silane (ODTES) (Table 6-1 outlines the used silanes) were all purchased from Gelest (Morrisville, PA), all used as received.

2.2. Microring Resonators.

The microring resonator system (Maverick M1 optical scanning instrumentation) and sensor array chips were purchased from Genalyte, Inc. (San Diego, CA). Detailed

descriptions of sensor fabrication and instrument operation has been described elsewhere.[13]

The 4 mm x 6 mm microring resonator chip consists of an array of 128 ring shaped optical cavities. Each individual microring is 30 μm diameter and has an adjacent linear waveguides, allowing for each sensor to be individually probed by an external tunable cavity diode laser centered at 1550 nm. Optical transmission is monitored as a function of wavelength, and dips in transmittance signal occur at resonant wavelengths defined by the following equation.

$$\lambda_r = \frac{2\pi r n_{eff}}{m}$$

where r is the ring radius, n_{eff} is the effective refractive index, and m is a constant. As changes are observed in the local refractive index at the sensor surface, such as analyte elution or analyte binding, the resonant wavelength will shift accordingly. These changes in resonance wavelengths correspond to changes in n_{eff} which are monitored as a function of time and referred to as relative shift in units of delta picometers (Δpm). [14,15]

2.3. Chip Functionalization via Silanization

The protective photoresist coating of the microring resonator chip is removed by immersing chips in acetone. This is followed by immersion of the chip in a 5% silane solution prepared in acetone except for ODTES which was prepared in THF and BH-APTES which was prepared in ethanol. Following incubation in the silane solution the chips were immersed in fresh solvent to remove residual silane. For APTES, CPTES,

HTDS, and TGS the fresh solvent was acetone, for ODTES the fresh solvent was THF and for BH-APTES the fresh solvent was ethanol. Chips were then rinsed in isopropanol and water before drying under nitrogen. Chips were all used immediately after silanization.

Silanization of the silicon surface of the microring resonator chip results in the formation of -Si-O-Si- bonds. This occurs via the displacement of the hydroxyl groups of the silicon surface by the alkoxy groups on the alkoxysilanes. This process is shown in Figure 6-1 and the structures of the obtained silane monolayers is shown in Figure 6-2.

2.4. Chip Functionalization via Oxidation

Prior to use, the protective photoresist coating was removed by successively immersing chips in acetone and isopropanol baths, followed by an acetone rinse. (For use of untreated chips this is the only necessary prep.) Chip surfaces were oxidized by by one of two different approaches, either piranha treating or oxygen plasma treating. As for piranha treating, chips were immersed in a 130 ^{o}C piranha solution (3:1 sulfuric acid:hydrogen peroxide) for 30 seconds, rinsed with water and dried under nitrogen. As for oxygen plasma treatment, chips were placed in the vacuum chamber of a plasma cleaner (PDC-32G, Harrick Plasma) utilizing oxygen as the ionizing gas for approximately 5 minutes before use. Chips were all used immediately after treatment.

2.5. Stand-Alone Microring Resonator Experimental

The microring resonator flow cell is assembled by placing the sensor chip on an anodized aluminum cartridge base followed by a polyethylene terephthalate (Mylar)

gasket and a polytetrafluoroethylene (Teflon) cartridge top. The Mylar gasket and Teflon cartridge top direct fluid flow across the chip and the whole assembly is secured together by screws. 1/16″ PEEK tubing with a 0.25 mm flangeless 1/4-28 interface where directly coupled to a Harvard Apparatus (Holliston, MA) Standard Infuse/Withdraw Pump 11 Elite Programmable Syringe Pump, which was operated at 0.1 mL/min in withdraw mode. Solvent changes were made manually by swapping the vial from which the syringe pump was pulling.

2.6. HPLC-MRR Interface for On-line Experiments

Solvent gradient delivery was performed by the Waters Alliance e2695 separation module (Milford, MA) equipped with a Waters 2424 ELSD detector. No column was used since the microring resonator chip is mimicking a column for these experiments. A schematic of this experimental design is shown in Figure 6-3. A 0.4 mL min^{-1} flow rate was maintained for a gradient of toluene to tetrahydrofuran (THF) or cyclohexane to THF. The Waters 2424 ELSD detector, when used was placed in-line after the microring resonators to detect any polymer that was released from the chip surface ELSD was operated at a gain of 20, gas pressure of 20 psi, drift tube temperature of 50 °C, and a nebulizer temperature of 12 °C.

The microring resonator flow cell is assembled as described earlier. 1/16″ PEEK tubing with a 0.25 mm flangeless 1/4-28 interface were used to couple the HPLC directly to the microring resonator cartridge, as described previously.[10]

2.7. Data Analysis

Data analysis was carried out using custom software written in R (version 3.4.1), previously described in more detail.[10] Briefly, microring resonator chromatograms typically show an averaged responses from 4-36 microrings depending on the experiment. The averaged signal intensity is plotted as a function of time.

3. Results and Discussion

3.1. Investigation of Silane-Polymer Interactions with Stand-alone Operation of Microrings

Silanes were the first approach for creating column mimics at the chip surfaces and preliminary work with these silanized chips were executed in the stand-alone operation of the microrings. In other words no LC was used in these experiments rather syringe pumps drove solvent across the chip surface. The hope of these experiments was to find a silane that exhibited strong interactions with PMMA/PMMA-PS so that these "systems" could later be translated into on-line LC experiments where the silanized chip replaces the LC column. The approach for these experiments involved the following. First, flow a weak solvent/adsorption promoting solvent to achieve a baseline, and in Figure 6-4 the weak solvent was toluene which is highlighted in blue. Next, flow a polymer solution prepared in a solvent which should promote adsorption. In other words we want to find a solvent system where our polymers are soluble but also have a preference for the chip surface, which is not easy. As shown in Figure 6-4 PMMA (highlighted in yellow) and 82% PS-PMMA (highlighted in red) were prepared at 1 mg/mL in toluene. If adsorption happens with this step a Langmuir binding profile will be observed, this is seen in Figure 6-4A, B, and E when 82% PS-PMMA is flowing and in Figure 6-4F we see this for both PMMA and 82% PS-PMMA although it is showing a negative refractive index difference.

If no adsorption occurs a square like step is observed, this is seen Figure 6-4A, B, E when PMMA is flowing and in Figure 6-4C-D this is observed for both PMMA and 82% PS-PMMA. The third step goes back to our weak solvent, toluene. Any non-binding cases should just show a step in the refractive index change as the polymer solution flows across the chip, with a return to the original baseline upon return to the weak solvent. Any binding or adsorption to the silane would be expect to exhibit a continuous increase of the baseline at that point. However, that is not observed in any of the cases where binding is observed instead a downward sloping trace was observed indicating removal of any mass that may have been held at the chip surface. This rapid disappearance of polymer indicates very weak interactions that would likely not hold up to chromatography interfaced experiments. Additionally with these experiments most of the chosen silanes were polar, as such PMMA would be expected to have more affinity for the chip surface in comparison to 82% PS-PMMA, however generally that trend was not observed.

3.2. Untreated Microring Resonator Chip Experiments

Investigating the untreated chip response was explored given the oxidized silicon surface potentially best replicates the surface of silica, which is conventionally used for chemical composition characterization via solvent gradient LC.[11] The same stand-alone microring resonator experimental approach was used in Figure 6-5; however, here an unfunctionalized chip was utilized to investigate the silicon-polymer interactions. Here evidence of binding was observed for both PMMA (highlighted in yellow) and 82% PS-PMMA (highlighted in red). Then looking at the toluene step (highlighted in blue) following the flow of polymer it is observed that with PMMA we are not observing rapid loss like we

are with 82% PS-PMMA or as was observed in Figure 6-4. The loss off the 82% PS-PMMA was not an immediate concern considering that with increasing PS content there is a decrease in polarity, meaning a decrease in affinity for the silicon surface. In other words, we are looking at two extremes polar PMMA and mostly non-polar 82% PS-PMMA with these experiments. Given that we see interactions responding according to polarity we can speculate that copolymers in between would show loss rates corresponding to their PS content which would have the potential to dictate separations once translated to chromatography. One important thing to mention is that in our previous paper, we used a similar system for the refractive index based detection of solvent gradient elution. In this study no adsorption to the chip surface was observed and should not be observed since a column was used so separations occurred before detection by the microrings. In other words, with previous LC-microring resonator studies analytes only come in contact with the sensor chip once they are in favorable solvents mitigating any affinity which is very different from what we are doing with these current studies.

Given the potentially promising observations in Figure 6-5, untreated chips were further pursed as a column mimic in on-line experiments. On-line meaning interfaced to the LC module but operated without a column, which is true for all “on-line” experiments in this chapter. The first attempt at this is shown in Figure 6-6, where the initial hold of the gradient (100% toluene) was run at 0.1 mL/min to replicate the stand-alone experiments and the gradient portion was run at 0.4 mL/min (100 toluene to 50:50 toluene:THF). Detection of this method by the microrings is seen in Figure 6-6A. The peak at the beginning of the traces is detection of pressure ripple from the injection. There is an upward ramping of the initial hold portion indicating potential adsorption, however no

indication of polymer leaving the chip surface is observed during the gradient. This is verified in Figure 6-6B, which shows detection by ELSD connected in series with the microrings. Thus any polymer that was adsorbed at the chip surface should be released and observed with ELSD detection. Rather what is seen with ELSD post microring resonators is a large peak with the solvent front indicating that much of the injection is not retained. By zooming into the baseline a small peak was observed for PMMA, however given that nothing was observed with the microrings, confidence that this is retained polymer is very low.

The unpromising results from Figure 6-6 inspired an alternative approach to exploring “on-line” experiments, which is provided in Figure 6-7. Here the stand-alone approach was combined with the “on-line” method, where a pre-loading of the chip was performed with 100% PMMA in stand-alone operation before interfacing with the LC module which is shown in Figure 6-7A. Following the pre-loading of the untreated microring resonator chip the microring resonator flow cell was connected to the LC without a column so that a solvent gradient could be delivered across the chip surface, with the hopes that at some point during the gradient PMMA would be released from the chip surface. Looking at Figure 6-7B we don’t see any obvious indication of PMMA release there is a small negative “blip” in the gradient at approximately 25 minutes, however this is not showing up with post detection by ELSD (Figure 6-7C). Which indicates that even though we were seeing what appeared to be decent interactions in the stand-alone experiments that these interactions appear to be too weak to translate to chromatography.

3.3. Oxidized Microring Resonator Chip Experiments

Given that untreated microring resonator chips showed more promise over silanized chips the next approach explored how we could make the silicon surface further resemble a silica column. Piranha treatments and oxygen plasma treatments were used for oxidizing the chip surface. Figure 6-8 shows the investigation of the oxidized silicon surface with various polymers was explored using the stand-alone operation of the microring resonators. These experiments were run much like Figures 6-4 and 6-5, however here an additional step was added which flowed 50:50 toluene:THF after the second weak solvent/toluene step to regenerate the chip surface before flowing another polymer solution. Taking a closer look at these, off-sets are observed in the baseline. Looking at Figure 6-8, toluene (light blue) is first flown to establish a baseline which is followed by 14% PS-PMMA (purple) and then another toluene step (light blue). Comparing the two toluene steps we can see that these are not lining up rather they are off-set by 18 ∆pm for the piranha chips and 12 ∆pm for the oxygen plasma chips. Next, 50:50 toluene:THF is flown (highlighted in darker blue) we see a significant negative shift which is followed by another toluene step that re-baselines to match the initial toluene step. This off-set in the baseline in weak solvent indicates that polymer was retained at the chip surface and released once strong solvent was flown. This was seen when each investigated polymer was flown across the oxidized chip surfaces, for the piranha treated chip (Figure 6-8A),a 65 ∆pm off-set is observed with 54% PS-PMMA (green) and a 42 ∆pm off-set is observed for 82% PS-PMMA (red). As for the oxygen plasma treated chip (Figure 6-8B),a 45 ∆pm off-set is observed with 54% PS-PMMA (green) and a 41 ∆pm off-set is observed for 82% PS-PMMA (red). The dashed line in Figure 6-8 provides a guide for the eye to observe these changes in the baseline.

Given that polymer appeared to be retained in stand-alone experiments by the oxidized chip surface in weak solvent conditions use of the oxidized surface was further pursed as a column mimic in on-line experiments. With the toluene THF solvent system no indication of adsorption was observed, therefore weaker adsorption promoting conditions were sought after. The weakest solvent condition where our polymers were still soluble was 80:20 toluene:THF however in “on-line” experiments this did not work as expected as seen in Figure 6-9. Here we were having challenges with our injections precipitating out before the chip regardless of the size of the injection which is not ideal for the study at hand. A peak was observed once PMMA was solubilized by the appropriate gradient composition, ELSD in-line observed the same occurrence. Although, oxidized chip surfaces appeared the most promising for translating to a “chromatography-like” experiment, these were no longer pursued given the weak interactions and challenges with precipitation and dissolution.

4. Conclusion

Various surface modifications for the microring resonator chip surface were pursued with the interest of mimicking a column. Although some hints of success were observed with stand-alone experiments, none showed success in on-line experiments. For example, even though decent polymer affinity for oxidized silicon chips across a range of PS-PMMA copolymers was observed, the same response was not observed when an injection was delivered by the LC rather than bulk polymer solutions flown across the chip surface. Because of this much work went into finding conditions that better promote adsorption, however this meant moving to less soluble solvent conditions which caused

persistent challenges with precipitation that were not avoidable. All and all, further consideration needs to be dedicated to the differences between the two experiment types. The biggest obvious difference is the flow of bulk polymer solutions versus small plugs of injections from the LC. Better replicating the LC injection potentially with an injection valve or such in the stand-alone experiments could have been useful for screening chemical conditions/interactions which better replicate the “on-line” experiments.

Although little success was found with the presented study, there was one such occasion where the on-line experiment “worked,” however it failed to be reproducible. This experiment is shown in Figure 6-10, the point of presenting this is not to make revolutions or say this was a success, rather it is shown here to illustrate to the reader what we were hoping to have seen. Figure 6-10A shows the raw gradient traces for two 31% PS-PMMA injections onto a APTES functionalized chip, here it is observed that with the copolymer injections that there is an off-set on the trace in comparison to the blank until a certain point where there is a vertical drop in the trace at approximately 30 minutes after this point the trace of the 31% PS is identical to the blank trace. The shift or off-set of the 31% PS traces is likely because mass was being pulled onto the chip surface and the re-baselining likely occurred once that mass was released at the appropriate solvent condition. Which again was not something that could be replicated unfortunately.

The hope of this work was to utilize the functionalizable chip surface to add another separation dimension at the chip surface with the first dimension being an actual column such as gel permeation. This is still ultimately something that can be pursued, given that it was not necessarily the experimental design which failed but rather the system, with a

more appropriate system such as reverse phase gradient with highly soluble small molecules these experiments may still be possible. However, an alternative approach has been taken to utilize the functionalizable chip surface with biological capture agents, the high affinity of these capture agents allows for analyte pull down even in on-line experiments.

Table 6-1: Silane Overview

Alkoxysilanes	Abbreviation	Surface Modification	Structure
3-aminopropyltriethoxy silane	APTES	Induces hydrophilicity	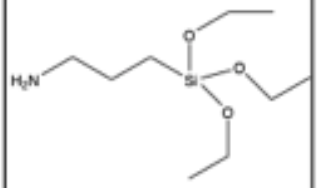
N,N-Bis(2-Hydroxylethyl)-3-aminopropyltriethoxy silane	BH-APTES	Induces hydrophilicity	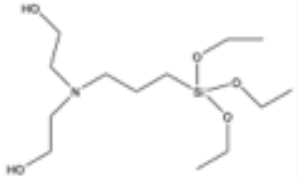
Cyanopropyltriethoxy silane	CPTES	Induces hydrophilicity	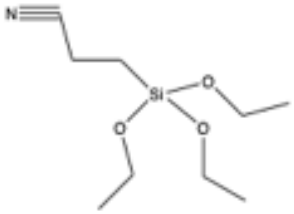
2-Hydroxy-4-(3-triethoxysilylpropoxy) diphenylketone) silane	HTDS	Induces hydrophilicity	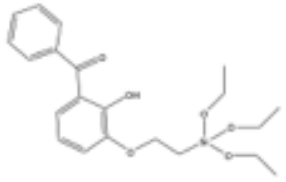
N-(3-Triethoxysilylpropyl) gluconamide silane	TGS	Induces hydrophilicity	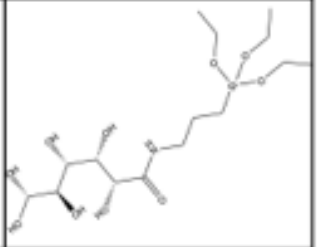
Octadecyltriethoxy silane	ODTES	Induces hydrophobicity	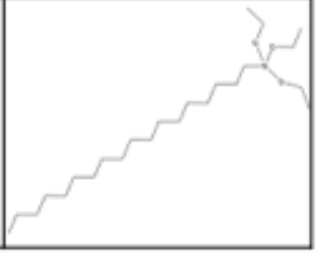

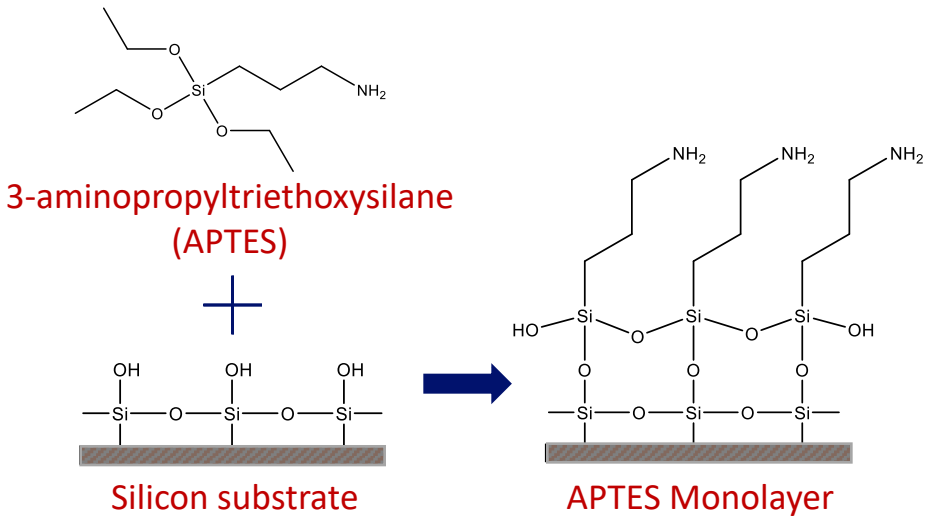

Figure 6-1: Example of Chip Functionalization via Silanization. Here the hydroxyl groups of the silicon surface of the microring resonator chip displace the alkoxy groups on the alkoxysilanes (in this example 3-aminopropyltriethoxysilane), forming covalent –Si-O-Si- bonds.

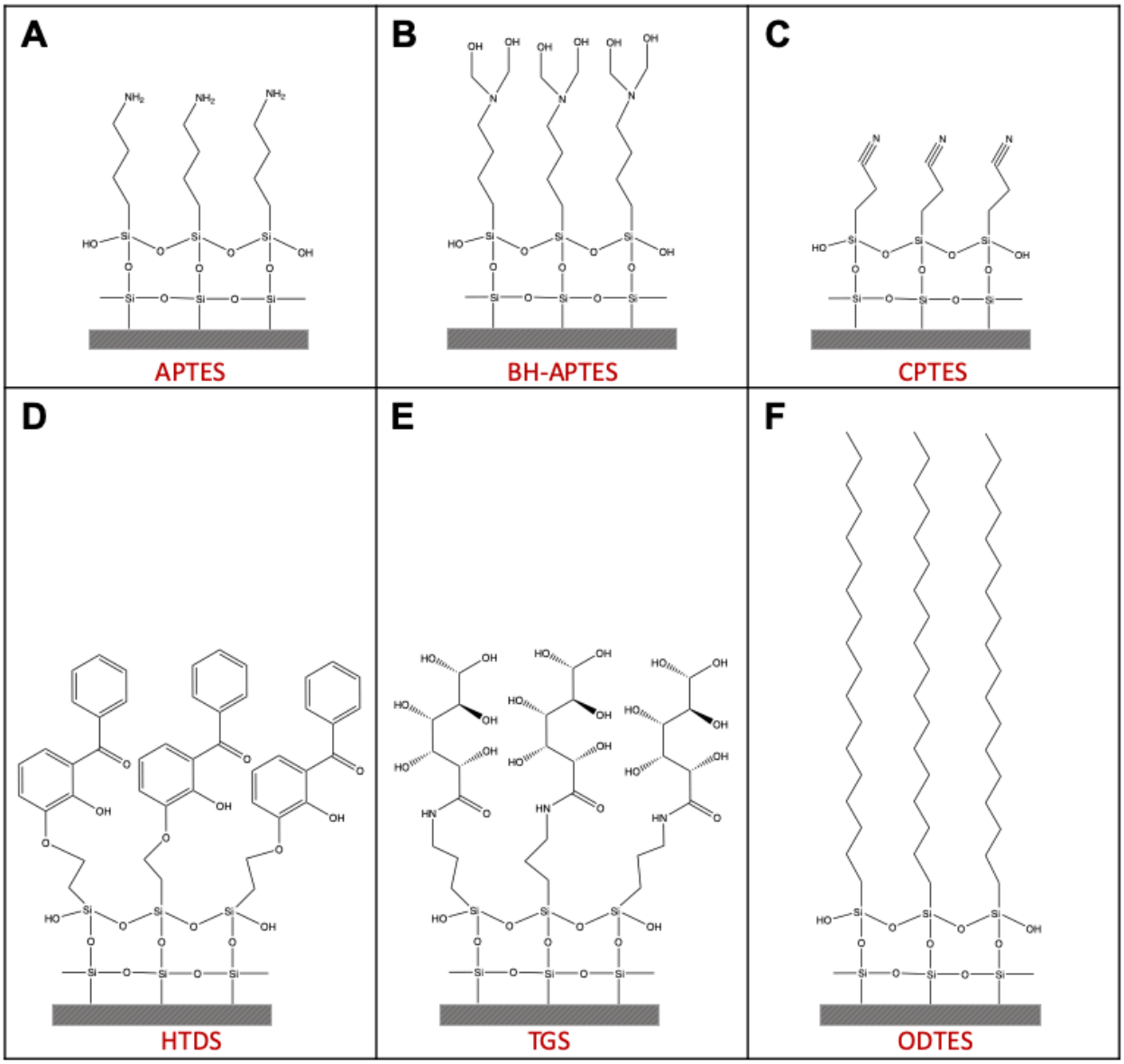

Figure 6-2: Structure of Silane Monolayers on Silicon Surface of Microring Resonator Chips. (A) APTES**,** 3-aminopropyltriethoxy silane monolayer. (B) BH-APTES, N,N-Bis(2-Hydroxylethyl)-3-aminopropyltriethoxy silane monolayer. (C) CPTES, Cyanopropyltriethoxy silane.(D) HTDS, 2-Hydroxy-4-(3-triethoxysilylpropoxy) diphenylketone) silane monolayer. (E) TGS, N-(3-Triethoxysilylpropyl)gluconamide silane monolayer. (F) ODTES, Octadecyltriethoxy silane monolayer. Surface functionalization/modification achieved using the process depicted in Figure 1.

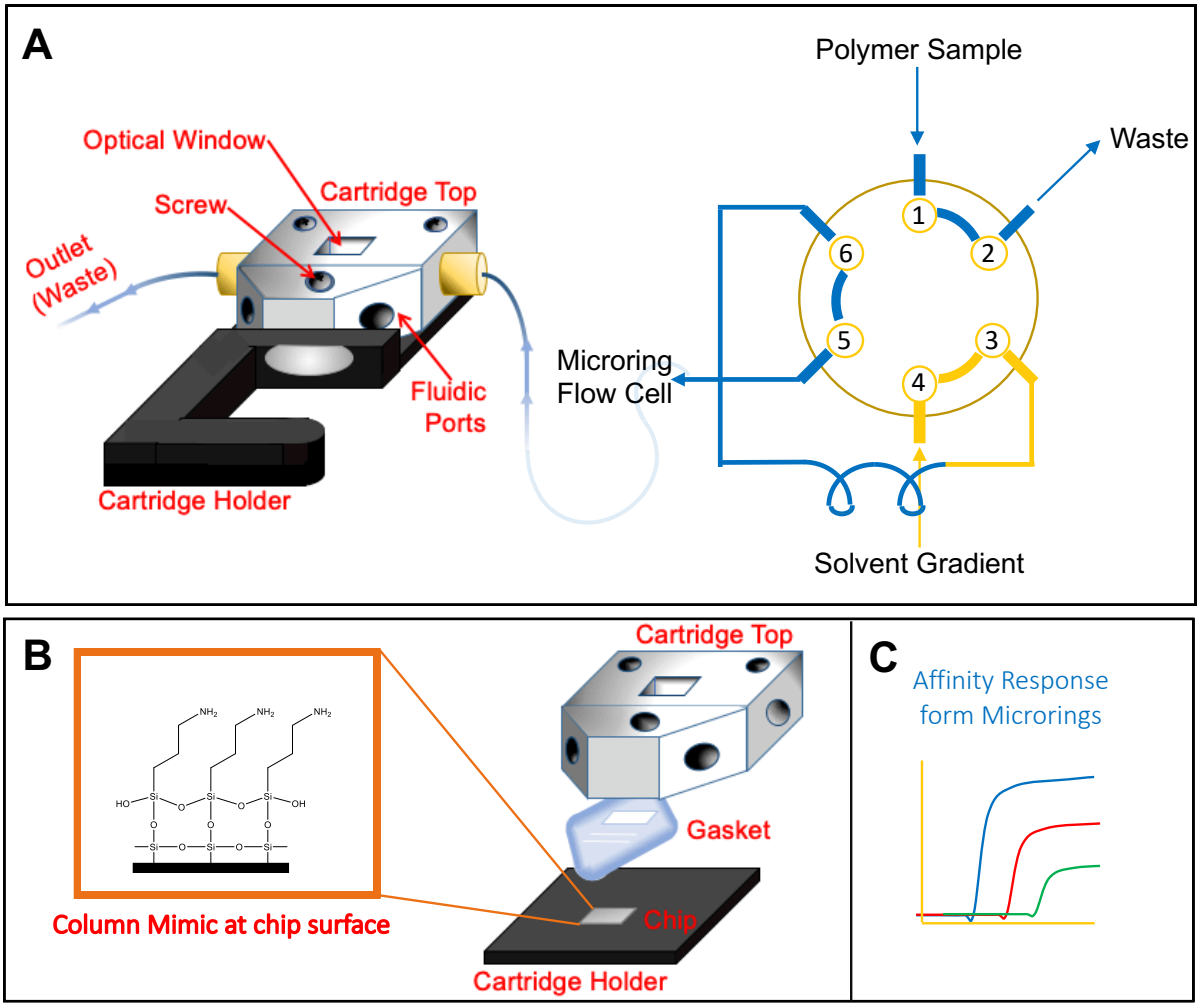

Figure 6-3: Experimental Design Schematic. (A) HPLC-Microring resonator interface/flow path. (B) Expanded view of microring resonator flow cell showing an example chemical modification of the chip surface. (C) Sketch of microring resonator binding chromatogram.

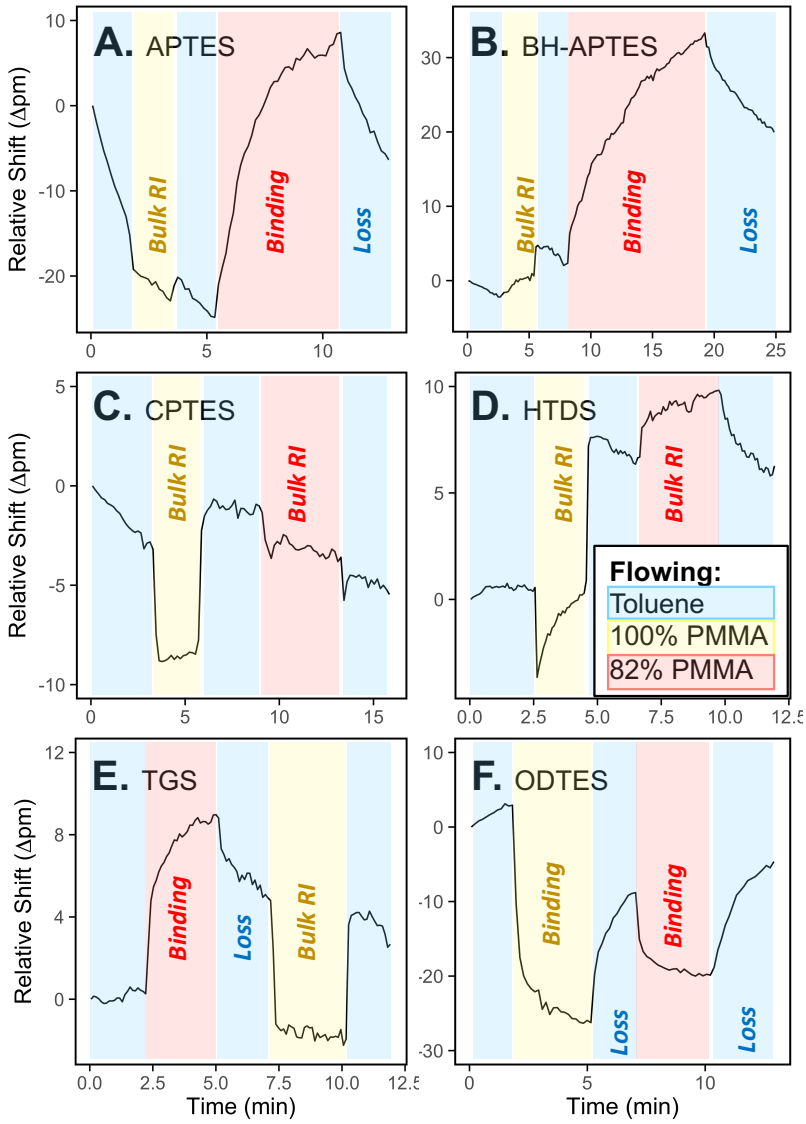

Figure 6-4: Investigation of Silane-Polymer Interactions with Stand-alone Operation of the Microring Resonator Platform. (A) APTES functionalized chip surface, with the flow (0.1 mL/min) of alternating blank weak solvent/toluene (highlighted in blue) and 1 mg/mL polymer solutions (100% PMMA, highlighted in yellow and 82% PMMA-PS, highlighted in red). (B) BH-APTES functionalized chip surface, with the flow of alternating blank solvent and polymer solution steps. (C) CPTES functionalized chip surface, with the flow of alternating blank solvent and polymer solution steps.(D) HTDS functionalized chip surface, with the flow of alternating blank solvent and polymer solution steps. (E) TGS functionalized chip surface, with the flow of alternating blank solvent and polymer solution steps. (F) ODTES functionalized chip surface, with the flow of alternating blank solvent and polymer solution steps. The observations are annotated on the figure itself where “bulk RI” means no polymer is adsorbed to the chip surface, “binding” means a Langmuir binding profile is observed indicating polymer retention, and toluene steps following previous binding step which experience loss of the retained polymer are labeled “loss” indicating weak interactions. Re-baselining toluene (blue) steps in between polymer steps are unlabeled.

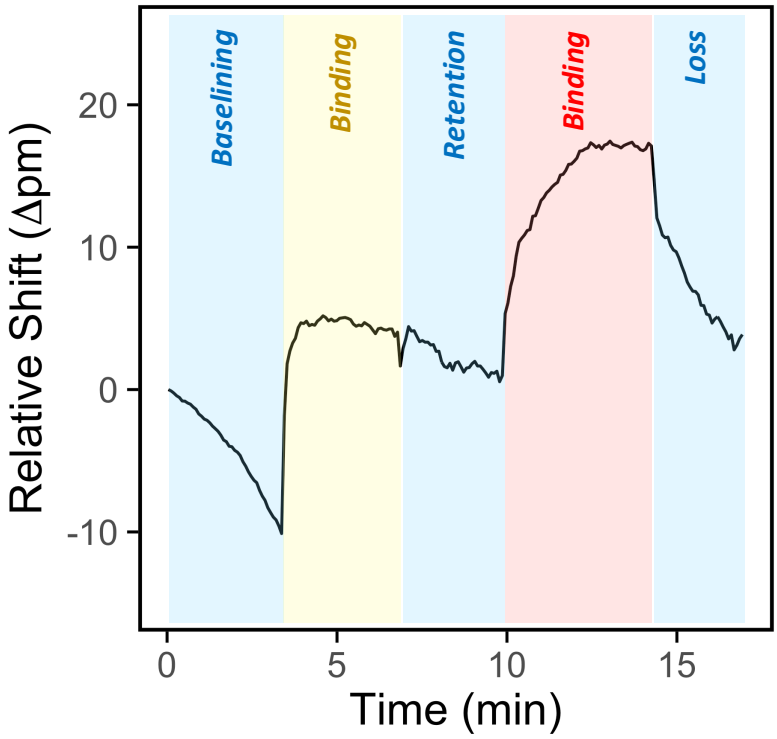

Figure 6-5: Investigation of Silicon-Polymer Interactions with Stand-alone Operation of the Microring Resonator Platform. Unfunctionalized/untreated chip surface, with the flow (0.1 mL/min) of alternating blank solvent (toluene) and 1 mg/mL polymer solutions (100% PMMA and 82% PMMA-PS). The observations are annotated on the figure itself where "binding" means a Langmuir binding profile is observed indicating polymer retention, the toluene steps following previous binding step are labeled either "retention" for strong interactions or "loss" for weak interactions.

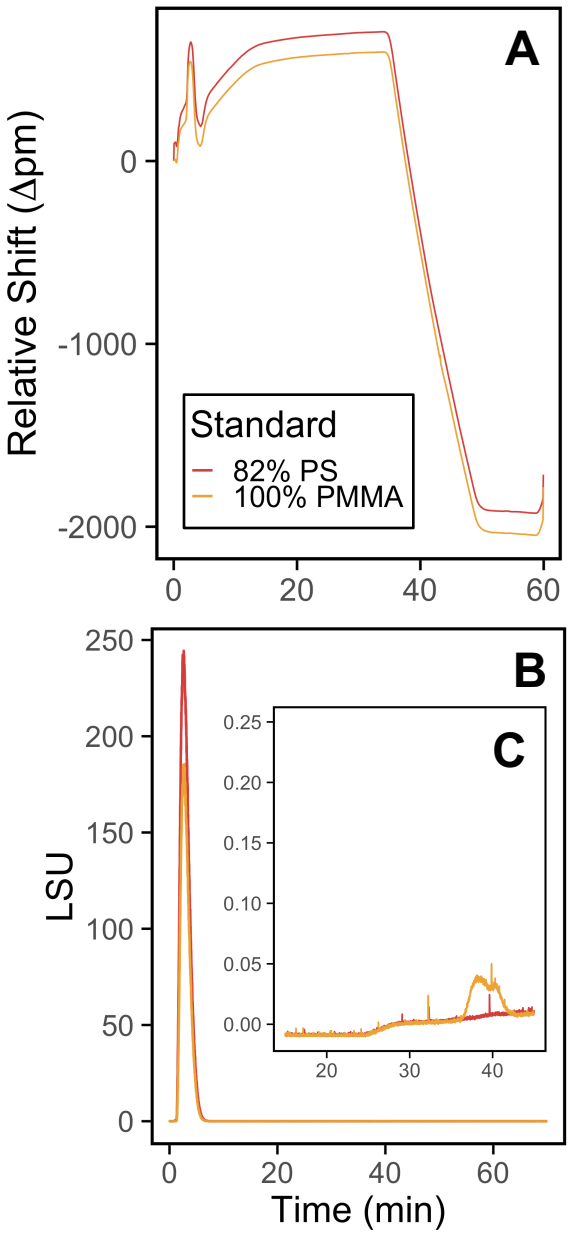

Figure 6-6: On-line Experiment with Untreated Chip and No Column in Order to best Mimic the Stand-alone Experiments. (A) Raw gradient traces obtained from microring resonators. The method used was a 100:0 Toluene:THF to 50:50 Toluene:THF gradient, where the initial hold of the gradient was run at a 0.1 mL/min flow rate to allow for adequate adsorption time and the remaining method was run at 0.4 mL/min. (B) The microring resonators and ELSD were connected in series, therefore any polymer that was adsorbed at the chip surface should be released and observed with ELSD detection. (C) Zooming in on the ELSD chromatogram shows a very small peak for the 100% PMMA injection however no indication of this mass at the microring surface is observed in (A).

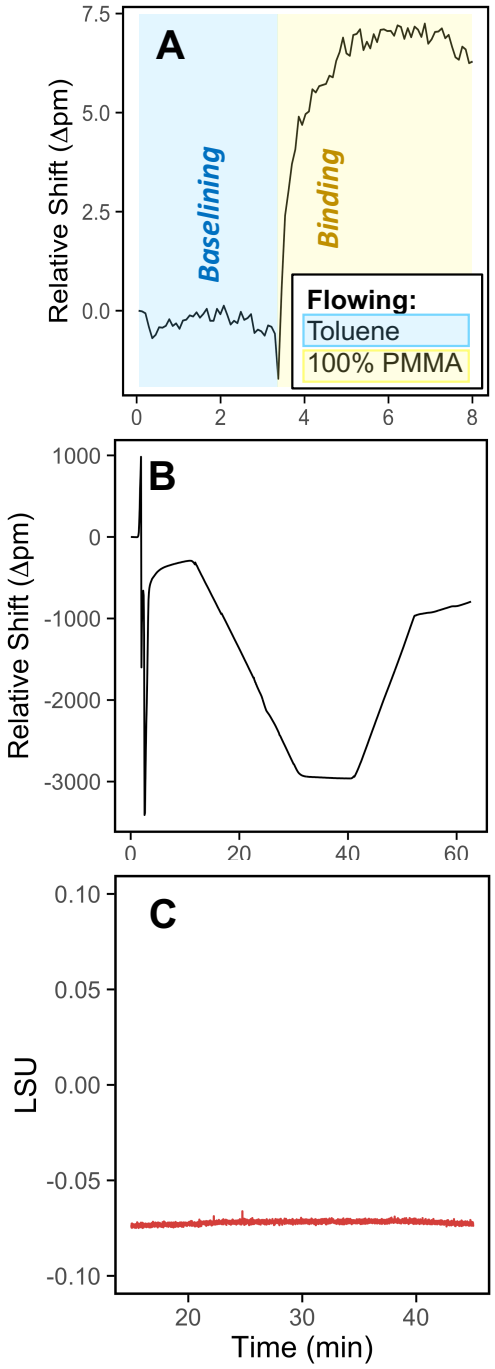

Figure 6-7: "Pre-Loading" PMMA on Untreated Chip in Off-line Experiment Followed by a Solvent Gradient Delivered by the LC. (A) Mimicking the conditions from Figure 6-5, in stand-alone operation PMMA was pre-adsorbed/pre-loaded onto the unfunctionalized microring chip before running a solvent gradient. (B) Following the pre-loading experiment, the microring resonator flow cell was connected to the LC which delivered a toluene:THF gradient. (C) The microring resonators and ELSD were connected in series, therefore any polymer that was released from the chip surface should be observed detection by ELSD.

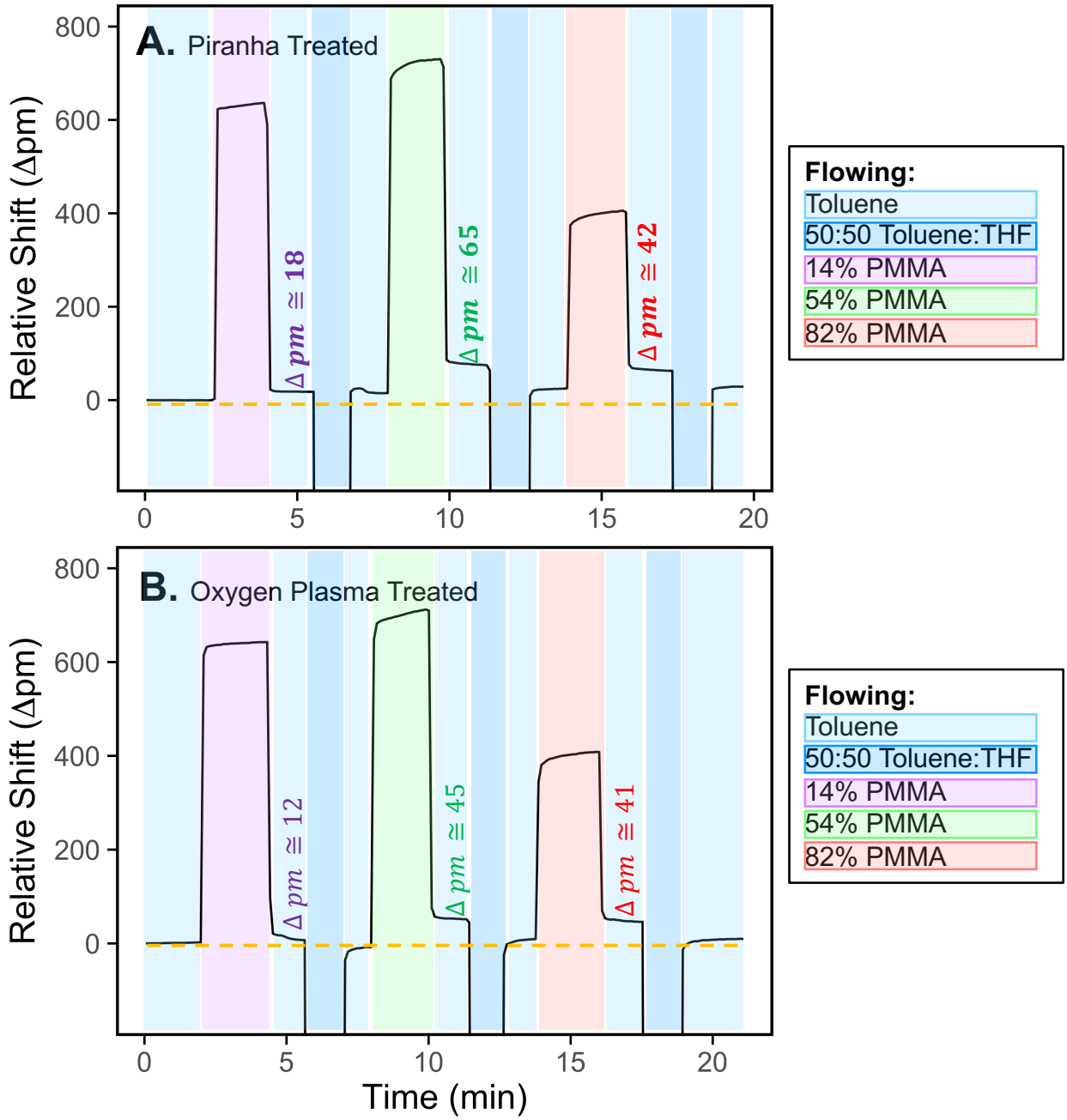

Figure 6-8: Investigation of Oxidized Silicon Surface-Polymer Interactions with Stand-alone Operation of the Microring Resonator Platform. (A) Piranha treated chip surface, with the flow (0.1 mL/min) of weak/blank solvent (toluene), various 1 mg/mL polymer solutions (14% PMMA-PS, 54% PMMA-PS, and 82% PMMA-PS), and strong solvent (50:50 Toluene:THF) for surface regeneration. (B) Oxygen plasma treated chip surface, with the same flow conditions as (A). Presented traces are zoomed in for optimal visualization. Off-sets are observed in the baseline in these experiments when polymer is held at the chip surface and following the flow of a strong solvent the baseline is re-established. Approximate shifts are annotated on the figure along with a dashed line to serve as a guide for the eye to observe these off-set changes in the baseline.

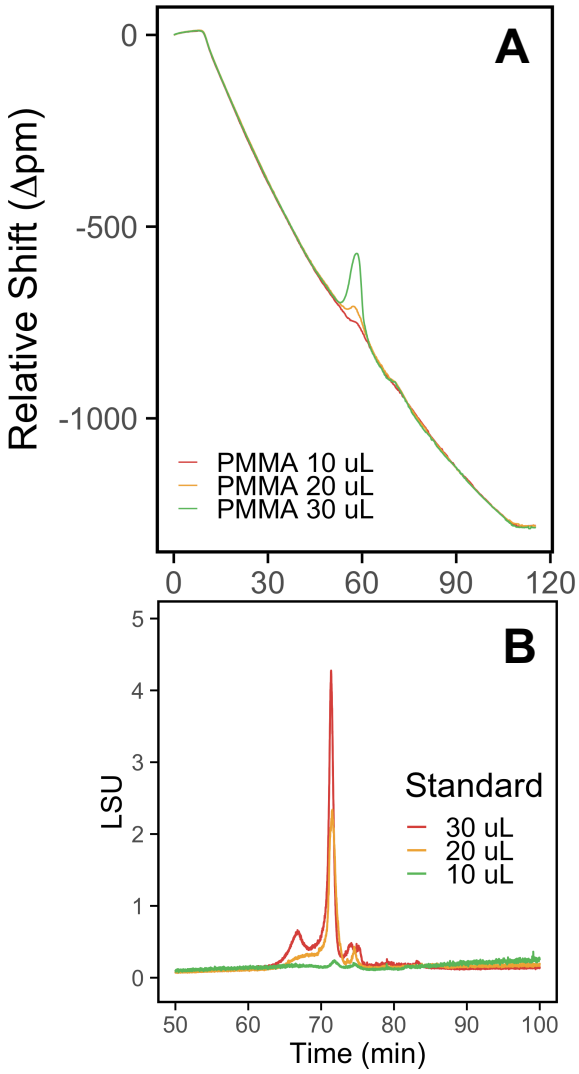

Figure 6-9: Persistent Precipitation Dissolution Method Challenges, On-line Experiment Using Oxidized Chip and No Column. (A) Raw microring resonator traces showing PMMA peak eluting in the middle of the gradient even though there is no column (1 mg/mL PMMA, varied injection volumes). (B) In-line ELSD chromatogram verifying the same occurrence.

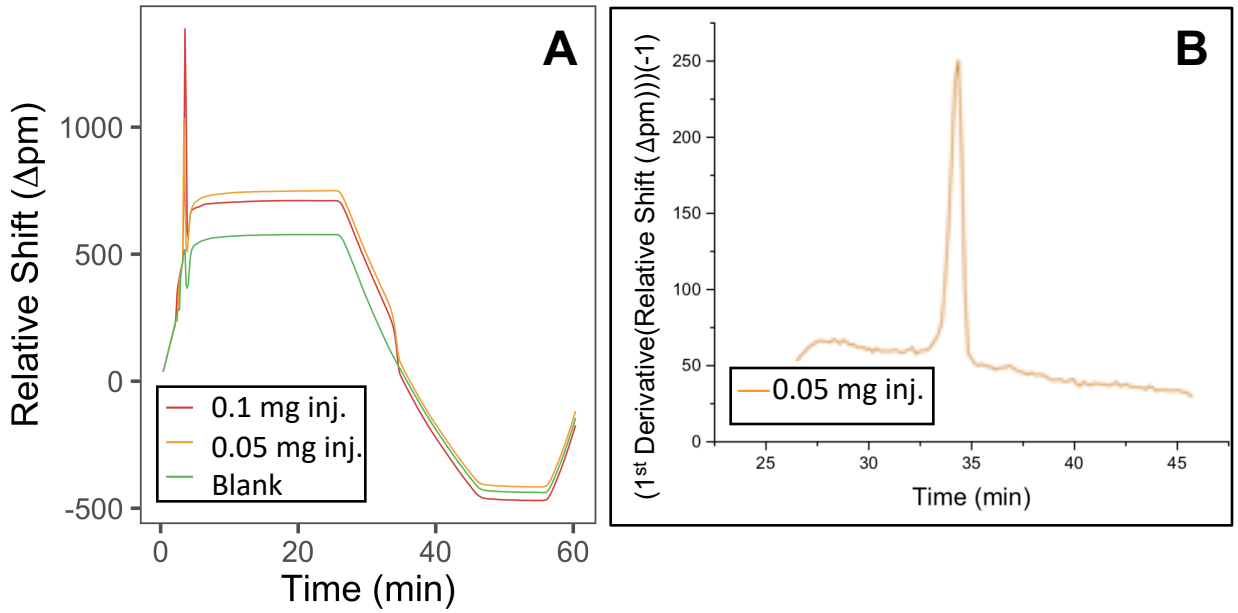

Figure 6-10: On-line Experiment with APTES Functionalized Chip and No Column. (A) Raw microring resonator traces showing injection of 31% PS-PMMA (0.1 and 0.05 mg) being retained at the chip surface and being released mid cyclohexane–THF gradient. (B) First derivative of data shown in (A).

5. Reference

(1) Schoenmakers, P.; Aarnoutse, P. Multi-Dimensional Separations of Polymers. *Anal. Chem.* **2014**, *86* (13), 6172–6179. https://doi.org/10.1021/ac301162b.

(2) Pasch, H.; Trathnigg, B. Two-Dimensional Liquid Chromatography. In *Multidimensional HPLC of Polymers*; Pasch, H., Trathnigg, B., Eds.; Springer Laboratory; Springer: Berlin, Heidelberg, 2013; pp 95–181. https://doi.org/10.1007/978-3-642-36080-0_6.

(3) Baumgaertel, A.; Altuntaş, E.; Schubert, U. S. Recent Developments in the Detailed Characterization of Polymers by Multidimensional Chromatography. *J. Chromatogr. A* **2012**, *1240*, 1–20. https://doi.org/10.1016/j.chroma.2012.03.038.

(4) Cardenosa-Rubio, M. C.; Graybill, R. M.; Bailey, R. C. Combining Asymmetric PCR-Based Enzymatic Amplification with Silicon Photonic Microring Resonators for the Detection of LncRNAs from Low Input Human RNA Samples. *Analyst* **2018**, *143* (5), 1210–1216. https://doi.org/10.1039/C7AN02045G.

(5) Graybill, R. M.; Para, C. S.; Bailey, R. C. PCR-Free, Multiplexed Expression Profiling of MicroRNAs Using Silicon Photonic Microring Resonators. *Anal. Chem.* **2016**, *88* (21), 10347–10351. https://doi.org/10.1021/acs.analchem.6b03350.

(6) Robison, H. M.; Escalante, P.; Valera, E.; Erskine, C. L.; Auvil, L.; Sasieta, H. C.; Bushell, C.; Welge, M.; Bailey, R. C. Precision Immunoprofiling to Reveal Diagnostic Signatures for Latent Tuberculosis Infection and Reactivation Risk Stratification. *Integr. Biol.* **2019**, *11* (1), 16–25. https://doi.org/10.1093/intbio/zyz001.

(7) Muehl, E. M.; Gajsiewicz, J. M.; Medfisch, S. M.; Wiersma, Z. S. B.; Morrissey, J. H.; Bailey, R. C. Multiplexed Silicon Photonic Sensor Arrays Enable Facile

Characterization of Coagulation Protein Binding to Nanodiscs with Variable Lipid Content. *J. Biol. Chem.* **2017**, *292* (39), 16249–16256. https://doi.org/10.1074/jbc.M117.800938.

(8) Washburn, A. L.; Shia, W. W.; Lenkeit, K. A.; Lee, S.-H.; Bailey, R. C. Multiplexed Cancer Biomarker Detection Using Chip-Integrated Silicon Photonic Sensor Arrays. *Analyst* **2016**, *141* (18), 5358–5365. https://doi.org/10.1039/C6AN01076H.

(9) Wade, J. H.; Alsop, A. T.; Vertin, N. R.; Yang, H.; Johnson, M. D.; Bailey, R. C. Rapid, Multiplexed Phosphoprotein Profiling Using Silicon Photonic Sensor Arrays. *ACS Cent. Sci.* **2015**, *1* (7), 374–382. https://doi.org/10.1021/acscentsci.5b00250.

(10) Mordan, E.; Wade, J. H.; Wiersma, Z. S. B.; Pearce, E.; Pangburn, T. O.; deGroot, A. W.; Meunier, D. M.; Bailey, R. C. Silicon Photonic Microring Resonator Arrays for Mass Concentration Detection of Polymers in Isocratic Separations. *Anal. Chem.* **2018**. https://doi.org/10.1021/acs.analchem.8b04263.

(11) Mordan, E. H.; Wade, J. H.; Pearce, E.; Meunier, D. M.; Bailey, R. C. A Linear Mass Concentration Detector for Solvent Gradient Polymer Separations. *Analyst* **2020**. https://doi.org/10.1039/C9AN02533B.

(12) Orlet, J. D.; Bailey, R. C. Silicon Photonic Microring Resonator Arrays as a Universal Detector for Capillary Electrophoresis. *Anal. Chem.* **2020**, *92* (2), 2331–2338. https://doi.org/10.1021/acs.analchem.9b05271.

(13) Wade, J. H.; Bailey, R. C. Refractive Index-Based Detection of Gradient Elution Liquid Chromatography Using Chip-Integrated Microring Resonator Arrays. *Anal. Chem.* **2014**, *86* (1), 913–919. https://doi.org/10.1021/ac4035828.

(14) Iqbal, M.; Gleeson, M. A.; Spaugh, B.; Tybor, F.; Gunn, W. G.; Hochberg, M.; Baehr-Jones, T.; Bailey, R. C.; Gunn, L. C. Label-Free Biosensor Arrays Based on Silicon Ring Resonators and High-Speed Optical Scanning Instrumentation. *IEEE J. Sel. Top. Quantum Electron.* **2010**, *16* (3), 654–661. https://doi.org/10.1109/JSTQE.2009.2032510.

(15) Wade, J. H.; Bailey, R. C. Applications of Optical Microcavity Resonators in Analytical Chemistry. *Annu. Rev. Anal. Chem.* **2016**, *9*, 1–25. https://doi.org/10.1146/annurev-anchem-071015-041742.

CHAPTER VII

Conclusions and Preliminary Results for Future Directions

Acknowledgements

I would like to acknowledge the many contributions of my co-worker John D. Orlet for his contributions in the following ventures still underway. Assisting with experimental design and execution for collection of the preliminary nanoflow data. As for the SEC-antibody capture work, John is responsible for chip functionalization, sample preparation, and microring resonator data work up. I am responsible for SEC method development, SEC operation and UV/vis data work up. Unmentioned task are of shared responsibility. I would

also like to thank Professor Zachary Schultz of Ohio State University for bring the potential nanoflow LC work to our attention.

1. Dissertation Summary and Conclusions

This dissertation presented here works toward demonstrating the versatility and utility of the microring resonators as an alternative high performance liquid chromatography (HPLC) detector for various types of separations. Three main approaches were presented, including bulk refractive index detection, in-line functionalized sensor chips, along with much flow cell design and testing for further optimization of the microring resonator platform for future liquid chromatography (LC) applications. In summary, chapters 2 and 5 shows work that utilizes the microring resonator platform as a bulk refractive index (RI) detector. Chapters 3-4 illustrate flow cell design approaches and chapter 6 shows work that takes advantage of the functionalizable chip surface.

1.1. Microring Resonators as a Bulk RI LC Detector

Chapters 2 and 5 present work that utilizes the microring resonator platform as a bulk RI detector, meaning the senor chip is untreated and no fouling/binding is observed. Chapters 2 sets the stage for the microring resonator as an LC detector using isocratic gel permeation chromatography (GPC) separations of polystyrene (PS). Here molecular weight distributions were determined and the linear mass detection capability of the microring resonators was demonstrated.[1] Chapter 5 builds upon this by detecting the solvent gradient separation of polystyrene -co- polymethyl methacrylate polymers (PS-

PMMA) according to chemical composition. Here direct comparisons were made to non-linear evaporative light scattering (ELSD) with various calibrations and quantification of blend components.[2] With both these chapters comparable function of the microring resonator platform to conventional HPLC detectors, such as UV/vis, differential refractive index (dRI) and ELSD was observed. More so, many added benefits were obtained by using the microring resonators over conventional detectors, such as the universal detection of solvent gradient elution along with linear mass detection presented in chapter 5, both of which cannot be offered by a single commercial detector.

1.2. Microring Resonators Flow Cell Design Ventures

Although chapters 3 and 4 use bulk RI detection of LC eluents, a different goal was in mind: further development of the microring resonator flow cell for LC applications. In chapter 2 a molecular weight dependence was observed which showed lower sensitivity to the upper molecular weight range. Given that the microrings are a surface sensitive detector it is understood that sensitivity will depend on proximity to the sensor surface. Given that we were observing this sensitivity challenge with large polymers in solution it was hypothesized that this was a result of poor mass transfer. Therefore, in chapter 3 an alternative flow cell geometry was utilized in hopes of improving the mass transfer of high molecular weight polymers. Through this work a series of flow cell lids and gaskets were employed for the detection of PS separated by GPC and with peak integrations performance was evaluated. Ultimately with this work it was found that the molecular weight dependence is very reproducible and no significant improvements with this fall-off are observed with alternative flow cells or by varying other experimental parameters such

as flow rate. As a result, it assumed that this challenge is not due to mass transfer issues alone, requiring further consideration of the limitations of the evanescent field.

Chapter 4 also revolved around flow cell design but with the interest of making one compatible for high temperature LC applications. Here a series of three designs were presented and the final design was tested with full operation. Overall the flow cell was successful, maintaining flow and temperature, the challenge was that microring resonator signal became unusable at these elevated temperature. The exact cause of the unusable signal is still unclear, it is possible that this could be due to solvent incompatibility or poor coupling of light at such temperature requiring software changes that are beyond our expertise. In other words, there is more work that needs to be done here to fully conclude if this work can be successful in the future.

1.3. Functionalized Microring Resonator Chips In-line with Upstream Separations

Bulk RI detection is not typical function of the microring resonator platform. Conventional operation of the microring resonators utilizes functionalized chip surfaces to execute binding assays. Chapter 6 took one approach for utilizing the functionalize chip surface by creating column mimics at the sensor surface with the interest of performing multi-dimensional separations. Precipitation-dissolution challenges arose with the system chosen with this approach presented in Chapter 6 making execution of these experiments unsuccessful. It is suspected that if the same experimental design was used along with small molecules and a reverse phase solvent system that these experiments would be more successful. A different approach was sought which is presented in more detail later in this chapter. Briefly, this approach took inspiration from traditional microring resonator

operation, using biomolecular capture agents in-line with size exclusion chromatography (SEC) separations. The preliminary data is discussed in the next section. Taking this work into consideration along with completed work, fully shows the versatility of the microring resonator platform as an LC detector along with the unique capability to adding another dimension of data post separation.

1.4 Final Remarks

In conclusion**,** there is a continuing need for a LC detector which is universal, gradient compatible and linear in response to increasing mass, this challenge is especially encountered through polymer analysis by LC methods. This goal in a detector can be achieved by the microring resonator platform as demonstrated throughout this dissertation. However, the microring resonators are not optimized as a LC detector and because of this many challenges have been encountered such as a small signal to noise ratio (S/N), the average signal to noise ratio of the microrings is approximately 4 orders of magnitude smaller than UV and ELSD. The microring resonators also suffer from elevated limits of detection (LOD), where on average the LOD of the microring resonators is approximately 5 orders of magnitude greater than the LOD for both UV and ELSD. Then finally the molecular weight dependence of the microring resonators, the microring resonators experience decreased sensitivity to polymers which have a 2Rg (radius of gyration) that equals or exceeds the 25 nm sensing region. All these outlined challenges are limitations of the microring resonator platform as an LC detector, ideally with further optimization of the microrings flow cell for LC applications some of these areas can be improved upon.

2. Future Directions and Preliminary Results

2.1. Microring Resonators as a Complementary Detector for Nanoflow LC

Use of microring resonators a bulk RI LC detector can be used for many applications especially those that traditionally use ELSD or charged aerosol (CAD) such as pharmaceutical analysis.[3–6] Along with other LC applications the microring resonators can also have potential promise as a nanoflow LC detector. This is heavily motivated by recent work interfacing the microring resonators with capillary electrophoresis (CE) since flow rates and solvent consumption used here are much more comparable to those used in nanoflow LC.[7] Preliminary data is presented here showing detection of flow injections delivered with nanoliter flow rates (Figure 7-1).

The development of nanoflow LC has made analysis in sample limited applications much easier. Typically nanoflow LC is hyphenated with electrospray ionization mass spectrometry (ESI-MS) making for a powerful tool for many bioanalytical applications including proteomics and metabolomics. However, challenges arise when samples consist of poorly ionizable analytes, structural isomers or even unknown metabolites. When such challenges are encountered, there is a need for an orthogonal detector. UV/vis and fluorometric detection schemes have been pursued for orthogonal detection, however both these techniques are non-universal detection schemes, which would require tagging analytes or using an indirect method for incompatible analytes.[8] Surface enhanced ramen spectroscopy (SERS) has recently been hyphenated with nano-LC as an alternative to LC-MS metabolomics. Here LC-SERS was employed for metabolomics-based tumor diagnosis and comparable detection to MS was observed. However the

overlap between LC-SERS and LC-MS was non-ideal. In other words SERS seemed to only be selective for a different subset of metabolites which does not eliminate the need for another orthogonal detector.[9] It is important to mention that another alternative to LC-MS especially in the metabolomic space is nuclear magnetic resonance (NMR). However, NMR does suffer from lower sensitivity and typically requires higher concentrations of significant volume for optimal detection making the nanoflow LC-MS a better choice in sample limited situations.[10]

A more universal orthogonal detection method for nanoflow LC-MS applications would be desirable, which is where the microring resonator platform comes in. The microring resonators represent a refractive index (RI) based detector which has shown with preliminary results to be compatible with detection of nanoliter flow rates. Here the microring resonator CE flow cell was interfaced to syringe pumps using 75 μm capillary tubing, the delivered flow rate was 500 nL/min. The data obtained with this set up is presented in Figure 7-1, where Figure 7-1A shows a solvent step of water and acetonitrile and Figure 7-1B shows detection of riboflavin plugs. This preliminary data verifies the operation of the microring resonators at 100's of nanoliter/min flow rates. Future work would require further minimizing the channel dimensions of the gasket to match those of the separation, which would be done using a laser cutter as explained in chapter 3, and then actual nanoflow LC-microring resonators experiments can be pursued.

2.2. Hyphenation of Size Exclusion Chromatography with Antibody Capture Array

One of the unique features of whispering gallery mode sensing methods are the ability to monitor biomolecular interactions, making this an attractive technique for

bioanalytical applications. Silicon photonic microring resonators are one type of such sensors which have been heavily applied to various biosensing studies. In these studies the sensor chip is modified with immobilized target-specific capture agents such as DNA or antibodies for the detection of various binding events. These studies provide useful information on target affinity and capture specificity, which has the potential to add another dimension of data if coupled to an upstream separation. The microring resonator platform has been thoroughly explored for various liquid chromatography (LC) applications and has demonstrated great utility for linear mass concentration detection, isocratic separations, gradient separations and chemical signature lacking analytes. Coupling similar LC methods of mixtures to multiplexed microring resonator arrays will not only provide typical separation data but also information on the affinity of various mixture components. Similar studies have been performed with surface plasmon resonance (SPR) optical sensing with great success, however SPR cannot be multiplexed easily so screening analyte affinity across various capture agents and/or the detection of multiple mixture components was a challenge here. With this mind, the study presented here addresses these limitations of pervious LC-SPR studies and further explores the versatility of the microring resonator platform for LC applications by utilizing multiplexed biosensing detection.

2.2.1. Introduction

Silicon photonic microring resonators are optical resonant sensors, a class of whispering gallery mode sensors, which are most often used for the observation of molecular binding events or immunoassays. This is typically employed as a diagnostic

tool, where insight on analyte specificity and binding kinetics can be inferred from diagnostic markers. Traditionally samples in complex matrices are flowed across a multiplexed microring resonator chip, which have been functionalized with tethered capture agents such as antibodies or DNA. Here analytes with specificity for tethered capture agents are pulled down, resulting in Langmuir binding response.[11–14] This technology will be hyphenated with size exclusion chromatography (SEC) to provide binding data post separation.

Previous work has used the microring resonator platform in a non-conventional way by hyphenating with upstream separations. Such studies have interfaced with capillary electrophoresis and both isocratic and gradient high performance liquid chromatography (HPLC). Much of this work was focused on demonstrating the competitive performance of the microring resonators as a detector when compared to commercial detectors such as UV/visible (UV/vis), differential RI (dRI), evaporative light scattering (ELSD) and charged aerosol detectors (CAD). Because they offer both a linear mass response and universal detection for solvent gradient separations, microring resonators offer certain advantages over commercially available detectors. In all previous studies involving microring resonators for LC, they were used as bulk refractive index (RI) detectors only. This means that the sensor chips were untreated so no analyte binding was observed. [1,2,7,15]

In this study, we will hyphenate SEC separations with microring resonator chips that have been functionalized with antibody capture agents. This means that we will separate antibody samples by size via SEC before flowing across our functionalized chips

where we will get affinity response from the microring resonators. Similar approaches have been used with surface plasmon resonance (SPR) in-line with various separations. SPR is another optical technique that monitors binding events. However, unlike the microring resonator platform SPR lacks the ability for multiplexing which means only one biomolecular interaction can be screened at a time.[16–26] To our knowledge this is the first time that multiple biomolecular interactions will be screened in a single experiment post separation.

2.2.2. Experimental

Materials

IgG and IgA captures were purchased from R&D Systems (Minneapolis, MN), both of which recombinant monoclonal antibodies purified from human serum. The IgM capture, specifically AffiniPure Goat Anti-Human IgM (which is specific for Fc5μ fragment), was purchased from Jackson Immuno Research Laboratories, Inc. (West Grove, PA). IgG, IgA, and IgM samples from human serum were purchased from Millipore Sigma (St. Louis, MO), samples were prepared in phosphate buffered saline at various concentrations. Phosphate buffered saline (PBS) was reconstituted as directed from powder packets purchased from Millipore Sigma (St. Louis, MO) to obtain a 1X PBS solution at pH 7.4 + 0.05% sodium azide for use as mobile phase. All reagents were used as received.

Microring Resonators

The microring resonator system (Maverick M1 optical scanning instrumentation) and sensor array chips were purchased from Genalyte, Inc. (San Diego, CA), detailed descriptions of sensor fabrication and instrument operation have been described elsewhere.[27] In overview, the microring resonators are ring shaped optical cavities 30 μm in diameter with adjacent linear waveguides. Light from an external tunable cavity diode laser centered at 1550 nm propagates down the waveguide individually probing each microring. Optical transmission is monitored as a function of wavelength and dips in transmittance signal are observed at resonant wavelengths (λ_r), defined by the following equation:

$$\lambda_r = \frac{2\pi n_{eff}}{m} \qquad \textit{Eq. 1}$$

Here r is the ring radius, n_{eff} is the effective refractive index, and m is a constant. As changes in n_{eff} are observed, such as analyte elution or binding, there is a shift in the λ_r, which is measured and referred as the relative shift in delta picometers (Δpm). These changes in the λ_r corresponded to changes in the n_{eff} and are monitored as a function of time.[1,15,28]

Each sensor chip is 4 x 6 mm silicon-on-insulator (SOI) wafer which has a SiO_2 surface that is highly chemically resistant. The microring resonator chip consists of an array of 128 individual microring resonators.[15] Prior to microring resonator functionalization, the protective photoresist coating is removed by immersing chips in acetone. The microring resonator functionalization protocol is discussed in the next section.

Microring Resonator Functionalization

Microring resonator chips were first rinsed in acetone to remove a protective coating, this was followed by silanization in a 1% APTES solution and rinses in both acetone and isopropyl alcohol. Sensor chips were then rinsed with deionized water and dried under nitrogen. A crosslinking reagent, consisting of 2 mM acetic acid and 5 mM BS3 crosslinker, was then manually spotted onto the chip clusters comprised of 4 individual microrings. This was followed by the manual spotting of immunoglobulin solutions of 0.25 mg/mL in 10 mM PBS and 5% glycerol. Multiple clusters were spotted with each capture for repetitive measurements, additionally different captures were spotted with spatial considerations made. Functionalization was concluded with incubation in a humidity chamber and coating with DryCoat before being stored in a desiccator at 4°C.[11]

HPLC

Size exclusion chromatographic separations were performed on a Waters Alliance e2695 separation module (Milford, MA) furnished with a Waters 2489 UV/Visible (UV/vis) Detector. The column used was an GE Superdex^{TM} 200 Increase 3.2/300 (Marlborough, MA), with dimensions of 3.2 mm × 300mm and a bed volume of 2.4 mL. The column was kept at ambient temperature and maintained a flow rate was 0.075 mL/min of 0.01 M PBS (pH 7.4) + 0.05% sodium azide. UV/vis wavelength was 280 nm and sample temperature was kept at 5 °C.

SEC-Microring Resonator Interface

The microring resonator assembly consists of an anodized aluminum cartridge holder, Mylar gasket and flow cell lid. Sandwiched between the holder an gasket is the freshly functionalized sensor chip. This whole assembly, which is analogous to a detector flow cell, was interfaced to the HPLC via the following connections. The HPLC outlet was connected to a 0.25 mm flangeless 1/4−28 and then to a ZDV 10−32 PEEK low pressure union. The PEEK union adapted the HPLC fittings to the microring resonator cartridge. The same interface HPLC-microring resonator interface has been discussed previously.[1,2,15] The experimental set-up is presented in Figure 7-2.

Data Analysis

Data analysis was carried out using custom software written in R (version 3.4.1). Briefly, raw microring resonator chromatograms typically show an averaged response from 4-10 microrings. The averaged signal intensity is plotted as a function of time (Figure 7-3A). The raw data undergoes a first derivative transformation using Origin (Figure 7-3B) and these traces are further smoothed using a Savitzky–Golay filter (Figure 7-3C).

2.2.3. Results and Discussion

SEC-Microring Resonator Binding Chromatograms

SEC separations of 10µL injections of 10 µg/mL immunoglobulin solutions utilizing the SEC- microring resonator interface were performed, with the resulting chromatograms shown in Figure 7-3. Here the raw chromatogram traces are presented in Figure 7-3A and the first derivative transformed traces are presented in Figure 7-3B-C. The different shapes of the binding profiles observed here are a result of the different binding kinetics

of the three different antibodies. Additionally, here a specific response is observed without any cross-reactivity. This binding chromatogram response was investigated further in Figure 7-4, looking at the reproducibility of these interactions. Here repetitive SEC separations of 6 µL injections of 0.25 mg/mL immunoglobulin solutions were performed, again utilizing the SEC-microring resonator interface with a different sensor chip each time. The multiple binding chromatograms are all plotted on the same axis shown in Figure 7-4A, the error bars here are the spread in the measurements made on each chip. Visual inspection of these binding traces show very reproducible binding profiles, this is further verified by the small range in the binding maximums when converting the chromatograms to box plots shown in Figure 7-4B.

SEC-Microring Resonator Bulk RI Chromatograms

The bulk microring resonator signal is dependent on the refractive index contrast between the mobile phase and the analyte. This means that when the RI difference is small sensitivity will suffer which is visualized in Figure 7-5. Figure 7-5A shows the bulk RI detection of SEC separations of 10 µL injections of 0.25 mg/mL immunoglobulin solution, here no immunoglobulin peak is observed. A peak for IgM is observed once injected concentration is significantly increased to 1.0 mg/mL, seen by the first peak in in Figure 7-5B. The second peak here, also observed in Figure 7-5A, in an unknown unbinding sample component possibly a sugar. As a reference dRI data was collected in a separate experiment shown in Figure 7-5C-D, here a larger injection volume (10 µL of 0.25 mg/mL) and higher flow rate (0.1 mL/min) were used due to detector flow cell requirements. Figure 7-5C shows the full dRI chromatogram and Figure 7-5D zooms in

on the small immunoglobulin peaks. These dRI chromatograms further show that RI detection of the immunoglobulins is challenged by small RI differences between the analyte and mobile phase, which supports the results seen with bulk microring resonators detection. This data is presented here to show that by having molecular captures at the microring resonator surface a significant signal enhancement is observed.

Comparison of HPLC Assay and Conventional Flow Assay

Conventionally assays with the microring resonators are performed in flow by stand-alone operation of the microring resonators. Such use of the microring resonators is presented in Figure 7-6A, here a concentration of 100 µg/mL were allowed to flow over the functionalized sensor chip for 5 minutes. Much like in the SEC assay, specific responses were observed between target-capture pairs and no cross-reactivity was observed. The biggest difference observed by comparing to the SEC assay traces presented in Figure 7-6B is the shape of the binding profile. This is especially evident by looking at Figure 7-6C-D which shows the binding profiles of IgA and IgM superimposed on the same axis. Comparable binding and kinetics is mostly observed with IgM (Figure 7-6D) however, whereas the SEC assay of IgA seems to have slower kinetics in comparison to the conventional flow assay which is mostly attributed to experimental differences (i.e. continuous flow of dilute IgA solution versus small concentrated injection of IgA) (Figure 7-6C).

Investigation Into Concertation Response

SEC separations of 10 µg/mL immunoglobulin solutions utilizing the SEC-microring resonator interface were performed this time varying the injection volume, as shown in Figure 7-7. Looking at the raw binding chromatograms (Figure 7-7A) it is observed that the binding shift increases with increasing mass injected, this is observed in peak form after the first derivative transformation presented in Figure 7-7B. The first derivative of the raw data is directly comparable to the UV/vis chromatogram shown in Figure 7-7C.

2.2.4. Conclusion

This preliminary work presented here explores the robustness of SEC hyphenated with multiplexed microring resonator senor chips to perform SEC assays. The chosen system successfully demonstrated specific antibody interactions without cross-reactivity, representing an important step for more complex analyses yet to come. Future work will demonstrate the utility of having an assay type experiment in-line with separations. This will be done by analyzing mixtures potentially of a biological matrix to infer sample component affinity, which is not data typically obtained from a traditional HPLC detector. Additionally, more quantitative analysis will be performed by quantifying mixture component abundance by using binding response and concertation calibrations of the microring resonator platform. Upon completion, this work along with other completed work will further highlight the unique versatility of the microring resonator platform as an HPLC detector.

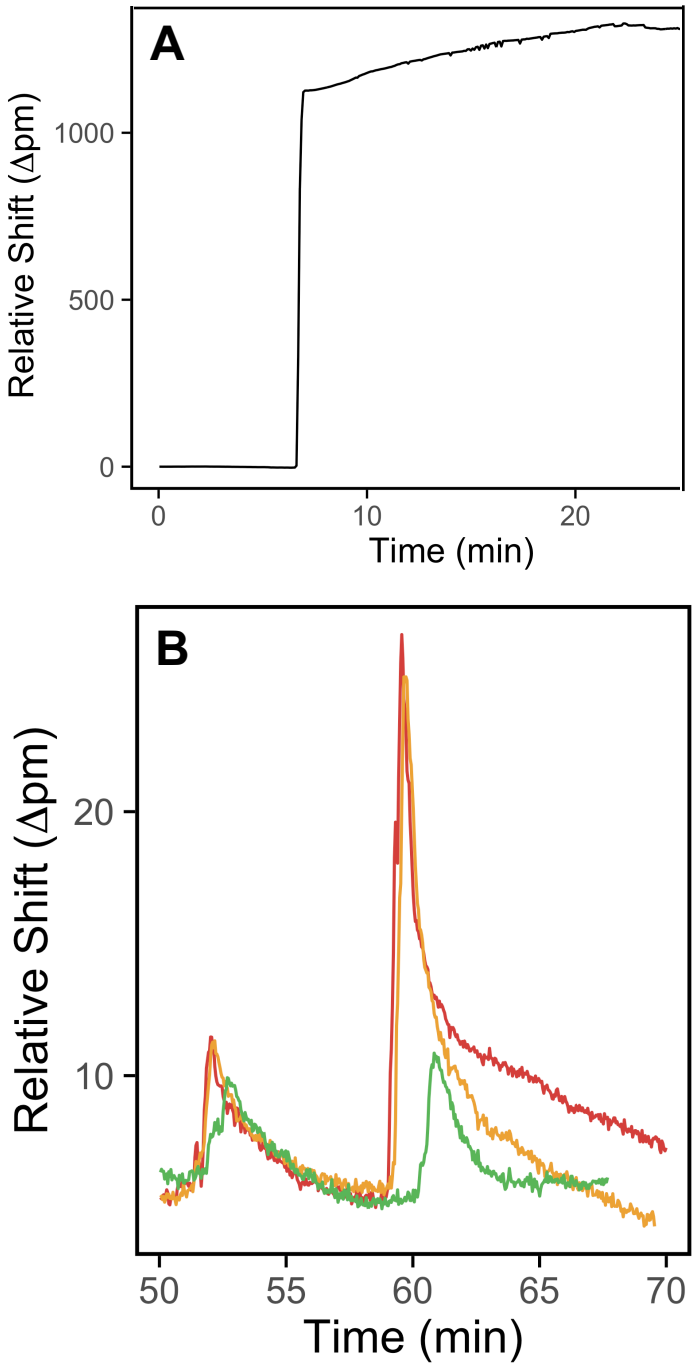

Figure 7-1: Microring Resonator Performance at Nanoliter Flow Rates. Here the microring resonators where interfaced with syringe pumps to deliver flow at a 500 nL/min, (A) shows a solvent step from water to acetonitrile and (B) shows flow injections of riboflavin of varied injection sizes.

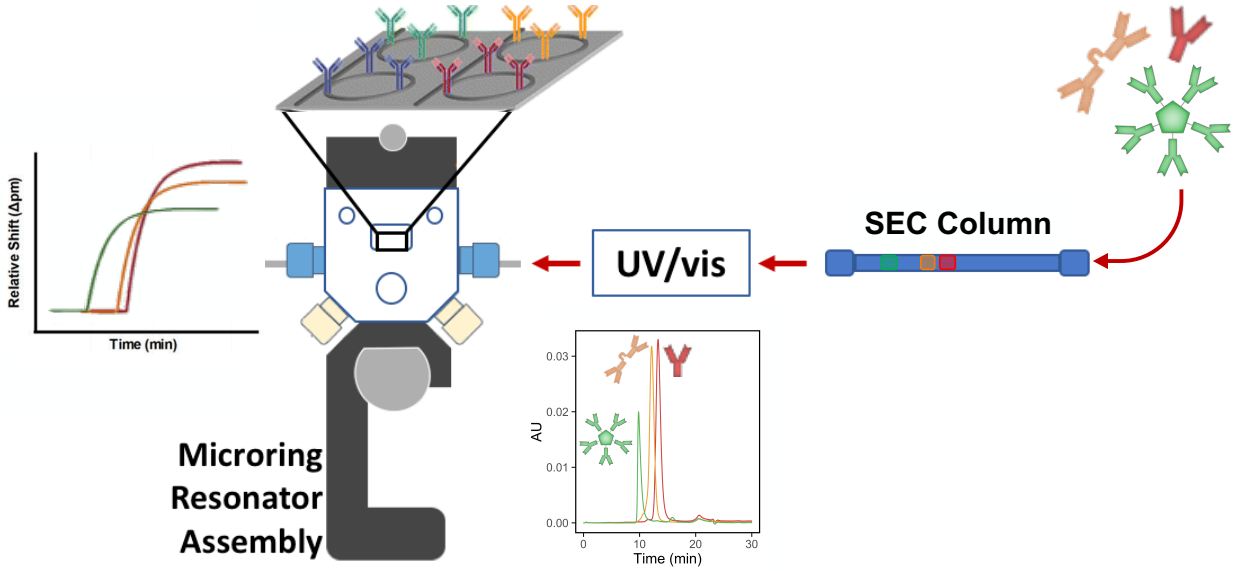

Figure 7-2: Hyphenation of Size Exclusion Chromatography with Antibody Capture Array Experimental Set-up/Flow Path.

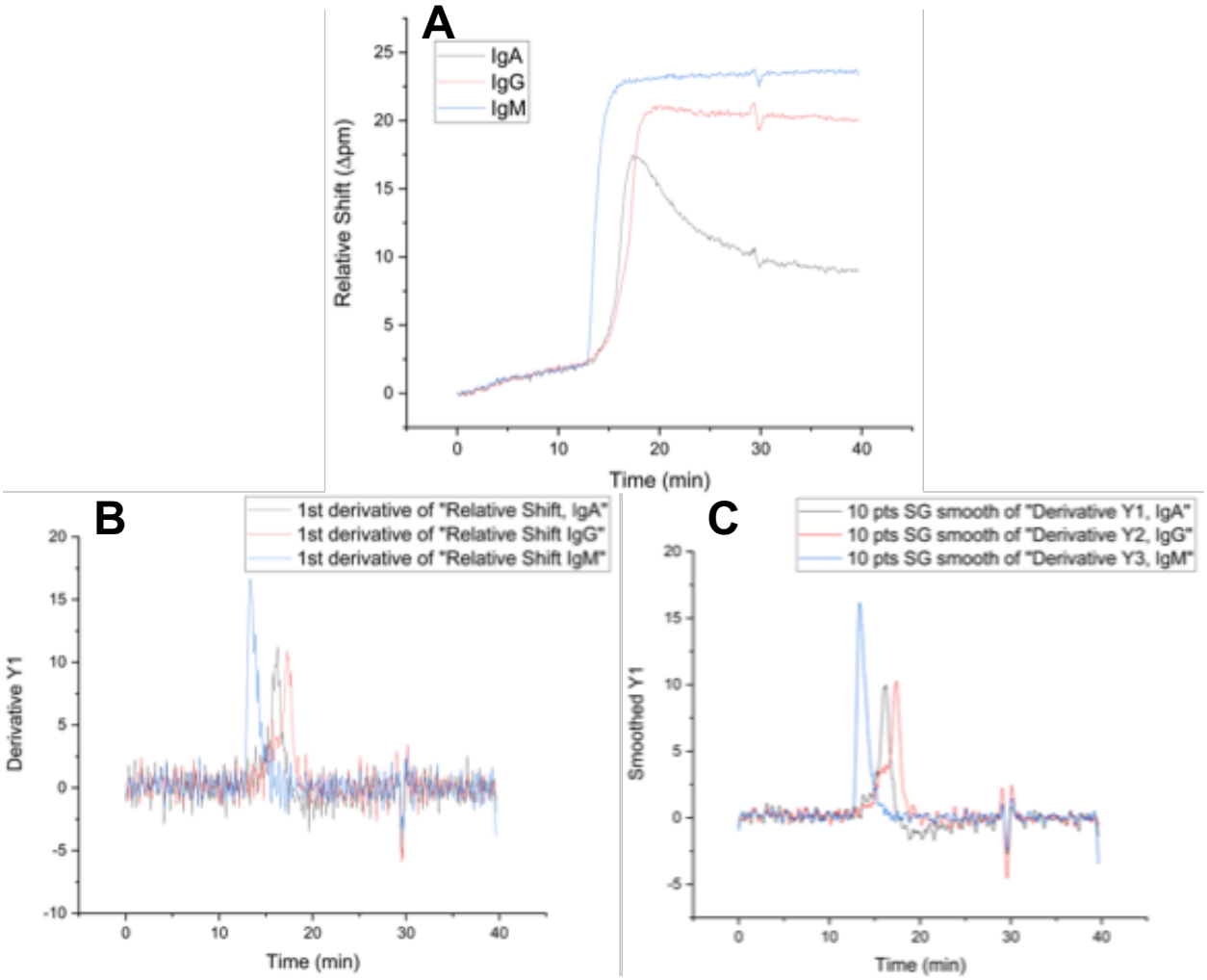

Figure 7-3: SEC-Microring Resonator Binding Chromatograms. Various immunoglobulins prepared at 10 µg/mL in phosphate buffered saline were separated by SEC with a 0.075 mL/min flow rate of 0.01M phosphate buffered saline. A. Raw binding chromatograms of a 10µL injection. B. First derivative transformation of the raw binding chromatograms. C. Savitzky–Golay filter smoother applied to the first derivative traces.

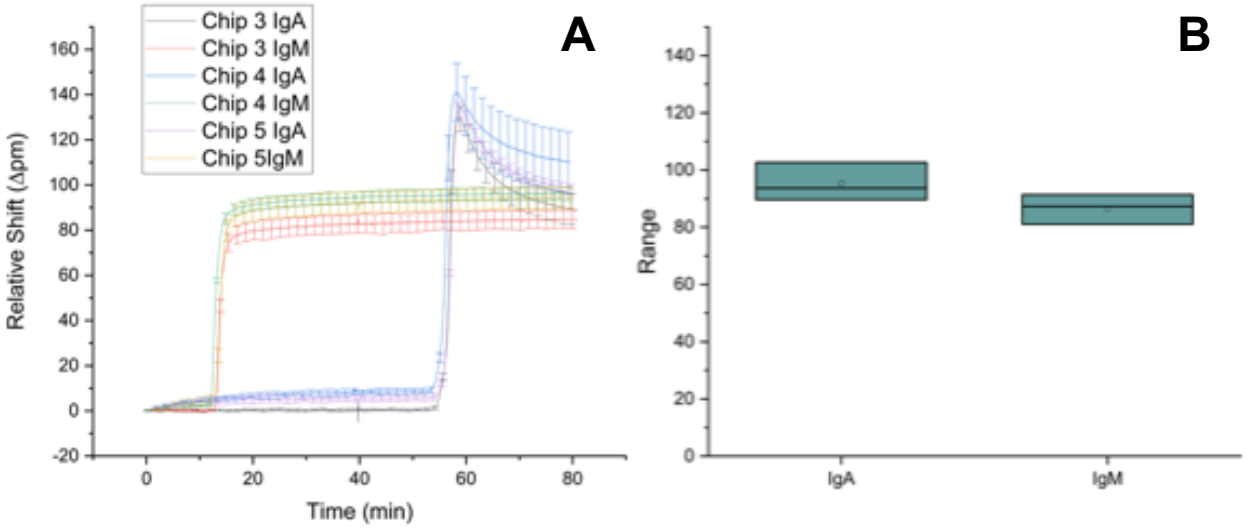

Figure 7-4: SEC-Microring Resonator Binding Chromatogram Reproducibility from Chip to Chip. A. Raw binding chromatograms obtained from three different chips with error bars showing ring spread from a single chip. B. Plots the range of the max shifts observed across three different chips in a box plot format.

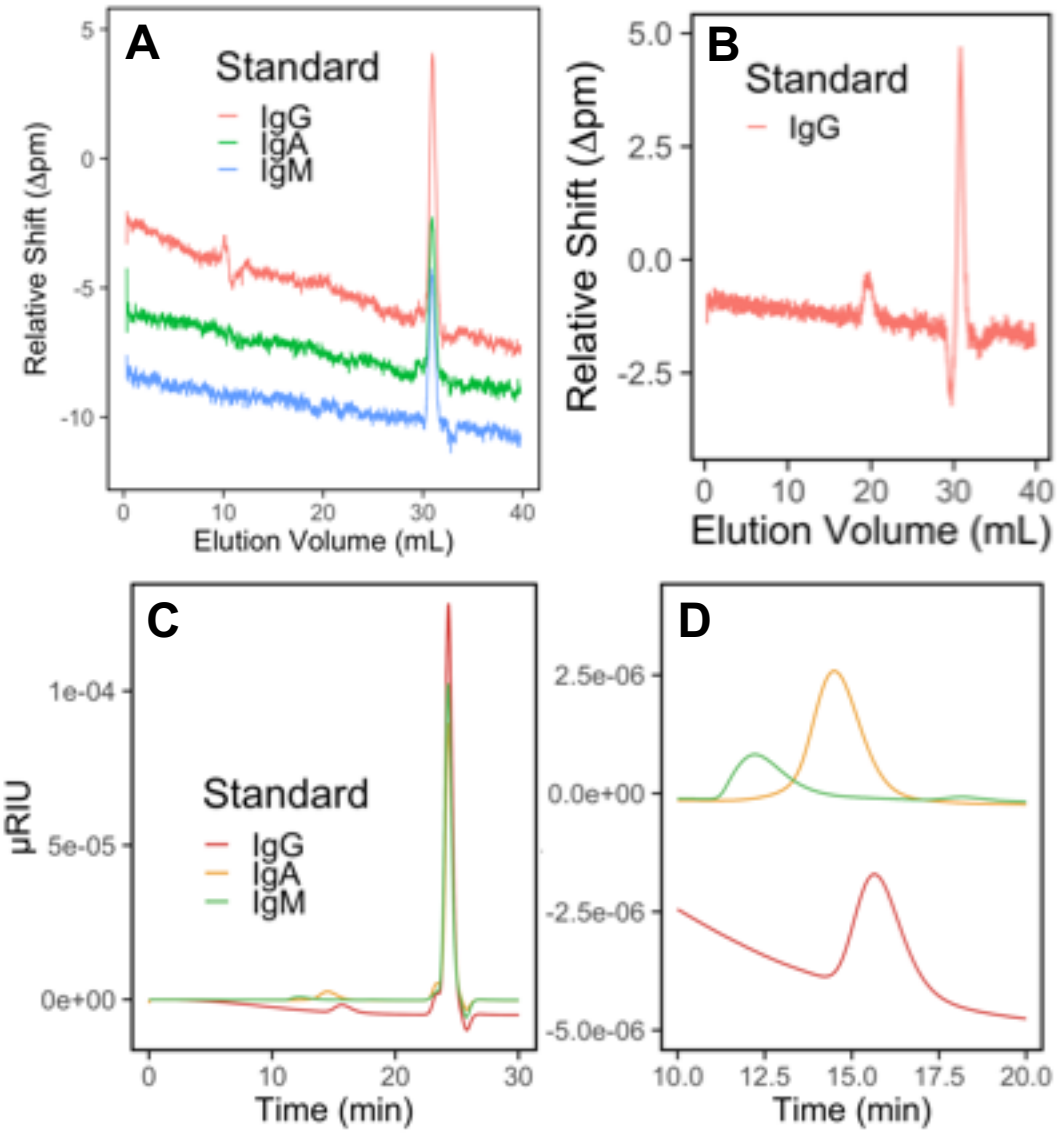

Figure 7-5: Bulk RI Response from the Microring Resonators and Detection by dRI. A. Raw SEC chromatograms of 10 μL injections of 0.25 mg/mL immunoglobulin solutions (separation performed at 0.075 mL/min flow rate of 0.01M phosphate buffered saline) . B. Raw SEC chromatograms of 10 μL injections of 1.0 mg/mL immunoglobulin solutions (separation performed at 0.075 mL/min flow rate of 0.01M phosphate buffered saline). C. Differential refractive index chromatogram of 10 μL injections of 0.25 mg/mL immunoglobulin solutions (separation performed at 0.1 mL/min flow rate of 0.01M phosphate buffered saline).

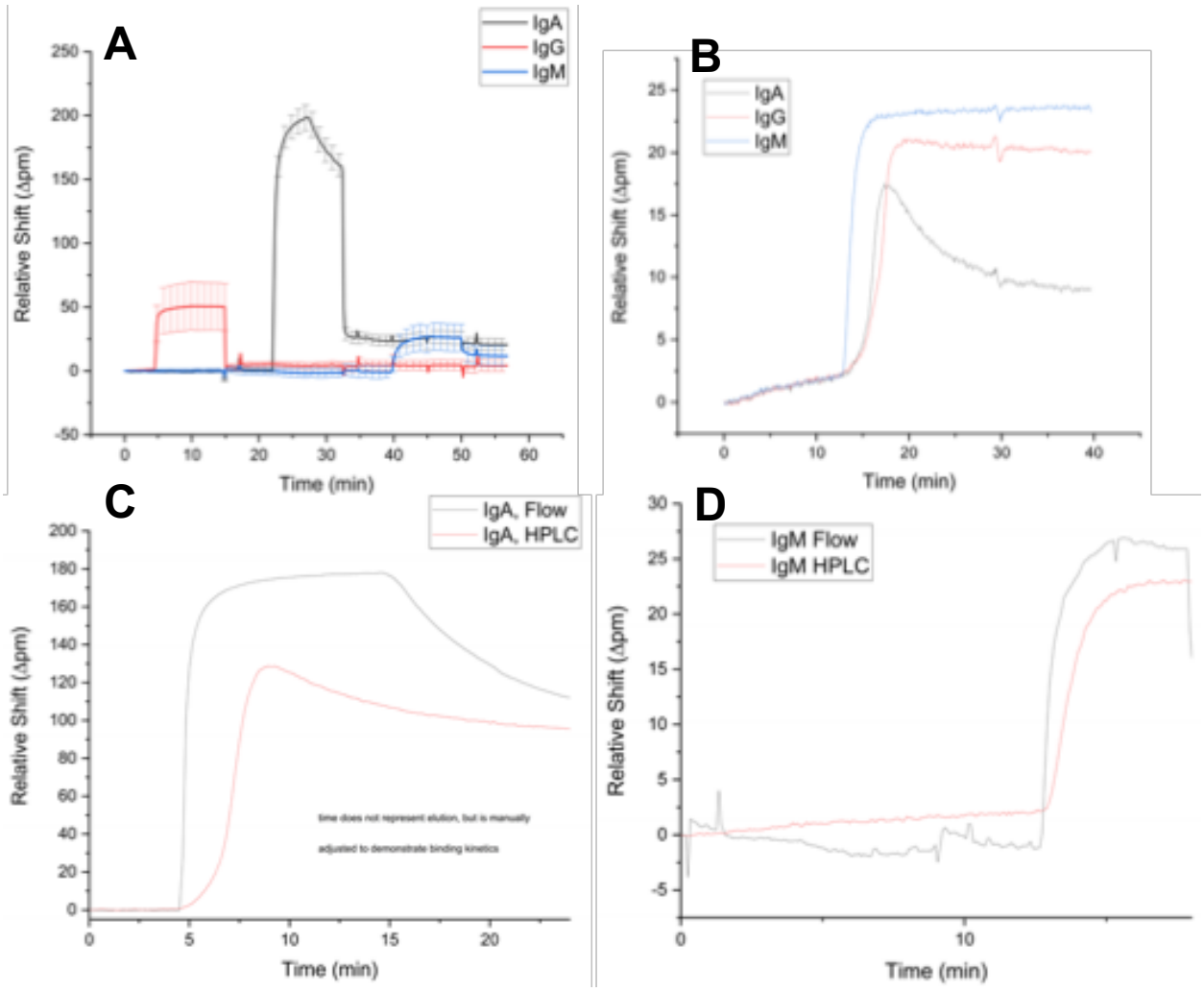

Figure 7-6: Comparison of SEC Assay and Conventional Flow Assay. A. Conventional flow assay of 100 µg/mL immunoglobulin solutions. B. Raw SEC chromatograms of 10 µL injections of 10 µg/mL immunoglobulin solutions (separation performed at 0.075 mL/min flow rate of 0.01M phosphate buffered saline). C. Overlapping binding profiles for IgA from the two different assay types. D. Overlapping binding profiles for IgM from the two different assay types.

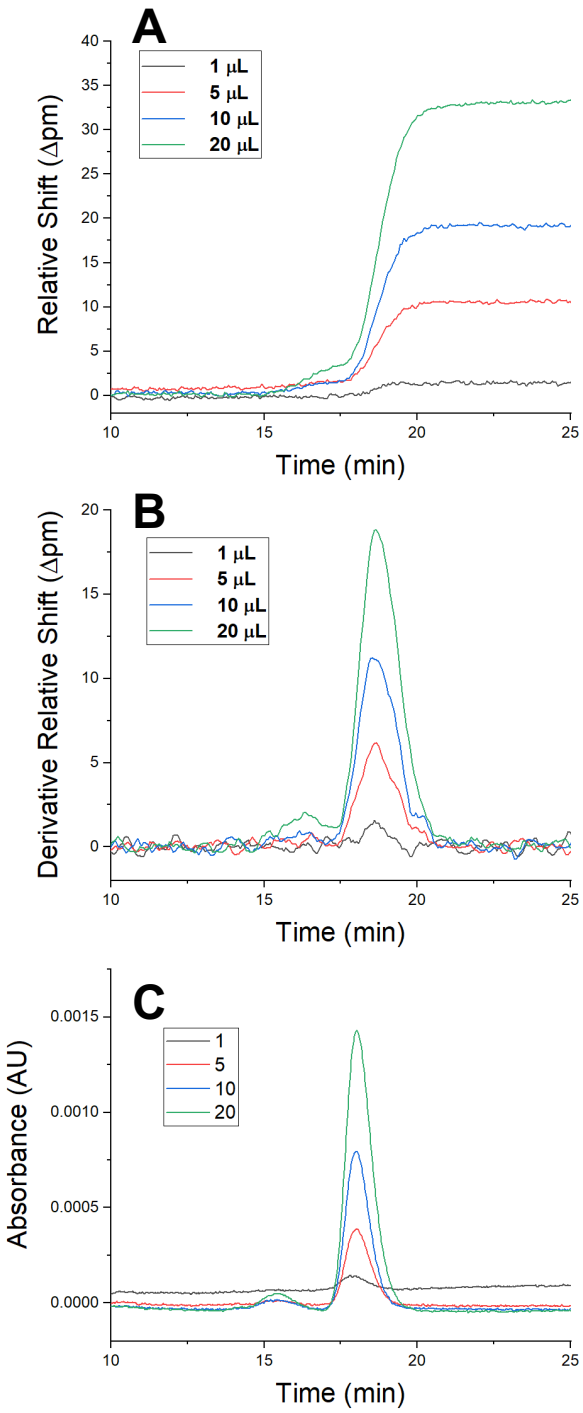

Figure 7-7: Concentration Response with increasing Injection Volume. A. Raw SEC chromatograms of 10 µg/mL IgG injected at varied volumes (1-10 µL). B. First derivative transformation of raw binding chromatograms. C. In-line UV/vis chromatograms (separation performed at 0.075 mL/min flow rate of 0.01M phosphate buffered saline).

3. References

(1) Mordan, E. H.; Wade, J. H.; Wiersma, Z. S. B.; Pearce, E.; Pangburn, T. O.; deGroot, A. W.; Meunier, D. M.; Bailey, R. C. Silicon Photonic Microring Resonator Arrays for Mass Concentration Detection of Polymers in Isocratic Separations. *Anal. Chem.* **2019**, *91* (1), 1011–1018. https://doi.org/10.1021/acs.analchem.8b04263.

(2) Mordan, E. H.; Wade, J. H.; Pearce, E.; Meunier, D. M.; Bailey, R. C. A Linear Mass Concentration Detector for Solvent Gradient Polymer Separations. *Analyst* **2020**. https://doi.org/10.1039/C9AN02533B.

(3) Almeling, S.; Ilko, D.; Holzgrabe, U. Charged Aerosol Detection in Pharmaceutical Analysis. *J. Pharm. Biomed. Anal.* **2012**, *69*, 50–63. https://doi.org/10.1016/j.jpba.2012.03.019.

(4) Jia, S.; Park, J. H.; Lee, J.; Kwon, S. W. Comparison of Two Aerosol-Based Detectors for the Analysis of Gabapentin in Pharmaceutical Formulations by Hydrophilic Interaction Chromatography. *Talanta* **2011**, *85* (5), 2301–2306. https://doi.org/10.1016/j.talanta.2011.04.012.

(5) Mondal, B.; Kote, M.; Lunagariya, C.; Patel, M. Development of a Simple High Performance Liquid Chromatography (HPLC)/Evaporative Light Scattering Detector (ELSD) Method to Determine Polysorbate 80 in a Pharmaceutical Formulation. *Saudi Pharm. J.* **2020**, *28* (3), 325–328. https://doi.org/10.1016/j.jsps.2020.01.012.

(6) Soliven, A.; Haidar Ahmad, I. A.; Tam, J.; Kadrichu, N.; Challoner, P.; Markovich, R.; Blasko, A. A Simplified Guide for Charged Aerosol Detection of Non-Chromophoric Compounds—Analytical Method Development and Validation for the HPLC Assay of

Aerosol Particle Size Distribution for Amikacin. *J. Pharm. Biomed. Anal.* **2017**, *143*, 68–76. https://doi.org/10.1016/j.jpba.2017.05.013.

(7) Orlet, J. D.; Bailey, R. C. Silicon Photonic Microring Resonator Arrays as a Universal Detector for Capillary Electrophoresis. *Anal. Chem.* **2020**, *92* (2), 2331–2338. https://doi.org/10.1021/acs.analchem.9b05271.

(8) Heus, F.; Giera, M.; de Kloe, G. E.; van Iperen, D.; Buijs, J.; Nahar, T. T.; Smit, A. B.; Lingeman, H.; de Esch, I. J. P.; Niessen, W. M. A.; Irth, H.; Kool, J. Development of a Microfluidic Confocal Fluorescence Detection System for the Hyphenation of Nano-LC to on-Line Biochemical Assays. *Anal. Bioanal. Chem.* **2010**, *398* (7), 3023–3032. https://doi.org/10.1007/s00216-010-4210-x.

(9) Xiao, L.; Wang, C.; Dai, C.; Littlepage, L. E.; Li, J.; Schultz, Z. D. Untargeted Tumor Metabolomics with Liquid Chromatography–Surface-Enhanced Raman Spectroscopy. *Angew. Chem. Int. Ed.* **2020**, *59* (9), 3439–3443. https://doi.org/10.1002/anie.201912387.

(10) Emwas, A.-H.; Roy, R.; McKay, R. T.; Tenori, L.; Saccenti, E.; Gowda, G. A. N.; Raftery, D.; Alahmari, F.; Jaremko, L.; Jaremko, M.; Wishart, D. S. NMR Spectroscopy for Metabolomics Research. *Metabolites* **2019**, *9* (7). https://doi.org/10.3390/metabo9070123.

(11) Robison, H. M.; Escalante, P.; Valera, E.; Erskine, C. L.; Auvil, L.; Sasieta, H. C.; Bushell, C.; Welge, M.; Bailey, R. C. Precision Immunoprofiling to Reveal Diagnostic Signatures for Latent Tuberculosis Infection and Reactivation Risk Stratification. *Integr. Biol.* **2019**, *11* (1), 16–25. https://doi.org/10.1093/intbio/zyz001.

(12) Graybill, R. M.; Para, C. S.; Bailey, R. C. PCR-Free, Multiplexed Expression Profiling of MicroRNAs Using Silicon Photonic Microring Resonators. *Anal. Chem.* **2016**, *88* (21), 10347–10351. https://doi.org/10.1021/acs.analchem.6b03350.

(13) Washburn, A. L.; Shia, W. W.; Lenkeit, K. A.; Lee, S.-H.; Bailey, R. C. Multiplexed Cancer Biomarker Detection Using Chip-Integrated Silicon Photonic Sensor Arrays. *Analyst* **2016**, *141* (18), 5358–5365. https://doi.org/10.1039/C6AN01076H.

(14) Wade, J. H.; Alsop, A. T.; Vertin, N. R.; Yang, H.; Johnson, M. D.; Bailey, R. C. Rapid, Multiplexed Phosphoprotein Profiling Using Silicon Photonic Sensor Arrays. *ACS Cent. Sci.* **2015**, *1* (7), 374–382. https://doi.org/10.1021/acscentsci.5b00250.

(15) Wade, J. H.; Bailey, R. C. Refractive Index-Based Detection of Gradient Elution Liquid Chromatography Using Chip-Integrated Microring Resonator Arrays. *Anal. Chem.* **2014**, *86* (1), 913–919. https://doi.org/10.1021/ac4035828.

(16) Jungar, C.; Strandh, M.; Ohlson, S.; Mandenius, C.-F. Analysis of Carbohydrates Using Liquid Chromatography–Surface Plasmon Resonance Immunosensing Systems. *Anal. Biochem.* **2000**, *281* (2), 151–158. https://doi.org/10.1006/abio.2000.4565.

(17) Wu, X.-Z.; Nakagawa, M.; Nagamori, C.; Uchiyama, K.; Hobo, T. Detection Method Based on a Surface Plasmon Resonance and Its Application to Flow Injection Analysis and Liquid Chromatography. *Bull. Chem. Soc. Jpn.* **1996**, *69* (7), 1969–1974. https://doi.org/10.1246/bcsj.69.1969.

(18) Lakayan, D.; Haselberg, R.; Gahoual, R.; Somsen, G. W.; Kool, J. Affinity Profiling of Monoclonal Antibody and Antibody-Drug-Conjugate Preparations by Coupled

Liquid Chromatography-Surface Plasmon Resonance Biosensing. *Anal. Bioanal. Chem.* **2018**, *410* (30), 7837–7848. https://doi.org/10.1007/s00216-018-1414-y.

(19) Zhang, Y.; Shi, S.; Guo, J.; You, Q.; Feng, D. On-Line Surface Plasmon Resonance-High Performance Liquid Chromatography–Tandem Mass Spectrometry for Analysis of Human Serum Albumin Binders from Radix Astragali. *J. Chromatogr. A* **2013**, *1293*, 92–99. https://doi.org/10.1016/j.chroma.2013.04.015.

(20) Peng, M.; Zhang, Y.; Shi, S.; Peng, S. Simultaneous Ligand Fishing and Identification of Human Serum Albumin Binders from Eucommia Ulmoides Bark Using Surface Plasmon Resonance-High Performance Liquid Chromatography–Tandem Mass Spectrometry. *J. Chromatogr. B* **2013**, *940*, 86–93. https://doi.org/10.1016/j.jchromb.2013.09.032.

(21) Marchesini, G. R.; Hooijerink, H.; Haasnoot, W.; Nielen, M. W. F.; Buijs, J.; Campbell, K.; Elliott, C. T.; Nielen, M. W. F. Towards Surface Plasmon Resonance Biosensing Combined with Bioaffinity-Assisted Nano HILIC Liquid Chromatography / Time-of-Flight Mass Spectrometry Identification of Paralytic Shellfish Poisons. *TrAC Trends Anal. Chem.* **2009**, *28* (6), 792–803. https://doi.org/10.1016/j.trac.2009.04.008.

(22) Chen, H.; Wang, X.; Wu, H.; Zhan, S. A Novel Detector for Chromatography and Estradiol Immune Sensor Based on Surface Plasma Resonance. In *2010 3rd International Conference on Biomedical Engineering and Informatics*; 2010; Vol. 4, pp 1401–1404. https://doi.org/10.1109/BMEI.2010.5639402.

(23) Du, M.; Zhou, F. Postcolumn Renewal of Sensor Surfaces for High-Performance Liquid Chromatography−Surface Plasmon Resonance Detection. *Anal. Chem.* **2008**, *80* (11), 4225–4230. https://doi.org/10.1021/ac702632y.

(24) Cepria, G.; Castillo, J. R. Surface Plasmon Resonance-Based Detection An Alternative to Refractive Index Detection in High-Performance Liquid Chromatography. *J. Chromatogr. A* **1997**, *759* (1), 27–35. https://doi.org/10.1016/S0021-9673(96)00752-2.

(25) Castillo, J. R.; Cepriá, G.; de Marcos, S.; Galbán, J.; Mateo, J.; Ruiz, E. G. Surface Plasmon Resonance Sensor as a Detector in HPLC and Specific Lactate Determination. *Sens. Actuators Phys.* **1993**, *37–38*, 582–586. https://doi.org/10.1016/0924-4247(93)80100-U.

(26) Lakayan, D.; Haselberg, R.; Niessen, W. M. A.; Somsen, G. W.; Kool, J. On-Line Coupling of Surface Plasmon Resonance Optical Sensing to Size-Exclusion Chromatography for Affinity Assessment of Antibody Samples. *J. Chromatogr. A* **2016**, *1452*, 81–88. https://doi.org/10.1016/j.chroma.2016.05.033.

(27) Iqbal, M.; Gleeson, M. A.; Spaugh, B.; Tybor, F.; Gunn, W. G.; Hochberg, M.; Baehr-Jones, T.; Bailey, R. C.; Gunn, L. C. Label-Free Biosensor Arrays Based on Silicon Ring Resonators and High-Speed Optical Scanning Instrumentation. *IEEE J. Sel. Top. Quantum Electron.* **2010**, *16* (3), 654–661. https://doi.org/10.1109/JSTQE.2009.2032510.

(28) Wade, J. H.; Bailey, R. C. Applications of Optical Microcavity Resonators in Analytical Chemistry. *Annu. Rev. Anal. Chem.* **2016**, *9*, 1–25. https://doi.org/10.1146/annurev-anchem-071015-041742.